DESIGN AND TESTING OF A NOVEL BUILDING INTEGRATED CROSS AXIS WIND TURBINE

GWANI MOHAMMED

FACULTY OF ENGINEERING
UNIVERSITY OF MALAYA
KUALA LUMPUR

2018

DESIGN AND TESTING OF A NOVEL BUILDING INTEGRATED CROSS AXIS WIND TURBINE

GWANI MOHAMMED

THESIS SUBMITTED IN FULFILMENT OF THE REQUIREMENTS FOR THE DEGREE OF DOCTOR OF PHILOSOPHY

FACULTY OF ENGINEERING
UNIVERSITY OF MALAYA
KUALA LUMPUR

2018

UNIVERSITY OF MALAYA
ORIGINAL LITERARY WORK DECLARATION

Name of Candidate: **GWANI MOHAMMED**

Matric No: **KHA130042**

Name of Degree: **Doctor of Philosophy**

Title of Thesis ("this Work"): **Design and Testing of a Novel Building Integrated Cross Axis Wind Turbine**

Field of Study: **Energy**

I do solemnly and sincerely declare that:

(1) I am the sole author/writer of this Work;
(2) This Work is original;
(3) Any use of any work in which copyright exists was done by way of fair dealing and for permitted purposes and any excerpt or extract from, or reference to or reproduction of any copyright work has been disclosed expressly and sufficiently and the title of the Work and its authorship have been acknowledged in this Work;
(4) I do not have any actual knowledge nor do I ought reasonably to know that the making of this work constitutes an infringement of any copyright work;
(5) I hereby assign all and every rights in the copyright to this Work to the University of Malaya ("UM"), who henceforth shall be owner of the copyright in this Work and that any reproduction or use in any form or by any means whatsoever is prohibited without the written consent of UM having been first had and obtained;
(6) I am fully aware that if in the course of making this Work I have infringed any copyright whether intentionally or otherwise, I may be subject to legal action or any other action as may be determined by UM.

Candidate's Signature Date:

Subscribed and solemnly declared before,

Witness's Signature Date:

Name:

Designation:

DESIGN AND TESTING OF A NOVEL BUILDNG INTEGRATED CROSS AXIS WIND TURBINE

ABSTRACT

This thesis presents a novel design of a building integrated cross axis wind turbine (CAWT) that can operate under dual wind directions i.e. the horizontal wind from side and the vertical wind from the bottom of the turbine. The CAWT consisting of six horizontal blades and three vertical blades connected via connectors forms the cross axis configuration. An experiment was designed to test the performance of the CAWT on two different rooftops, i.e. on the gable and the vaulted shapes of a reduced-scaled building model. For benchmarking, the performance of a conventional straight bladed vertical axis wind turbine (VAWT) is tested under the same experimental conditions. The height of the CAWT and the VAWT above the rooftops were varied from Y = 100 to 250 mm. The effect of the roof shapes on the performance of CAWT was investigated. Comparisons were made between the performances of CAWT on the gable and vaulted rooftops. The CAWT was tested with different pitch angles, $\beta = 0^o$, 5^o, 10^o, and 15^o for the horizontal blades of the CAWT. The results obtained from the experimental study showed that at Y = 100 mm height above the gable and the vaulted rooftop, the maximum coefficient of power, $C_{p,\max}$ of the building integrated CAWT increased significantly by 266% at tip speed ratio, TSR (λ) of 1.1 and 246% at λ of 1.03, respectively, compared to the straight bladed VAWT. Further increase in CAWT height, Y above the gable rooftop showed that the CAWT outperformed the straight-bladed VAWT by 196%, 136% and 71 % at TSR of 1.16, 1.08, and 1.12 for Y = 150 to 250 mm respectively. Similar improvement in the performance of CAWT is also observed for all conditions of height above the vaulted rooftop. Furthermore, integrating CAWT on a building with gable or vaulted rooftop could yield 121% or 37% more energy than

a bare-CAWT. In addition, CAWT mounted on the gable rooftop produces 66% more energy compared to the vaulted one under the same experimental conditions. Furthermore, 10^{o} is the optimum pitch angle of the horizontal blade of the CAWT. Computational fluid dynamics (CFD) simulation results obtained from the flow field analysis indicated that the wind flow characteristics are strongly dependent on the profile of the roofs. Wind flowing above the vaulted rooftop has higher velocity, lower turbulence and lower pressure difference than the ones flowing above the gable rooftop. The double multiple streamtube (DMST) and blade element momentum (BEM) analysis produced similar pattern of graphs to the experimental results which indicates an agreement between the two analyses. Finally, an adaptive neuro-fuzzy inference system (ANFIS) methodology was used to predict the performance of power augmented VAWT. By using the root mean square error (RMSE), and the coefficient of determinant (R^2), the accuracy of the ANFIS techniques was evaluated against the experimental results. The results showed that the developed ANFIS model is very effective and reliable in predicting the performance of power augmented VAWT.

Keywords: Cross axis wind turbine, wind energy, renewable energy, building rooftop, vertical axis wind turbine

REKA BENTUK DAN PENGUJIAN KINCIR ANGIN BERPAKSI SILANG BERINTEGRASI BANGUNAN

ABSTRAK

Tesis ini membentangkan reka bentuk novel kincir angin berpaksi silang (CAWT) berintegrasi bangunan yang boleh beroperasi dalam arah angin dari arah mendatar dan juga menegak dari bawah. CAWT yang terdiri daripada enam bilah mendatar dan tiga bilah menegak yang disambungkan melalui penyambung membentuk konfigurasi berpaksi silang. Prestasi CAWT diuji pada dua bumbung berlainan, iaitu berbentuk tebar layar dan kubah pada model bangunan berskala kecil. Sebagai penanda aras, prestasi kincir angin konvensional berpaksi menegak lurus (VAWT) diuji di bawah keadaan eksperimen yang sama. Ketinggian CAWT dan VAWT di atas bumbung diuji dalam julat Y = 100 to 250 mm. Kesan bumbung bentuk pada prestasi CAWT disiasat. Perbandingan dibuat antara prestasi CAWT di atas bumbung tebar layar dan bumbung berkubah. CAWT juga diuji dengan sudut pic bilah horizontal yang berbeza, iaitu β = 0^o, 5^o, 10^o, dan 15^o. Keputusan yang diperoleh daripada kajian eksperimen menunjukkan bahawa pada ketinggian Y = 100 mm di atas tebar layar dan bumbung berkubah, pekali kuasa, Cp maksimum bangunan berintegrasi CAWT meningkat dengan iaitu ketara masing-masing sebanyak 266% pada nisbah laju tip, TSR (λ) 1.1 dan 246% pada λ 1.03, berbanding dengan VAWT. Peningkatan ketinggian CAWT, Y di atas atap tebar layar menunjukkan bahawa prestasi CAWT mengatasi VAWT masing-masing dengan 196%, 136% dan 71% pada TSR 1.16, 1.08, dan 1.12 untuk Y = 150 to 250 mm. Peningkatan yang sama dalam prestasi CAWT juga diperhatikan untuk semua ketinggian di atas bumbung berkubah. Selain itu, mengintegrasikan CAWT ke atas bangunan dengan bumbung tebar layar atau bumbung berkubah masing-masing boleh menghasilkan 121% atau 37% lebih banyak tenaga daripada yang CAWT yang tidak diintegrasikan pada bumbung bangunan. Di samping itu, CAWT yang dipasang di

bumbung tebar layar menghasilkan tenaga sebanyak 66% lebih tinggi daripada yang bumbung berkubah di bawah keadaan eksperimen yang sama. Selain itu, 10^{o} ialah sudut pic optimum bagi bilah mendatar CAWT. Hasil simulasi dinamik bendalir (CFD) diperolehi dari analisis aliran aliran menunjukkan bahawa ciri-ciri aliran angin sangat bergantung pada profil bumbung. Aliran angin di atas bumbung berkubah mempunyai kelajuan yang lebih tinggi, pergolakan yang lebih rendah dan perbezaan tekanan yang lebih rendah daripada yang mengalir di atas bumbung tebar layar. Analisis juga dijalankan untuk menentukan kuasa yang dihasilkan oleh bangunan berintegrasi CAWT menggunakan teori tiub aliran berkembar berganda (DMST) dan momentum unsur bilah (BEM). Pendekatan analitik yang digunakan menghasilkan tren graf yang serupa dengan hasil percubaan seterusnya menunjukkan persetujuan antara kedua-dua analisis. Akhir sekali, metodologi sistem adaptif inferensi neuro-kabur (ANFIS) digunakan untuk meramalkan prestasi penambahan kuasa kincir angin paksi menegak. Dengan menggunakan ralat akar min (RMSE), dan pekali penentu (R^2), ketepatan teknik ANFIS telah dinilai terhadap keputusan percubaan. Hasilnya menunjukkan bahawa model ANFIS yang dibangunkan sangat berkesan dan boleh dipercayai dalam meramalkan prestasi kuasa ditambah VAWT.

Keywords: Turbin angin paksi silang, Tenaga angin, Tenaga yang boleh diperbaharui, Membina bumbung, Turbin angin paksi menegak

ACKNOWLEDGEMENTS

Thanks, praises, total submission, and glorification are due to Allah (S.W.T) most gracious, most merciful, who in His infinite mercy guide, protect, and grant me success throughout my academic pursuit.

I wish to express my sincere gratitude, thanks, and appreciations to my supervisors Assoc. Prof. Dr. Chong Wen Tong and Dr. Tan Chin Joo for their guidance, supervision, constructive criticism and contributions, throughout the period of my study. Their constructive comments from their wealth of experience and academic competence serve as a means of inspirations towards making this thesis a reality despite all their academic constraint.

I would like to thank the University of Malaya for the PPP research grant (Project No. PG098-2014A). I would like to seize this opportunity to express my gratitude to the Tertiary Education Trust Fund (TETFUND) for the sponsorship given to me through Kebbi State University of Science and Technology, Aliero, Kebbi State Nigeria.

I would like to express my sincere appreciation to my friends and colleagues in the Renewable Energy and Green Technology Laboratory for their moral support, and fruitful discussion in conducting this research.

My profound gratitude, thanks and appreciation goes to my parents who prayed for my success every night and day, indeed they have contributed immensely toward making my dreams come true. I wish to express my sincere appreciation to my wife, my sons and daughter and my brothers and sisters for their prayers and well wishes.

Thank you all……

Gwani Mohammed

TABLE OF CONTENTS

LIST OF FIGURES

LIST OF TABLES

LIST OF SYMBOLS AND ABBREVIATIONS

Nomenclature

Latin Symbols

A	Swept area of the turbine	[m^2]
a	Induction factor	[-]
c	Blade chord length	[mm]
C_D	Drag coefficient	[-]
C_L	Lift coefficient	[-]
C_p	Power coefficient	[-]
CQ	Torque coefficient	[-]
F_D	Drag Force	[N]
F_n	Normal Force	[N]
F_t	Tangential Force	[N]
L	Lift Force	[N]
W	Relative Wind Speed	[m/s]
l	Length of horizontal blade	[mm]
P	Wind turbine power	[W]
P	pressure	[pa]
Q	Torque	[Nm]
R	Radius of the rotor	[m]
t	Time	[sec^{-1}]
T	Thrust force	[N]
U_∞	Wind speed	[m/s]
x	Distance between upper and lower arms	[mm]
$\dot{m}$	Mass flow rate	[m^3/s)
N	Blade number	[-]

Greek symbol

θ	Offset angle of the horizontal blade	[^{o}]
ρ	Density	[kg/m^3]
β	Pitch angle of the horizontal blade	[^{o}]
Ω	Rotor tip speed	[-]
σ	Solidity	[-]
ω	Angular velocity	(rad/s)

α	Angle of attack	[^{o}]
ϑ	Azimuthal angle	[^{o}]

Acronyms

AR	Aspect Ratio
CAWT	Cross axis wind turbine
CAD	Computer aided design
HAWT	Horizontal axis wind turbine
NACA	National Advisory Committee for Aeronautics
RPM	Revolution per minute
TSR (λ)	Tip speed ratio
VAWT	Vertical axis wind turbine

subscript

∞	Free stream
a	Induce velocity
i	instantaneous
R	Relative velocity

LIST OF APPENDICES

CHAPTER 1: INTRODUCTION

1.1 Energy

The Socio-economic growth of any nation often depends on the availability of energy in that nation (Mathew, 2006). Different countries have outlined different policies and approaches in planning their future energy demands (Tan et al., 2013). Fossil fuel contributes about 78% of the global energy consumption despite the environmental deterioration (EIA 2016). This has necessitated an urgent search for an alternative energy sources to meet the challenges of the present day energy demand (Sharpe & Proven, 2010). Owing to our commitment to reduce the greenhouse gas (GHG) emission caused by the use of these fossil fuels and make available sufficient energy to both the developed and developing nations, various nations have made efforts to complement the energy base with renewable energy sources in the future energy scenario (Mathew, 2006). As a result of these, renewable energy has become a critical component of many researchers and governmental organization by ever-increasing the quantity of generated power from renewable energy resources (Zhao et al., 2012).

1.2 Renewable energy

In the global energy markets, renewable energy resources have been facing an increasing growing attention recently (Jha, 2011). Renewable energy has gone mainstream, accounting for the majority of capacity additions in power generation today. It provides access to clean, secure, reliable and affordable energy therefore many countries can meet their sustainable development goals with renewable energy (International Renewable Energy Agency, 2012). However, there are some disadvantages associated with the use of these renewable energy sources for example; there is high initial investment cost and dangerous radiation effects associated with nuclear power generation, while solar energy-based power is not available during nights or in heavily clouded environments. Wind turbines technology is the most attractive

renewable energy source which generates large amounts of electrical energy at lower cost and inflicts no adverse environmental impacts (Jha, 2011). Wind energy is currently viewed as one of the most significant, fastest growing commonly used, cost effective and commercially attractive source of energy (Mostafaeipour, 2011). The competitive cost of generation of electricity from wind energy system with fossil fuel has encouraged many countries around the world to pay a greater attention during the past few years toward using wind energy systems with USA, Germany, China and India being the most successful countries in order of installed wind turbines in recent years.

1.3 Wind energy

The generation clean energy is very important in every aspect of energy consumption (Sahin, 2005). The energy that is captured from the wind can help to reduce the dependence on fossil fuel, and it is a pollution-free resource (Raymond & Winchester, 2010). Wind represents a mainstream energy source of new power generation and it is duly acknowledged as a leading technology due to its technical maturity and speed of deployment (Wei, 2010). Wind energy is globally recognized as one of the world fastest growing technology among other renewable energy sources with more than 26% annual growth rate since 1990 (Gipe, 2004; Mostafaeipour, 2011). In developed, and developing countries, wind energy is already making a significant contribution to emissions reduction. Under a new 2020 climate agreement, a substantial savings of CO_2 could be achieved since wind energy alone could contribute a very large portion of the emissions reductions under the pledges put forward so far (GWEC, 2014).

1.3.1 Global wind energy

The growing concerns on future global energy demand and environmental pollution (Saidur et al., 2011), has necessitated an urgent need for clean, and sustainable indigenous power sources for economic growth through Africa, Asia and Latin America

which is increasingly being met through wind power (Global Wind Report, 2014). Considered as a clean source of renewable energy, wind energy is fast growing and gaining acceptance worldwide (Lawan et al., 2014). The Global installed cumulative capacity of wind energy increased rapidly from only 6 GW in 1996 to 487 GW of installed capacity in 2016 Figure 1.1 (Ren 21, 2014, Ren 21, 2017).

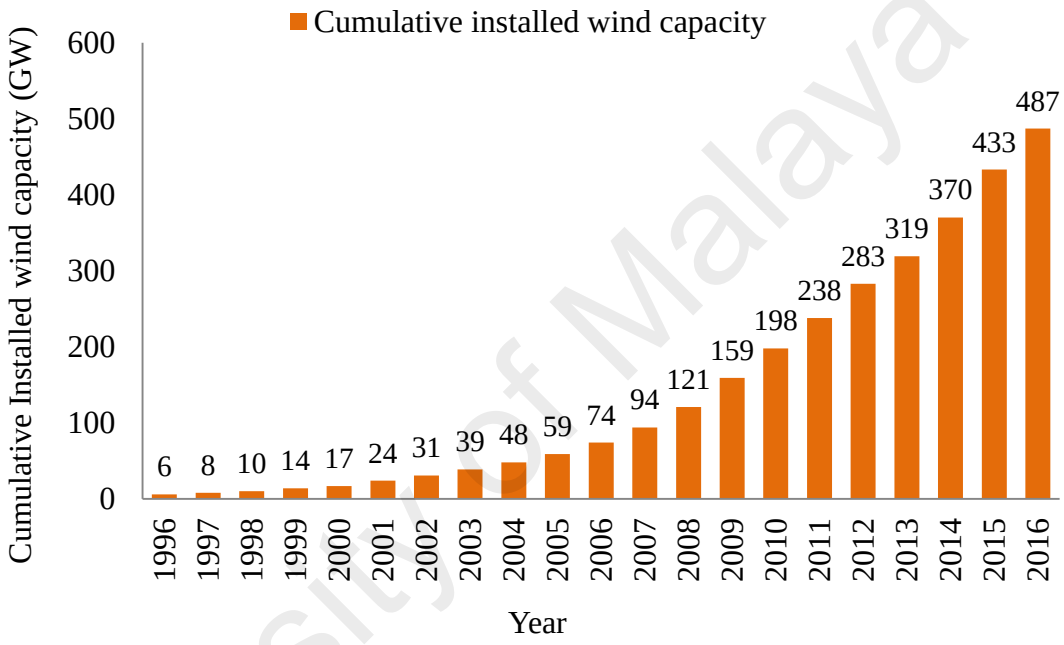

Figure 1.1: Global cumulative installed wind capacity 1996-2016 (Ren 21, 2014, Ren 21, 2017)

Wind turbines have been installed in at least 83 countries (ESMAP/WB, 2011.). However, developed countries like Germany, Australia, Denmark etc. accounts for the largest share of electricity supply by wind as shown in Figure 1.2

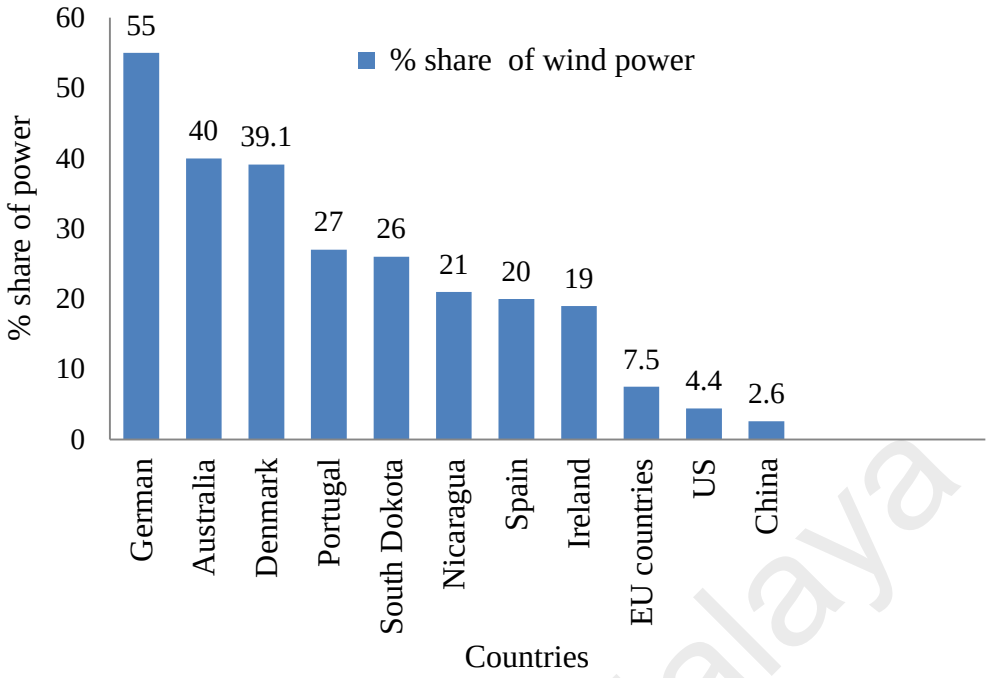

Figure 1.2: Share of electricity supply by wind power 2014 (Ren 21, 2014 a)

While countries like the China, United State, and Germany account for the highest cumulative installed wind capacity with the china topping the list as shown in Figure 1.3.

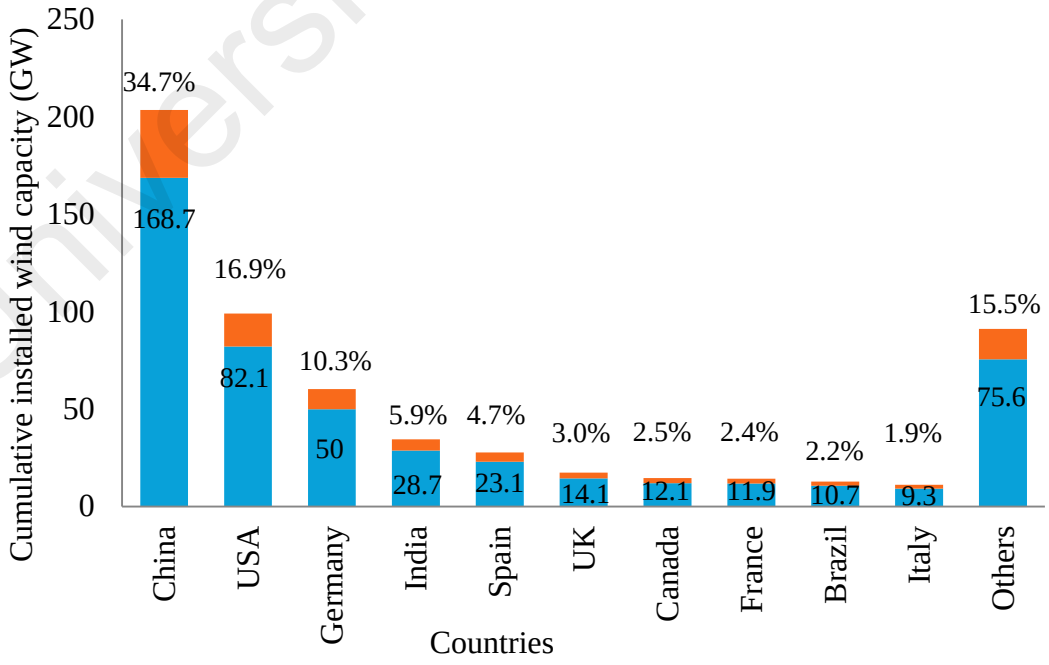

Figure 1.3: Top 10 countries with cumulative installed wind capacity, 2016 (Ren. 21, 2014)

However, despite the high growth rates of wind energy in recent years, its contribution is very small, accounting for only 2-3% of the global electricity supply (Ren 21, 2012). The economic potential of wind energy depends upon factors such as average wind speed, statistical wind speed distribution, turbulence intensities and the cost of wind turbine systems (Joselin Herbert et al., 2007).

1.4 Energy status in Malaysia

Malaysia's energy sources primarily comprise of oil, natural gas, hydro power, coal, and renewable energy source which are currently being exploited (Poh & Kong, 2002). Malaysian energy sector was highly dependent only on a single source of energy which is crude oil (Mohamed & Lee, 2006). Oil contributes about 87.7% in the Malaysia energy mix before the four-fuel diversification strategy was implemented in 1981, after the two occurrences of international oil crises (Oh et al., 2010). For the past 60 years, quite a number of energy-related policies have been formulated by the Malaysian government to ensure sustainability, security and environmentally friendly energy supply (Islam et al., 2009; Haslenda & Ho, 2011). The five-fuel diversification strategy energy mix was adopted by Malaysian government in 1999, with the five main energy sources like oil, natural gas, coal, hydro and renewable energy. Renewable energy is the fifth-fuel strategy which was introduced to promote its usage due to the rising global concern of climate change. It is targeted to contribute 5% of the total energy mix (Haslenda & Ho, 2011). Many countries recognized that the existing energy trends are not sustainable; therefore there is need to have a better balance between security of energy, environmental protection, and economic development of which Malaysia is not an exception. To achieve these, renewable energy is the solution and one of these renewable energy sources is wind energy (Sitti et al., 2011). The growth of wind power is as a result of its competitive pricing, and energy security (Global Wind Report, 2014).

1.5 Problem statement

Building integrated wind turbine represents the future outlook of wind energy generation in the urban environment. Mounting wind turbine on the rooftop of urban buildings is considered as one of the potentially low-cost renewable sources of energy. Low wind speed, high level of turbulence and aerodynamic noise has limited the number of installations of wind turbines on the building despite their great potential (Ledo et al. 2011, Kosasih, & Cooper, 2011). Another problem that hinders the installation of wind turbines in the urban environment is the design type or category of the wind turbine. At present, two main categories of wind turbines have been used for electricity generation in the urban environment; the horizontal axis wind turbines (HAWTs) and the vertical axis wind turbines (VAWTs). Both turbines have their merits and demerits.

The HAWT very effective in generating electricity from the wind (suitable for open plains), and is capable to self-start at low wind speed. However, the HAWT has some disadvantages which includes; accepting wind only in one direction therefore, it needs a yaw mechanism to rotate the turbine in the direction of the wind. It has a high cost of maintenance and repairs because the transmission and electrical generation equipment are placed at the hub. Furthermore, it is dangerous to surrounding and has a high noise level therefore; it is not suitable for the urban environment.

Owing to these disadvantages of the HAWT, the VAWT has attracted a lot of attention recently, in comparison to the HAWT. The VAWT is omni-directional, and hence averts the need for a yawing mechanism. It has ease of maintenance and repairs because the transmission and electrical generation equipment are placed at the ground level, and it generates power at low wind speed, and The VAWT is smaller in size, lighter in weight and generates low level of noise therefore; it is more suitable to be installed in the urban environment. However, the problem associated with the VAWT is

that it cannot self-start at low wind speed; this is considered as one of its main set-backs. (Kentfield, 1996, Ackermann & Soder, 2000, Hyun et al 2012, Johnson & Manhatta 2001). To overcome this challenges, many researchers have proposed the idea of integrating the H-Darrieus VAWT systems onto the urban buildings to take advantage of the increase wind speed in the urban environment, these systems features either additional augmentation system (Chong et al. 2013) or by using the geometry of the building or retrofitted onto the building (Mertens 2003, Sharpe & Proven, 2010, Ledo et al. 2011, Bianchini et al. 2012).

Another problem that affects the H-Darrieus VAWT is the supporting struts. The supporting struts of the H-Darrieus VAWT generate parasitic drag that reduces the net power output (Islam et al. 2008, Ramkissoon & Manohar, 2013). Although, the prospects of harnessing wind energy in urban areas is not very promising owing to low wind speeds and the turbulence caused by surrounding obstacles. The challenges can be overcome through an improved design of wind turbine that is operational under dual wind direction and can self-start at low wind speed.

To overcome the disadvantages of both the HAWT and VAWT in the urban environment, a novel wind turbine known as the cross axis wind turbine (CAWT) is designed and tested. The CAWT which function with airflow coming from both the horizontal and vertical direction is integrated onto the building rooftop to take advantage of the increase wind speed at the top of the roof. The effect of the roof shape creates a skew flow condition at the rooftop which was utilized by the CAWT to enhance the self-starting capability and improve its overall performance. The skewed wind at the rooftop modify the region of interaction of the downwind blade passage with the upwind generated wake therefore allowing the downwind blade to experience an undisturbed flow with larger energy content The “roof effect” on the gable roof gives higher skewed angle which increase the area of interaction of the downwind blade

passage and improve the efficiency of the CAWT on the gable rooftop. The new type of wind turbine can utilize the merits of both the HAWT and VAWT while overcoming their respective demerits.

1.6 Research objectives

This thesis presents a novel design of building integrated CAWT in order to overcome the disadvantages of both the HAWT and the VAWT in the urban environment while utilizing their advantages to improve the self-starting behavior and overall performance. The objectives of this research are;

i) To develop, design, fabricate and test a novel building integrated cross axis wind turbine

ii) To evaluate and compare the efficiency between the cross axis wind turbine and the conventional vertical axis wind turbine

iii) To investigate the effect of roof shapes on the performance of cross axis Wind turbine and analyze the flow Field on gable and vaulted roof shapes of the Building

vi) To analytically predict the performance of the building integrated cross axis wind turbine using double multiple stream tube and blade element Momentum model

v) To predict the performance of power augmented vertical axis wind turbine using soft computing methodology

1.7 Thesis outline

In this thesis the design and testing of a novel building integrated cross axis wind turbine is presented. The thesis structure is as follows;

Chapter 1 contains the introductory parts detailing the background of related study regarding energy, renewable energy such as wind energy system and global wind energy. This is followed by the energy status in Malaysia. Furthermore, the problem statement, the objectives of the research and the thesis outlines is also shown in this chapter.

Chapter 2 covers the literature review of wind turbines and the related studies including but not limited to the evolution of researches in wind turbines. The review also covers the different types of wind turbine design and their historical development and investigation of a number of existing state-of-the-art of wind turbine. In this chapter, the various models developed for the performance prediction of the wind turbines (HAWT and VAWT) were discussed, these include the double multiple streamtube (DMST) and the blade element momentum (BEM). Where needed; additional investigations were carried out in order to establish a thorough understanding of the performance and challenge to be faced.

Chapter 3 contains a detail description of wind energy in the urban environment, these includes; the building integrated wind turbines technologies including architectural integrations, aesthetics functional demands, technical and economic issues.

Chapter 4 described the methodology used in this study. This includes design description and methodology. This stage involved the development of the conceptual design, building and experimental testing of the developed models. Designing and fabricating the rotor blades models and the test rig. In this stage, the functional components and mechanism were discussed. The selection procedure of airfoil section and rotor blade decision was performed based on the information from the literature review. The procedure for the double multiple streamtube and the blade element momentum analysis used to predict the performance of the turbine is also explained in

this chapter. Furthermore, the computational fluid dynamic simulation conducted on the building models and the application of soft computing methodology on the performance investigation of wind turbine were also discussed.

Chapter 5 comprises of the results and discussions. The experimental result includes power coefficients, rotational speed and the start-up behavior of the CAWT and the VAWT configurations. The effect of the pitch angles of the horizontal blades of the CAWT, and the effect of roof shapes on the performance of CAWT were discussed in this chapter. The Variation of the heights of the CAWT and the VAWT above the rooftop of the building models (gable and vaulted roof shapes), and the comparison of the Performance of the CAWT on the gable and vaulted rooftops were also discussed. The result of the computational fluid dynamics simulations (cfd) performed on the two roof shapes was analyzed. The analytical results obtained from the combined method of the double multiple streamtube (DMST) and blade element momentum (BEM) method were also discussed. Moreover, the performance prediction of the power augmented VAWT using soft computing methodology (Adoptive neuro-fuzzy inference system), ANFIS was discussed in this chapter.

Chapter 6 contains the conclusion and recommendation. All the major findings from the study (both from experimental, analytical, CFD simulation and soft computing approach) are summarized in this chapter.

CHAPTER 2: LITERATURE REVIEW

A wind turbine is a device that exploits the wind's kinetic energy by converting it into useful mechanical energy. It basically consists of rotating aerodynamically surface (blades) mounted on a hub/shaft assembly, which transmit the produced mechanical power to the selected energy utilizer (Maalawi, 2011). Although the genesis of wind turbine are lost in antiquity, but its existence as a provider of useful mechanical power for the last thousand years has been authoritatively established (Shepherd, 2009). The utilization of wind energy can be traced back thousands of years to many ancient civilizations. The human history has revealed that wind energy was discovered and used independently at several sites of the earth (Wei, 2010).

2.1 Historical development of windmills with vertical axis

The first reliable information about the existence of windmills from historical sources originates from the year 644 A.D from the Persian (present Iran) and Afghan border region of Seistan (Hau, 2006). There are written evidence that the first accepted establishment of the use of windmills was in the tenth century in Persia. It is documented by reliable writers and reinforce by ancient drawings that correspond to the remains of old mills and to modern ones still in used in 1963 (Dennis, 2009). The remains of these wind mills that were running for centuries can be found in Iran and Afghanistan, Figure 2.1. The world's oldest windmills had a vertical axis of rotation, and braided mats were attached to the axis. The mats caused drag forces and, therefore, were taken along with the wind as shown in Figure 2.2a. In Persian windmills, an asymmetry was created by screening half the rotor with a wall. This way the drag forces could be utilized for driving the rotor (Gasch & Twele, 2012).

Figure 2.1: An existing windmill of the Persian type in Neh (Dennis, 2009)

The Chines windmills which is also dated back a long time as similar asymmetry is created by sails which rotate out of the wind on their way back, i.e. when they advance into the wind. these chinese drag wheels dated back to approximately 1000 AD. Just as the Persian mills, the chinese windmills had a vertical axis and used braided mats as sails, Figure 2.2b. However, in constrast to the Persian mills, they had the typical advantage of vertical axis windmills to utilised the wind independent of its directions

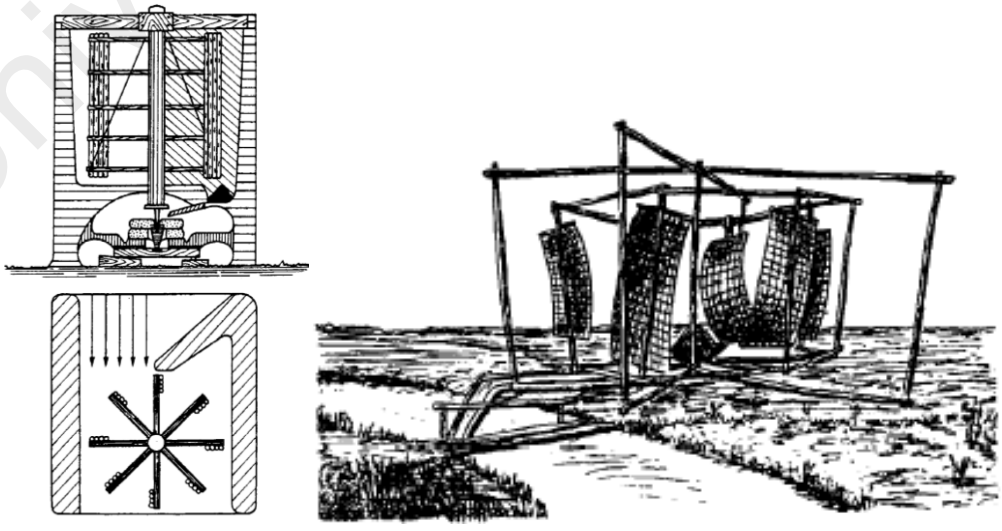

(a) **(b)**

Figure 2.2: (a) Persian wind mill, (b) Chines windmill (Simiu et al., 2011; Gasch & Twele, 2012)

2.2 Historical development of windmills with horizontal axis

The first recorded appearance of windmills was in the 12th century in northern Europe (England). The appearance of this windmills are noticeably different to the Persian windmills (Manwell et al., 2009). These early windmills had horizontal axes, the shaft carrying the sails was oriented horizontally rather than vertically as in the Persian mill, and in a relatively short time, tens of thousands of what is call horizontal-axis European windmills were in use for a variety of duties (Dennis, 2009). Figure 2.3 shows the early mills which of four blades, they were used for pumping of water, and grinding of grains (Manwell et al., 2009).

Figure 2.3: European post windmill (Mathew, 2006)

2.2.1 Wind power

The first experiment to generate electricity with wind mill began at the end of the eighteen century (1890) in Denmark using a 23 m diameter wind turbine, and by 1910, several hundred units with capacities of 5 to 25KW were in operation in Denmark

(Johnson, 2001). With the evolution of mechanical insight and technology, the last decades of the 20th century, in particular, saw the development of machines which efficiently extract power from the wind (DNV/Riso., 2002).

Today large wind power plant are competing with economic utilities in supplying economical clean power in many parts of the world, it stands out to be one of the most promising new sources of electrical power in the near term with many countries promoting the wind-power technology by national programs and market incentives (Mukund, 1999). Due to modem technological developments remarkable advances in aerodynamics, structural dynamics, and micrometeorology have been achieved since 1980, and have contributed up to 5% annual increase in energy yield of the turbines. Currently, research techniques are producing stronger, lighter, and more efficient blades for the turbines; this improvement increases the annual energy output enormously and reduces the weights and noise by half over the last few years (Joselin Herbert et al., 2007).

2.3 Modern wind turbine systems

Wind turbine technology has a unique technical identity and demands in terms of the methods used for its design (Joselin Herbert et al., 2007). It is has the capability to generate larger amounts of electrical energy with zero greenhouse effects compared to other energy generating schemes including Solar cell, tidal wave, biofuel, hydrogen, biodiesel and biomass technology (Jha, 2011).

2.3.1 Classification of wind turbines

The significant improvement in the operating efficiencies of wind power systems makes them more economically competitive to other energy generation techniques (Pope et al., 2010). At present, two main categories of wind turbines have been used for electricity generation based on the axis about which the wind turbines rotate; the

horizontal axis wind turbines (HAWTs) and the vertical axis wind turbines (VAWTs) (Islam et al., 2008; Wang et al., 2016).

2.3.1.1 Horizontal axis wind turbine

The horizontal axis wind turbine (HAWT) is a lift-type turbine which consists of airfoil sections that capture the wind energy in the form of a lift force. This lift force produces torque on a shaft, which can then be connected to a generator to produce electricity as power output (Mohammed, 2013). HAWT has emerged as the dominant wind energy technology, it is effective in generating electricity, can achieve higher energy efficiencies and can self-start at low wind speed (Pope et al., 2010). HAWT are further classified according to their number of blades these includes; single bladed, double bladed, three bladed and multi bladed wind turbines, Figure 2.4. Due to savings on blade materials, the single bladed wind turbines are cheaper, but a counter weight has to be placed opposite to the hub to balance the blade. The two bladed and the multi-bladed wind turbines also have some draw backs but to a lesser amount when compared with the single bladed turbine. The three bladed turbines are accepted generally because of the advantages it offers when compared to the single, and two bladed wind turbines. Presently most of the commercial wind turbines are the three bladed wind turbines (Mathew, 2006).

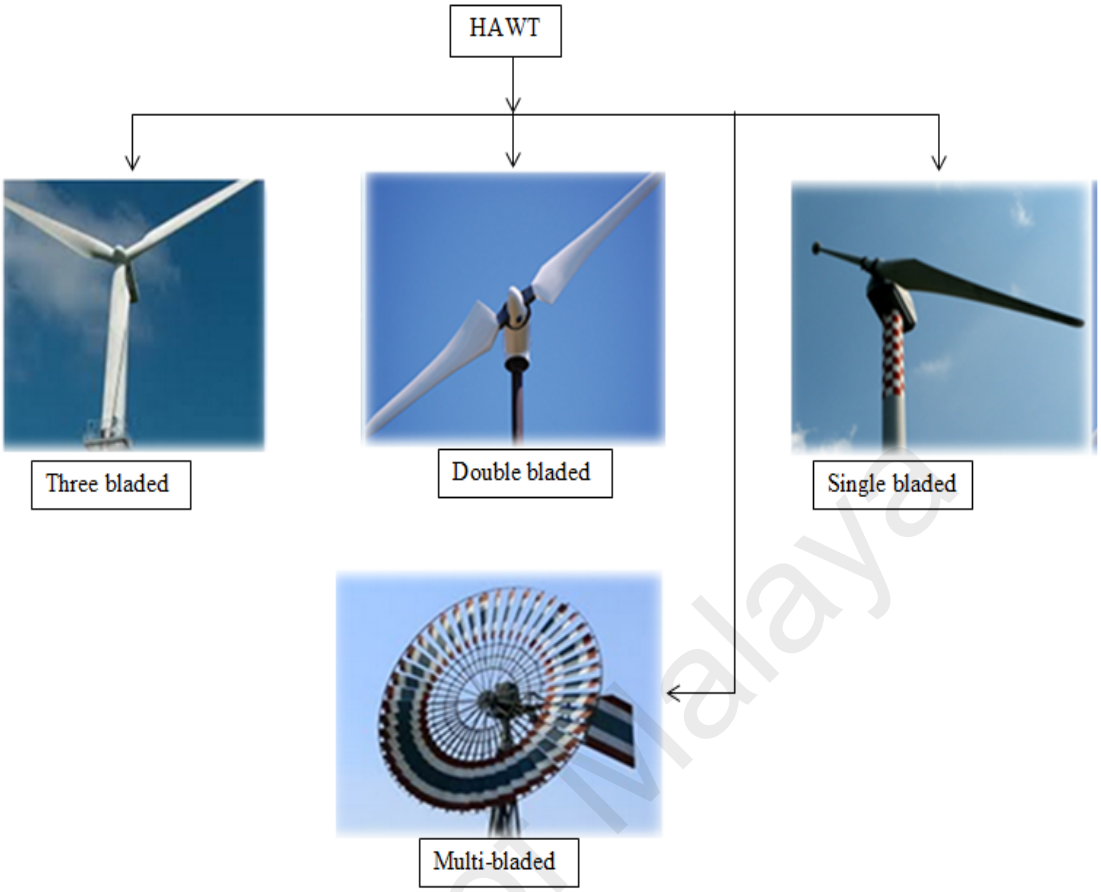

Figure 2.4: Classification of horizontal axis wind turbine

The HAWT can be further categorized into upwind and downwind turbine; the rotor of the upwind turbine is directly facing the wind, to keep the rotor continually confronting the wind, a yaw mechanism is essential for these designs. The downwind machines may not require a yaw mechanism because they are more flexible but rather they might be uneven stacking on the blades as it goes through the shadow of the tower when the rotor are put at the lee side of the tower (Mathew, 2006). The disadvantages of the HAWT are that it accept wind only in one direction, and thus requires a yaw mechanism to direct the turbine into the wind direction. It also has a high cost of maintenance and repairs due to the tower structure, and the placement of the transmission and electrical generation equipment at the hub (Pope et al., 2010). It is larger in size, heavier in weight, and generates high level of noise therefore; it is not suitable for the urban environment (Nils et al., 2000).

2.3.1.2 Vertical axis wind turbine

The vertical axis wind turbines (VAWT) have attracted a lot of attention recently due to the disadvantages of HAWT especially in the urban environment. The VAWT is omni-directional and hence averts the need for a yawing mechanism. The transmission and electrical generation equipment can be located at the ground level, making the installation, operation and maintenance much easier, It is smaller, lighter and safer hence it is more suitable for the urban environment. The VAWT operates with any horizontal wind directions, Figure 2.5 (Hau, 2006).

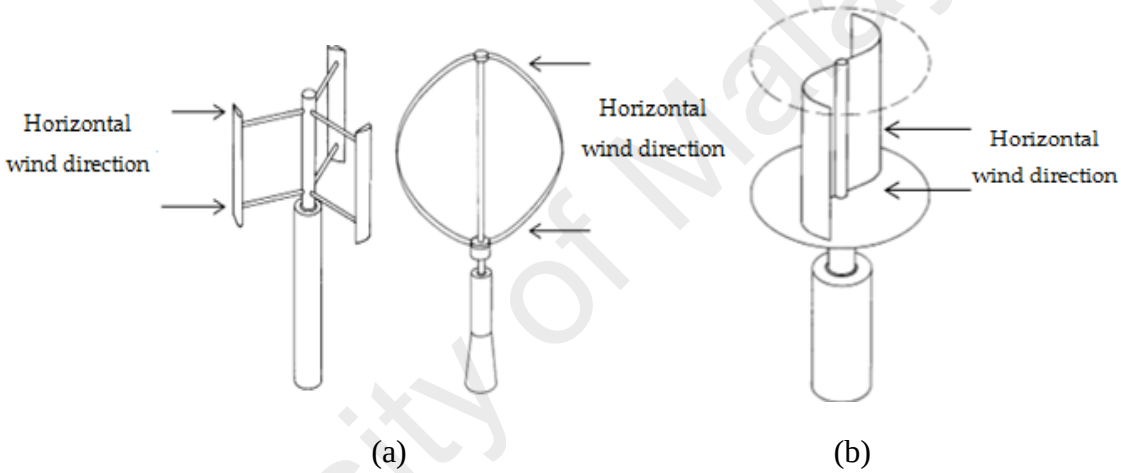

(a) (b)

Figure 2.5: VAWT operating under any horizontal wind direction (Hau, 2006), (a) Darrieus rotor; (b) Savonius rotor

The VAWT is further subdivided into the lift type (Darrieus rotors), the drag type (Savonius rotor), and the hybrid VAWT (combination of both the lift and drag type turbine).

(a) ***Darrieus rotors***

The Darrieus rotors are lift-type turbines which captures the wind energy in the form of a lift force (Mohammed, 2013). The Darrieus rotors are further subdivided into H-rotor and egg beater turbines Figure 2.6a.

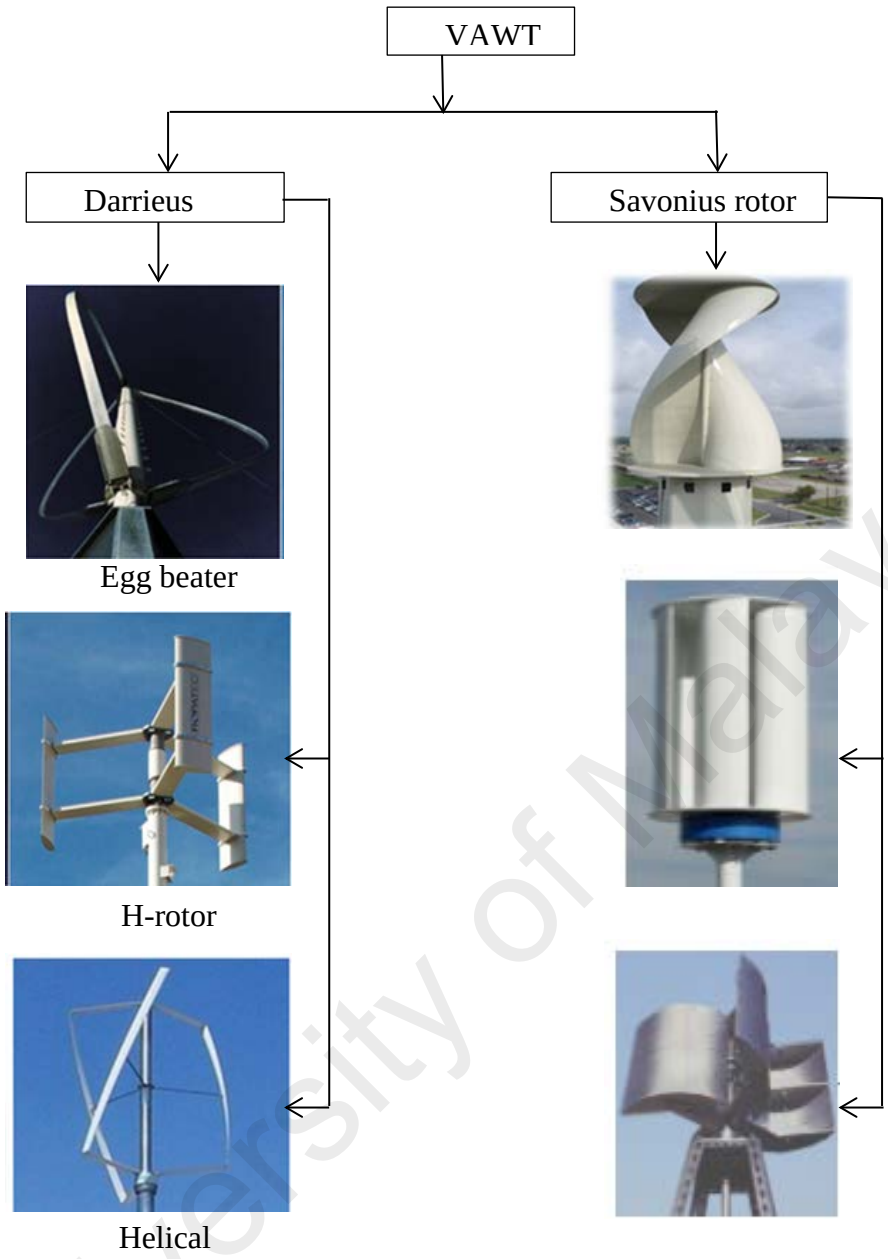

Figure 2.6: Rotor configuration of vertical axis wind turbine (a) Darrieus rotor, (b) Savonius rotor (Ragheb, 2015)

The H-rotor has H' shaped blades and a central shaft, while the Darrieus rotor egg-beater, have its blades shaped like egg beaters or troposkein, the bending stress experienced by the blades is minimize by the blade configuration. Usually the Darrieus rotors are effective for wind electric generators due to the fact that it works at high tip speed ratio, but its disadvantage lies on the fact that they don't the capability to self-start, therefore, needs an external excitation (Hau, 2006).

(b) ***Savonius rotor***

The Savonius rotor is a drag-based wind turbine which produces mechanical power using the drag force to (Mohammed, 2013). It consists of two hollow half cylinders displaced so that both the convex face and concave face are facing the wind. The torque for most but not all wind direction is produce by the difference in drag on the two sides, Figure 2.6 b (Kirke, 1998). At low tip speed ratio, the Savonius rotor produces large amount of torque due to the large surface area facing the wind. The disadvantage of the Savonius rotor is that the same drag of the advancing blades which is used to produce power can also reduce the peak amount of power that can be obtained since the returning blades work against the turbine (Mohammed, 2013). To ensure self-starting at least two rotors are placed at two directions. The drawback of this type of turbine is its low efficiency despite the fact that it is easy to build, it has an efficiency of < 25%, it has excessive weight and its inability to turn into the wind direction makes it of disadvantage (Kirke, 1998).

Saha & Rajkumar (2006) investigated the feasibility of twisted bladed Savonius rotor for power generation in a low wind speed tunnel, and compared its performance with a conventional semicircular blade with twist angle of 0^{o}. The results obtained showed that the twisted bladed rotor has great potential in terms self-starting, capability, and higher efficiency compared to the conventional semicircular bladed rotor. Arifin et al (2017) reported that the performance of a Savonius rotor can be improved by combining a conventional blade with an elliptical blade into a combined blade rotor. Similar studies on the Savonius rotor are reported in (Kamoji et al., 2009; Guta et al. 2013, Menet, 2004).

2.4 Hybrid vertical axis wind turbine

A hybrid turbine consists of the combination of common VAWT rotors for optimal performance. The Savonius rotor can self-start at low wind speeds, and creates high torque, but it is relatively low in terms of efficiency. The Darrieus rotors have much higher efficiency than the Savonius rotor but they cannot self-start. Therefore, the combination of these two rotors increases the total power of the turbine in lower wind speeds, Figure 2.7.

The Savonius rotor is used to self-start either the straight bladed or egg-beater Darrieus rotor. Hybrid VAWT has better self-starting capabilities and conversion efficiency. This design combines the Advantages of both Savonius and Darrieus rotor while attempting to reduce their various disadvantages (Letcher, 2010).

Figure 2.7: Hybrid VAWT (Letcher, 2010)

Many studies have been reported for the improvement of the self-starting ability and efficiencies of vertical axis wind turbine. Letcher (2010), reported that the combination of rotors (Savonius rotor and straight bladed Darrieus rotors) increases the performance of the turbine at low wind speeds. Alam & Iqbal (2009), presented a study on hybrid vertical axis turbine (a straight bladed Darrieus rotor and Savonius rotor) on the same

shaft to be operated on water, the results indicates that the hybrid VAWT is capable to self-start by itself and has better efficiency at higher flow speed.

2.5 Benchmarking study of Darrieus Vertical Axis Wind Turbine

This section describes the benchmarking study of Darrieus vertical axis wind turbines. This study shall set a basis from which the design in the current work can develop its improvements beyond the state of the art.

The Darrieus vertical axis wind turbine is a lift based wind turbine that is distinguished by its simplicity and relative low manufacturing cost. The VAWT potentially performs better in the urban environment despite the continuous change in direction of the wind flow. However, Darrieus VAWT difficulty to self-start which may affects its overall performance (Qing'an et al. 2016; Kentfield, 1996; Ackermann & Soder, 2000; Hyun et al., 2012; Hau 2006). To overcome this challenges, many researchers have proposed the idea of integrating the H-Darrieus VAWT systems onto the urban buildings to take advantage of the increase wind speed in the urban environment, these systems features either additional augmentation system (Chong et al. 2013, Bailey & Jonh, 2010, Valsamides 1995) or by using the building geometry or retrofitted onto the building (Mertens 2003, Merten 2006, Sharpe & Proven, 2010, Ledo et al. 2011, Bianchini et al. 2012).

Many studies have been conducted on the Darrieus type VAWT in an attempt to improve the performance of the VAWT (Manabu et al., 2009; Robert et al., 2010; Aslam Bhutta et al., 2012; Nilesh & Shiekh, 2014; Siddiqui et al., 2015). Although Darrieus wind turbine was previously known for difficulty in self-starting, recent studies have shown that these wind turbines can self-start under certain conditions. Dominy et al. (2007) and Hill et al. (2009) demonstrated that it is possible to have a self-start three-bladed H-rotor VAWT using a fixed geometry and symmetrical airfoils.

Bianchini et al. (2011) uses a numerical code to evaluate the transient behavior of H-Darrieus turbines under generic wind conditions in terms of velocity and direction. The influence of the airfoil type and the blade shape on the startup capabilities of the rotor as a function of the initial position of the rotor and the oncoming wind velocity was also investigated. Dominy et al. (2006) asserted that under steady wind condition a lightly loaded, three-bladed rotor has the potential to self-start. Similar studies on the self-starting ability of VAWTs are reported by (Barker, 1983; Batista et al., 2015; Worasinchai et al., 2015 & Kirke 1998).

Cantwell & Amargosa (2014) filed a patent on a low wind vertical axis dual stage wind turbine power generator that comprises of a structural support tower, with four turbine assemblies stacked on top of one another within individual turbine bays. Bailey et al., (2010) showed the concept of shrouded vertical axis dual-turbine generator; it comprises of a structure in the shape of a double airplane wings symmetrical foil, having a vertical axis turbine set into each camber at each side of the foil. Other patent filed on the improved performance of VAWT includes (Valsamidis, 1995; Donald, 1999; Joe, 2008; Hanjun et al., 2012; Joo-soo & Busan, 2013).

Researchers also conduct study on how the design parameters affect the performance of the VAWT. Islam et al. (2008) reported that proper selection of design parameters are important for a cost-effective smaller capacity SB-VAWT which can be considered as a candidate for urban, and off-grid rural applications. In an attempt to improve the performance of straight-bladed VAWT, Islam et al. (2007) designed a special purpose airfoil “MI-VAWT” for smaller capacity straight-bladed VAWT, results obtained from the study indicates that the performance of the special purpose airfoil is greater to that of LS-0417 at low Reynold number and comparable with NACA 0015 at medium Reynold number. The effect of wind velocity was studied by (Song et al., 2003; Li et

al., 2014; Islam et al 2008; Li et al., 2016) they found out from the study that the power performance of VAWT was better at the same tip speed ratio, when the wind velocity was higher. El-Samanoudy et al. (2010) studied the effect of the design parameters such as radius, airfoil, and chord length in an attempt to determine the optimum variation, the results obtained indicates that when the radius of the turbine is decrease, the performance was decreased greatly. Brusca et al., (2014) investigated how the aspect ratio affect the performance of the VAWTs, the results showed that as the aspect ratio fall, the Reynold number increases which in turn increases the performance of the VAWT.

A novel omni-direction guide vane (ODGV) that surrounds a VAWT is presented by Chong et al. (2013), the ODGV improved the performance of the VAWT by increasing the wind speed before interacting with the VAWT. Muller et al. (2009) presented the design of vertical axis resistance wind turbine for used in building; results obtained showed that the design improvements can lead to an increase of the theoretical efficiency by 48% (conservative), or 61% (optimistic).

The primary reason for the extensive literature on the design, and development of existing system of the VAWTs is to establish performance benchmarks that can be used as the boundaries or constraints in the design and development of the novel building integrated wind turbine in this current work. The state of the art" on the vertical axis wind turbine has been established in order to set criteria for the evaluation and development of the new wind turbine in the current work.

2.6 Latest Development of Darrieus Vertical Axis Wind Turbine

Recently, many new design of wind turbine has been explored by many researchers with the aim of improving the performance and versatility of the Darrieus vertical axis wind turbines. Current research techniques used now a day are producing stronger,

lighter, and more efficient blades for the turbines. The vertical axis wind turbine system has become an object of intense research and development due to recent development of the technology sector. This can be achieved through the integration of new technologies such as magnetic levitation rotors to reduce friction, the introduction of innovative production processes such as 3D printing, up to completely new and futuristic technological approaches (Casini, 2016).

2.6.1 Recent Design of Darrieus Vertical Axis Wind Turbines

Wind turbine researchers and innovators have developed several new technology of Darrieus VAWT. Among the new ideas are vertical axis turbine airborne unit (D' Ambrosio, 2010), which is mounted at 300-500 m above the ground level. A Recent developed technology (Allaie & Andreopoulos, 2014, Allaie et al., 2015), INVELOX, Figure 2.8 has shown promising performance. While conventional wind turbines use massive turbine-generator systems mounted on top of a tower, INVELOX by contrast, funnel wind energy to ground-based generators. The INVELOX technology captures wind with a funnel and directs it through a tapering passageway that passively and naturally accelerates its flow which drives a generator that is economically installed safely at ground levels (Allaei et al. 2015).

Figure 2.8: INVELOX wind turbine (Allaie & Andreopoulos, 2014, Allaie et al., 2015)

A funnel based wind energy harvesting system (FBWEHS) was design and tested by Kumar et al. (2015). The FBWEHS has a nested funnel structure which is used for capturing the wind because it has the ability to capture wind from all directions and the funnel is design to enhance for smooth flow of wind into the duct by designing opening of funnel with best suitable angle. van de Wiel (2015) design and developed a high solidity Tulip-shaped vertical axis wind turbine for low visual impact and cost efficient system in suburban environments. Boatner (2010) developed a Blackhawk wind turbine which has a passively controlled rotor that automatically adjusts the tilt of its vertical blades for a better angle of attack. The horizontal component of the oncoming wind interacts with the vertical blade, and in turn, the mechanical system of the turbine tilts the vertical blades accordingly.

IMPLUX, Figure 2.9 is another novel wind turbine design by Sureshan, (2008). The design is an omni-directional device which consists of a shroud that captures wind from any direction and directing it to flow vertically through a throat section where an airfoil multi-bladed rotor is mounted.

Figure 2.9: IMPLUX wind turbines, (Sureshan 2008)

Gorlov (1998) patented the design for helically twisted turbine blades for use in flowing water. The Gorlov helical turbines (GHT) are a water turbine evolved from the Darrieus turbine design by altering it to have helical blade/foils. The concept of helical vertical axis wind turbine was introduced by Song et al. The helical VAWT consists of 3 blades comprising of a main wind blade with tow blades as connecting arms, which was supported by the hubs in the center (Song et al., 2012).

Aerotecture developed another novel wind turbine known as Aeroturbines, Figure 2.10. The Aeroturbines can be mounted horizontally, essentially becoming HAWT. The Aeroturbines takes advantage of the prevailing winds from North-East and from South-South West without breaking the strick local height limits for building, which would have prevented the traditional vertical mounting (Casini, 2016, Jahn, 2007).

Figure 2.10: (a) Aerotechure turbines on Mercy housing Lakefront rooftop-Chicago (Casini, 2016, Jahn, 2007)

Hara et al. (2014) introduced the idea of a double-blade wind turbine Figure 2.11 (a) which was designed to improve the self-starting behavior of the turbine by using

additional blades with reduced radius to the current blades. This idea was later transformed into a butterfly wind turbine (BWT), Figure 2.11 (b) which consists of closed-loop blades (Hara et al. 2014), The BWT has a better self-starting capability, and high efficiency.

(a) (b)

Figure 2.11: (a) Double-blade vertical axis wind turbine, (b) butterfly wind turbine (Hara et al. 2014)

Qu et al. (2012) envisages a novel Darrieus straight bladed VAWT with added feature, this added features includes the ability of the blades to open and close along its length via a hinge. The authors concluded that the turbine has greater starting capability than a rigid bladed Darrieus rotor with a similar design. Hwang et al. (2006) improves the efficiency of four bladed VAWT rotors by employing a control strategy which utilizes a small micro-controller, several sensors and motors, 30% more power is generated using this method compared to a fixed blade approach.

Takao et al. (2009) experimentally investigate the effect of various arc plates configuration used as guide vanes with vane configurations using 1, 2, 3, and 4,to determine an optimum spacing of vanes. It was found that the power and the torque coefficients were independent of the number of guide vanes used.

Based on exiting literature, VAWT has shown to have improved performance with innovative designs skewed flow conditions, and even performs better compared to the HAWT. However, there is no Darrieus type VAWT designed to specifically extract wind energy by utilizing the vertical and horizontal component of the wind. The main aspect of this work is to provide insight into the development of a new type of building integrated cross axis wind turbine that can function with those two components of wind flow and at the same time improve the energy output of the wind rotor. The CAWT which consists of vertical and horizontal blades that are linked through specially designed connectors to provide a larger swept area with robust structural integrity can be integrated at the rooftop of urban building to take advantage of the increase wind speed at the rooftop. The horizontal blades which are also the supporting struts of the CAWT can adequately utilized the skewed wind at the rooftop to improve the self-starting behavior and overall performance of the wind turbine system.

2.7 Wind turbine in skewed flow

The performance of H-Darrieus VAWT in skewed flow can be increase when by the region of interaction of the downwind blade passage with the upwind generated wake is modified. When the skewed angle is increased, the area of the downwind blades passage which is operating outside the upwind generated wake is also increased thus the turbine will experience an incoming flow with larger energy content (Ferreira, 2006). According to Mertens et al. (2003) and Balduzzi et al. (2012) H-Darrieus VAWT produces increase power output in skewed flow. The skewed angle is defined as the angle between the velocity vectors outside the recirculation region. The skewed angle varies with:

- Sizes of the buildings
- Position on the roof

- Upwind edge rounding
- Roughness of the upwind area.

The velocities close to the building are high and decrease with increasing distance to the building. Consequently the pressures close to the building are low and increase with increasing distance to the building. This pressure gradient forces the flow in a curved path. On the curved path, the radius of the curvature is defined as the equilibrium between the force caused by the pressure gradient and the centrifugal caused by the curvature (Simiu & Scanlan, 1996; Mertens, 2006).

The effect of the roughness and size of the building on the skew angle can be understood from the amount of lateral momentum caused by blockage of the building. On the other hand, a high roughness results in a smaller mass-flow towards the building (reduced velocities in the boundary layer for high roughness) compared to a low roughness. This results in less lateral momentum because a smaller mass-flow has to move around the building. For small building sizes, the same augmentation is valid. Therefore, the flow stays closer to the building for high roughness or small building sizes compared to low roughness and large building size (Mertens, 2006).

The H-Darrieus rotor does not suffer from frequent changes in wind directions, therefore the use of the H-Darrieus rotor in buildings seems a favorable proposition (Mertens et al., 2003). Wind turbine in urban buildings operates near, on, and in the wake of bluff bodies larger than the rotor scale and these flow conditions may result in skewed flow operation (Ferreira, 2006).

Many studies have been reported on H-Darrieus wind turbine in skewed flow. Bianchini et al. (2012) reported that an improve model which is based on momentum model was developed in order to predict the H-Darrieus rotor performance under skewed flow conditions. The model was properly modified to account for the variations

induced by the new directions of the flow which invests the rotor. Results from the study indicate that a notable agreement has been constantly obtained between simulations and experiments.

On the other hand, Balduzzi et al. (2012) critically evaluate the suitability of installing a Darrieus VAWT rotor on the rooftop of a building in a reference European city. Using numerical CFD analysis, the flow field characterization in the rooftop area of the buildings with different roof shapes and geometrical proportions were carried out. The results from the study show that notable increments (up to 70%) of the attended capacity factor in the rooftop area of an installation building in the urban environment can be achieved. Further results indicate that the skew angles (15-30^{o}) increase up to 12% of the attended energy harvesting.

The variation in optimal performance of a H-Darrieus VAWT in skewed flow has been studied by Simao-Ferreira et al. (2006), using analytical approach, the variation in thrust, torque, tip speed ratio, and power generated was predicted using the momentum method, a high correlation between experimental and theoretical results can be achieved. Similarly Ferreira (2006) measured the incoming flow and the wake of the VAWT in skewed and non-skewed flow, the results obtained indicates that for the non-skewed flow case the flow in the rotor around the downwind passage of the blade and in the wake, is mainly defined by the upwind passage of the blade.

Mertens et al. (2003) studied the behavior of an H-Darrieus VAWT in skewed flow condition and compared it with a model based on the blade element momentum theory. The results indicate that the H-Darrieus produces an increased power output in skewed flow. Zanforlin & Letizia (2015) investigated the effectiveness of combining the concentration effects generated by a dual-pitched roof and a diffuser-shaped wall

mounted over a Darrieus turbine. The results showed that by integrating the actions of rooftop and diffuser a significant power increasing is obtained in skewed winds.

2.8 Basics of wind energy conversion

The available energy in the wind is mainly the kinetic energy of huge masses of air moving over the surface of the earth which is received by the wind turbine blades and is then transformed to mechanical energy and then to electrical energy. The efficiency of converting wind to other useful energy forms greatly depends on the efficiency with which the rotor interacts with the wind stream (Mathew, 2006).

2.8.1 Theoretical power available in the wind

Wind energy is the kinetic energy of the wind which can be extracted by using wind turbines to produce electric power. The wind kinetic power can be expressed as follows:

$$P_w = \frac{1}{2}\dot{m}U_\infty^2 \tag{2.1}$$

Where $\dot{m}$ is the mass flow rate of air which can be expressed as; $\dot{m} = \rho A U_\infty$

By substituting the mass flow rate in Equation 2.1, the power becomes;

$$\mathrm{P_w} = \frac{1}{2}\rho \mathrm{A} U_\infty^3 \tag{2.2}$$

Where

P is the power available (W)

ρ is the density of air (1.23 kg/m^3)

A is the area (m) and

U_∞ is the wind speed (m/s)

2.8.2 Wind turbine performance parameter

Wind turbine cannot extract completely the power from the wind because when the wind stream passes the turbine, a part of its kinetic energy is transferred to the rotor and the rest are carried away by the air leaving the turbine. Equation 2.2 shows the theoretical power available in the wind (Mathew, 2006). According to the Betz limit, the theoretical maximum power coefficient of any design of wind turbine is 59.3%, this implies that only 59.3% of the kinetic energy of the wind can be converted into mechanical energy turning a rotor. The limited efficiency of a wind turbine is as a result of the power losses in the transmission and electrical system, and the swirl imparted to the air flow by the rotor (Magdi & Adam, 2011).

2.8.2.1 Coefficient of performance of wind turbine

The actual power produced by a wind turbine rotor depends on the efficiency at which the energy is transferred to the wind turbine rotor from the wind. This efficiency is usually called the power coefficient (C_p). The power coefficient of a wind turbine is the ratio of the actual power extracted by the wind turbine rotor to the theoretical power available in the wind. It can be expressed as;

$$C_p = \frac{2P}{\rho A U_\infty^3} \tag{2.3}$$

Where P is the power generated by the turbine.

2.8.2.2 Coefficient of torque

The Coefficient of the torque (C_T) is the ratio between the actual torque produce by the rotor to the theoretical torque. It can be expressed as;

$$C_T = \frac{2T}{\rho A U_\infty^2 R} \tag{2.4}$$

Where T is the actual torque developed by the rotor.

2.8.3 Tip speed ratio (TSR)

Wind turbines are designed to operate at their optimal wind tip speed in order to obtain maximum and optimal rotor efficiency. Wind tip speed ratio TSR, (λ) depends on a particular wind turbine design, the airfoil profile, as well as the number of blades. The TSR, (λ) is the ratio between the velocity of the rotor tip and the wind velocity. The TSR can be expressed as;

$$\text{TSR}, (\lambda) = \frac{\Omega}{U_\infty} = \frac{\omega r}{U_\infty} \tag{2.5}$$

where

r is the radius of the rotor (m);

$\omega = 2\pi f$ *is* the angular velocity (rad/s);

f is the rotational frequency (H_z).

The C_p varies with the TSR, (λ). The C_p values increases with increase in λ the C_p reaches its maximum at a certain λ and then decreases with increase in λ. For a given rotor, there is an optimum λ at which the transfer of energy is most efficient and thus the coefficient of power is maximum, $C_{p,max}$ (Ragheb, 2014). The performance of a wind turbine rotor is usually characterized by the variations in its power with the tip speed ratio. Figure 2.12 shows the Cp-λ curve for different rotor performance irrespective of size and site parameters as both the parameters are dimensionless.

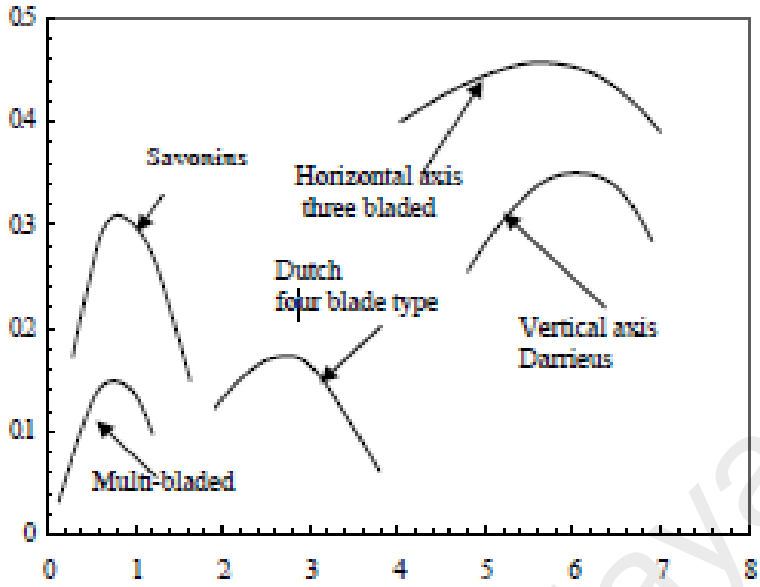

Figure 2.12: Performance characteristics of wind turbine rotors (Hau, 2006; Mathew, 2006)

2.9 Aerodynamics of wind turbine

The aerodynamic and dynamic properties of a wind turbine rotor have a decisive influence on the entire wind turbine systems (Hau, 2006). The mean wind generated the aerodynamic forces which determine the major aspect of a wind turbine performance (Manwell et al., 2009). The capability of the rotor to convert a maximum proportion of the wind energy flowing through its swept area into mechanical energy is the direct result of its aerodynamic properties. These aerodynamic properties largely determine the overall efficiency of the energy conversion in the wind turbine (Hau, 2006). The aerodynamic performance of a wind turbine rotor are analyze using several theories which are proposed to give an understanding to the performance of the rotor at changing working conditions (Manwell et al., 2009).

2.9.1 Forces acting on rotor blade

The amount of power that can be extracted from the wind at a given speed is determined by geometry of the rotor blade. Due to the effect of the wind, the shape of the cross sectional area of the rotor blade experiences several forces. Two types of

forces are responsible for the rotating of the blades when the air flows on the blades, these includes the lift and drag force.

2.9.1.1 Lift force

The lift force is the consequence of the unequal pressure on the upper and lower airfoil surfaces. The lift force, L arises in a direction that is perpendicular to the air stream (Manwell et al., 2002). There is higher stream velocity at the top compared to the bottom of the airfoil due to curvature on the top and hence a lower pressure, Figure 2.13.

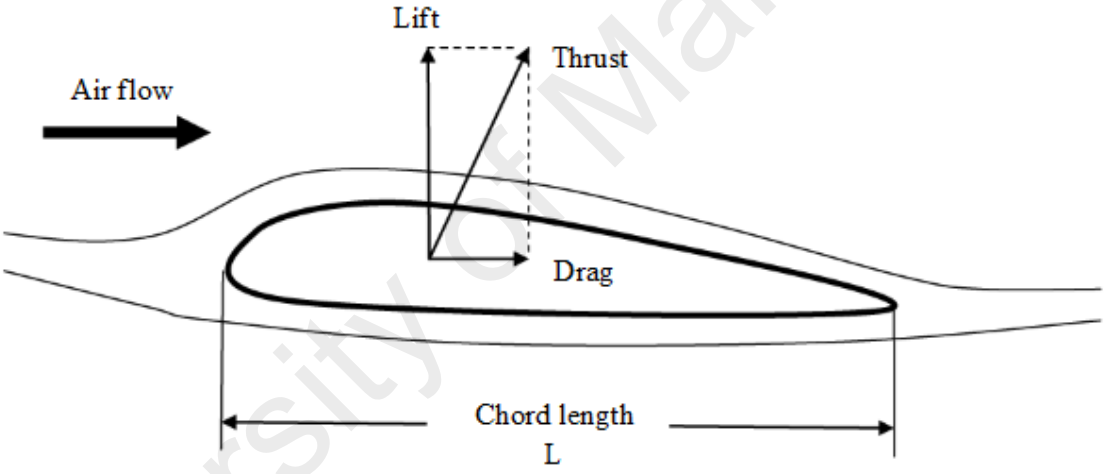

Figure 2.13: Geometry of force acting on airfoil (Ragheb 2013)

The lift force L is described by the coefficient of lift C_L:

$$C_L = \frac{(L/A_L)}{\frac{1}{2}\rho U_\infty^2} \quad (2.6)$$

Where:

A_L is the cross sectional area of the airfoil (m^2)

L is the lift force (N)

2.9.1.2 Drag force

The drag force is due to both the viscous friction forces at the surface of the airfoil and to unequal pressure on the airfoil surfaces facing toward and away from the oncoming wind. The drag force is the forces that arise in a direction that is parallel to the air stream as shown in Figure 2.13 (Manwell et al., 2002). The drag coefficient C_D can be expressed as:

$$C_D = \frac{(D/A_D)}{\frac{1}{2}\rho U_\infty^2} \quad (2.7)$$

Where:

A_D is area of the airfoil (m^2),

D is the drag force (N)

The lift and drag forces varies with the angle of attack, α (i.e. the angle that the rotor blade makes with the direction of the air stream). The thrust force, T which is the resultant of the lift and drag forces effectively rotates the rotor blade. The resultant ratio of lift to drag L/D for a given airfoil section, is a function of the angle of attack α. To attain maximum efficiency for a turbine rotor blade, the maximum value of the L/D ratio profile must correspond to the optimal angle of attack (Ragheb, 2013).

2.9.2 Linear momentum theory

The aerodynamic behavior of wind turbines can be analyzed by considering the energy extraction process without any turbine design (Kulunk, 2011). In linear momentum theory the fluid is assumes to be inviscid, incompressible and irrotational (with no swirl) where the turbine is modeled as a homogeneous actuator disc with infinite number of blades (Messam Abbas Naqvi et al., 2015).

2.9.2.1 Actuator disc model

A simple model that can be used to determine the power from an ideal turbine rotor, the thrust of the wind on the ideal rotor, and the effect of the rotor operation on the local wind field was developed by Betz, in 1926 (Mathew, 2006). The model is based on linear momentum theory. The actuator disc model is the simplest model of wind turbine where the wind turbine is replaced by a circular disc through which the airstream flows with a velocity U_∞, and across which there is a pressure drop from P_u to P_d as shown in Figure 2.14 *(Kulunk, 2011).* The turbine is represented by a uniform 'actuator disc' which creates a discontinuity of pressure in the streamtube of air flowing through it. It is important to note that this analysis is not limited to any particular type of wind turbine (Mathew, 2006; Messam Abbas Naqvi et al., 2015).

The following assumptions are used for the actuator disc model;

- No frictional drag,
- Homogenous incompressible steady state flow;
- Infinite number of blades;
- Uniform thrust over the disc or rotor area; a non-rotating wake;
- The static pressure far upstream and far downstream of the rotor is equal to the undisturbed ambient static pressure (Mathew, 2006; Kulunk, 2011).

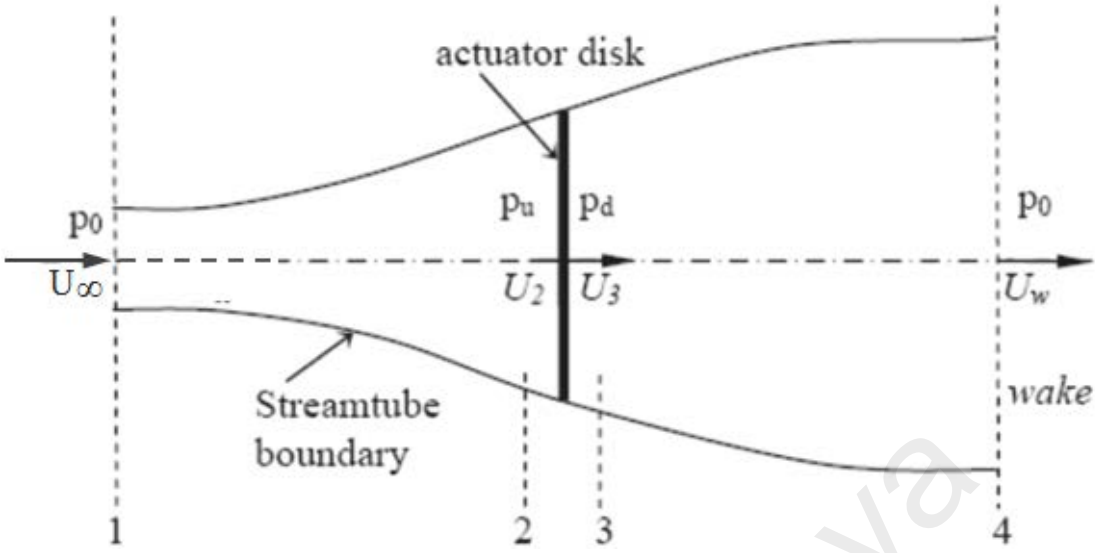

Figure 2.14: Actuator disc model of a wind turbine; U, mean air velocity, 1, 2, 3, 4 indicate locations (Mathew, 2006; Kulunk, 2011)

The analysis assumes a control volume, in which the control volume boundaries are the surface of a streamtube and two cross-sections of the streamtube. In order to analyze this control volume, four stations (1: free-stream region, 2: just before the blades, 3: just after the blades, and 4: far wake region) need to be considered as shown in Figure 2.14 (Kulunk, 2011). The mass flow rate remains the same throughout the flow. So the continuity equation along the streamtube can be written as;

$$\rho A_\infty U_\infty = \rho A_d U_d = \rho A_w U_w \quad (2.8)$$

Assuming the continuity of velocity through the disk gives Equation 2.9

$$U_2 = U_3 = U_R \quad (2.9)$$

For steady state flow, the mass flow rate is given by Equation. 2.10

$$\dot{m} = \rho A U_R \quad (2.10)$$

The net force of the wind on the wind turbine which is equal and opposite to the thrust, T, can be obtained by applying the conservation of linear momentum on both sides of the actuator disc,

$$T = \dot{m}(U_\infty - U_w) \Rightarrow \rho A U_R (U_\infty - U_w) \quad (2.11)$$

The positive thrust implies that the velocity, U_w behind the rotor is less than the free stream velocity, U_∞. Bernoulli equation can be applied on both sides of the rotor since the flow is frictionless and there is no work or energy transfer done, and by assuming that the static pressured at section 1, 2, and 3,4 is equal to the undisturbed ambient static pressure. In the streamtube, the upstream and downstream of the disc can be written as Equation 2.12 and Equation 2.13 respectively.

$$P_O + \frac{1}{2}\rho U_\infty^2 = P_U + \frac{1}{2}\rho U_R^2 \quad (2.12)$$

$$P_O + \frac{1}{2}\rho U_w^2 = P_d + \frac{1}{2}\rho U_R^2 \quad (2.13)$$

The pressure decrease $\acute{P}$ can be obtained by combining Equation 2.12 and Equation 2.13 given as;

$$\acute{P} = \frac{1}{2}\rho(U_\infty^2 - U_w^2) \quad (2.14)$$

The thrust on the actuator disk rotor is given by

$$T = A\acute{P} \quad (2.15)$$

Where

$$\acute{P} = (P_u - P_d) \quad (2.16)$$

The thrust is expressed in a more explicit form by substituting Equation 2.14 into Equation 2.15.

$$T = \frac{1}{2}\rho A(U_\infty^2 - U_w^2) \quad (2.17)$$

Combining Equation 2.11, and Equation 2.17, and solving for U_R the velocity through the disk can be obtained as

$$U_R = \frac{U_\infty + U_w}{2} \quad (2.18)$$

Therefore Equation 2.18 implies that at the rotor section the velocity of the wind stream is the average of the velocities at its upstream and downstream sides. The fractional decrease in wind velocity between the free stream and the rotor plane is called the axial induction factor, a, given as;

$$a = \frac{U_\infty - U_R}{U_\infty} \tag{2.19}$$

This implies that

$$U_R = U_\infty (1\text{-}a) \tag{2.20}$$

From Equation 2.18 and solving for the wake velocity U_w

$$U_w = U_\infty (1\text{-}2a) \tag{2.21}$$

The wake induced velocity is twice that of the induced velocity in the plane of the rotor. The power output of the rotor can be calculated using Equation 2.22;

$$P = TU_R \tag{2.22}$$

By substituting Equation 2.17 into Equation 2.22 the power output can be obtained as;

$$P = \frac{1}{2}\rho A(U_\infty^2 - U_w^2)U_R \tag{2.23}$$

Also substituting Equation 2.20 and Equation 2.21 into Equation 2.23 gives;

$$P = 2\rho A U_\infty^3 a(1-a)^2 \tag{2.24}$$

The Performance parameters of a wind turbine rotor (power coefficient, C_p, thrust coefficient C_T, and the tip speed ratio λ can be expressed in dimensionless form which is given by Equation 2.25, Equation 2.26, and Equation 2.27 respectively

$$C_p = \frac{2P}{\rho U_\infty^3 \pi R^2} \quad (2.25)$$

$$C_T = \frac{2T}{\rho U_\infty^2 \pi R^3} \quad (2.26)$$

$$\lambda = \frac{R\Omega}{U_\infty} \quad (2.27)$$

Equation 2.24 is substituted into Equation 2.25, and the coefficient of power of the rotor can be rewritten as

$$C_p = 4a(1-a)^2 \quad (2.28)$$

Also using Equation 2.17 and Equation 2.21 the axial thrust on the disk can be written as

$$T = 2\rho A a U_\infty^2 (1-a) \quad (2.29)$$

And by substituting Equation 2.29 into Equation 2.26 gives the coefficient of thrust of the rotor.

$$C_T = 4a(1-a) \quad (2.30)$$

For C_p to be maximum $\frac{dC_P}{da} = 0$. Differentiate Equation 2.28 and equating to zero

$$\frac{dC_P}{da} = 4a(1-a)^2 \quad (2.31)$$

$$(1-4a-3a^2) = 0 \quad (2.32)$$

Solving for 'a' gives 'a' = 1, or 1/3

Therefore, the maximum power occur at a = 1/3, substituting, a = 1/3 into Equation 2.28 gives the maximum power coefficient ($C_{p,max}$) value of $\frac{16}{27}$ = 0.593. This is called the Betz limit. In practice, three factors led to a decrease in the maximum achievable power coefficient:

- Rotation of the wake behind the rotor;
- Finite number of blades and associated tip losses;
- Non-zero aerodynamic drag. (Manwell et al., 2009)

2.10 Blade element theory

Froude and Taylor initially proposed the Blade element theory (BET). In this approach it is considered that the blades are made up of a number of strips arranged in the span wise direction. The strips are aerodynamically independent, have infinitesimal thickness, and there is no interference between them. To find the torque and power produce by the blade, one need to estimate and integrate the lift and drag forces that are acting on the strip over the total blade span by incorporating the velocity terms, and the total rotor torque is obtained by further multiplying by the number of blades (Mathew, 2006). The BET assumes each turbine blade to be a rotating wing which comprises of small blade elements along the blade span. To produce the aerodynamic forces (lift, and drag) and moment (pitching moment), each blade element behaves like a two dimensional airfoil due to the collective influence of the incoming wind speed, induced velocity, and rotational velocity. Due to the radial placement, each blade element experiences different rotational velocity, therefore, they will experience a slightly different airflow as compared to other elements as shown in Figure 2.15.

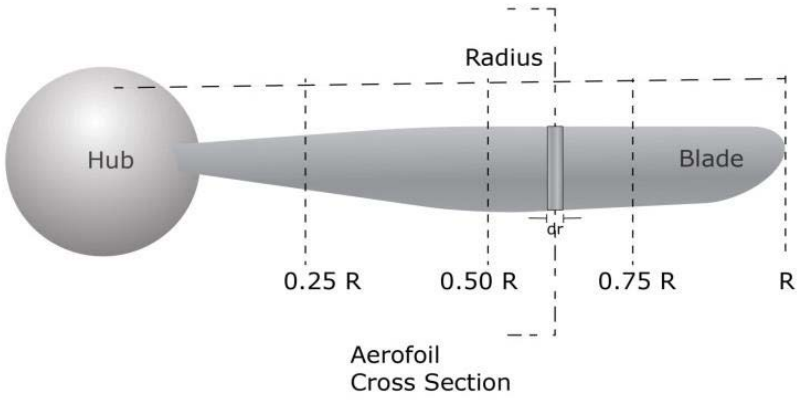

Figure 2.15: Distribution of blade into small elements (Messam Abbas Naqvi et al., 2015)

The relationship between the properties of the airfoil, the thrust that the rotor experienced, and the power developed by it can be best understood using the BET. This analysis is based on some assumptions which include no aerodynamic interactions between different blade elements and the force on the blade elements are solely determined by the lift and drag coefficients. Since each of the blade elements has a different rotational speed and geometric characteristics, the theory states that the blade should be divided into a sufficient number (usually between ten and twenty) of elements and the flow at each one is calculated. The blade element model is shown in Figure 2.16

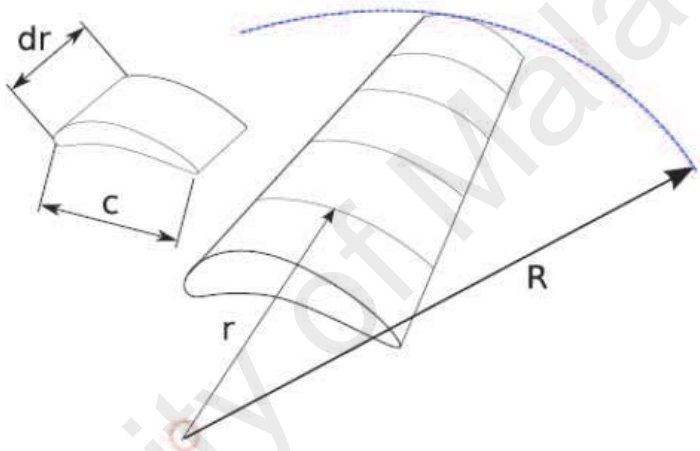

Figure 2.16: Blade element model (Kulunk, 2011)

The overall performance characteristics of the blades can be determined by using numerical integration along the blade span. Since most wind tunnels testing is done with the airfoil stationary, therefore data for the coefficient of lift and drag are obtainable for a variety of airfoils from wind tunnel data (Kulunk, 2011). The general form of elemental torque and thrust equations can be expressed as;

$$dQ = \sigma\pi\rho \frac{U_\infty^2(1-a)^2}{sin^2\varphi} (C_L \sin\varphi - C_D \cos\varphi)\, r^2\, dr \quad (2.33)$$

$$dT = \sigma\pi\rho \frac{U_\infty^2(1-a)^2}{sin^2\varphi} (C_L \cos\varphi - C_D \sin\varphi)\, rdr \quad (2.34)$$

the thrust on the differential element can be expressed as:

$$dT = 4\,\pi\rho U_{\infty}^{2} a(1\text{-}a)\,rdr \tag{2.35}$$

the torque on the differential element can be expressed as:

$$dQ = 4\pi\rho U\Omega\acute{a}(1-\acute{a})r^{3}dr \tag{2.36}$$

by integrating the elemental torque from the root to the tip of the blade, the total torque produced by the rotor can calculated, and by multiplying this torque by its angular velocity, the rotor power can be estimated (Mathew, 2006).

2.11 Blade element momentum (BEM)

The performance parameters of a rotor for ideal, steady operating conditions can be predicted using the blade element momentum (BEM) theory. The BEM theory combines the linear momentum theory and the blade element theory (BET) to analyze the aerodynamic performance of a wind turbine (Kulunk, 2011). In this theory, the aerodynamic forces and moments were computed by change in momentum of the air passing through the annulus swept by each element along with determination of axial and tangential induced velocities (Messam Abbas Naqvi et al., 2015). The momentum balance on a rotating annular streamtube passing through a turbine is analyzed by the momentum theory, and the forces generated by the airfoil lift and drag coefficients at various sections along the blade were examined by the BET (Kulunk, 2011).

BEM assumes no radial interaction between the rotating elements, and the total forces and moments are calculated by integration over the entire blade span. Considerable accurate results are produce by the BEM theory at smaller range of the local angles of attack of the blade (axial flow conditions). However, when the local angle of attack is high, or yawed flow conditions the blade aerodynamic load distributions cannot be accurately be predicted by BEM theory (Messam Abbas Naqvi et al., 2015). According to the general momentum theory, the thrust on the differential element is given as;

$$dT = 4\pi\rho U_{\infty}^{2} a\,(1-a)\,rdr \tag{2.37}$$

For the blade element theory, the thrust is given as

$$dT = \sigma\pi\rho \frac{U_{\infty}^{2}(1-a)^{2}}{sin^{2}\varphi} (C_L \cos\varphi - C_D \sin\varphi)\, dr \tag{2.38}$$

By equating Equation (2.37) and (2.38) we can obtain the following expression

$$\frac{a}{(1-a)} = (\sigma C_L)\frac{\cos\varphi}{4sin^{2}\varphi}[1 + (C_D/C_L)\tan\varphi] \tag{2.39}$$

Also according to the general momentum theory, the torque on the differential element is given as

$$dQ = 4\pi\rho U\Omega\acute{a}(1-\acute{a})r^{3}dr \tag{2.40}$$

for the blade element theory, the torque is given as

$$dQ = \sigma\pi\rho \frac{U_{\infty}^{2}(1-a)^{2}}{sin^{2}\varphi} (C_L \sin\varphi - C_D \cos\varphi)\, r^{2}dr \tag{2.41}$$

by equating Equation 2.40 and Equation 2.41 in the same manner gives

$$\frac{\acute{a}}{(1-a)} = \frac{(\sigma C_L)}{4\lambda_r sin\varphi}[1 - (C_D/C_L)\cot\varphi] \tag{2.42}$$

Equation 2.42 can further be written as

$$\frac{\acute{a}}{(1+\acute{a})} = \frac{(\sigma C_L)}{4\cos\varphi}[1 - (C_D/C_L)\cot\varphi] \tag{2.43}$$

The induction factor a, and $\acute{a}$, are calculated by setting C_D to zero. Equation 2.39, Equation 2.42, and Equation 2.43 can be written as;

$$\frac{a}{(1-a)} = (\sigma C_L)\frac{\cos\varphi}{4sin^{2}\varphi} \tag{2.44}$$

$$\frac{\acute{a}}{(1-a)} = \frac{(\sigma C_L)}{4\lambda_r sin\varphi} \tag{2.45}$$

$$\frac{\acute{a}}{(1+\acute{a})} = \frac{(\sigma C_L)}{4\cos\varphi} \tag{2.46}$$

The power of each differential annular element can be integrated from the radius of the hub to the radius of the rotor to calculate the total power of the rotor, Equation 2.47

$$P = \int_{rh}^{R} dP = \int_{r_h}^{R} \Omega dQ \quad (2.47)$$

Therefore the power coefficient is given by

$$C_p = \frac{P}{\frac{1}{2}\rho A U_\infty^3} = \frac{\int_{r_h}^{R} \Omega dQ}{\frac{1}{2}\rho U_\infty^3 \pi R^2} \quad (2.48)$$

2.12 Aerodynamic of vertical axis wind turbine

Darrieus wind turbine has attracted a lot of attention recently therefore, there is need to develop a model that can be used to accurately predict the performance of the wind turbine. With such model in place large scale rotor systems can be properly engineered and optimized. The model predicts the performance of small scale rotors for which test data is currently available. There are several models from which one could select, ranging from very complex to reasonable simple (Strickland, 1975). Most of this method uses either a conservation of momentum method or a vortex method for determining the forces on a blade.

2.12.1 General mathematical expressions for aerodynamic analysis of straight-bladed Darrieus VAWTs

The straight-bladed Darrieus-type VAWT is the simplest type of wind turbine, however its aerodynamic analysis is quite complex. The following sections describe the general mathematical expression at a specific location of the blade.

2.12.1.1 Variation of local angle of attack

Figure 2.17 shows the flow velocities of the VAWT. From the Figure, one can observe that at upstream and downstream sides of the Darrieus-type VAWTs the flow velocities are not constant and the flow is consider to occur in the axial direction.

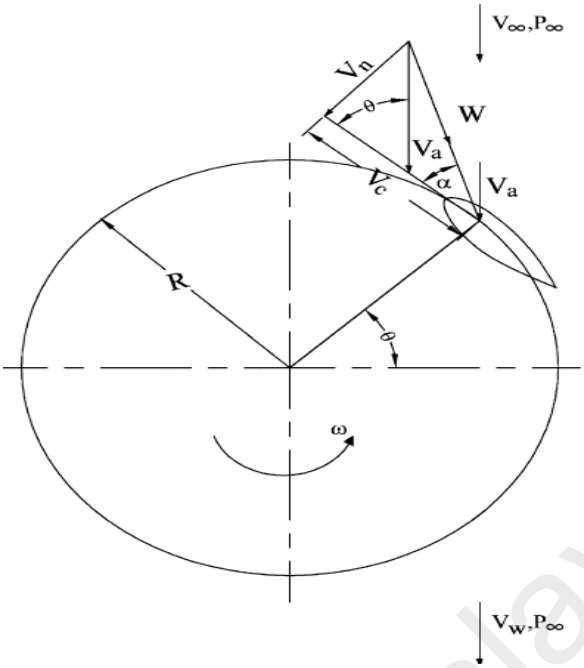

Figure 2.17: Flow velocity of straight-bladed Darrieus rotor (Islam et al., 2008)

From the figure, the chordal velocity component V_c and the normal velocity component V_n are given by Equation 2.49 and Equation 2.50 respectively.

$$V_c = R\omega + V_a\cos\theta, \tag{2.49}$$

$$Vn = V_a \sin\theta \tag{2.50}$$

Where V_a is the axial flow velocity (i.e. induced velocity) through the rotor, ω is the angular velocity, R is the radius of the turbine, and θ is the azimuth angle. The angle of attack (α) can be expressed as;

$$\tan\alpha = \frac{Vn}{Vc} \tag{2.51}$$

$$\alpha = \tan^{-1}\left(\frac{\text{Va}\sin\theta}{Va\cos\theta + Rw}\right) \tag{2.52}$$

By non-dimensionalizing Equation 2.52, and referring back to Equation 2.20 and substituting U_R with V_a and U_∞ with V_∞

$$\alpha = \tan^{-1}\left(\frac{(1-a)\sin\theta}{(1-a)\cos\theta + \lambda}\right) \tag{2.53}$$

where $\frac{R\omega}{V_a}$ is the tip speed ratio given by λ. considering the blade pitching,

$$\alpha = \tan^{-1}\left(\frac{(1-a)\,sin\theta}{(1-a)\,cos\theta+\lambda}\right) - \beta \quad (2.54)$$

Where β is the blade pitch angle

2.12.1.2 Variation of local relative flow velocity

Using the cordial velocity component, Equation 2.49 and the normal velocity component, Equation 2.50, the relative velocity component (W) can be obtained. From Figure 2.17, the relative velocity (W) is given by:

$$W = \sqrt{V_c^2 + V_n^2} \quad (2.55)$$

If the values of V_c and V_n is inserted in this Equation, and by non-dimensionalizing, the relative velocity can be calculated as

$$W = \sqrt{(R\omega + V_a cos\theta)^2 + (V_a sin\theta)^2} \quad (2.56)$$

$$\frac{W}{V_\infty} = \sqrt{\left(\frac{R\omega}{V_\infty} + \frac{V_a}{V_\infty} cos\theta\right)^2 + \left(\frac{V_a}{V_\infty} sin\theta\right)^2} \quad (2.57)$$

Referring to Equation 2.20 and substituting U_R with V_a and U_∞ with V_∞, Equation 2.57 can be re-written;

$$\frac{W}{V_\infty} = \sqrt{(\lambda + (1-a)cos\theta)^2 + ((1-a)sin\theta)^2} \quad (2.58)$$

Where "a" is the induction factor and "λ" is the TSR.

2.12.1.3 Variation of tangential and normal forces

Figure 2.18 shows the directions of the lift and drag forces, and their normal and tangential components. The normal force coefficient (C_N) can be define as the difference between the normal components of lift and drag forces. Similarly, the tangential force coefficient (C_T) is basically the difference between the tangential components of the lift and drag forces. For each streamtube, the normal and tangential

forces coefficients are evaluated as a function of the blade position using the blade airfoil sectional force coefficients. The expressions of C_N and C_T can be written as

$$C_N = C_L \cos \alpha + C_D \sin\alpha \quad (2.59)$$

$$C_T = C_L \sin \alpha - C_D \cos\alpha \quad (2.60)$$

The blade airfoil section lift and drag coefficients C_L and C_D can be obtained by interpolating the available test data using both the local Reynolds number and the local angle of attack (Ibrahim et al., 1995).

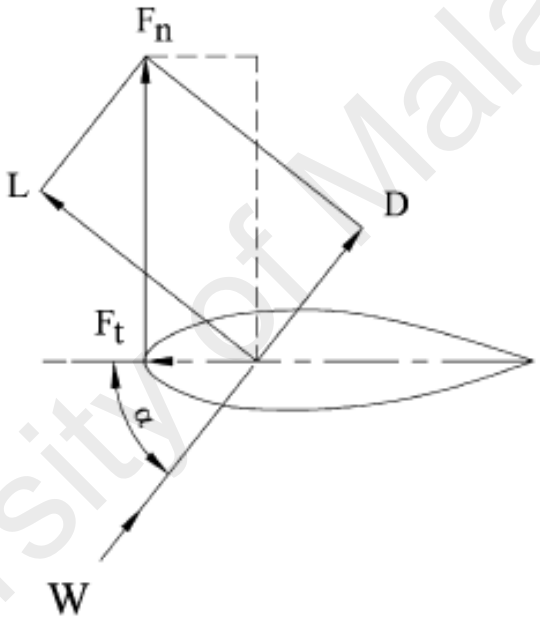

Figure 2.18: Force diagram of blade airfoil (Islam et al., 2008)

The net tangential and normal forces can be defined as

$$Ft = Ct \frac{1}{2} PCHW^2 \quad (2.61)$$

$$Fn = Cn \frac{1}{2} PCHW^2 \quad (2.62)$$

Where ρ is the air density, C is the blade chord and h is the height of the turbine.

At certain θ, the instantaneous thrust force (T_i) on one single airfoil is given by

$$T_i = \frac{1}{2} \rho V^2 (hc)(C_t cos\theta - C_n sin\theta) \quad (2.63)$$

Where the height, and chord length of the blade is denoted by, h and c, respectively.

Also at certain θ, the instantaneous torque (Q_i) on one single airfoil is given by;

$$Q_i = \frac{1}{2}\rho V_R^2 (hc) C_t * R \quad (2.64)$$

2.13 Computational models for Darrieus type straight-bladed VAWT

In recent years, different researchers across the globe have developed many mathematical models based on several theories to predict the performance prediction and design of Darrieus-type VAWTs. According to literature survey the most studied and validated models are the momentum model, the vortex model and the cascades model (Beri & Yao, 2011). For the purpose of this study the momentum model is chosen to predict the performance of CAWT as it is fast and provide reasonable accurate prediction.

2.13.1 Momentum models

Generally, the induced velocity field of the turbine is evaluated using aerodynamic models, the knowledge of the velocity field can be used to determine all the forces on the blade and the power generated by the turbine (Ibrahim et al., 1995). A complete state of the art review including the appropriate reference is given by Strickland (1986), and Paraschivoiu (1988). To calculate the flow velocity through the turbine in momentum models, the streamwise aerodynamic forces on the blades are equated with the rate of change of momentum of air, and this is equal to the overall change in velocity times the mass flow rate (Islam et al., 2008).

2.13.1.1 Single streamtube model

Templin (1974) developed the first method to study the flow field around VAWT. In his approach, the rotor is consider to be an actuator disk enclosed in a simple streamtube, and the induced velocity through the swept volume of the turbine is

assumed to be constant (Ibrahim et al., 1995). The single streamtube model is first and most simple prediction method for the calculation of the performance characteristics of a Darrieus-type VAWT, Figure 2.19.

In the single streamtube models the entire turbine is assumed to be enclosed within a single streamtube, and the air flow through the turbines as if through a single streamtube (Paraschivoiu., 2002). The concept of the windmill actuator disc theory was incorporated into the analytical prediction model of a Darrieus-type VAWT, and the induced velocity (rotor axial flow velocity) which is assumed to be constant throughout the disc can be obtained by equating the streamwise drag with the change in axial momentum (Islam et al., 2008). The effect of airfoil stalling, geometric variables such as blade solidity and rotor height-diameter ratio, and the effect of zero-lift-drag coefficient on the performance characteristics are taken into account in this theory.

The uniform velocity through the rotor according to the Gluert Actuator Disk theory is given by equation;

$$U_R = \frac{U_\infty + U_w}{2} \tag{2.65}$$

Where U_w is the wake velocity. Calculations are done for a single blade.

The streamwise drag force (F_D) due to the rate of change of momentum is given by

$$F_D = \dot{m}\,(U_\infty - U_w) \tag{2.66}$$

Where $\dot{m}$ (= $A\rho U_R$) is the mass flow rate. The rotor drag coefficient (C_{DD}) is defined as

$$C_{DD} = \frac{F_D}{1/2\rho A U_R^2} \tag{2.67}$$

From Equation 2.54 and Equation 2.55 we can find that

$$C_{DD} = 4\left(\frac{U_\infty - U_R}{U_R}\right) \tag{2.68}$$

$$\frac{U_R}{U_\infty} = \left(\frac{1}{1+\frac{C_{DD}}{4}}\right) \tag{2.69}$$

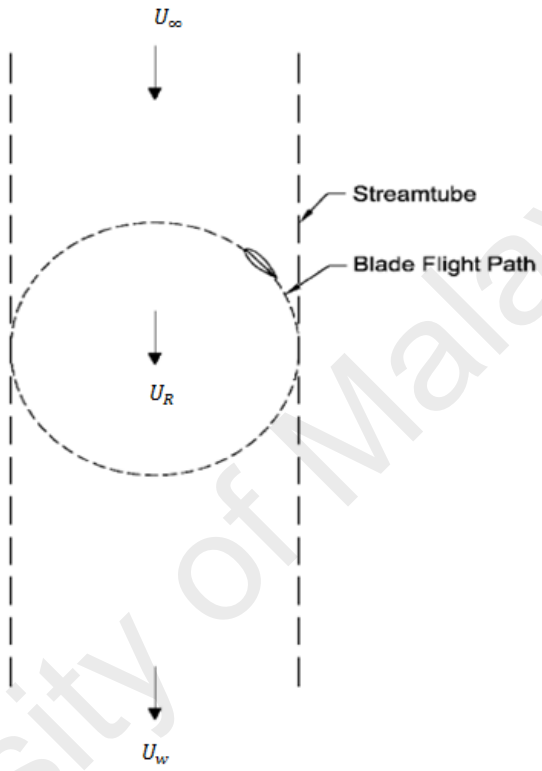

Figure 2.19: Schematic of single streamtube (Islam et al., 2008)

2.13.1.2 Multiple streamtube

The multiple streamtube which is an improvement of the single streamtube models add more streamtube in the plane perpendicular to the airflow was introduced by Wilson and Lissaman in 1974 (Islam et al., 2008). By considering the swept volume of the turbine as a series of adjacent streamtube, Strickland (1975) developed an extension of this method to the multiple-streamtube model (Ibrahim et al., 1995). The multiple streamtube models is a variation of the single streamtube model, where the single streamtube is divided into several parallel adjacent streamtube that are independent

from each other and have their own undisturbed, wake and induced velocities (Batista et al., 2012) as shown in Figure 2.20.

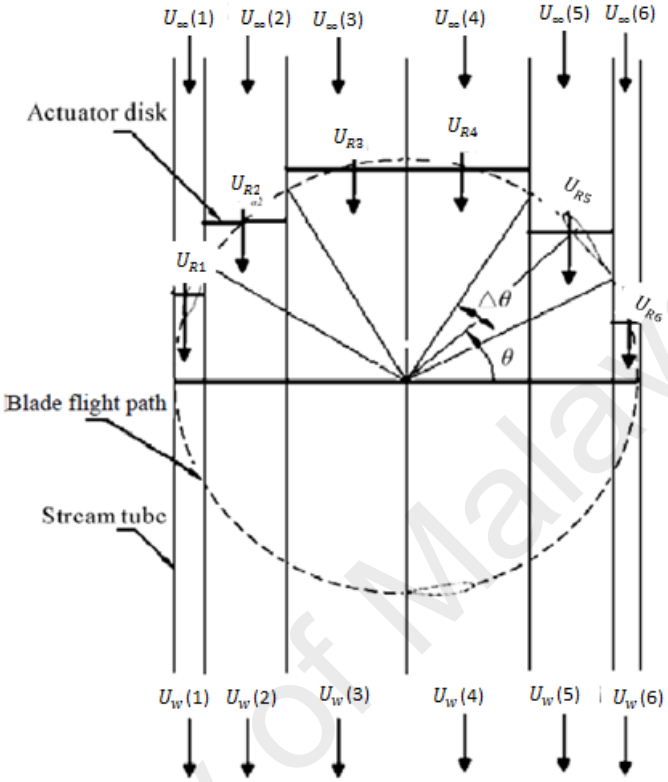

Figure 2.20: Multiple streamtube model for VAWT (Beri & Yao, 2011)

For each streamtube, the blade element and the momentum theories are then employed. In calculating the induced velocity through the streamtube they consider the flow as inviscid and incompressible, therefore, only the lift force appears in the calculation of the induced velocity (Islam et al., 2008). Equation 2.63 gives the instantaneous thrust force on a single blade, and the average aerodynamic thrust is given by Equation 2.70.

$$C_T = \frac{T_a}{\frac{1}{2}\rho u^2 (hR\Delta\theta sin\theta)} \tag{2.70}$$

$$= \left(\frac{NC}{2R}\right)\left(\frac{U_R}{U_\infty}\right)^2 \frac{2}{\pi}\left(C_t \frac{\cos\theta}{\sin\theta} - C_n\right) \tag{2.71}$$

Also Equation 2.64 gives the instantaneous torque on a single blade. In one complete revolution, the average torque (Q_a) on rotor by "N" blades can be expressed as;

$$Q_a = N * \sum_{i=1}^{2m} \frac{\left[\frac{1}{2}\rho V^2 (hc) C_{t*R}\right]}{2m} \quad (2.72)$$

Where m the number of streamtube, and 2m is the number of $\Delta\theta$. The torque coefficient (C_Q) and the power coefficients (C_p) can be expressed as;

$$C_Q = \frac{Q_a}{\frac{1}{2}\rho V^2 (Dh) * R} \quad (2.73)$$

$$= \left(\frac{NC}{D}\right) \sum_{i=1}^{2m} \frac{\left[\left(\frac{V_R}{V_\infty}\right)^2 C_t\right]}{2m} \quad (2.74)$$

$$C_p = C_Q \lambda \quad (2.75)$$

Where D is the diameter of the turbine

2.13.1.3 Double multiple streamtube

The double multiple streamtube theory which was introduced by Paraschivoiu (1981) is the widely used model for the performance prediction of a Darrieus wind turbine. The double multiple streamtube model takes the multiple streamtube model and uses it twice, once upstream and once downstream of the rotor. These methods each provide increasing more accurate performance predictions, as shown by Paraschivoiu (2002). In this model the calculation is done separately for the upstream and downstream half cycles of the turbine. The upstream and downstream induced velocities are obtained at each level of the rotor, using the principle of two actuator discs in tandem. Vertical variation of the induced velocity (like that in the multiple streamtube models) is considered for both the upstream and downstream half cycles Figure 2.21. The wake velocity for the upstream half-cycle can be expressed as;

$$V_e = V_{\infty i}\left(2\frac{V_{au}}{V_{\infty i}} - 1\right) = V_{\infty i}(2U_u - 1) \quad (2.76)$$

Where $V_{\infty i}$ is the local ambient wind velocity, U_u ($= \frac{V_{au}}{V_{\infty i}}$) is the interference factor for the upstream half-cycle, and V_{au} is the induced velocity. V_e is the input velocity for the

downstream half-cycle of the rotor. Therefore, the induced velocity for the downstream half-cycle, V_{ad} is given by Equation 2.77

$$V_{ad} = U_d Ve = U_d (2U_u\text{-}1)\, V_{\infty i} \tag{2.77}$$

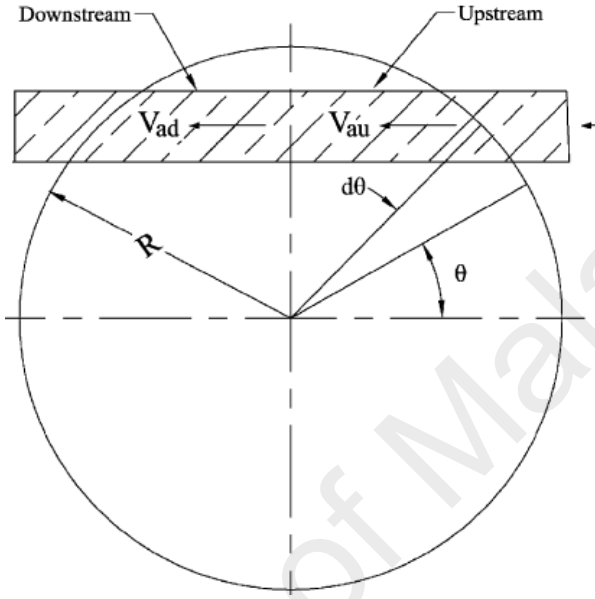

Figure 2.21: Double multiple streamtube (Islam et al., 2008)

Where U_d ($= \frac{V_{au}}{V_{\infty i}}$) is the interference factor for the downstream half-cycle.

Many studies have been conducted on the performance prediction of vertical axis wind turbine using the DMST (Strickland, 1975; Kulunk, 2011; Batista et al., 2012; Biadgo et al., 2013; Soraghan et al., 2013). Beri & Yao (2011) presents the unsteady flow analysis of VAWT using the DMST model; the results obtained from the DMST model were compared with the simulation results using CFD analysis. The results indicate that a improved performance can be achieved with the CFD simulation at low tip speed ratio for the modeled turbine. The DMST model gives good correlation between the calculated and experimental results can be obtained. However, this model gives over prediction of power for a high solidity turbine (Islam et al., 2008).

2.14 Soft computing methodology for performance prediction of wind turbines

2.14.1 Adaptive neuro-fuzzy inference system (ANFIS)

Adaptive neuro-fuzzy inference system (ANFIS) is a soft computing methodology that can be used to predict the behavior of several systems that are uncertain. Despite the fact that various new numerical approaches have been proposed for the performance prediction of wind turbines, there are many disadvantages of these new approaches like the challenges in computing time. Artificial neural network systems (ANN) could be utilized as elective to logical approach as ANN offers favorable circumstances, for example, no obliged learning of inward framework parameters, minimal answer for multi-variable issues (Shamshirband et al., 2014). Artificial neural networks are flexible modeling tools with the capability of learning the mathematical mapping between input and output variables of nonlinear systems. The ANFIS is a powerful neural network system which excels learning and predicting, it is an effective tool for dealing with doubts in any system (Jang J-SR., 1993; Petkovic et al., 2014).

ANFIS, as a hybrid technique, has the proficiency to automatically learn and adopt (Petković et al., 2012; Petković et al., 2012). It is a unique neural network which has good learning and predicting capabilities (Jang, 1993). Because of these capabilities, ANFIS is a very effective instrument to deal with when encountering doubts in any system (Petković et al., 2012; Petković et al., 2012). Due to its estimation accuracy, many studies have been conducted on real-time identification and estimation for many different systems using the application of ANFIS (İnal, 2008; Khajeh et al., 2009; Ekici & Aksoy, 2011). The main core of ANFIS is the Fuzzy Inference System (FIS). The FIS can be used to predict the behavior of several systems that are uncertain as it is based on skill which is expressed in ‘IF- THEN’ rules. One of the advantages of FIS is that the precondition for its applications does not need knowledge of fundamental physical procedure. Therefore, the ANFIS incorporates the FIS through neural network back-

propagation learning algorithm. With this method, the fuzzy logic has the ability to familiarize with the parameters of the membership function which allows the given input and output data to be tracked by the related FIS (Akcayol, 2004; Grigorie & Botez, 2009; Wahidabanu et al., 2011).

Many studies have been conducted on the power-augmentation-devices for the VAWT. Altan et al. (2008) reported that the performance of the Savonius rotor is improved by 38.5% by introducing a curtain arrangement in front of a Savonius rotor. Takao et al. (2009) increases the power coefficient of a straight-bladed VAWT by 1.5 times with the guide vane. Irabu & Roy (2007), reported that the coefficient of a Savonius rotor can be improve by a factor of 2.3 times, by adjusting the inlet mass flow rate with a rectangular guide-box tunnel.

Nobile et al. (2013) reported that the introduction of an omni-direction stator around the VAWT increases the power coefficient by 1.35 times compared to the open case. Chong et al. (2012) asserted that the introduction of an innovative power-augmentation-guide-vane that surrounds the VAWT increased the rotor torque by 2.8 times and the power output by 5.8 times. Tourlidakis et al. (2014) presented a numerical study on a VAWT (bare and shrouded), the results showed that a significant improvement on the performance of the shrouded wind turbine can be achieved. Alidadi & Calisal (2014) reported that the power output from hydro-current vertical axis turbine can be increased by 74% when it is enclosed within a well-designed duct than in a free stream condition.

2.15 Summary

An overview of wind turbine technology, and the related studies including but not limited to the evolution of researches in wind turbines have been studied extensively. The review covers the different types of wind turbine design and their historical development and investigation of a number of existing state-of-the-art of wind turbine.

Several attempts made by researchers for studying various design concept and developing innovative ideas on how to improve the performance of wind turbine including developing various models for the performance prediction of the wind turbines (HAWT and VAWT) have been discussed. Benchmarking study of H-Darrieus wind turbine has been discussed extensively in order to have an insight into the limitation of the H-Darrieus wind turbine and the research efforts made to improve its performance.

According to the literature, many researchers have developed innovative designs to improve the performance of the H-Darrieus VAWTs, while others in an attempt to maximize the energy extraction of the VAWT, design an additional augmentation device (guide vanes) to improve the wind speed before interacting with the turbines which in turn improve the performance of the wind turbine. Some other researchers have applied soft computing methodology in predicting the performance of the wind turbine. It has been seen that most of the research worked on integrating H-Darrieus VAWT on the building rooftop focuses on utilizing the skewed wind at the rooftop to improve performance which may also be affected due to the inherent disadvantages of the VAWT. However, none of the design goals focused on utilizing both the vertical blades and the supporting strut (in these case horizontal blades) in harnessing the wind energy at the rooftop. The motivation of the current research is on how to overcome the disadvantages of the VAWT since building integrated wind turbine represents the future outlook of wind energy generation in the urban environment. Thus a novel wind turbine would be developed to give better performance compared with the conventional H-Darrieus VAWT.

The current works provide an insight into a novel building integrated cross axis wind turbine (CAWT). The CAWT which functions with airflow coming from both the

vertical and horizontal direction can be integrated on to a building rooftop in order to take advantage of the increasing wind speed at the rooftop. The supporting strut of the CAWT is made of the horizontal blade which is capable of utilizing the deflected airflow from the building rooftop to improve the self-starting capability and overall performance. It will be shown later in this thesis that the novel wind turbine can actually function efficiently in the urban buildings.

CHAPTER 3: BUILDING INTEGRATED WIND TURBINE

Building integrated wind turbine can be an excellent location for wind turbines not only because of the increase wind speed at the top of the building but also because it helps to reduce the cost of support towers (Casini, 2016). Building integrated wind turbines exploits any augmentation that the building causes to the local wind flow. They can be incorporated within the building design or supported independently to the building (Dutton et al., 2005). Integrating wind turbines onto buildings is considered a low-cost and effective way to harness renewable energy for buildings (Stankovic et al., 2009).

The first modern concepts to integrate wind energy converters for electricity generation into buildings were put forward in the 1930s and 1940s in Germany by engineer Hermann Honnef who proposed gigantic multi-rotor wind power tower of a height of more than 400 m with rotors of a maximum diameter of 160 m (Heymann, 1998; Muller et al., 2009). Since the mid-1990s, building integrated wind energy generation has become increasingly debated and pursued in research projects (Campbell & Stankovic, 2000; Dannecker & Andrew, 2002).

Drew et al. (2013) suggest that the poor performance of wind turbines in the urban settings can be attributed to two reasons which include: designing wind turbine without any consideration to the complex nature of the wind resource at the roof level and poor placement of wind turbine on the rooftop of urban buildings. Blackmore, (2010) reported that the power output of a roof mounted wind turbine may be close to zero for substantial periods of time if the turbine is mounted at the wrong position. The wind flow in and around high-rise buildings was analyzed by Lu and Sun, (2014). They recommended that the annual wind flows over buildings should be model using an

integrated method of both macro (weather data and domain topography) and micro aspects (Computational Fluid Dynamics, CFD).

Park et al. (2015) proposes a new building-integrated wind turbine system with a specially design guide vane which directly utilizes the building skin. The incoming wind was effectively collected by the combination of a guide vane which increase its speed. The results showed that the proposed building integrated wind turbine system can sufficiently increase the coefficient of power by accelerating the wind using the specially design guide vane.

Ledo et al. (2011) asserted that the characteristics of wind flow are strongly dependent on the profile of the roofs. Abohela et al. (2011) asserted that mounting wind turbine on the vaulted roof shape would yield 56% more electricity than a freestanding wind turbine in the same location under the same wind conditions. A concept of utilizing the building shape for wind energy harvesting is also presented by Sharpe & Proven (2010). The study indicates that improved visual integration into new and existing buildings and augmentation airflow can be achieved by utilizing a lightweight cowling system.

Dayan, (2006) suggested the mounting of wind turbines on top of high-rise buildings for a greater opportunity for wind energy generation in an urban area, and on buildings with special roof shapes (Cochran & Damiani, 2008). Mertens, (2003) asserted that the shape of buildings can offers possible benefits by augmentation of wind flow around buildings for wind energy generation. Wind turbines on the rooftop operates in about 20% higher wind speed compared to undisturbed wind speed (Mertens et al., 2002), due to the slope of the roof which has an effect on the wind speed of the buildings (Padmanabhan, 2013).

Dutton et al. (2005) suggested that the location of the acceleration effects over different roof shapes should be investigated in order to take advantage of the increased wind speed which translates into more energy yield. Rafailidis (1997) reported that the building roof shape is one of the main factors affecting the performance of roof-mounted wind turbines. Muller et al. (2009) conducted a study on a Sistan type wind mill energy converter for building integration. Building mounted wind turbines (BMWTs).

Mounting wind turbines on the rooftop of urban buildings are coming under increasing scrutiny as part of a group of technologies that is suitable for domestic micro-generation applications (Walker, 2011). Building mounted wind turbines are linked to the structure of the building and the structure must be able to support the turbine both in terms of loads and within noise and vibration constrains (Dutton et al., 2005). There are several possibilities on which wind turbine can be integrated on the building (Mertens, 2002; Dayan, 2006).

3.1.1 Mounting wind turbine on top or alongside the building

Wind turbines are sited on the roof or alongside a building, Figure 3.1 (Mertens, 2002). The wind turbine on top or alongside a building operates in the higher wind speed area close to the building. At the rooftop, the flow separates at the leading edge of the roof at an angle of 45^{o} to the horizontal roof, the effect will have less impact for Darrieus rotor, because the blades will experience flow that is almost horizontal for common tip speeds. On the other hand the tilt will have a larger influence on the HAWT, this influence includes the stalling of the airfoil, and reduction in the aerodynamic efficiency, which makes the Darrieus rotor to be more suitable for locating on the roof (Mertens, 2002).

(a)

(b)

Figure 3.1: wind turbine on-top or alongside the building (a) horizontal axis wind turbine, (b) vertical axis wind turbine (Dayan, 2006)

3.2 Building augmented wind turbine (BAWT)

Building augmented wind turbines (BAWT) refers to the wind turbine that operates in the wind energy concentrated by the building (Mertens, 2006). BAWT is seen as having great potential for new buildings, it is a concept that has been developed over a number of years (Dayan, 2006). BAWT requires careful planning and design as they are integral part of the building. The world Trade Centre in Bahrain is the first high-rise building integrating a building augmented wind turbine. The building which is recently completed incorporates three horizontal axis wind turbines of 29 m diameter (Muller et al., 2009).

The wind turbines make use of the buildings as a concentrator of the wind. Wind turbine are always located in high wind speed zones, which only exist close to the buildings, therefore the concentrator effect will only be present for small wind turbine

dimensions. For a building with dimension of around 100 m, this limits BAWT dimensions up to 20% of the characteristics buildings, the BAWT diameter can only be up to about 20 m which is relatively small compared to the 100 m rotor dimensions found in conventional wind turbines (Mertens et al., 2002). BAWT can be categorized into two viz: (a), siting wind turbine between the diffuser shapes of the building in order to enhance airflow towards the turbine, thus increasing its efficiency and (b), siting wind turbine in a duct through a building (Mertens, 2002; Ragheb, 2014).

3.2.1 Siting wind turbine between the diffuser shapes of the building

In this approach, the buildings act as a diffuser for the wind turbine. In the past numerous tests on the operating conditions and attainable aerodynamic efficiency were conducted due to the interest in the diffuser augmented wind turbine. The entire test carried out was based on the horizontal axis wind turbine in ring shaped diffusers (Mertens et al., 2002). According to the test conducted by Igra (1975) the possibility of raising the aerodynamic efficiency in this configuration is high. The drawback is that the diffuser needs to be long in order to generate an applicable gain in aerodynamic efficiency. However, shorter diffuser such as buildings that depend less on wind direction as shown in Figure 3.2, can perform better, this configuration is known as the short “diffuser configuration” Although the configuration exclusively operate as a combination of “diffuser and duct” (Mertens, 2002).

Figure 3.2: Wind turbine located between the diffuser shaped of the building (Dutton et al., 2005; Haase & Lofstrom, 2015)

3.2.2 Siting wind turbine in a duct through the building

The pressure difference between the windward and leeward side initiates the flow through the duct in the building. The local pressure is higher than the undisturbed pressure far before the building due to the stagnation condition at the windward. In contrast, there exists a low pressure at the leeward side of the building that is induced by the high velocity flow at the sides and roof of the buildings. From the latter it can be concluded that there are few advantages of rounding the building at the sides as this can cause lower separating velocities at the sides that cause the pressures difference across the building to become less. So the basic design of this concentrator can look like a flat plate with a duct though the building and can be described as a flat plate concentrator, Figure 3.3 (Mertens, 2002).

Figure 3.3: wind turbine in a duct through the building (flat plate concentrator) (Dutton et al., 2005)

They are some advantages of rounding the edges for the inlet flow when the flow angles are not perpendicular to the front, in this case the flow will be guided more smoothly to the entrance of the turbine. The change in wind direction does not affect the aerodynamic efficiency of the rotor because the pressure difference between the windward and leeward side is not very sensitive to changes in wind direction (Mertens et al., 2002).

3.3 Selection of sites

Optimal location of mounting wind turbine on the building can augment the power output of a wind turbine, and counteract effectively the adverse effects of low urban wind conditions (Dutton et al., 2005). The energy yield of wind turbine depends on the selection of the site. Generally, safety, noise, visual impact, and the availability of land are some of the significant issues that must be taken into account when selecting a site for mounting wind turbine (Turan et al., 2007). In application, the characteristics of local terrain, and the obstructions as well as the regime of flow should be investigated

for a feasible site selection. Bahaj et al. (2007) reported that urban wind turbines will always suffer from being installed in unfavorable locations compared to the large scale wind turbines due to their sitting at low heights within dense urban areas. Stankovic et al. (2009) pointed that there is difficulty in sourcing out a small-scale wind turbines when compared to large ones. According to WINEUR (2007) report, the following should be considered when siting a wind turbine in the urban environments

- Investigate which turbine type and model is the best for the chosen building and locations
- Investigate if the building and the surroundings are suitable for urban wind turbines (UWTs) development.
- Ensure acceptance of the turbine installation in the neighborhood
- Investigate the visual impact and give enough attention to the aesthetic aspects of the integrations (WINEUR, 2007).

The ease of maintenance, installation, and proximity to the building electrical system should be taken into consideration in site selection (Dutton et al., 2005).

3.4 Selection of wind turbines for urban environment

HAWT are the most common type of wind turbine in built environment due to the good performance, and competitive cost of installation. However, the disadvantage of the HAWT is that it accepts wind only in one direction and therefore to keep the turbine rotor faced the varying direction of the wind a yaw mechanism is needed in order to make full use of the wind energy (Muller et al., 2009), which in application it can leads to great constraint (Li et al., 2010). The vertical axis wind turbine (VAWT) is being installed in built environment due to the disadvantage of the HAWT. The VAWT are better suited for built environment due to their omni-directions and better performance

in skewed and turbulent flow (Dayan, 2006; Bahaj et al., 2007). Although the VAWT has gain some acceptance over the HAWT in the urban environments, it also has its own disadvantage which is its inability to self-start at low wind speed, therefore there is need to design a wind turbine that can overcome these disadvantages of both the VAWT and the VAWT while utilizing their various advantages.

In this study, a novel cross axis wind turbine (CAWT) that operates with dual wind directions is introduced. The novel CAWT can overcome the disadvantages of both the HAWT and VAWT in the urban environment and utilize their advantages to improve the performance of building integrated wind turbines in the urban environment. The introduction of the CAWT will assist greatly in overcoming the challenges being faced by the HAWT (accepting wind in only one direction) and the VAWT (difficulty to self-start) in the urban environment thus making the wind turbines to be more attractive among the populace.

CHAPTER 4: DESIGN DESCRIPTION AND METHODOLOGY

4.1 Design description of the novel cross axis wind turbine (CAWT)

The challenges being faced in installing wind turbine on buildings are due to the demerits of both the HAWT and the VAWT in the urban environment. However, the challenges can be overcome through the design of a novel building integrated cross axis wind turbine (CAWT) that can function with dual wind directions (i.e. from horizontal and vertical directions). The CAWT is a new type/category of wind turbine that captures wind energy from both the horizontal and vertical directions (Chong and Kong, 2016). The CAWT in this study was designed to overcome the disadvantages of the HAWT and the VAWT in the urban environment while utilizing their advantages to maximize the power out and improve the overall performance. The revolutionary design of the CAWT can potentially displace the existing wind turbine rotor technology. The vertical and horizontal blades of the CAWT maximizes the wind energy power generation and the lifespan is extended due to the better load distribution and aero-levitation forces generated by the CAWT which lowers the friction in the bearing and generator. The CAWT possesses self-starting capability due to its unique design. The CAWT functions with airflows coming from the horizontal and vertical directions which help to increase the total wind energy potential, improve, the wind turbine self-starting behavior, and overall performance.

4.1.1 General arrangement of the CAWT

The CAWT comprises of three vertical blades and six horizontal blades arranged in a cross axis orientation. The horizontal and vertical blades are connected via connectors to form the cross axis arrangement; Figure 4.1 shows the general arrangement of CAWT. Due to its compact design, it can easily fit into any high-rise or low-rise buildings via different rooftops. The vertical blades are connected to the horizontal blades via some connectors and the horizontal blades are mechanically joined to the

upper and lower hubs through the axle holes. Both hubs are attached to a center shaft with a relative distance of 100 mm. A total of six connectors were used in the design, three top connectors were used to connects the top horizontal blades to the upper part of the vertical blades through the axle hole of the connectors, and the three bottom connectors were used to connects the lower horizontal blades to the lower parts of the vertical blade by screwing through the axle hole of the connectors.

To maximize the interaction of the vertical flow, the lower horizontal blades are offset by 60^o from the upper horizontal blades. Offsetting the upper horizontal blade from the lower horizontal blades will enable the free flow of the vertical wind stream from the bottom of the turbine to the upper horizontal blades. Furthermore, the offset 60^o of the upper and lower horizontal blades gives better force distribution to reduce vibration. The drive shaft of the CAWT can be fixed directly to the generator which converts the kinetic energy in the wind to mechanical energy at the shaft and then to electrical energy. The upper and lower horizontal blades can be pitched at different pitch angles, $\beta = 0^o$, 5^o 10^o, and 15^o to allow for better performance of the CAWT. The purpose of the pitch angle is to maintain a near uniform rotor speed under different wind conditions in order to maximize the power output from the turbine. The choice of the pitch angle was arrived at after conducting an experimental study on four (4) different pitch angles, $\beta = 0^o$, 5^o, 10^o, 15^o to ascertain the optimum pitch angle for the horizontal blades of the CAWT. The whole system is attached to a small pole and can be mounted on a building of any roof shape.

For benchmarking, the performance of a conventional straight-bladed vertical axis wind turbine (VAWT) is tested under the same experimental conditions. The lab scale VAWT model used for the comparison consists of a straight-bladed H-rotor, and it has a 50 mm chord length and 300 mm height. A flat plate metal was used as the connecting

strut for the VAWT. The lab scale CAWT and VAWT model which are used in the experiment are depicted in Figure 4. 6 (a, b). The material selection for the CAWT and VAWT is as shown in Table 4.1.

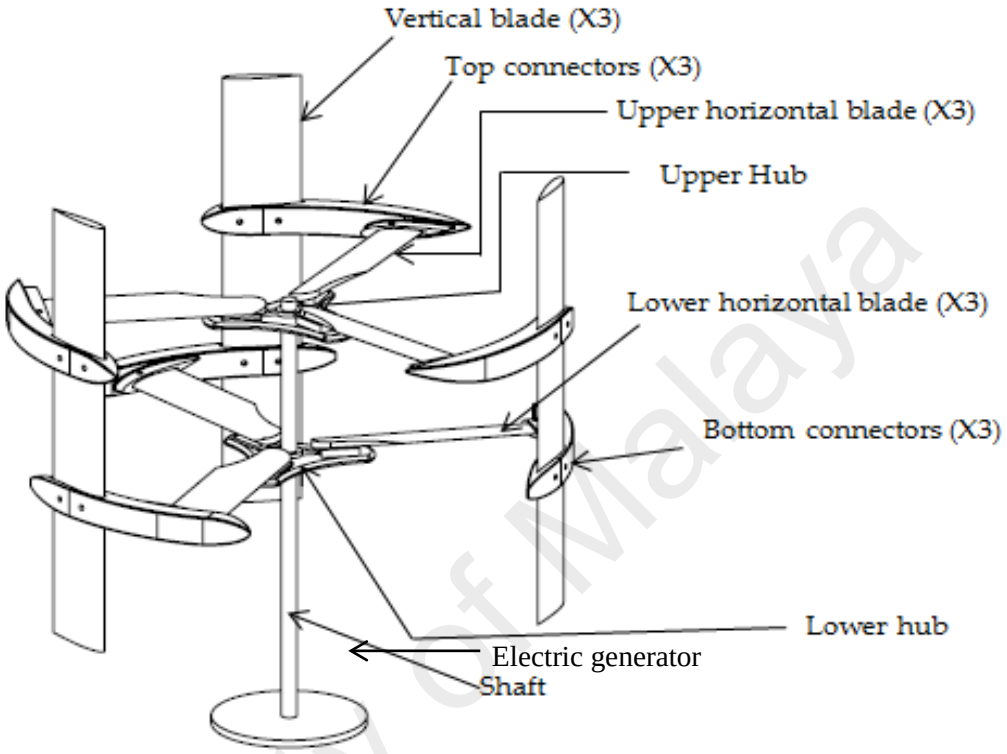

Figure 4.1: General arrangement of CAWT

Table 4.1: Materials selection for the CAWT and VAWT

Component	CAWT	VAWT
Vertical blades	Carbon fibre	Carbon fibre
Horizontal blades	Carbon fibre	N/A
Connectors	3D printing – Acrylonitrile Butadiene Styrene (ABS)	N/A
Generator	10 W	10 W
Shaft	Mild steel	Mild steel
Hubs	3D printing (ABS)	N/A
Supporting strut	Airfoil (Horizontal blades)	Flat plate metal sheet

4.1.2 Working principle of the CAWT

The CAWT is designed to operate either as a building integrated wind turbine or as a stand-alone wind turbine system. However, due to its compact design and its ability to operate under dual wind directions, the CAWT can be integrated onto urban buildings to take advantage of the accelerating effects on the building. Furthermore, it can easily

fit onto any high-rise or low-rise buildings with different roof shapes such as vaulted roof, gable roof, doom roof, etc. When integrated on the rooftop of a building, the horizontal blades located at the bottom and top of the CAWT collects the upward wind streams that strike the wall and roof of the buildings. These wind streams interact with the horizontal blades and allow for self-starting as well as improved efficiency performance.

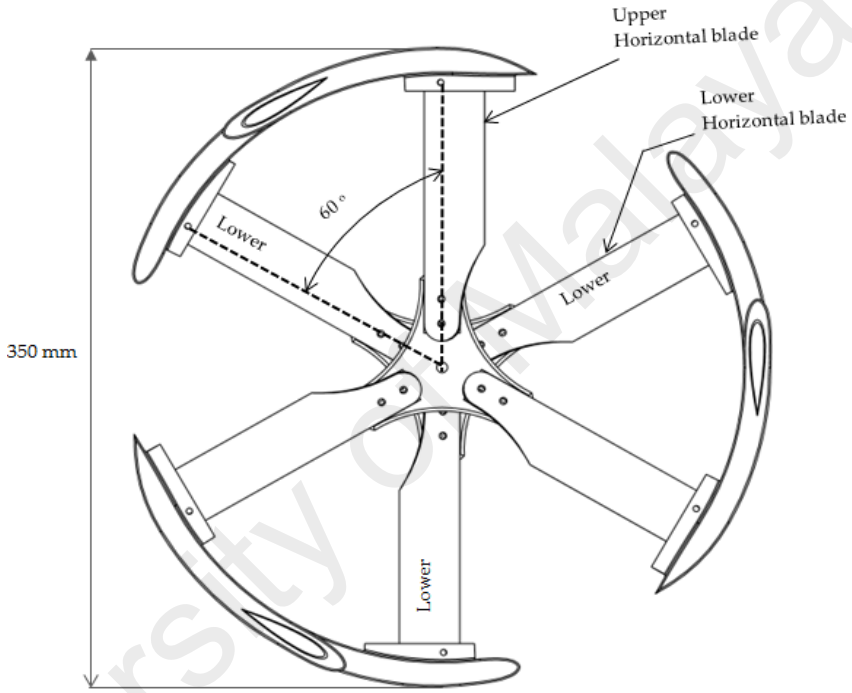

(a) Top view of CAWT showing the 60^{o} offset angle

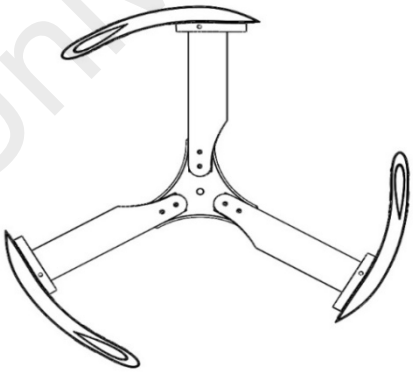

(b) Top rotor

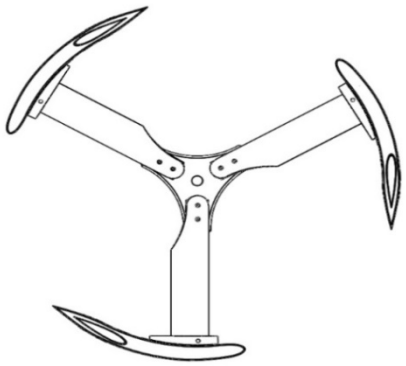

(c) Bottom rotor

Figure 4.2: Arrangement of the horizontal blades of the CAWT, (a) top view showing the offset angle, (b) the top rotor, and (c) bottom rotor

The offset angle of 60^{o}, Figure 4.2 (a) maximizes the interaction of the vertical flow since the vertical wind streams that escape from the bottom horizontal blades without interacting with the blades will be captured by the top horizontal blades. Moreover, offsetting the bottom horizontal blades by an angle of 60° from the top horizontal blades may provide large pocket area to allow for the deflected flow to interact with the top horizontal blades without impinging the bottom blades which allow for a good start-up, and improved efficiency. The top and bottom horizontal rotor is shown in Figure 4.2 (b, c).

The wind turbine is designed to overcome the disadvantages of both the HAWT and the VAWT, as it is operational under both horizontal and vertical wind from the bottom of the turbine, Figure 4.3. The CAWT is an omni-directional device and needs no yaw mechanism. Another unique feature of the CAWT is its ability to intercept the vertical wind stream from the bottom of the turbine through the horizontal blades as shown in Figure 4.3. This vertical wind stream can be due to the accelerating effect on the wind at the leading edge of the building (Dannecker & Grant, 2002), or guided by a guide vane or a deflector to direct the vertical wind stream upward to the horizontal rotor when installed as a stand-alone wind turbine system.

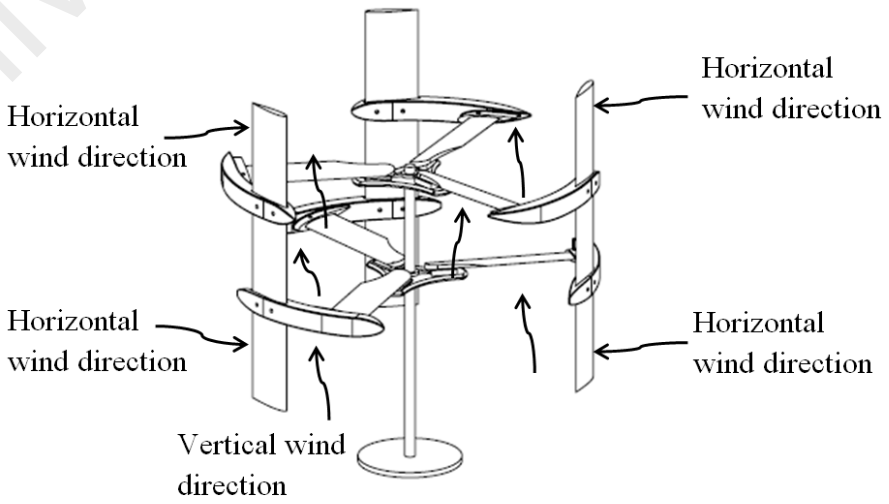

Figure 4.3: CAWT operating under horizontal and vertical (bottom) wind directions

The shape of the roof will act as an augmentation device by deflecting the wind that strikes the roof upward to the horizontal blades. The axis of orientation of the CAWT with its simplicity and improved aerodynamic rotation are the main advantages of the CAWT. An artist's impression showing the CAWT integrated onto a building with a gable roof-shape is shown in Figure 4.4, and the CAD design of the CAWT and VAWT are shown in Figure 4.5 (a, b).

Figure 4.4: Artist's impression of a building integrated CAWT

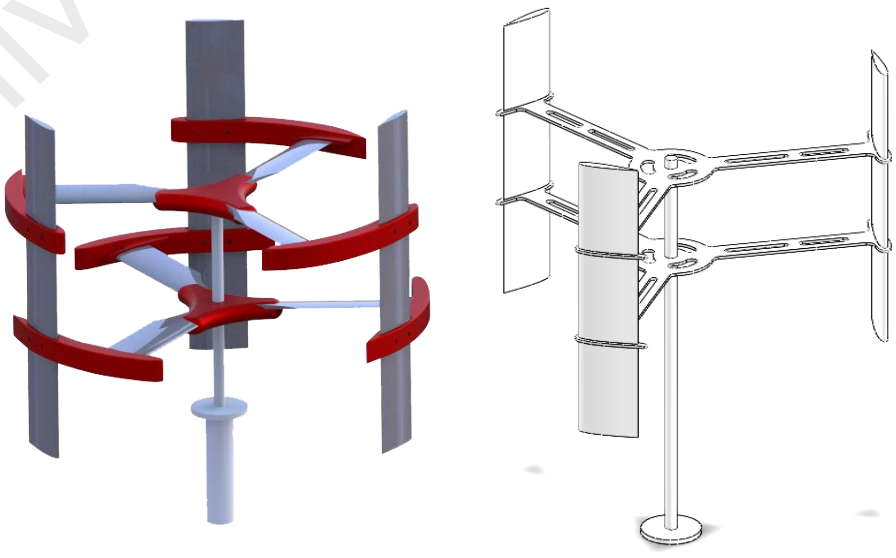

(a) **(b)**

Figure 4.5: CAD design of (a) CAWT, and (b) VAWT

4.2 Design description of the vertical axis wind turbine (VAWT)

For benchmarking a lab scale VAWT model was design and used for comparison with the CAWT, the VAWT consist of a straight-bladed H-rotor, it has 50 mm chord length and 300 mm height. The supporting struts that connect the vertical blades to the hub consist of a 150 mm flat plate, with width and thickness of 25 mm, and 2.03 mm respectively. The profile of the vertical blades is NACA 0015 (Table 4.5). The computer aided design CAD of the CAWT and VAWT is shown in Figure 4.5 (a, and b) while the lab scale CAWT and VAWT model which are used in the experiment are depicted in Figure 4.6 (a, and b), Table 4.5 presents the parameter comparison between the two models.

(a) **(b)**

Figure 4.6: Lab scale model of (a) CAWT and (b) VAWT

4.2.1 General arrangement of the vertical axis wind turbine (VAWT)

The VAWT functions with airflows coming from any horizontal directions. The VAWT comprises of three vertical blades and six supporting struts. The supporting struts connect the vertical blade to the drive shaft which in turn is connected to the generator. Figure 4.7 shows the general arrangement of VAWT and Figure 4.8 shows the top view of the supporting struts. Due to its compact design, it can easily fit into any

high-rise or low-rise buildings via different rooftop. The vertical blades are connected to the center shaft via supporting struts, and the vertical blades are mechanically joined to the upper and lower supporting struts. The lower and upper supporting struts are placed at a relative distance of 100 mm. A total of six supporting struts were used in the design, three top supporting struts connects the upper part of the vertical blades to the shaft while the other three bottom supporting struts connects the lower parts of the vertical blades to the shaft, Figure 4.7.

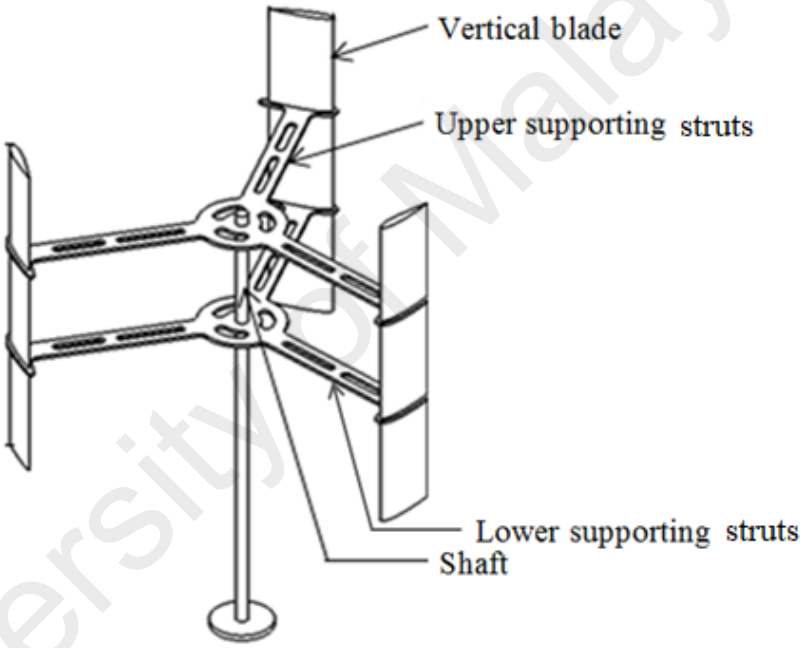

Figure 4.7: General arrangement of VAWT

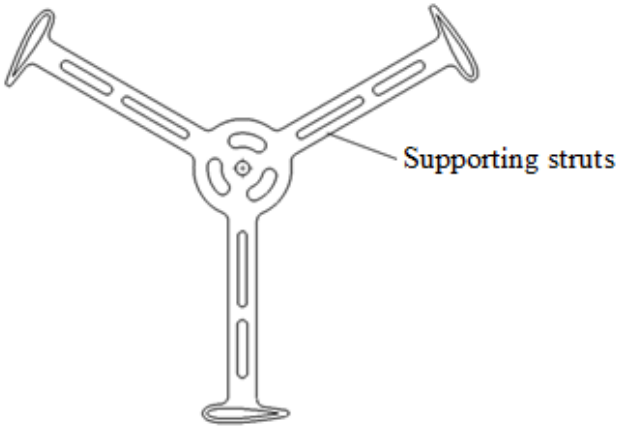

Figure 4.8: Top view of vertical axis wind turbine

4.3 Design parameters

The main design parameters related to a small-scale CAWT and the VAWT are discussed in the following sub sections. Parameters such as the choice of airfoil, supporting strut configuration and shape, solidity, material are more sensitive and critical for a successful final product.

4.3.1 Selection of airfoils

The choice of a suitable airfoil section can significantly improve both the peak performance and the starting characteristics of a wind turbine. Symmetrical NACA 0015 airfoil with a 15% thickness to chord ratio has been chosen for this study. It is an indisputable fact that a cambered airfoil is preferable for the VAWT, due to the curved nature of the airfoil as reported by (Beri & Yao, 2011; Sayed Mohamed et al., 2012; Rainbird et al., 2015). However, VAWT researchers have used one of the original NACA four digit series airfoil sections, usually either a NACA 0012 or a NACA 0015 section. This is because their lift, drag, and pitching moment characteristics are presumably well documented thus making validation of theoretical predictions easier (Kirke, 1998). Bravo et al. (2007) reported that a maximum C_p of 0.32 at TSR (λ) of 1.6 could be achieved with a symmetrical NACA 0015 airfoil. Hameed & Afaq (2013) reported that the symmetrical airfoil is utilized for small scale VAWTs in order to have the same characteristics of lift and drag on the upper and lower surfaces. They asserted that the major advantage is that symmetrical airfoils provide lift from both sides of the airfoil and therefore it will provide lift during the complete 360° rotation of the turbine.

Although cambered airfoils are usually used in wind turbines because of their high L/D ratio (compared to symmetrical airfoils) at positive incidence (relative wind approaching the concave side of the airfoil), however they perform poorly at negative incidence (relative wind approaching the convex side of the airfoil). Because the angle

of attack (α) on a VAWT blade reverses twice per revolution, it is impossible to avoid negative incidence. It has apparently been assumed by most researchers that any performance gain by a cambered airfoil when angle of attack (α) is positive would be more than offset by the reduction in performance when the angle of attack (α) reverses, and symmetrical airfoils have usually been used on VAWTs (Kirke, 1998).

4.3.2 Blade aspect ratio

The Aspect ratio, H/c of the blade plays a very significant role in improving the performance of the wind turbine. According to Kirke (1998) a low blade aspect ratio should be avoided to achieve acceptable peak efficiency, and it must be considerable higher than 7.5. The blade performance deteriorates if the aspect ratio is reduced (Hameed & Afaq, 2013). It has been reported by Islam et al. (2008a) that when the aspect ratio is increased the swept area also increases for the same chord length and diameter of the SB-VAWT, therefore more energy will be captured. Long slender blades with high value of aspect ratio are therefore recommended for straight bladed VAWTs (Islam et al., 2008a; Hameed & Afaq, 2013). Worasinchai et al. (2015) reported that rotors self-start in the following ranges of aspect ratio: $5.71 \leq AR \leq 16.7$. The blade aspect ratio for the CAWT is 6 indicating that it is within the AR range reported by Worasinchai et al. (2015). Table 4.2 summarizes some design parameters of CAWT in comparison with the VAWT.

Table 4.2: Comparisons of design parameters of between VAWT and CAWT in terms of solidity, aspect ratio and c/D ratios

Configuration	Bianchini et al. (2011)	Balduzzi et al. (2012)	Hill et al. (2009)	CAWT
Number of blade	3	3	3	3
solidity	0.45	0.45	0.66	0.43
Blade aspect ratio	6.6	6.7	7.229	6
c/D	0.15	0.15	0.14	0.14

4.3.3 Solidity

The solidity (σ) is key design parameters of wind turbine. It is define as the ratio of blade surface area to the frontal swept area that the rotor passes through. When the solidity is increased, the weight and manufacturing cost of VAWT also increases. In general, a rotor with high solidity turns slowly and produces high starting torque (Islam et al., 2008a; Kirke, 1998). The advantage of a rotor with high solidity is that it has low tip speed ratios and produces higher torque. The solidity can be expressed as;

$$\text{solidity, } (\sigma) = \frac{Nc}{D} \tag{4.1}$$

where N is the number of blade, c the chord length and D is the diameter of the turbine. The solidity of CAWT in comparison with other VAWT is shown in table 4.2

4.3.4 Number of blades

Wind turbines that are mostly used for electricity generation have three blades. The advantage of the three bladed turbine is that the polar moment of inertia with respect to yawing is constant (Manwell et al., 2009). Technically, a single blade VAWT is feasible. However, to balance the mass of the single blade, a counter weight would be required, and a parasitic drag will be generated by this counter weight. Moreover, a single blade wind turbine will not self-start because forward torque is not produced at all blade positions (Kirke, 1998). Two bladed VAWT produces more torque than the single bladed ones, but it has been responsible for damaging fatigue stresses in a number of VAWT rotors (Paraschivoiu., 2002). However, the response is more favorable for the case of a three bladed rotor, compared to the two bladed rotor of the same chord length due to fact that it is omni-directional.

A turbine with three blades tends to run smoothly because of lower fluctuation of energy in each revolution, three bladed VAWT have the advantage of better choice of fabrication technique, and better structural dynamics (Islam et al., 2008a). In view of

these, 3 vertical blades were used in the design of the CAWT. The tip speed ratio, and the power coefficient that could be achieved according to the number of blades is as presented in Table 4.3

Table 4.3: Effect of increase in number of blades on Darrieus VAWT (Castelli et al., 2012)

Number of blades	Tip speed ratio (TSR)	Maximum Coefficient of power ($C_{p,max}$)
3	2.58	0.40
4	2.33	0.38
5	2.04	0.34

4.3.5 Supporting struts

The supporting struts connect the central rotating column to the blades. They stabilize the blade during survival winds, transfer torque to the central column, reduce operating mean and fatigue stresses in the blades and strongly influence some natural frequencies of the rotor (Islam et al., 2008a). The main purpose for the supporting struts is to attach the blades to the main shaft and provide mechanical support to the blades. Usually, these struts have no aerodynamic characteristics. Struts that are commonly used are round pipes or flat metal plates (Ramkissoon & Manohar, 2013). It has been observed that the supporting struts generate parasitic drag which reduces the net power output (Islam et al., 2008a; Ramkissoon & Manohar, 2013). However, using a streamline-shaped object (i.e. airfoils) as the supporting struts will significantly reduce the parasitic drag.

A streamline shaped object maintains a smooth laminar flow and the resistance can be substantially reduced ("Streamlining and Aerodynamics," 27 September, 2016). Islam et al. (2008a) reported that the supporting struts with airfoil shape will improve the aerodynamic performance of the VAWT. Ramkissoon & Manohar (2013) reportedly reduced the resistance of their supporting struts by 15% by modifying the original struts to a round pipe shape. For this study, the supporting strut use in the design of the

CAWT is an airfoil, NACA 0015. Airfoil shapes have less resistance which makes them more favorable to replace the normal supporting struts for VAWT.

4.3.6 c/D ratio

Another aspect that can be considered is the c/D ratio. According to Worasinchai et al. (2015) rotors that have c/D ratio of 0.05 or less will not start whatever the value of the blade aspect ratio. On the other hand rotors with c/D values of around 0.10, can self-start because the Reynolds number is sufficiently high for the rotor to be able to generate sufficient torque to start spinning. The c/D ratios of the CAWT in comparison with other VAWT is shown in Table 4.4. The c/D ratio of CAWT is within the range of c/D ratio used by Worasinchai et al. (2015).

Table 4.4: Comparisons of c/D ratios between VAWT and CAWT

Configuration	Bianchini et al. (2011)	Balduzzi et al. (2012)	Hill et al. (2009)	CAWT
c/D	0.15	0.15	0.14	0.14

4.3.7 Pitch angles of the horizontal blades

Pitching of wind turbine blades is thought to improve the performance of the wind turbine. The role of a pitch angle is to maintain a near uniform rotor speed under different wind conditions in order to maximize the power output from the turbine. For this study, four different pitch angles were used for the horizontal blades. This pitch angles ranges from, $\beta = 0^o, 5^o, 10^o$, and15^o, Table 4.5. To select the optimum pitch angle for the horizontal blades, experiments was conducted for the different pitch angles with the CAWT integrated on the gable and vaulted rooftop. The design parameters of the CAWT in comparison to the VAWT are shown in Table 4.5.

4.3.8 Turbine Aspect Ratio

The aspect ratio, h/R of a turbine is an important design parameter that affects the performance of a wind turbine, to maximize the power output of a wind turbine; the turbine aspect ratio must be as small as possible. Low turbine aspect ratio h/R = 0.4 has

higher power compared to high turbine aspect ratio h/R = 2. When the aspect ratio is low, the radius of the turbine increases which in turn increases the chord length of the turbine, when the chord length of the turbine blade is increased, the Reynold number rises and this can cause an increase in power coefficient of the turbine (Brusca et al. 2014).

Table 4.5: Summary of design parameters of the prototype CAWT and straight bladed VAWT

Parameters	CAWT	VAWT
Diameter of rotor, *d* (mm)	350	350
Height of vertical blade, *h* (mm)	300	300
Chord length of vertical blade, *c* (mm)	50	50
Length of horizontal blade, *l* (mm)	150	N/A
Connecting strut of VAWT (mm)	N/A	150 (flat plate: W = 25 mm, thickness = 2.03 mm)
Chord length of horizontal blade, *c* (mm)	34	N/A
Type of airfoil	Symmetrical airfoil	Symmetrical airfoil
Profile of airfoil	National Advisory Committee for Aeronautics (NACA) 0015	NACA 0015
Pitch angle of the horizontal blade, β	$\beta = 0^o, 5^o, 10^o, 15^o$	N/A
Pitch angle of the vertical blade, β	0	0
Solidity, σ	0.43	0.43
Blade Aspect Ratio (*AR*)	6	6
Swept area (*m)*	0.105	0.105

4.4 Fabrication of CAWT

Fabrication of CAWT consists of different parts which are needed to be fabricated as part of the main assembly. The parts fabricated for the CAWT includes the blades, shaft, supporting disc, and base fabrication. A micro scale prototype CAWT was built and mounted/integrated on low-rise building models with a vaulted and gable roof shape. The feasibility of integrating CAWT onto building with gable and vaulted rooftop, and as a stand-alone system was investigated through an experimental study.

The performance of the CAWT integrated on the building was compared with the performance of a conventional straight bladed VAWT of the same dimension and under the same experimental conditions. The design parameter of the innovative CAWT and the straight bladed VAWT is shown in Table 4.5.

4.4.1 Fabrication of the building model

A scaled-down building model was constructed for the laboratory test. The models were made from a ply wood and zinc metal sheet which is use for the rooftop. The building models consist of two different shapes; one is the gable rooftop with a pitch angle of 35^{o} Figure 4.9 (a), and the other is the vaulted rooftop Figure 4.9 (b).

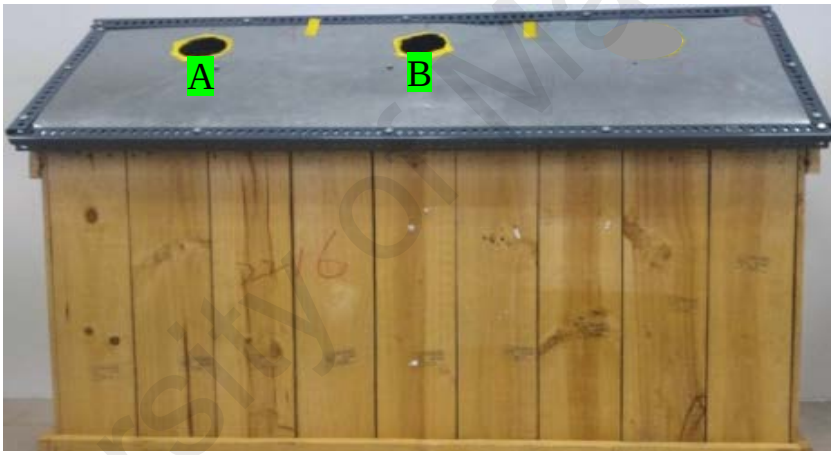

(a)

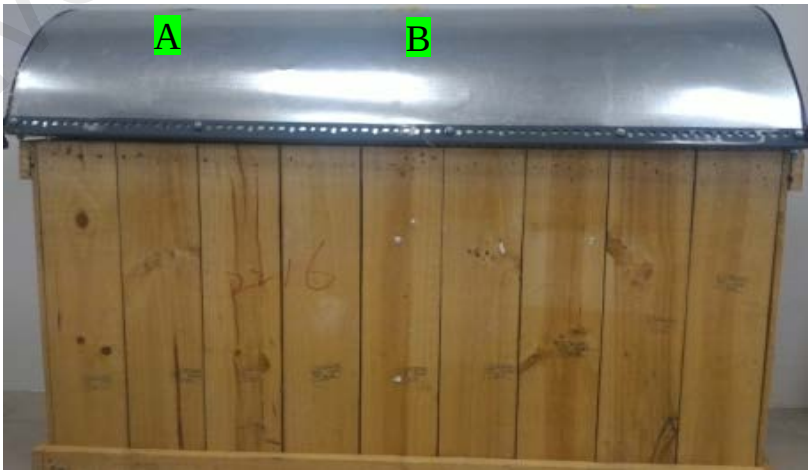

(b)

Figure 4.9: Building model for (a) gable roof shape (b) vaulted roof-shape

The length, height, and width of the building models 1450 mm x 1364 mm x 740 mm respectively, Figure 4.11 and Figure 4.13. The wind turbine is mounted at position A, and B above the rooftop as shown in Figure 4.9. The lab scale building models are shown in Figure 4.9 (a, and b).

4.5 Experimental set-up

Figure 4.10, Figure 4.12, and Figure 4.14 shows the experimental set-up for this study, the set-up consists of two lab scale building models with gable and vaulted rooftops having similar dimensions (length, width, and height) 1450 mm x 740 mm x 1364 mm, Figure 4.10, and Figure 4.12. The set-up for Figure 4.14 is mainly for the bare-CAWT. The CAWT and the straight bladed VAWT were mounted at a varying height of Y = 100 mm; 150 mm; 200 mm; and 250 mm above the rooftop of the building models as shown in Figure 4.11 and Figure 4.13.

The experiment was conducted in an open air test rig; this is though more realistic scenario since air blown ventilation fans performs in a similar manner to the field environment where the wind stream is swirling and turbulent (Chong et al., 2012), and the boundary effects typical of a wind tunnel can be excluded, the main advantages being of course that the wind speed cannot be controlled (Muller et al 2009). The experimental procedures used in this study is similar to those in (Amirante et al. 2017, Chong et al., 2012), where industrial stand fans were used to generate the wind speed. Similar open air test rig experiment for wind turbine was also reported in (Muller et al 2009).

The wind speed measurements were taken downstream of ventilation fans placed at a distance of 3500 mm and 4000 mm away to the building model. The ventilation fans were arranged in array in a 3 x 3 configuration as shown in Figure 4.10 and Figure 4.12. The schematic diagram with detail dimension for the building models and the

ventilation fans is shown in Figure 4.11 and Figure 4.13. Also the detail dimension of the bare-CAWT is shown in Figure 4.15. An arrangement 3 x 3 equally spaced grid points which covers a cross-section of 1.0 m by 1.0 m (Figure 4.16) downstream of the fan array was used for the measurement of the wind speed which was set at average wind speed of 4.5 m/s and 4 m/s for a distance 3500 mm, and 4000 mm away to the building model. The wind direction is set at 0^o (i.e. perpendicular to the building model). Since the flow was not controlled, the blower was directed orthogonal to the test section area and the wind speed was measured at different lengths to conform spatial uniformity. Hence the average wind speed of 4.5 m/s ± 0.2 (3500 mm) and 4.0 m/s ± 0.1 (4000 mm), was obtained. The central axis of the turbine was taken as the center point, the wind speed measurements were taken at each measuring points by using a vane anemometer over a period of 5 min. repeatability and airflow uniformity were ensured by repeating the measurements for 10 times at each point.

The rotor of both the CAWT and the straight bladed VAWT were in free-running conditions where only the inertial and bearing friction were applied. Measurement of the rotational speed of both the turbines started immediately after switching on the ventilations fans until the stabilized rotational speed is achieved. The measurement was performed with a dynamometer controller system which consists of a rectifier and resistive dump load. For current and voltage measurement, the alternating current (AC) voltage from the generator is rectified to direct current (DC).

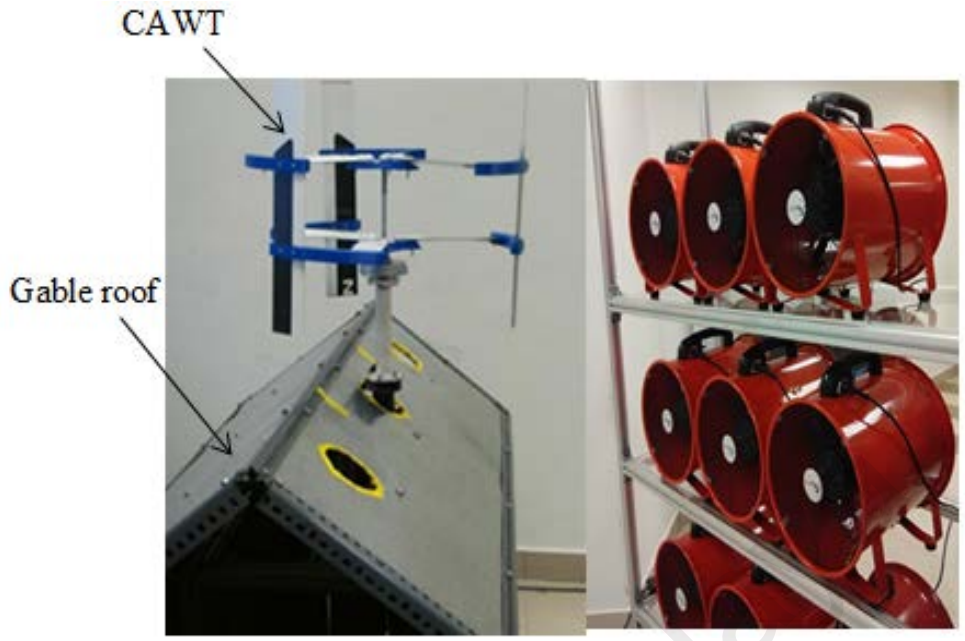

Figure 4.10: Experimental set-up of the CAWT integrated on a building with a gable rooftop

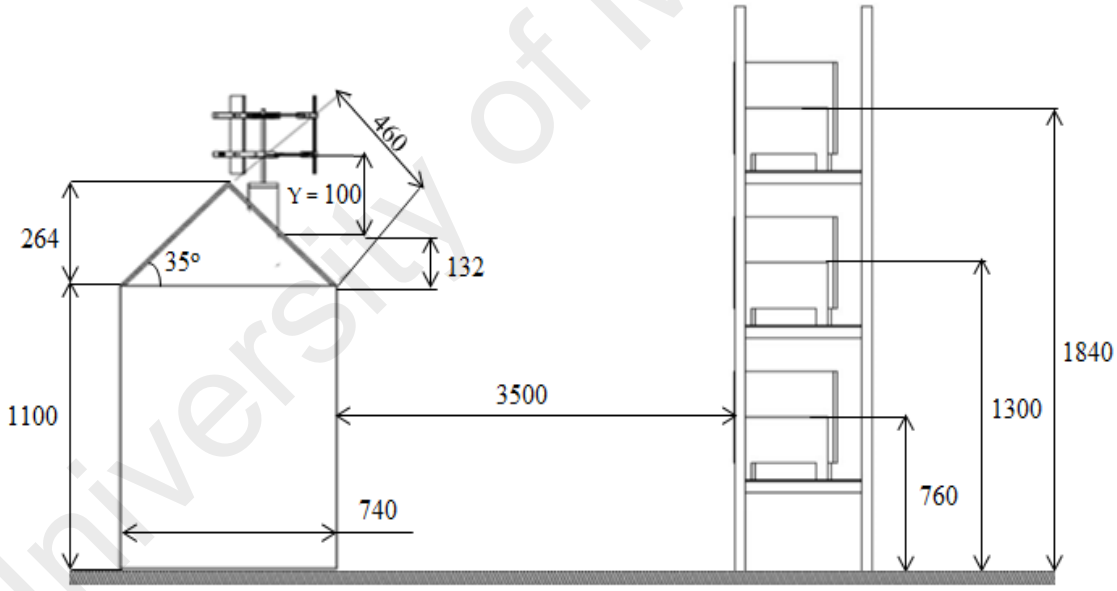

Figure 4.11: Detailed dimensions of a gable rooftop building model integrated with a CAWT and dimension of the ventilation fans (all dimensions in mm)

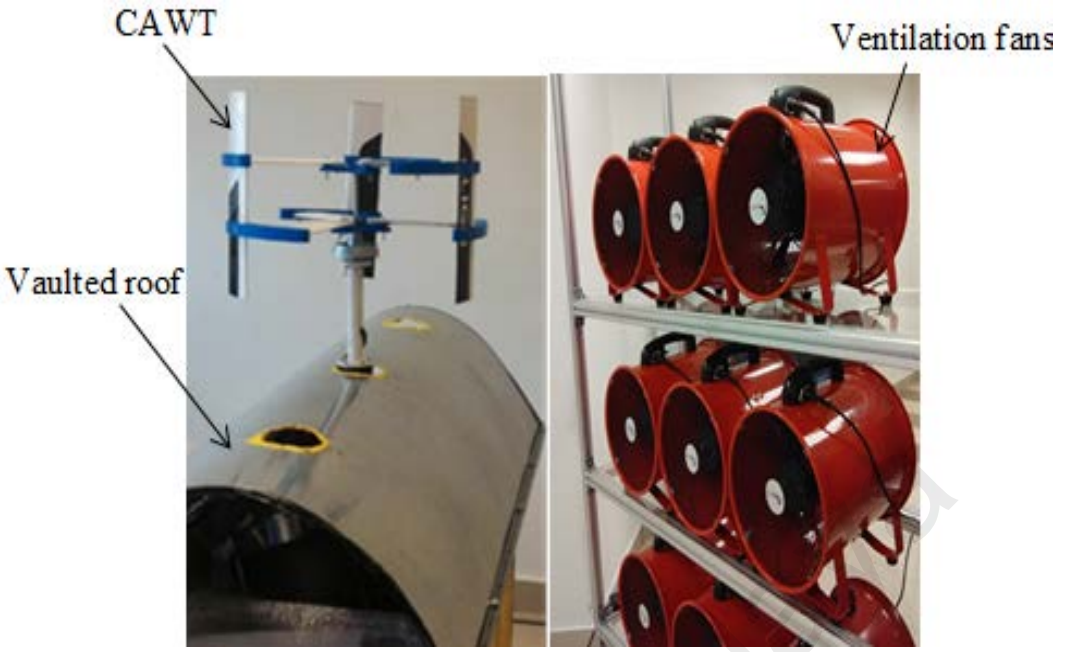

Figure 4.12: Experimental set-up of the CAWT integrated on a building with a vaulted rooftop

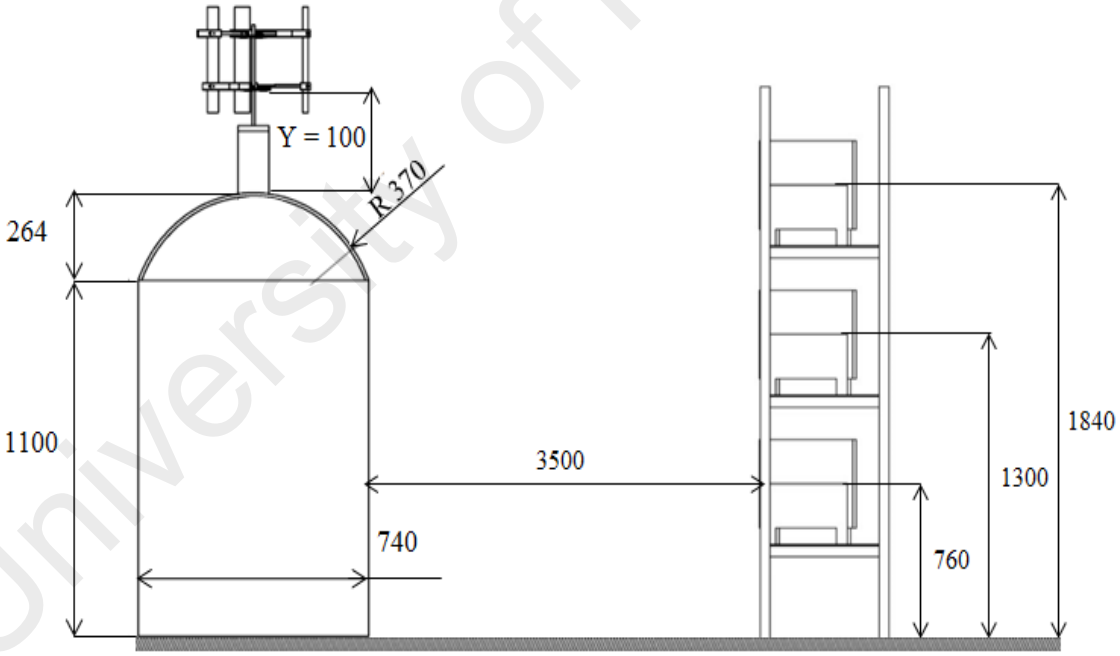

Figure 4.13: Detailed dimensions of a vaulted rooftop building model integrated with a CAWT and dimension of the ventilation fans (all dimensions in mm)

Figure 4.14: Experimental set-up of the bare-CAWT

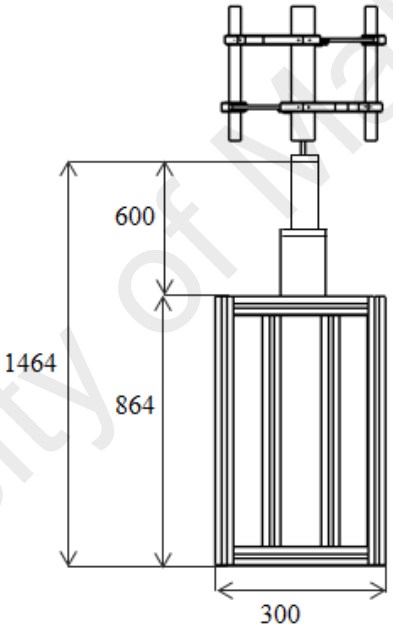

Figure 4.15: Detailed dimensions of the bare-CAWT (all dimensions in mm)

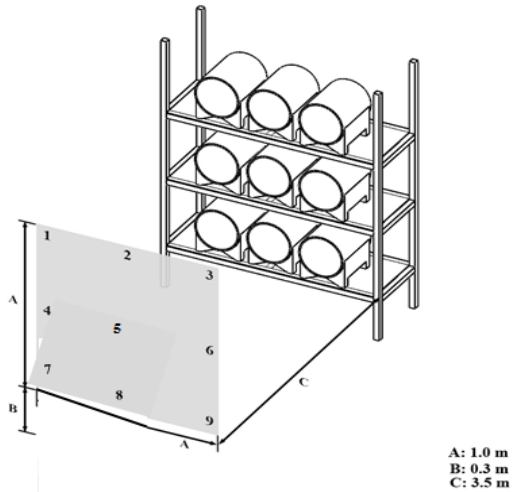

Figure 4.16: Wind speed measurement area (shaded region)

4.5.1 Dynamometer controller

The controller system logged the rotor performances. The parameters recorded by the controller system include the voltage, current, electrical power and the turbine rotational speed. The dynamometer controller, Figure 4.17 allows the user to control the dynamometer in several different modes: Manual, speed, Torque, Road Load (RPM^2) and computer (remote) mode. Each of these modes to use depends on the specifics of the testing to be carried out. Manual control mode is used for simple loading of an engine (i.e. adding and reducing the load) while speed control mode is used for constant speed operations (Torque will vary).

Figure 4.17: Dynamometer controller

For computer communications, a computer can be connected to the dynamometer controller for logging data from the dynamometer controller. The data acquisition systems are via serial ports. The dynamometer controller includes a data acquisition system (DAQ). This system is for reading signals from various sensors commonly used in engine testing such as thermocouples, pressure sensors, voltages and etc. Several channels are available for the use, and are logged along with the standard controller data (e.g. speed, torque, %load, control mode, alarm Status), Figure 4.18. All of these sensors can be read by the computer data logging software for display and recording.

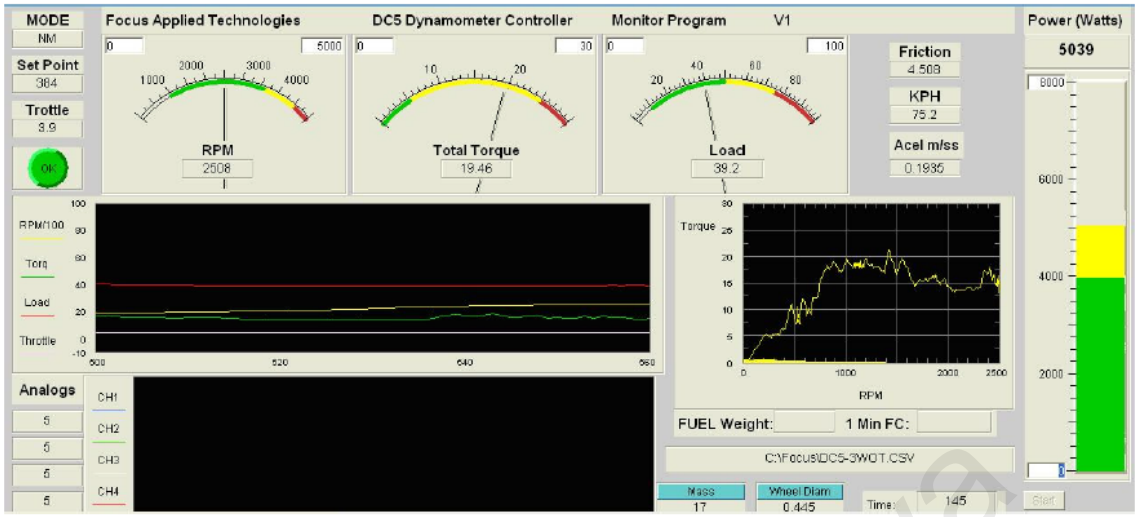

Figure 4.18: Dynamometer controller display

The dynamometer is designed to operate at up to 5000 RPM, giving a roller speed of 2500 RPM. This corresponds to a vehicle speed of 78 kph, or about 50 mph. The dynamometer has a frictional torque of approximately 2 Nm, and the maximum torque rating is approximately 35 Nm. This gives a maximum mechanical power of approximately 9 Kw (Stankovic et al., 2009).

4.6 Analytical method for the cross axis wind turbine

The aerodynamic prediction model for wind turbines is use to determine the velocity field of the blades which allows the aerodynamic forces on the blades and power generated by the turbine to be determined (Soraghan et al., 2013). An analytical model based on the double multiple streamtube (DMST) method and blade element momentum (BEM) theory is proposed for calculating the rotor performance and aerodynamic blades forces for the CAWT. The output from the aerodynamic prediction using this model is compared with experimental data for validation purpose. The model is discussed in detail in chapter two subsection 2.13.1.3, and 2.11 respectively. In the proposed model, the DMST and BEM model which were used independently for both the vertical blades (DMST) and the horizontal blades (BEM), were combined to determine the power output of the CAWT.

4.6.1 Double multiple streamtube (DMST) Analysis

The aerodynamic behavior of the vertical blades of CAWT was analyzed using the DMST theory, which was explained in detail in chapter 2, subsection 2.13.1.3. As explained earlier in the design parameter, an airfoil, NACA 0015 with maximum thickness of 15% was used for the experiment. The parameter of wind velocities and rotor rotational speeds are taken from the experiment using semi-empirical approach. The lift and drag coefficients used for this computation were obtained from the online airfoil database at Reynolds number of 2.5×10^4. According to Sheldahl & Klimas (1981) the angle of attack of an airfoil of VAWT continuously changes from positive to negative and back to positive as it revolves about the vertical axis. Therefore it is possible to be at an angle of attack approaching $\pm$ 180^o at low TSR throughout the revolution. However, due to the fact that the airfoil study is focused on aircraft wing application, the available data is only limited to a small range of angle of attack. Since the angle of attack of the blades varies continually during the rotation it is therefore essential to get a complete range of angle of attack through an extrapolation model which was developed by Montgomerie, (2004). For the analysis in the DMST theory, the swept volume of the turbine is divided into 18 streamtube for each of the upstream and downstream sides. Using the actuator disc principle in tandem, the upstream and downstream half cycles of the turbine were calculated separately as reported by Lapin, (1975), and at each level of the rotor the induced velocities at upstream and downstream are obtained.

The assumption made was that the wind velocity profile is uniform for all the streamtube. Analysis was done separately for the wind in the upwind and downwind regions of the turbine that interacts with the blades. It also assumed that the wake from the upwind pass has fully expanded in which the ultimate wake velocity is reached before it interacts with the blades in the downwind pass. On the other hand, the blades

on the downwind region interact with a reduced 'free-stream' velocity. The variation of the flow through the turbine can be accurately represented using this approach. Therefore, for each streamtube of the DMST model, the wind stream intersects the airfoil of the vertical blades twice (upwind and downwind regions). The turbine is assumed to be replaced by a tandem pair of actuator discs upon which the flow may exert force at these intersections. Two equations for the stream-wise force at the actuator disk were solved simultaneously by the DMST model; one is obtained by the conservation of momentum and the other is based on the aerodynamic coefficients of the airfoil and the local wind velocity. These equations are solved twice; one for the upwind and the other for the downwind part of the rotor. The turbine was divided into 18 streamtube (each of upwind and downwind) where the size of each streamtube is 10^o and the free stream and induced velocity were assumed to be perpendicular to the turbine swept plane.

4.6.1.1 Procedures for the DMST calculation

The rotational speed, turbine and airfoil dimension, azimuth angle, and wind velocity are the parameters needed for the DMST calculation. After assuming the axial induction factor "a" to be 1/3, the induced velocity and angle of attack is calculated. Furthermore the lift and drag coefficient at a particular angle of attack is obtained from a reliable airfoil database. After which the tangential, normal coefficient and torque is calculated as explained in chapter 2.

4.6.2 Blade element momentum (BEM) analysis

For the proposed approached, Firstly, measurement were taken for the oncoming wind velocity near the horizontal blades of the CAWT integrated on the building models at different azimuth angle of the rotor, Figure 4.19 using the vane anemometer. 36 local points were selected, starting from the azimuth angle of 5^o to 355^o at 10^o increment. The

location of the points are r = 16 cm, (r/R: 91%), 12 cm, (r/R: 69%), and 8 cm, (r/R: 46%) from the centre of CAWT or span from the central axis. Measurement of the wind velocity was done on the plane of the bottom rotor of the CAWT, where at each point the horizontal (x-axis) and vertical (y-axis) wind velocities were measured. All the measurement was taken in the absence of the CAWT. To reduce the uncertainties arising from the use of instrument careful consideration were made during the measurement. To quantify for repeatability, the mean velocities at each local point were measured repeatedly. The ranges of flows encountered by the horizontal wind velocity ($V_{ob,x}$) and the mean vertical wind velocity, V_{aby} were covered by the local points. The deflected flow angle, ϑ and the resultant wind flow velocity, V_{ob} can be obtained at each azimuth angle by treating these values as vectors. The essence of this method is to determine the induced velocity V_{ab} seen by the blade and thus the local angle of attack α_b. When the local angle of attack is determined, the lift and drag coefficient can be looked up in an airfoil's database and therefore, the forces acting on the local area of the horizontal blade element can be explained.

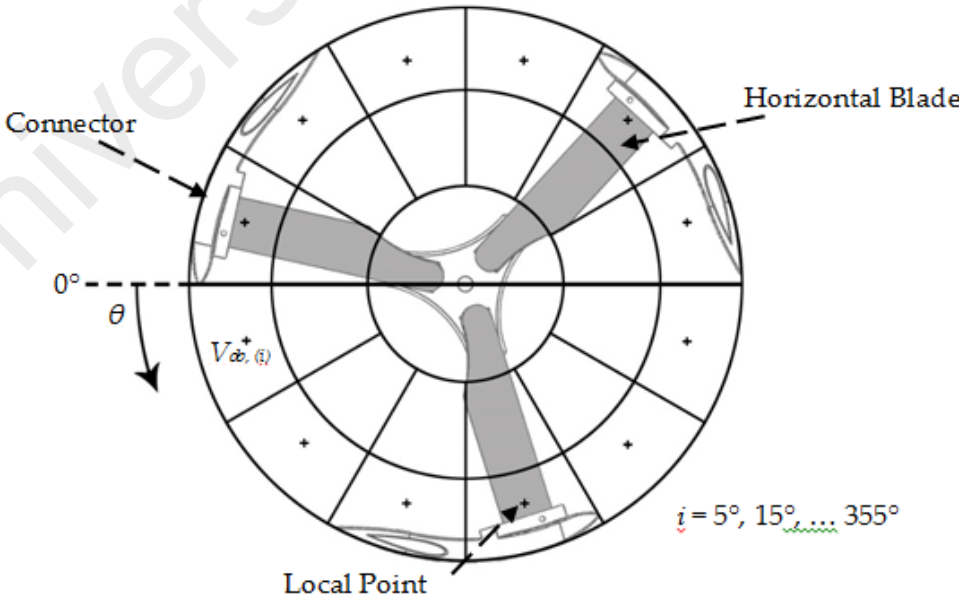

Figure 4.19: Top view of the CAWT showing local points

In the proposed approach, the axial (a) and angular induction factors (a′) are assumed to be functions of the radius of the wind turbine, R. The lift and drag force are perpendicular and parallel to the relative wind of the horizontal blade, V_{Rb}. Moreover, by using trigonometrical method, the vector velocity triangle can be obtained as shown in Figure 4.20.

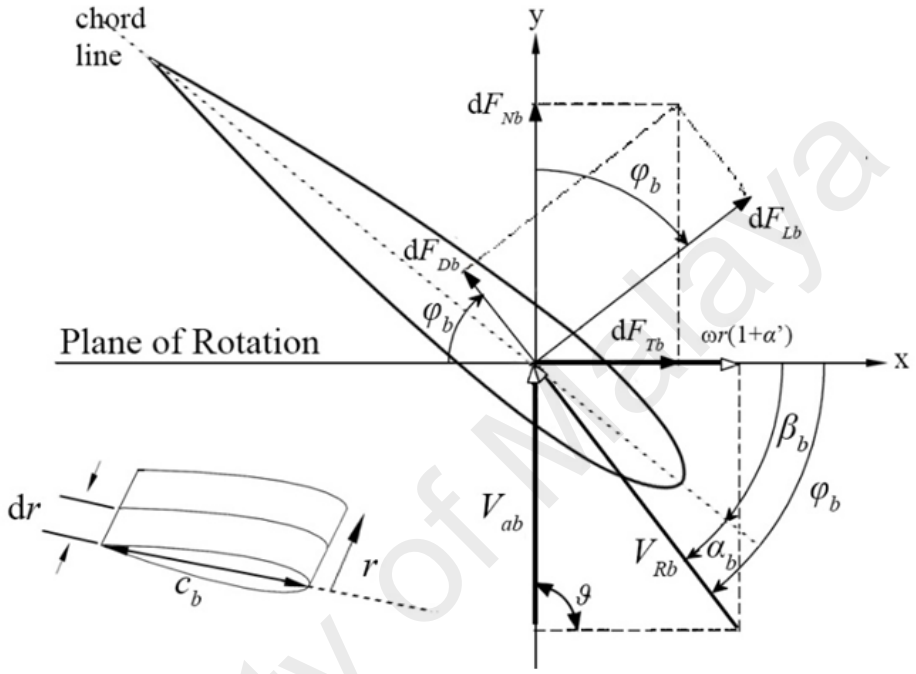

Figure 4.20: Blade geometry for analysis of a horizontal blade of the CAWT

The relative wind is the vector sum of the induced wind velocity at the horizontal blade, V_{ab}, and the wind velocity due to rotation of the blade, $\omega r(1 + a')$. The relationship of the various angles, forces, and velocities at the horizontal blade of the CAWT is shown by the blade geometry in Figure 4.20. The angle between the chord line and the plane of rotation is called the pitch angle of the horizontal blade (β_b), and the angle between the chord line and the relative wind is called the angle of attack (α_b), and the sum of the pitch angle and the angle of attack gives the angle of the relative wind;

$$\varphi_b = \beta_b + \alpha_b \tag{4.2}$$

The relationship between the angle of the relative wind and the angular speed of the horizontal blade can be determined from Figure 4.20;

$$\tan \varphi_b = \frac{V_{ab}}{\omega r(1+a')} = \frac{V_{ob}(1-a)}{\omega r(1+a')} = \frac{1-a}{(1+a')\lambda_{rb}} \tag{4.3}$$

Where, λ_{rb} is the local tip speed ratio, and V_{ob} is the resultant wind velocity approaching the horizontal blade. The incremental lift and drag forces are given by;

$$dF_{Lb} = \frac{1}{2} C_l \rho {V_{Rb}}^2 c_b dr \tag{4.4}$$

$$dF_{Db} = \frac{1}{2} C_d \rho {V_{Rb}}^2 c_b dr \tag{4.5}$$

The incremental force normal to the plane of rotation (contributes to thrust), and the incremental force tangential to the circle swept by the horizontal blades (contributes to torque), are given by:

$$dF_{Nb,i} = dF_{Lb} \cos \varphi_b + dF_{Db} \sin \varphi_b \tag{4.6}$$

$$dF_{Tb,i} = dF_{Lb} \sin \varphi_b - dF_{Db} \cos \varphi_b \tag{4.7}$$

If B is the number of blades, then the total normal force on the horizontal blade at a distance, *r*, from the hub and at an azimuthal position of θ is given by;

$$dF_{Nb,i} = \frac{1}{2} B \rho {V_{Rb}}^2 (C_l \cos \varphi_b + C_d \sin \varphi_b) c_b dr \tag{4.8}$$

Whereas, the differential torque due to the tangential force acting at a distance, *r*, from the hub with respect to azimuth angle, θ can be expressed as;

$$dQ_{b,i} = B r dF_{Tb,i} = \frac{1}{2} B \rho {V_{Rb}}^2 (C_l \sin \varphi_b - C_d \cos \varphi_b) c_b r dr \tag{4.9}$$

By integrating Equation 4.9 over a known distance, $r - r_h$, the torque contributed by the horizontal blade can be calculated. The torque produced by the horizontal blade at each azimuth angle can be obtained by applying the conservation of momentum and the aerodynamic properties of the airfoil (i.e. lift and drag coefficients), together with calculating the local wind velocity. Therefore, the total torque is obtained by adding all the instantaneous torques at the selected blade segment and azimuthal positions.

4.6.3 Combined DMST and BEM models for CAWT

As stated earlier, NACA 0015 was chosen for both the horizontal blades and the vertical blades. The NACA 0015 data was obtained from (AID Airfoil Investigation Database; Sheldahl & Klimas, 1981) for Reynolds number of 2.5 x 10^4 for both he horizontal blades and vertical blade. The characteristic of airfoils beyond the stall angle was predicted using the model where all airfoils essentially have the same characteristics as a flat plate. For the case of the induction factors, it is assumed that the models described in previous sections have no wake rotation, therefore the value of radial induction factor is $a' = 0$, and the axial induction factor, a is assume as 1/3 at all conditions for both models. This is the optimum value of axial induction factor where the flow is decelerated to 2/3 and 1/3 of its original free-stream velocity at the rotor disc and in the far wake, respectively (Geurts et al., 2010). Finally, the theoretical power generated by the CAWT for a specific λ is simply the sum of the power contributions by the Vertical (DMST) and horizontal (BEM) blades of the turbine:

$$P_{THEORETICAL} = P_{DMST} + P_{BEM} = \omega(Q_a + Q_b) \quad (4.10)$$

4.7 Numerical simulation for the roof models

In industry and cutting-edge research, ANSYS Fluent software is regularly utilized in the area of numerical simulation because of the broad scope of displaying physical modeling techniques, time effective solution and accurate numerical results (Shahizare et al., 2016).

4.7.1 Computational fluid dynamics simulation

This section describes 2D computational fluid dynamics (CFD) calculation on the turbulence separation over the gable and vaulted building models, carried out with the commercial code Fluent 16.1. The CFD gives an insight into the flow patterns that are difficult, and expensive to study using experimental methods. The choice of the method used is generally made based on the details of the flow to be obtained and the

computing resources available (Ledo et al., 2011). The building model for the CFD calculation has a height of 1.36 m and a width of 0.74 m. The flow-solver is based on the two-dimensional Reynold Average Navier-Stokes equations (RANS), which formulate the principles of conservation of mass, momentum and energy in the form of partial differential equation.

The shear stress transport (SST) k-ω turbulence model was used in the simulation because this model could produce more accurate and reliable results (ANSYS Fluent 14.0 User's Guide). The SST k-ω model is also known to have reduced sensitivity to far field values of turbulence frequency, ω, and a more balanced performance for a wide range of flow types compared to other general purpose two equation model, as demonstrated by (Menter et al., 2003). The discretization is carried out with the first-order upwind scheme and the velocity-pressure flow field is determined using the SIMPLE model (Fluent 5 User's Guide 2). This is due to the computational efficiency, and robustness in iterating the coupled parameters.

The buildings are modelled with the dimensions 1.45 m (L) × 0.74 m (W) × 1.36 m (H), which is the same size as the prototype. The pitch angle for the case of the gable roof was 35° (Figure 4.11). In the simulation only wind velocity, the pressure profile and turbulence intensity on the two building models were considered. The roughness level of the roof surface was ignored. Wind flow around buildings has been previously model using the computational fluid dynamic (CFD) methods (Abohela et al., 2011; Ledo et al., 2011; Ozmen et al., 2016).

4.7.2 Modelled parameter

As stated above, the height of the building is 1364 mm. The wind direction is 0^{o} perpendicular to the main axis of the building and the inlet wind speed is 4.5 m/s. Using the Fluent 16.2 program, the physical properties of the flow have been defined,

turbulence model have been selected; analysis technique and the number of iterations and convergence values have been determined by entering the values of the boundary conditions.

4.7.3 Governing equations

In the analysis of turbulent flow, standard k-ω turbulence model has been used with logarithmic surface function. Momentum equation, x and y components of velocity, and turbulent kinetic energy (k) was solved by using this program. Simple analysis algorithm has been used in calculating the pressure and velocity distributions. The equation of mass and momentum, turbulence kinetic energy and turbulence dissipation rate are expressed as;

Continuity equation:

$$\frac{\partial}{\partial x_j} + \left(\rho \, . \, u_j\right) = 0 \tag{4.11}$$

Momentum equation:

$$\frac{\partial}{\partial t}(\rho\vec{v}) + \nabla \, . \, (\rho\vec{v}\,\vec{v}) = -\nabla P + \nabla \, . \, \bar{\bar{\tau}} + \rho\vec{g} + \vec{F} \tag{4.12}$$

Where p is the static pressure, $\vec{v}$ is the velocity component, $\rho\vec{g}$ and $\vec{F}$ is the gravitational body force and external body forces (that arises from interaction with the dispersed phase) respectively. $\vec{F}$ Contains other model-dependent source terms such as porous-media and user-defined sources and τ is the stress tensor given by

$$\tau = \mu\left(\nabla\vec{v} + \nabla\vec{v}^{T} - \frac{2}{3}\nabla \, . \, \vec{v}\, I\right) \tag{4.13}$$

Where μ is the molecular viscosity, I is the unit tensor.

The following transport equation is use to obtain the turbulence kinetic energy, k.

$$\frac{\partial}{\partial t}(\rho k) + \frac{\partial}{\partial x_i}(\rho k U_i) = \frac{\partial}{\partial x_j}\left[\left(\mu + \frac{\mu t}{\sigma k}\right)\frac{\partial k}{\partial x_j}\right] + G_k + G_b + -\rho\varepsilon - Y_M + S_K \tag{4.14}$$

And the turbulence dissipation rate

$$\frac{\partial}{\partial t}(\rho\varepsilon) + \frac{\partial}{\partial x_i}(\rho\varepsilon U_i) = \frac{\partial}{\partial x_j}\left[\left(\mu + \frac{\mu t}{\sigma\epsilon}\right)\frac{\partial k}{\partial x_j}\right] + C_{1\varepsilon}\frac{\varepsilon}{K}(G_K + C_{3\varepsilon}G_b) - C_{2\varepsilon}\rho\frac{\varepsilon^2}{K} + S_\varepsilon \quad (4.15)$$

Where G_k represents the generation of turbulence kinetic energy due to mean velocity gradients, and $C_{1\varepsilon}$, $C_{2\varepsilon}$, σk and $\sigma\epsilon$ are constant (ANSYS Fluent User's Guide Released 14.0 ANSYS Inc.).

4.7.4 Computational mesh

A mesh independence study was carried out for the two roof shapes to determine the dependence of the flow field on the refinement of the mesh. Grid types on solution domain are performed near the building model with increasing intensity as shown in Figure 4.21 and Figure 4.22 respectively. The meshes are highly denser to capture the complex flow structure with lower expected error. To ensure attainment of grid-independent results, sensitivities of both grid numbers and grid distributions are tested and the mesh used is refined for the building models. The buildings are modelled with the dimensions 1.45 m (L) × 0.74 m (W) × 1.36 m (H), which is the same size as the prototype. The domain size for the CFD simulation for both roof models is (H) 10000 and (L) 28000 mm. The pitch angle of the gable roof was 35° (Figure 4.11). In the simulation, the inlet wind speed was set as 4.5 m/s, this is to perform the simulation under the same condition as the experiment where the wind speed used for the actual test is 4.5 m/s.

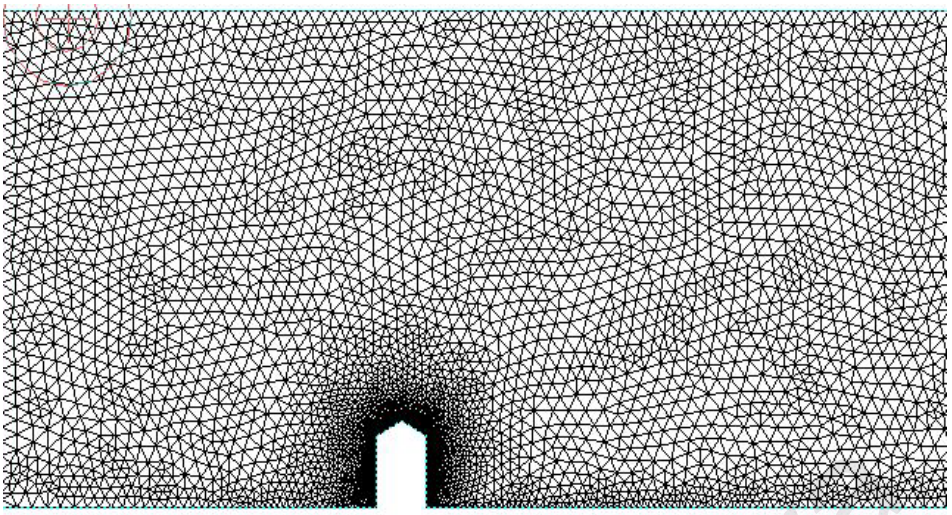

Figure 4.21: Mesh refinement area around the gable shape

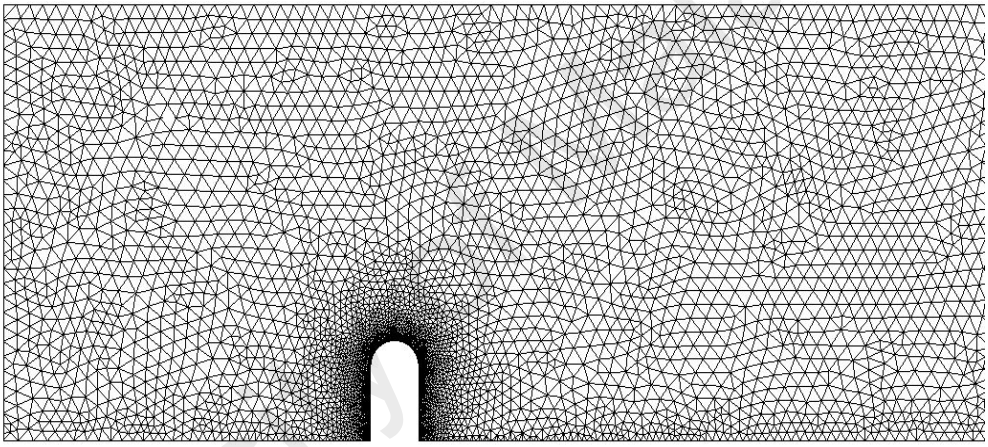

Figure 4.22: Mesh refinement area around the vaulted roof shape

4.8 Soft computing methodology for the performance prediction of power augmented VAWT

4.8.1 Adaptive neuro-fuzzy application

Adaptive neuro-fuzzy inference system (ANFIS) can be used as a basis for constructing a set of fuzzy 'IF-THEN' rules with an appropriate membership to generate the stipulated input-output pairs. In this study, the ANFIS system that is functionally equivalent to the first-order Sugeno fuzzy model was used. A typical rule set with a fuzzy 'IF-THEN' rule can be expressed as:

$$\text{if } x \text{ is } A \text{ then } f_1 = p_1 x + t \tag{4.16}$$

The ANFIS architecture for three inputs of x, y and z (wind speed, time, and PAGV) is shown in Figure 4.23. Nodes at the same layer have the same purposes. $O_{l,i}$ denotes the output of the ith node in layer 1. The input variable membership functions (MFs) is in the first layer, which supply the next layer with the input values. The adaptive node can be a function of:

$$O_{l,i} = \mu(x, y, z)_i \text{ for } i = 1,2 \tag{4.17}$$

Where $x, y =$ ith node input and m $\mu(x, y, z)_i$ = embership functions.

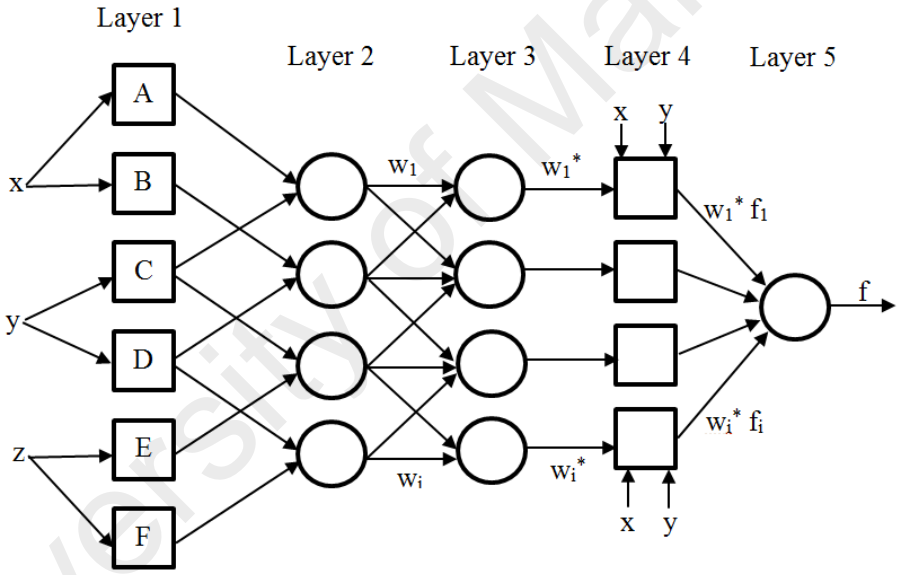

Figure 4.23: Three inputs, one output and two rules ANFIS structure

The MFs can be defined by a bell-shaped function:

$$f(x; a, b, c) = \frac{1}{1+\left(\frac{x-c}{a}\right)^{2b}} \tag{4.18}$$

Where $\{a, b, c\}$ is the parameter set.

The second layer (membership layer) sends the product out after it multiplies the incoming signals from the first layer. The output of every single node signifies the firing power of a rule or weight:

$$O_{2,i} = w_i = \mu(x)_i \cdot \mu(x)_{i+1}\ ,\ i = 1,2 \tag{4.19}$$

The rule layer which is the third layer is non- adaptive, in this layer, The ratio of the rule's firing strenght to the sum of all rules' firing strenght is calculated by every node i:

$$O_{3,i} = w_i^* = \frac{w_i}{w_1 + w_2}, \text{ where } i = 1,2 \tag{4.20}$$

This layer's output is called normalized firing strengths or normalized weights. The defuzzification layer which is the fourth layer provides the output values which results from the inference rules, where each node i is an adaptive node with node function.

$$O_{4,i} = w_i^* \cdot f_i = w_i^*(p_i x + q_i y + r_i) \tag{4.21}$$

Where $\{p_i, q_i, r_i\}$ is consequent parameters.

The classification results of the fuzzy were converted into a crisp output after all the inputs from the fourth layer is sums up by the fifth layer. The overall output of all the incoming signals was computed by the node in the fifth layer which is no adaptive;

$$O_{5,i} = \sum_i w_i^* \cdot f_i = \frac{\sum_i w_i \cdot f_i}{\sum_i w_i} \tag{4.22}$$

4.8.2 Evaluation of model performances

To assess the performance of the developed ANFIS model, the following statistical indicators are utilized:

(a) Root-Mean-Square Error (RMSE)

$$\text{RMSE} = \sqrt{\frac{\sum_{i=1}^{n}(O_i - P_i)^2}{n}} \tag{4.23}$$

(b) Coefficient of Determination (R^2)

$$R^2 = \frac{\left[\sum_{i=1}^{n}(O_i - \bar{O}_i)\cdot(P_i - \bar{P}_i)\right]^2}{\sum_{i=1}^{n}(O_i - \bar{O}_i)\cdot\sum_{i=1}^{n}(P_i - \bar{P}_i)} \tag{4.24}$$

$$r = \frac{n(\sum_{i-1}^{n} O_i - P_i) - (\sum_{i-1}^{n} O_i).(\sum_{i-1}^{n} P_i)}{\sqrt{(n\sum_{i-1}^{n} O_i^2 - (\sum_{i-1}^{n} O_i))^2 . (n\sum_{i-1}^{n} P_i^2 - (\sum_{i-1}^{n} P_i))^2}} \quad (4.25)$$

Where O_i is the predicted value by ANFIS technique, P_i is the measurement value. $\overline{O}_i$ is the mean values of O_i, $\overline{P}_i$ is the mean values of P_i, and n is the total number of test data. It should be noted that the smaller values of RMSE represent further accuracy in the predictions and in an ideal case it is zero. Also, the R^2 ranges between 0 and +1. The R^2 values around +1 indicates that there is a perfect linear relationship between the estimated values and measured ones whereas R^2 around zero shows that there is no linear relationship.

4.8.3 Experimental study of the PAGV

Using a drag type Sistan rotor wind turbine, a test was performed for the small scale PAGV device with the geometry and measurements as shown in Figure 4.24 to ascertain the possibility of incorporating the wind turbine with the PAGV. The experiments were performed for the following cases: (i) the case where the wind turbine is integrated with the PAGV and, (ii) the case without the PAGV. Three industrial fans were arranged in parallel to generate the wind stream. Two different experiments were conducted with two different average wind speeds. The first experiment was conducted using a wind speed of 4.24 ms^{-1} and the second experiment was conducted using a wind speed of 4.63 ms^{-1}. The wind rotor performance was measured using the laser tachometer over time, and a continuous measurement of the rotational speed was carried out until the data stabilized.

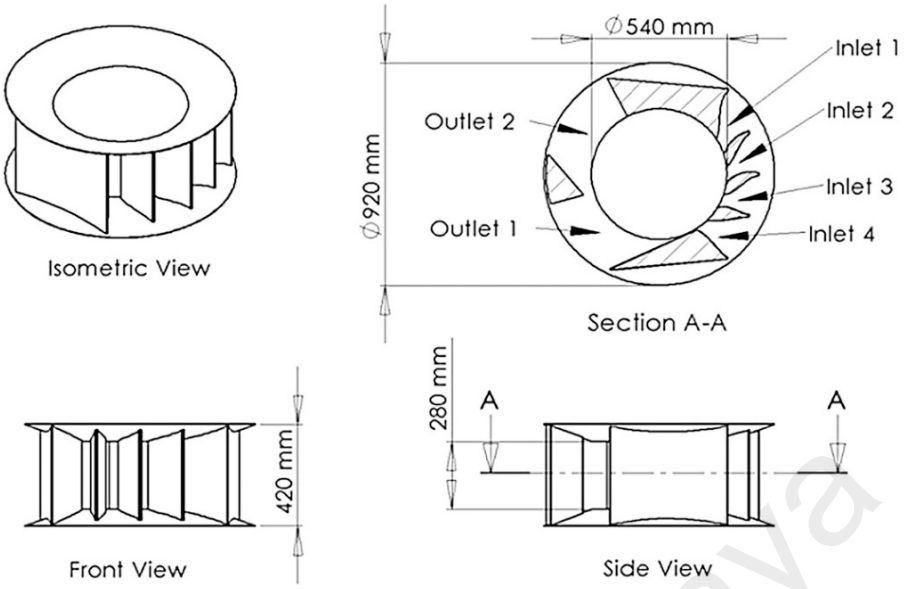

Figure 4.24: Fabricated PAGV model with dimensions (Chong et al., 2013)

4.8.3.1 Sistan rotor

Sistan rotors produce mechanical energy from the conversion of wind kinetic energy by using the drag principle. As shown in Figure 4.25 the oncoming air hits the surface of a Sistan rotor blade, S at velocity of V_0. Thus, the extractible power from the Sistan rotor using the principle of the drag force can be expressed as:

$$P_S = F_D V_S \tag{4.26}$$

Where F_D is the drag force and V_S is the wind surface velocity. The drag force produced by the Sistan rotor can be calculated as follows:

$$F_D = C_d \frac{\rho}{2} (V_0 - V_S)^2 S \tag{4.27}$$

Where C_d is the coefficient of drag of the blade, by combining Equations 4.26 and Equations 4.27, the resultant power extracted at 0^o azimuth angle from this wind turbine can be expressed as:

$$P_S = C_d \frac{\rho}{2} (V_0 - V_S)^2 S V_S \tag{4.28}$$

Using Equation 4.28, the various azimuth angles can be calculated as:

$$P_S = C_d \frac{\rho}{2} S\left(\overrightarrow{V_0} - \overrightarrow{V_S}\right)^2 \cdot \overrightarrow{V_S} \tag{4.29}$$

By summing up all the power extracted from the Sistan rotor at every azimuth angle in a single blade revolution, the average power extracted $P_{S(avg)}$ can be calculated from the Equation 4.30 as;

$$P_{S(avg)} = \frac{1}{2\pi} \sum_{i=0}^{2\pi} \left\{ C_d \frac{\rho}{2} S\left(\overrightarrow{V_{0_i}} - \overrightarrow{V_{S_i}}\right)^2 \cdot \overrightarrow{V_{S_i}} \right\} \tag{4.30}$$

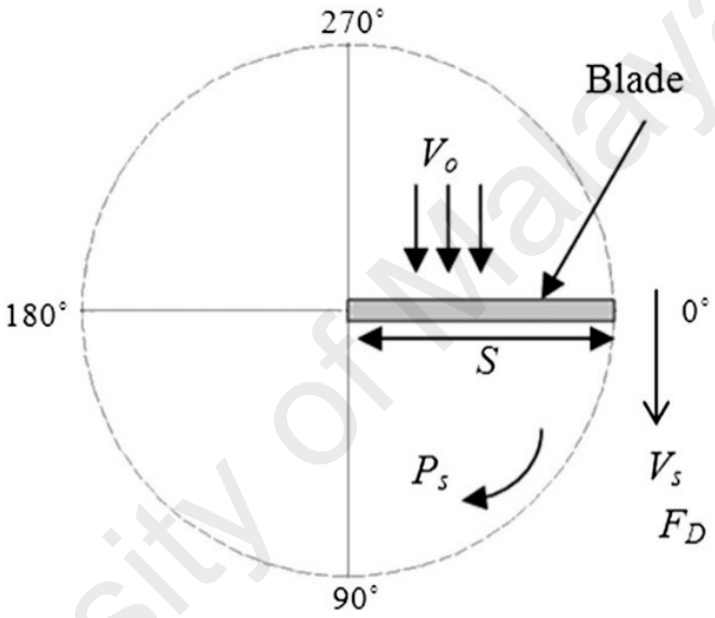

Figure 4.25: Single-bladed Sistan rotor

It should be noted that in Equation 4.30 the assumption was made that the blade is purely driven by the air drag force. No other aerodynamic behavior such as the turbulence flow and edge vortex generated after the moving fluid interacts with the Sistan rotor blade were considered. Through the use of computational fluid dynamics (CFD) software, the average power extraction and behavior of the VAWT can be simulated and predicted.

CHAPTER 5: RESULT AND DISCUSSION

5.1 Selection of wind turbine mounting location on the rooftop

Experiments were conducted in order to select the mounting location of the CAWT on the building with gable and vaulted rooftop. These mounting location includes the top corner of the rooftop (location A), and the top center of the rooftop (location B).

5.1.1 Mounting location on the gable rooftop

To identify the suitable location for the mounting of CAWT on the gable rooftop, experiments were conducted with the CAWT mounted at position A (top corner) and position B (top center) on the gable rooftop. The CAWT was mounted above the rooftop at a varying distance, *Y* i.e. *Y* = 100 mm; 150 mm; 200 mm; and 250 mm for each of the above mention locations. The wind speed used for the testing of the CAWT at these two locations is averaged wind speed of 4.5 m/s.

Figure 5.1 (a, b, c, and d) present the coefficient of power, C_p against the tip speed ratio, TSR (λ) of the CAWT mounted at position (A), and position (B) on the gable rooftop for *Y* = 100 mm, 150 mm, 200 mm, and 250 mm. The Figures demonstrated that position B which is the center position is more suitable for the mounting of the CAWT on the gable rooftop. The results showed that at *Y* = 100 mm the maximum C_p obtained by the CAWT mounted at location B is 0.115 at TSR (λ) of 1.13. In comparison, the maximum C_p obtained by the CAWT mounted at position A is 0.099 at TSR (λ) of 1.12. This indicates that mounting CAWT at position B would yield 16% more power compared to position A. This observation is the same for all condition of height where mounting of the CAWT at position B outperforms it performance at position A. For *Y* = 150 mm; 200 mm; and 250 mm, Figure 5.1 (b, c, and d) where the coefficient of power of the CAWT mounted at position B increases by 11.4%, 10,9% and 5.3% respectively. The improved performance of CAWT at the center location (position B) is due to the

larger surface area at the center, this larger surface area have higher concentration power than the position A, (top corner position). The result obtained is in agreement with Cochran & Damiani (2008). According to Cochran & Damiani (2008) the strongest wind locations for the case of the pitch roof are the center location.

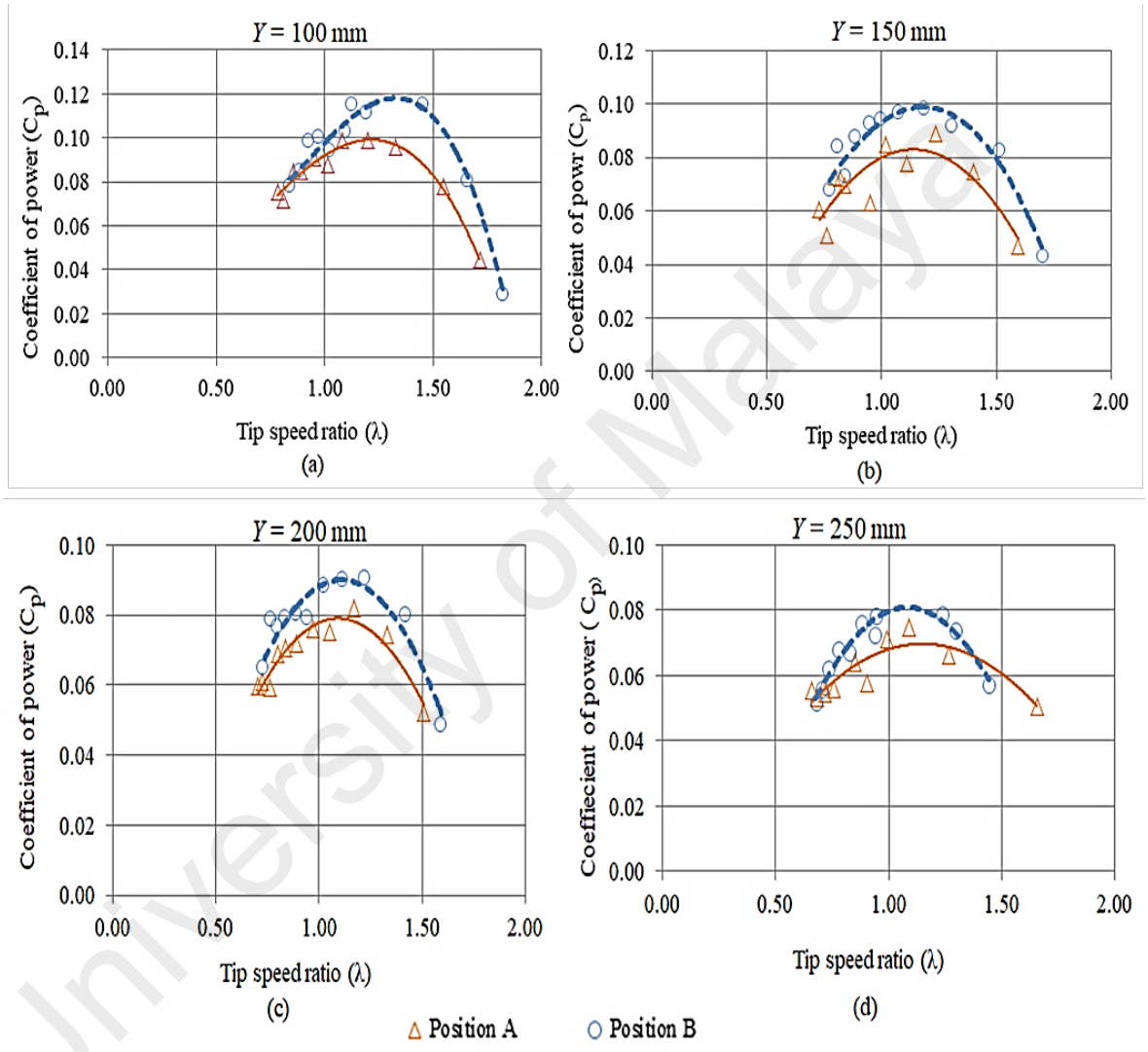

Figure 5.1: Coefficient of power against tip speed ratio for CAWT on the gable rooftop for (a) *Y* = 100 mm; (b) *Y* = 150; mm, (c) *Y* = 200 mm; and (d) *Y* = 250 mm

5.1.2 Mounting location on the vaulted rooftop

Similarly, experiments were conducted to select the mounting position of the CAWT on the vaulted rooftop. Two locations were investigated; position A which is the top corner location and position B is the top center position where the wind turbine is

mounted. The height of CAWT was varied from *Y*= 100 mm, 150 mm, 200 mm, and 250 mm. and the average wind speed used for this study is 4.5 m/s. The result is presented in Figure 5.2.

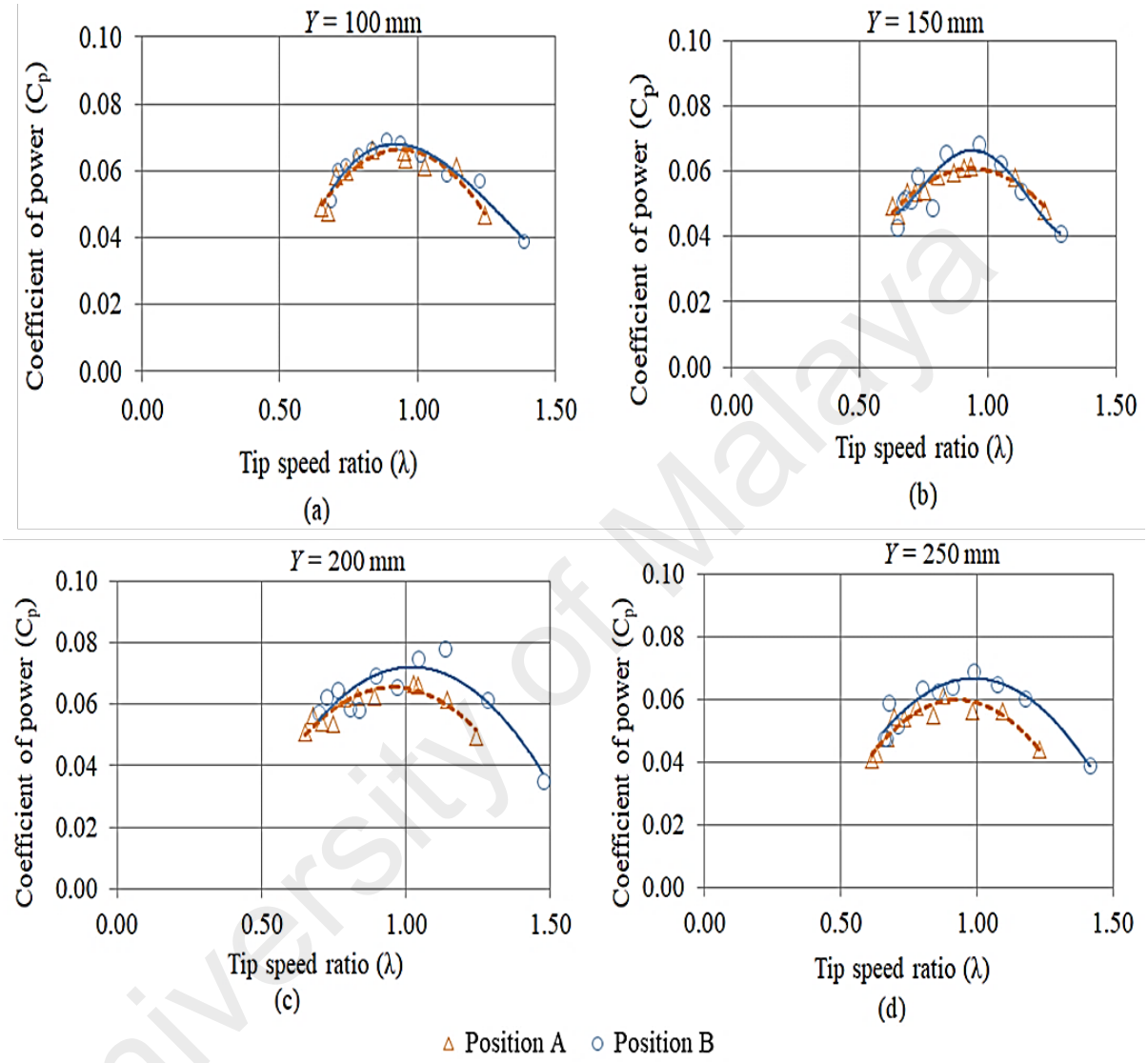

Figure 5.2: Coefficient of power against tip speed ratio for CAWT on the vaulted rooftop (a) *Y* = 100 mm; (b) *Y* = 150 mm; (c) *Y* = 200 mm; and (d) *Y* = 250 mm

Figure 5.2 (a,b, c, and d) present the C_p values against the TSR (λ) for the CAWT mounted on position A (top corner location) and position B (top center position) of the leading edge of the building with vaulted rooftop for *Y* = 100 mm, 150 mm, 200 mm, and 250 mm. From the Figures, it can be seen that CAWT has better performance when it is mounted on position B which is the top center position of the vaulted rooftop. The results showed that at *Y* = 100 mm height, Figure 5.2 (a) CAWT attain a maximum C_p

of 0.069 at TSR, (λ) of 0.89, at position B. The maximum C_p obtained by the CAWT At position A, is 0.066 at TSR (λ) of 0.83. In comparison, the power produce by CAWT mounted at position B is 5% higher compared to the power produce by the CAWT at position A. This observation is the same for all condition of height where CAWT mounted at position B outperformed its performance at position A. At *Y* = 150 mm; 200 mm; and 250 mm, the $C_{p,max}$ of CAWT mounted at position B increases by 16%, 11.5%, and 13% respectively. The improved performance of the CAWT at the center location (position B) is due to the larger surface area at the center, this larger surface area have higher concentration power than the corner location (position A).

5.2 Performance of CAWT at wind speed, V = 4 m/s, and 4.5 m/s

A range of wind speed measurement was used to test the performance of the building integrated CAWT. These wind speeds includes 4 m/s, and 4.5 m/s, and the pitch angle of the horizontal blade of the CAWT was set at 15^o. The purpose of the test is to investigate the effect of increase in wind speed in the performance of the building integrated CAWT. The experiment was conducted for four different CAWT height i.e. *Y* = 100 mm, 150 mm, and 200 mm height above the rooftop, as shown in Figure 5.3. From the figures it can be observed that the coefficient of power of CAWT increases with increase in wind speed.

Figure 5.3 (a-c) shows the performance of the CAWT integrated onto the building model at wind speed of 4 m/s. In the same figure, the performance of the CAWT at 4.5 m/s is also shown. From Figure 5.3 (a), At *Y* = 100 mm, the maximum coefficient of power, $C_{p,max}$ of the CAWT is 0.0854 at TSR, λ of 0.86. When the wind speed was increased from 4 m/s to 4.5 m/s a significant increment in the C_p values of the building integrated CAWT was observed, the C_p value of the CAWT increases from 0.0854 at TSR 0.86 to 0.1151 at TSR 1.23 which represent 35% increment for the 4.5 m/s wind

speed. The increment in the performance of CAWT at 4.5 m/s is due to the cubic power of the wind speed where the power is directly proportional to the cube root of the wind speed. Similar observation is made for each case of 150 mm, and 200 mm where the CAWT performs better at 4.5 m/s wind speed compared to the 4 m/s wind speed. From the study it was found that at the same tip speed ratio, when the wind velocity was higher, the power coefficient is better compared to the power coefficient at lower wind speed. From literature, both the thrust and the normal coefficient CN increase with increase in wind speed due to increase in the momentum of the wind (Sudhamshu, et al, 2016).

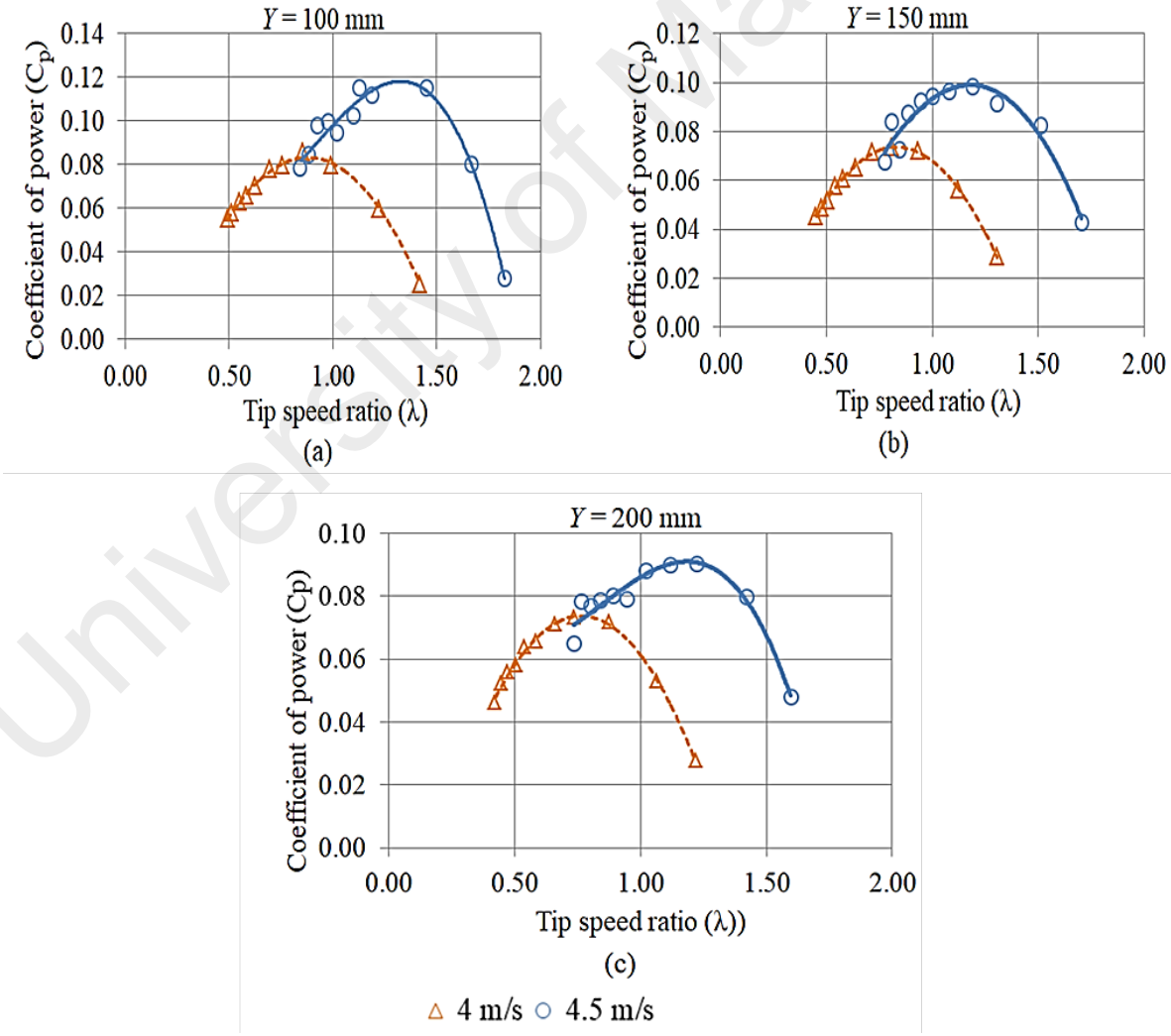

Figure 5.3: Coefficient of power against tip speed ratio for CAWT at 4 m/s, and 4.5 m/s

The free-run condition tests, which measure the rotational speeds of the CAWT until it reaches steady state conditions were carried out at wind speed 4, and 4.5 m/s as presented in Figure 5.4. Figure 5.4 (a-c) show the free-run rotational speed for the CAWT height, Y = 100 to 250 mm. Figure 5.4 (a), shows that the highest maximum rotational speed of the building integrated CAWT at wind speed of 4 m/s is 404 RPM at 222 seconds for CAWT height Y = 100 mm. When the wind speed was increased from 4 m/s to 4.5 m/s a significant increment in the RPM of the CAWT is observed. The rotational speed of the CAWT increases from 404 RPM to 507 RPM, which represent 25.5% increment in the rotational speed of CAWT at 4.5 m/s. Similarly improvement in rotational speed is also observed for each case of Y = 150 mm, and Y = 200 mm, Figure 5.4 (b and c) respectively.

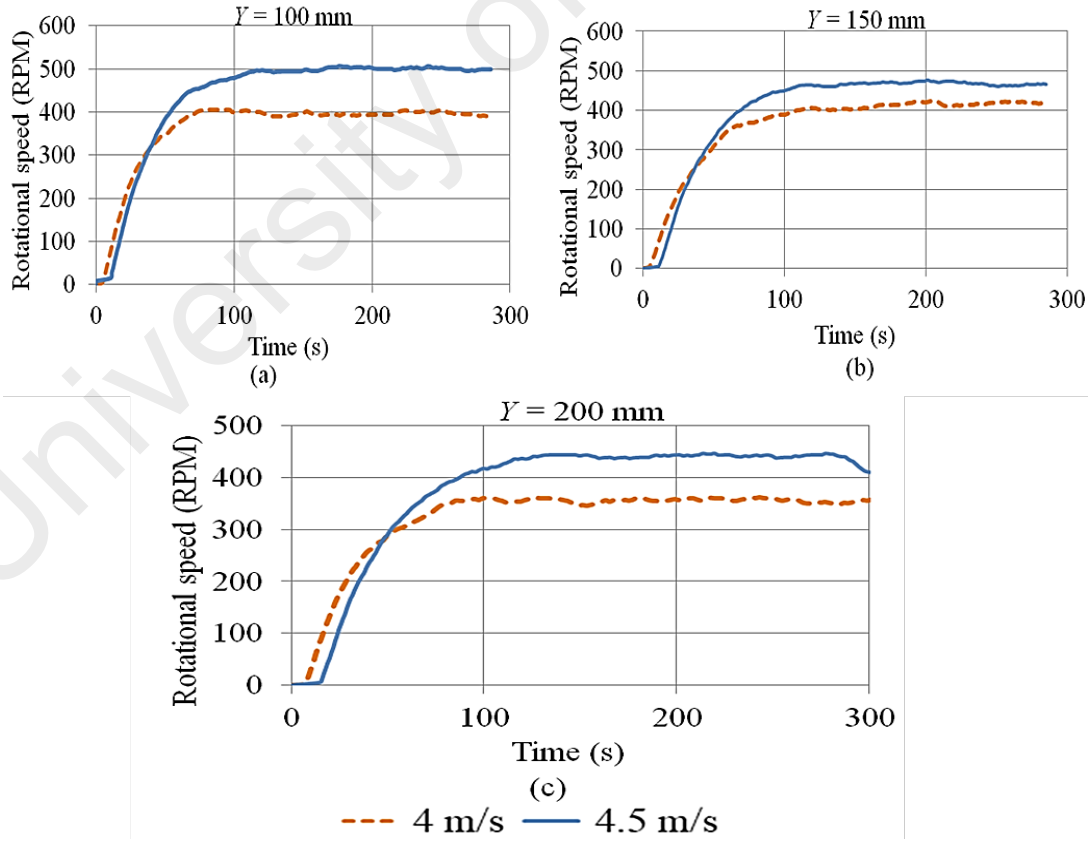

Figure 5.4: Free-run rotational speed for 4 m/s, and 4.5 m/s wind speed

5.3 Effect of pitch angle on the performance of CAWT

The role of the pitch angle is to maintain a near uniform rotor speed under different wind conditions in order to maximize the power output from the turbine. For this study the effect of the pitch angle for the horizontal blades on the performance of building integrated CAWT was investigated. The investigation cut across the two roof shapes, i.e. the gable roof shape and the vaulted roof shape. Four different pitch angles, $\beta = 0^o$, 5^o, 10^o, and 15^o at different CAWT height which also ranges from $Y = 100$ to 250 mm was investigated the wind speed was set at 4.5 m/s. The optimum pitch angle for the horizontal blade for both rooftops was selected based on this investigation for the subsequent experiments.

5.3.1 CAWT on gable rooftop

The results in this subsection are presented for different pitch angles, $\beta = 0^o$, 5^o, 10^o, 15^o of the horizontal blades of the CAWT. The height of the CAWT above the gable rooftop was varied for $Y = 100$ to 250 mm. Figure 5.5 (a-d) shows the C_p values against the TSR for the CAWT mounted on gable rooftop. The graph indicates that the 10^o pitch angle of the horizontal blades produced the highest C_p values among other pitch angles. The maximum C_p value obtained for the 10^o pitch angle, Figure 5.5 (a) at CAWT height, $Y = 100$ mm, is, $C_{p,max} = 0.1263$ at a TSR (λ) of 1.06. Similar improvement in power output of the CAWT at 10^o pitch angle is also noticed for the other height configurations i.e. $Y = 150$-250 mm height where the CAWT with 10^o pitch angle of the horizontal blades outperformed other pitch angles. Therefore, the 10^0 pitch angle is considered as the optimum pitch angle of the horizontal blade for the CAWT.

Furthermore, at $Y = 100$ mm, when the pitch angle was increased from the optimum value i.e.10^o to 15^o pitch angle, the C_p, max decreases by 10%, similarly when the pitch angle was decreased from the optimum value to 5^o pitch angle the $C_{p,max}$ further

decreases by 45%, and 94.5% for the 0^o pitch angle. The graphs in all other CAWT height configurations i.e. Y = 150-250 mm shows a decrease in the C_{pmax} when the pitch angle of the horizontal blade is either increase above the optimum value or decreases below the optimum value. Although, compared to the 0^o, and 5^o pitch angle, the 15^o pitch angle for the horizontal blades performs better.

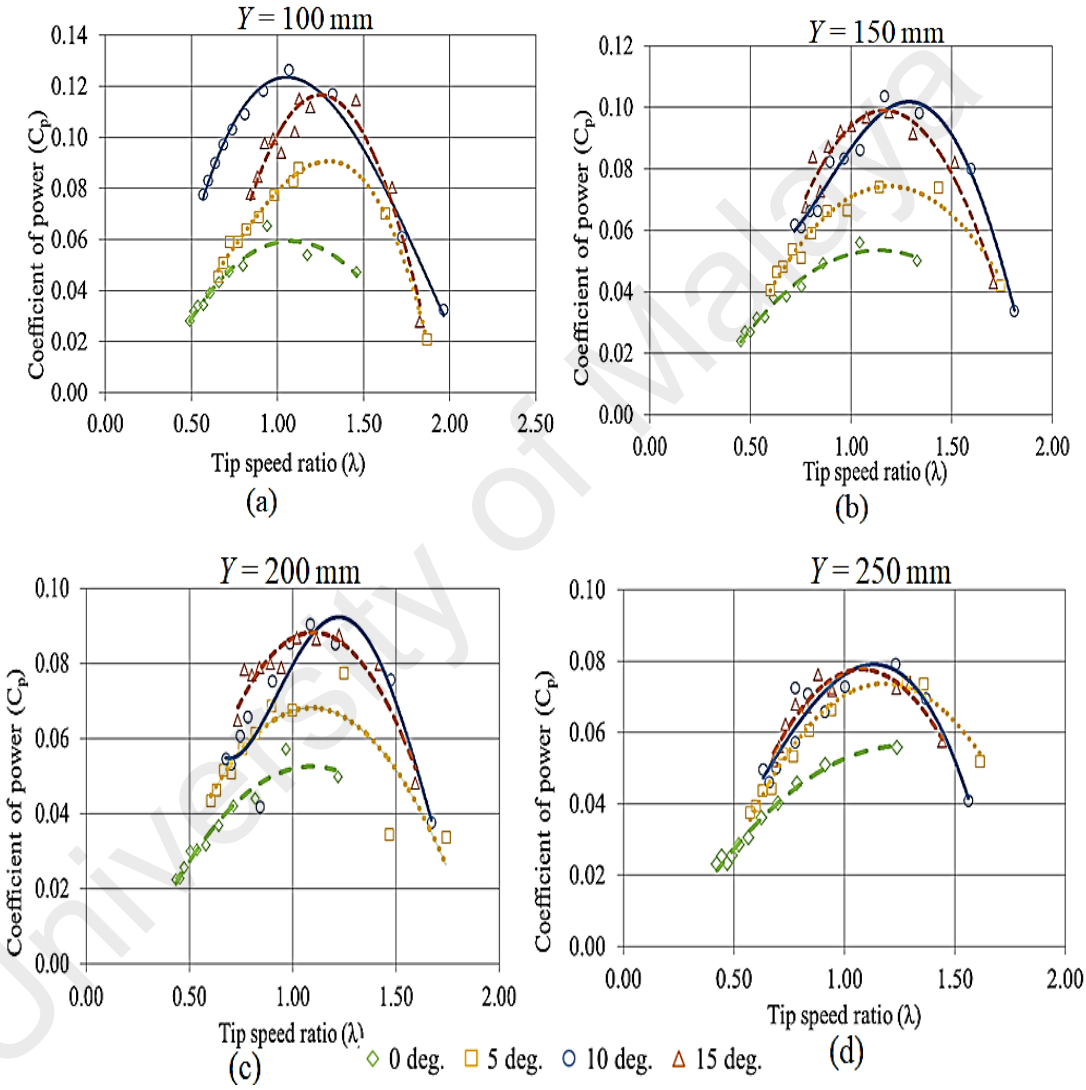

Figure 5.5: Coefficient of power against Tip speed ratio for CAWT at different pitch angle on the gable rooftop for (a) *Y* = 100 mm, (b) *Y* = 150 mm, (c) *Y*= 200 mm, and (d) *Y*= 250 mm

The distribution of the coefficient of power along the TSR for the entire pitch angle is similar to that of the optimum pitch angle, i.e.10^o. The higher the pitch angle the easier the wind turbine gets starts to rotate. Higher pitch angles exposes the horizontal

blades to the optimum angle of attack of the deflected wind stream therefore increasing the lift force and maximizing the torque produced by the blades. Using blade pitch angle higher than the optimum pitch angle can effectively reduce the mean load on the turbine while still permitting significant power extraction (de Jesus Henriques et al. 2016).

The experimental results indicates that the pitch angle of the horizontal blades is very vital in determining the optimum angle of attack during operation where the horizontal blades with the higher pitch angle delivered better performance in terms of the coefficient of power and also the tip speed ratio.

5.3.2 CAWT on vaulted rooftop

The results in this subsection are presented for different pitch angles, $\beta = 0^o$, 5^o, 10^o, and 15^o for the case of the CAWT mounted on the vaulted rooftop. The experiment was conducted for different CAWT height configuration for Y = 100 to 250 mm. Figure 5.6 shows the C_p values against the TSR for the various pitch angles tested. It can be seen from Figure 5.6 (a), that at Y = 100 mm height the 5^o pitch angle produced the highest C_p value compared to the other pitch angles. The maximum coefficient of power produced by the 5^o pitch angle is, $C_{p,max} = 0.117$ at a TSR of 1.65. However, this result is not consistent with the other heights i.e. Y = 150-250 mm. For these heights of CAWT, the 10^o pitch angle has better performance where the CAWT with the 10^o pitch angle of the horizontal blades outperformed other pitch angles of the horizontal blades. The 15^o pitch angle also has better performance compared to 0^o and 5^o pitch angles at theses heights. This suggests that the drag decreases with increase in pitch angle due to reduction in the horizontal blade airfoil's frontal area that interacts with the deflected airflow (Sudhamshu et al., 2016). Therefore, for the case of integrating CAWT on the vaulted rooftop, 10^o pitch angle is considered the optimum pitch angle for the horizontal blade of the CAWT.

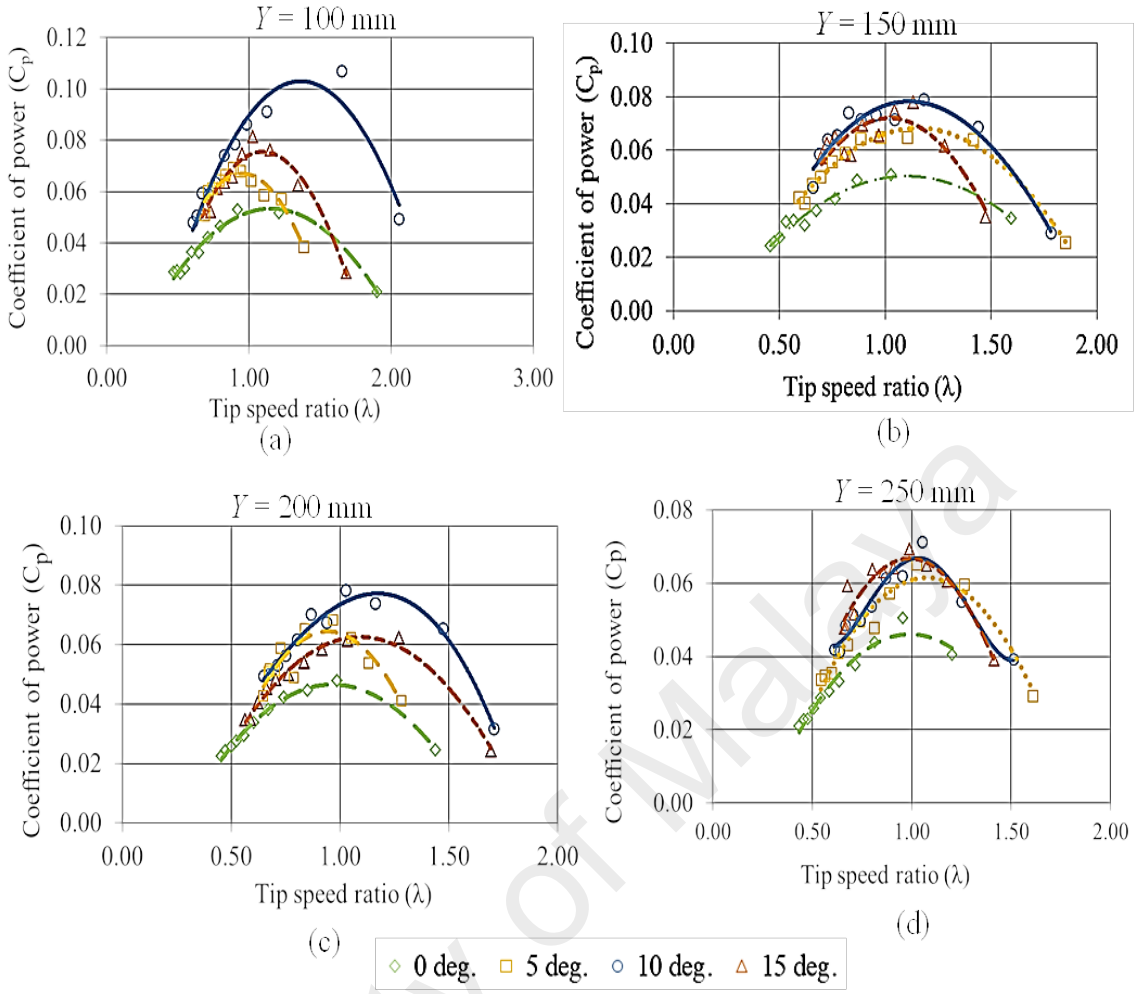

Figure 5.6: Coefficient of power against Tip speed ratio for CAWT at different pitch angle on the vaulted rooftop for (a) *Y* = 100 mm, (b) *Y* = 150 mm, (c) *Y* = 200 mm, and (d) *Y* = 250 mm

de Jesus Henriques et al. (2016) investigated the effect of pitch angle on the performance of model horizontal axis tidal stream turbine operating under wave current interaction, they concluded that the highest mean power is obtained at optimum pitch angle of 6^{o}, and increasing the pitch angle above the optimum can caused greater reduction in the coefficient of power, and associated decrease in turbine rotational speed, they infer that the changes in blade pitch angle can be used as a mechanism for reducing the loading on a HATT when operating with excessive wave-induced load, while still enabling a significant amount of the available power in the unsteady tidal stream to be extracted. Strom et al. (2015) reported that the conversion efficiency of a cross flow turbine increases from 5.4% with zero preset pitch angle to 18.2% at the

optimum pitch angle for a two-bladed case and from 8.8% to 14.0% for the four-bladed case.

5.4 Performance comparison between CAWT and VAWT on gable rooftop

After selecting the mounting position and pitch angle through an experimental study, a comparative study was performed for the performance of CAWT and VAWT on the gable rooftop. The heights of the two turbines (CAWT and VAWT) above the rooftop were varied for four different heights i.e. Y = 100 mm, 150 mm, 250 mm, and 250 mm and at an averaged wind speed of 4.5 m/s and for 10^o pitch angle of the horizontal blade. Both the CAWT and the VAWT are subjected to similar experimental conditions. For each case, the performance of the two turbines was evaluated based on the maximum, C_p. maximum RPM, and TSR, (λ).

5.4.1 Variation of height above the gable rooftop

The height of CAWT, and conventional straight bladed VAWT integrated onto a building with gable rooftop were varied for Y = 100 mm, 150 mm, 200 mm, and 250 mm above the gable rooftop. Figure 5.7 (a, b, c, and d) compares the C_p values between the building integrated CAWT and the conventional straight bladed building integrated VAWT at turbine height Y = 100 to 250 mm. Results showing similar trend of increasing in C_p with increase in TSR is shown in Figure 5.7 (a-d). Figure 5.7 (a) show the coefficient of power against the tip speed ratio of the CAWT and the VAWT placed at Y = 100 mm height above the rooftop of the building. The graph indicates that the coefficient of power of both the CAWT and the VAWT increases with increase in TSR, the Cp values of both turbines reaches it maximum value at optimum TSR and then decreases with increase in TSR. Based on the results obtained in Figure 5.7 (a), the CAWT is able to attain a maximum C_p of 0.1263 at a TSR (λ) of 1.1. The maximum C_p of the conventional straight bladed VAWT integrated on the same rooftop of a building

and subjected to similar experimental conditions is 0.0345 at a TSR (λ) of 0.59. The result shows that the $C_{p,max}$ for the CAWT increased by 266% compared to the straight bladed VAWT as shown in Table 5.1.

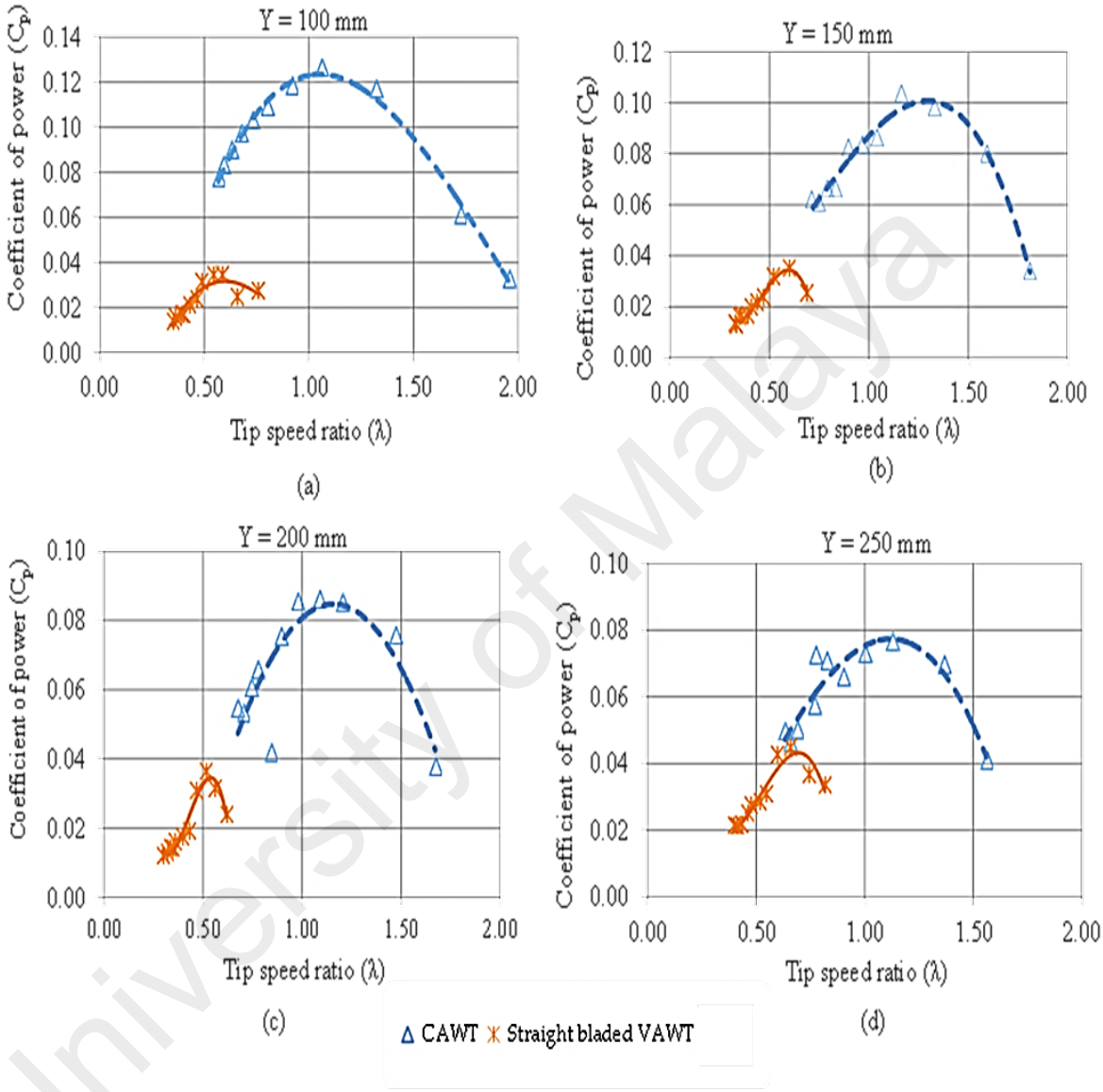

Figure 5.7: Coefficient of power against tip speed ratio for CAWT and straight bladed VAWT at various heights above the gable rooftop: (a) *Y* = 100 mm; (b) *Y* = 150 mm; (c) *Y* = 200 mm; and (d) *Y* = 250 mm.

Figure 5.7 (b) compares the C_p values between the CAWT and the straight bladed VAWT placed at *Y* = 150 mm height above the building model, the result showed that the $C_{p,\,max}$ recorded by the CAWT at *Y* = 150 mm height is 0.1035 at a TSR (λ) of 1.16 higher than the $C_{p,max}$ value recorded by the straight bladed VAWT whose highest C_p is

0.0350 at a TSR (λ) of 0.60. This shows that at Y = 150 mm height above the gable rooftop, the CAWT outperformed the conventional straight bladed VAWT by 196%. This increase in C_p values by the CAWT is attributed to the horizontal blades which serve as a horizontal axis wind turbine by interacting with the vertical airflow that is deflected from the building.

Figure 5.7 (c) presents the C_p values against the TSR of the building integrated CAWT and the straight bladed VAWT for Y = 200 mm. It can be observed that the CAWT integrated onto the building with gable rooftop outperformed the conventional straight bladed VAWT. The results showed that the C_p value attained by the CAWT is higher than that recorded by the VAWT. The maximum C_p value recorded by the building integrated CAWT and VAWT are 0.0859 at a TSR (λ) of 1.08 and 0.0364 at a TSR (λ) of 0.51 respectively. In comparison, the maximum coefficient of power for the building integrated CAWT is 136% higher compared to the maximum C_p value of the building integrated VAWT. The improved performance of the building integrated CAWT may be attributed to the horizontal blades which utilized the vertical wind deflected by the building, and the pitch angle of the horizontal blades which exposes the horizontal blade at an optimum angle of attack of the vertical wind. Similarly, the result presented in Figure 5.7 (d) for Y = 250 mm indicates that the C_p value of the building integrated CAWT increases by 71% compared to the conventional straight bladed VAWT under the same experimental conditions. The maximum C_p value recorded by the building integrated CAWT and VAWT at Y = 250 mm are 0.0765 at a TSR (λ), of 1.12, and 0.0448 at a TSR, (λ) of 0.66 respectively. The results were summarised in Table 5.1.

In general, the building integrated CAWT is shown to have better performance compared to the conventional building integrated VAWT for all the configurations (100-250 mm height). Traditionally VAWT turbines are designed to intercept any horizontal

wind. Therefor interacting with the deflected wind from the building can cause power loss due to the supporting struts of the VAWT which are not airfoil and are not design for such purposes as compared to the CAWT whose supporting struts are airfoil. These significant improvements in the C_p value of the building integrated CAWT may be attributed to the cross axis orientation of the CAWT which enables it to operate with dual wind directions. The roof shape which acts as an augmentation device to further increase the wind speed due to the accelerating effects of the roof.

Table 5.1: Summary of the experimental results for the CAWT and the VAWT on the gable rooftop (data presented for 10^o pitch angle)

Height (mm)	Parameter	CAWT	Straight bladed VAWT	Percentage of Improvement (%)
Y = 100	RPM	554	179	209
	$C_{p\max}$	0.1263	0.0345	266
	TSR for $C_{p\max}$	1.1	0.59	86
Y = 150	RPM	512	189	171
	$C_{p\max}$	0.1035	0.0350	196
	TSR for $C_{p\max}$	1.16	0.60	93
Y = 200	RPM	474	212	123
	$C_{p\max}$	0.0859	0.0364	136
	TSR for $C_{p\max}$	1.08	0.51	112
Y = 250	RPM	449	233	93
	$C_{p\max}$	0.0765	0.0448	71
	TSR for $C_{p\max}$	1.12	0.66	70

The increased wind speed which is deflected from the roof of the building is utilized by the horizontal blades to increase the torque output of the CAWT by having a larger area for the oncoming wind to interact with the turbine. The case is not the same for the VAWT since the arm (supporting struts) of the VAWT is not an airfoil and thus does not utilize the deflected airflow from the accelerating effect of the roof. The low C_p output of the conventional straight bladed VAWT is attributed to the radial arms (supporting struts) of the VAWT, the supporting struts of the VAWT inevitably affects the power output of the turbine by adding additional drag (parasitic drag) on the turbine which may cause a significant reduction in the overall rotor performance of the VAWT

(Islam et al., 2008a; Sutherland et al 2012; Li & Calisal, 2010; Ramkissoon & Manohar, 2013).

Moreover, both the vertical blades of the CAWT and VAWT have 0^o pitch angle which may affect the performance of the turbine. According to literature, increase in pitch angle of the vertical blade can lead to substantial increase in the power output of the turbine. Although the study focus mainly on varying the pitch angle of the horizontal blades of the CAWT this is consider as the limitation of the current study. However, while this negative effect of the pitch angle of the vertical blades may have little effect on the CAWT due to the present of the horizontal blade (which is pitched at 10^o for optimum performance), as the supporting struts, the effect is much more pronounced in the VAWT due to the parasitic drag generated by the supporting strut. Variable pitch for the VAWTs are being regarded as a promising solution for the alleviation of the negative effects of the blades dynamic stall (efficiency loss, vibration), improvement of the rotor's self-starting capability and torque ripple smoothing (Hwang et al. 2006, Kirke, 1998, Paswey, 2002). (Rezaeiha et al., 2017), reported that optimum pitch angle can improve the performance of VAWT by more than 5% compared to 0^o pitch angle, and that introducing the pitch angle can create a significant difference in wake generation especially in the upwind and downwind parts of the turbine revolution. Zhang et al., 2014), reported that compared to the 0^o pitch angle, the optimized blade pitch angle has greatly improved the aerodynamic performance at upstream of S-VAWT.

Moreover, solidity is one of the most important parameters that can affect the performance of a turbine. According to Brusca et al. (2014) VAWTs performs better at a low solidity of 0.3, compared to the solidity of Brusca eta al., the solidity of both the CAWT and the VAWT which is 0.43 is higher, and this can have negative effect on the power output of the two turbines. For the case of the CAWT, the presence of the horizontal blade as supporting struts can significantly mitigate the negative effect of

high solidity, but for the case of the VAWT, the high solidity can have significant effect to the power output of the VAWT.

Similarly, turbine aspect ratio is seen as an interesting parameter that could increase the performance of the VAWT. However, if the aspect ratio is too high it could lead to lower efficiency of the turbine, according to Brusca et al. (2014) to maximize the power coefficient, the rotor's aspect ratio should be as small as possible i.e. h/R = 0.4, For the case of the VAWT, the aspect ratio is h/R = 1.71 this has negative effect on the efficiency of the building integrated VAWT. When the AR is low, the radius of the turbine increases, and this increases the chord length of the blade and in turn increase in the Reynold number, and an increase in Reynold number can increase the power coefficient of the turbine.

Figure 5.8 (a, b, c, and d) compares the rotational speed of the free running CAWT and the straight bladed VAWT placed at Y = 100 to 250 mm height above the gable rooftop of the building model. The results are presented for a free running condition where the rotors were subjected to inertia and bearing friction with no external load applied. Similarly the results are presented for the 10^{o} pitch angle and 4.5 m/s wind speed.

Figure 5.8 (a-d) shows the trend of the rotational speed against time for both the CAWT and the conventional straight bladed VAWT for all the height configurations, the time recording is started immediately after switching on the ventilation fans. Figure 5.8 (a) shows the rotational speed against time for the building integrated CAWT and the conventional straight bladed VAWT at Y = 100 mm. as shown in the graph, the RPM for both the wind turbines increases gradually with time until it reaches a maximum value of 554 and 179 RPM at t = 178 and t = 249s for the CAWT and the VAWT respectively. The rotational speed becomes constant (stabilize) after that. The maximum RPM recorded by the CAWT is 209% higher than the one for the VAWT under the same experimental conditions. Furthermore, the figure shows that the CAWT started to rotate

earlier than the VAWT. At Y = 150 mm height above the gable rooftop, the results shown in Figure 5.8 (b) indicate that the rotational speed recorded by the building integrated CAWT is 171% higher than the one recorded by the building integrated VAWT (Table 5.1).

Similarly, Figure 5.8 (c) and (d) presents the RPM of the building integrated CAWT and the conventional straight bladed VAWT placed for Y = 200 mm, and 250 mm height above the rooftop of the building. It can be observed from the figure that the CAWT integrated onto the building with gable rooftop outperformed the conventional straight bladed VAWT, by 123% and 93% increment in RPM respectively compared to the straight bladed VAWT mounted at the same height and subjected to the similar experimental conditions.

The improved performance of the building integrated CAWT is attributed to the cross axis orientation of the CAWT where the horizontal blades which is also the supporting struts of the CAWT utilized the vertical airflow that is deflected from the building thereby improving the overall performance of the CAWT. In addition, the vertical wind guided by the gable roof shape has successfully reduced the self-starting time and increased the maximum rotational speed of the CAWT resulting in a better efficiency. The increment in the rotational speed of the CAWT is attributed to the additional torque produced by the horizontal blade of the CAWT. Similar to the C_p performance of the VAWT, the parasitic drag generated by the supporting struts of the VAWT has greatly affects the rotational speed of the VAWT. According to Islam et al. (2008a), and Li & Calisal (2010) the arms (supporting struts) of the VAWT inevitably affects the power output of the turbine by adding additional drag on the turbine therefore affecting the overall performance of the VAWT.

Moreover, VAWT performance is directly related to the blade's Reynold number, the higher the Re the better the performance; this is because as the Re increase, the blade's

lift coefficient rises (Robert & Klimas 1980) and the drag coefficient decreases thus providing greater torque output (Brusca et al. 2014)

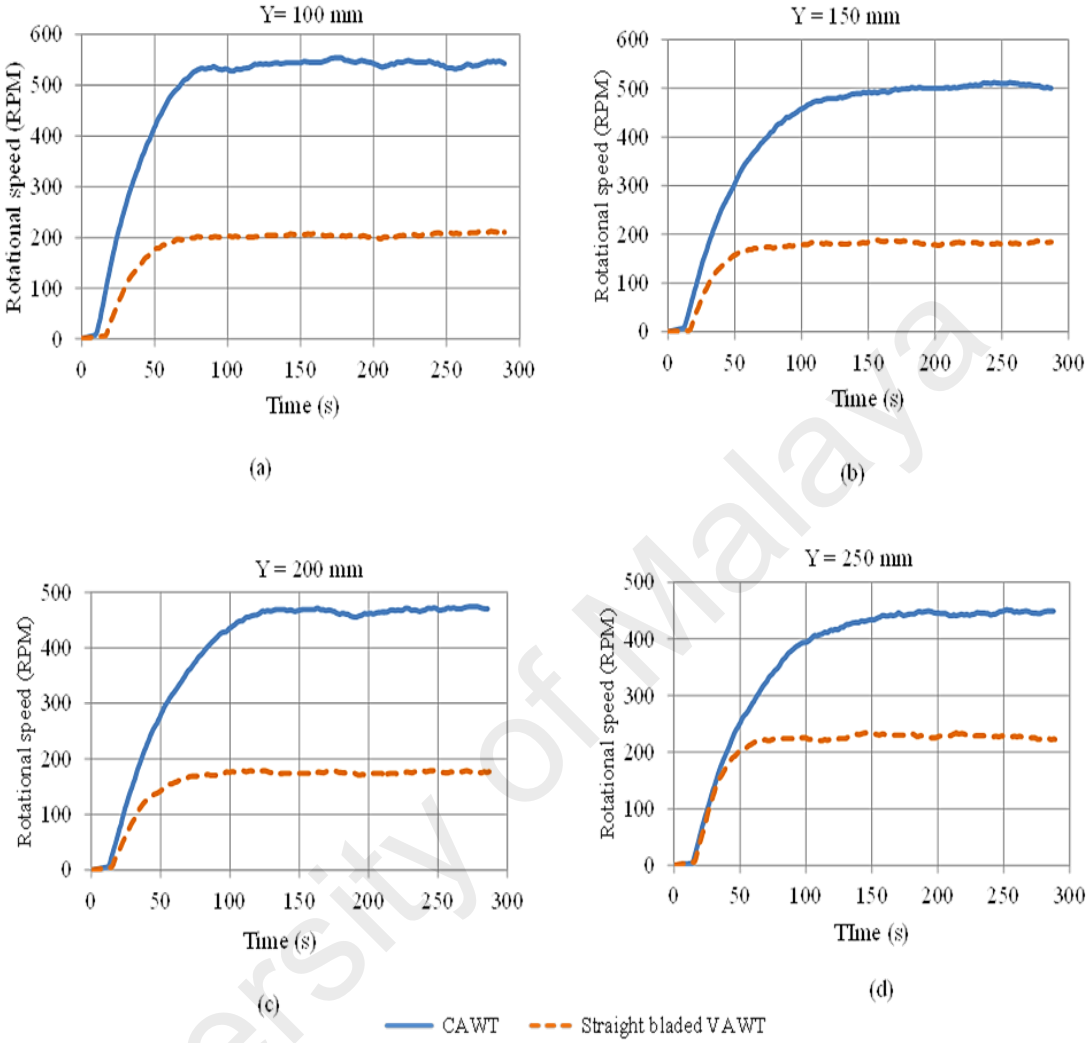

Figure 5.8: Rotational speed against time for building integrated CAWT and VAWT at various heights above the gable rooftop: (a) *Y* = 100 mm; (b) *Y* = 150 mm; (c) *Y* = 200 mm; and (d) *Y* = 250 mm

5.4.2 Effect of increase in height on the performance of CAWT on gable rooftop

Further study was conducted on the effect of the increase in turbine height on the performance of the building integrated CAWT. The height of the CAWT above the gable rooftop was varied for *Y* = 100 to 250 mm as shown in Figure 5.9 and Figure 5.10 respectively. The pitch angle used for this study is 15^{o} at an average wind speed of 4.5 m/s. Comparisons were made between the performances of the building integrated

CAWT at various heights above the building model in order to identify the height that is more suitable for the mounting of the CAWT. Figure 5.9 presents the coefficient of power of the CAWT against tip speed ratio at various heights above the gable rooftop. The figure shows that low performance of the CAWT is observed as it is mounted at higher positions above the rooftop of the building. This implies that the closer the CAWT is mounted above the rooftop, and utilizing the vertical wind deflected by the rooftop, a better performance can be expected from the CAWT.

Although the results showed a better performance closer to the roof, the air flow closer to the roof is turbulent and the machine experiences more turbulence and as a result more fatigue which may shorten the lifetime of the turbine. However, research has shown that VAWT can operate efficiently in a turbulence environment (van Bussel et al., 2004; Eriksson et al., 2008; Armstrong et al., 2012). Lubitz (2014) reported that Turbulence in the approaching wind can have a significant influence on the wind turbine power output; this is mainly significant for the smaller wind turbines which in practice are often situated near buildings, trees and other Impediments. According to Cochran, (2002) the turbulence intensity has a significant influence on the performance of a wind turbine due to the cubic variation of power with wind speed, more turbulent winds have greater power than less turbulent winds with the same mean wind speed. Evidence has shown that the turbulence level in the incoming flow affects the rate at which the velocity deficit reduces with downwind distance from the turbine (i.e. wake recovery rate), since the turbulence in the wake is an efficient mixer, it mixes the low velocity fluid in the wake with the high velocity fluid outside it. In this way momentum is transferred into the wake, the wake expands but the velocity deficit is reduced (Sanderse, 2009).

However Y = 100 mm is the minimum height in which CAWT can be mounted above the rooftop, at $Y < 100$ mm the distance will be too close that the vertical blade

almost touches the surface of the rooftop. The presence of the horizontal blades interacting with the deflected vertical winds enhances the self-starting capability of the CAWT and improves the overall performance of the CAWT. When the height of the CAWT above the rooftop of the building was increased from Y = 100 to 150 mm and from Y = 100 to 200 mm, the maximum C_p of the CAWT drops by 17% and 52%, respectively. Since there is non-uniform wind profile, the turbine at each position is expected to experience a different wind velocity and hence different amounts of available wind energy to be extracted. The summary of the experimental results for the variation of height is presented in Table 5.2.

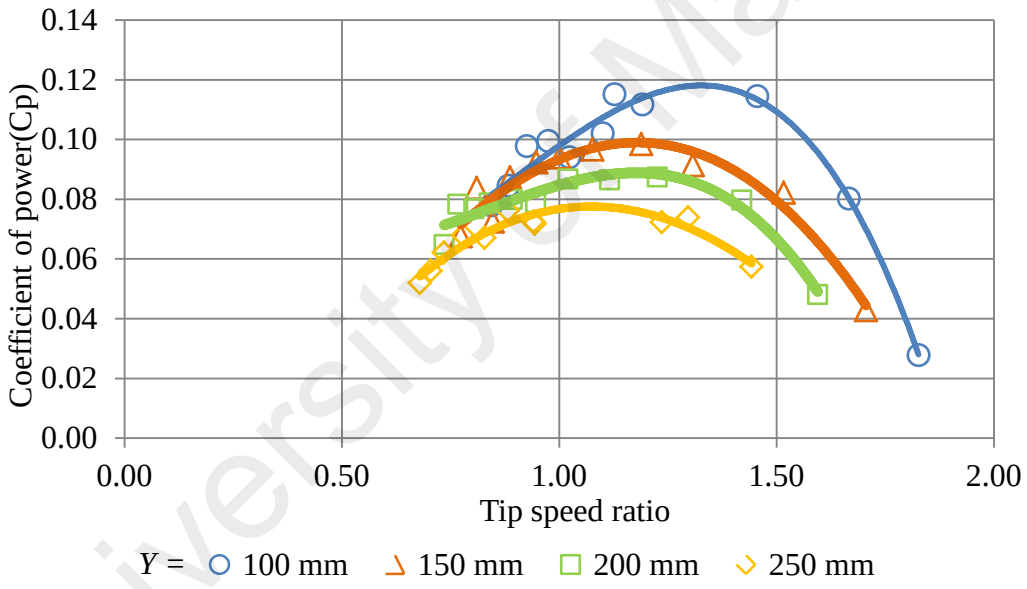

Figure 5.9: Coefficient of power against tip speed ratio for CAWT at different heights above the gable rooftop

Figure 5.10 show the rotational speed of the building integrated CAWT at various heights above the rooftop. The overall results and observations showed that as the height is increased, the performance of the CAWT reduces. This is because the horizontal blades of the CAWT which utilizes the vertical airflow that is deflected from the building is been positioned further away from the deflected wind flow. Therefore, at higher position above the rooftop, very small vertical (deflected) wind is experienced by

the horizontal blades. Hence, the reason for the poor performance of CAWT at higher positions above the rooftop. On the other hand, at lower positions, due to the speed up effect at the rooftop, more vertical (deflected) wind interacts with the horizontal blades therefore improving the performance of the CAWT. The presence of the horizontal blades of the CAWT is very important in case of the skewed flow, which could actually increase the lift production of the CAWT.

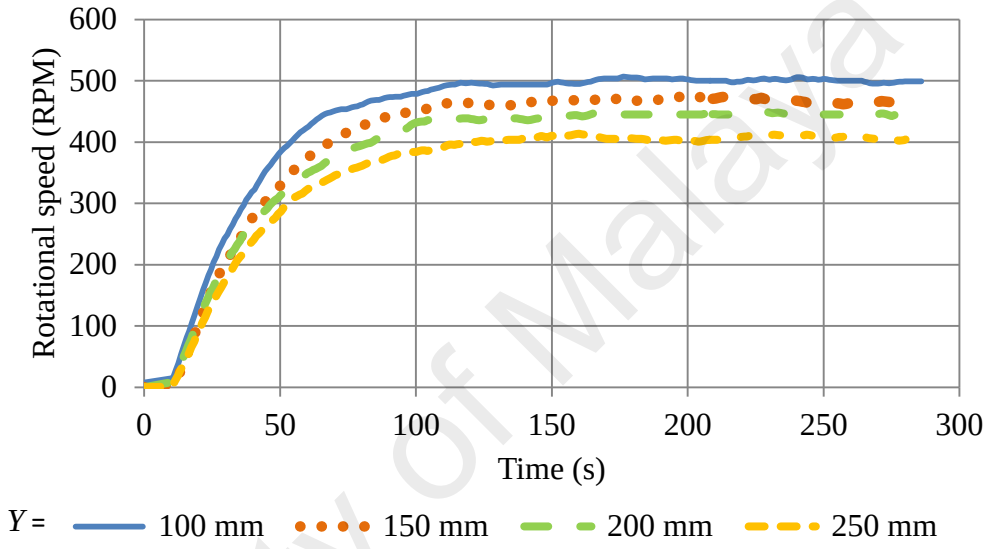

Figure 5.10: Rotational speed against time for CAWT at different heights above the gable rooftop

Table 5.2: Summary of experimental results on effect of increase in height of CAWT on the gable rooftop (data presented for 15° pitch angle)

Parameter	Height (mm)			
	100	150	200	250
RPM	506	477	449	412
C_{Pmax}	0.1152	0.0985	0.087	0.076
TSR for C_{pmax}	1.13	1.19	1.23	0.88

To verify the experimental result on the effect of increase in height of CAWT above the rooftop (Figure 5.9 and Figure 5.10), a simple CFD simulation was carried out to calculate the skewed angle of the wind at the rooftop as shown in section 4.9. For each height of the CAWT above the rooftop i.e. Y = 100 mm, 150 mm, 200mm, and 250 mm. the skewed angle is calculated. The result obtained for the calculated skewed angle

agrees well with (Mertens et al., 2003), where the skewed angle is largest close to the windward side of the roof edge. Figure 5.11 presents the results for the skewed angle for each of the turbine height Y = 100 mm, 150mm, 200 mm, and 250 mm above the rooftop. From the figure; it can be observed that the highest skewed angle is obtained at Y = 100 mm. This confirms the results obtained in Figure 5.9 and Figure 5.10 where the CAWT mounted at 100 mm height performs better than other heights. The figure show that the skewed angle decreases with increase in height. Therefore the performance of the CAWT increase with increase in skewed angle. Therefore mounting the CAWT at higher height will reduce the skewed angle. Similarly, improvement in the performance of VAWT turbine due to skewed flow is also reported in (Mertens, 2003; Balduzzi et al., 2012; Zanforlin & Letizia, 2015).

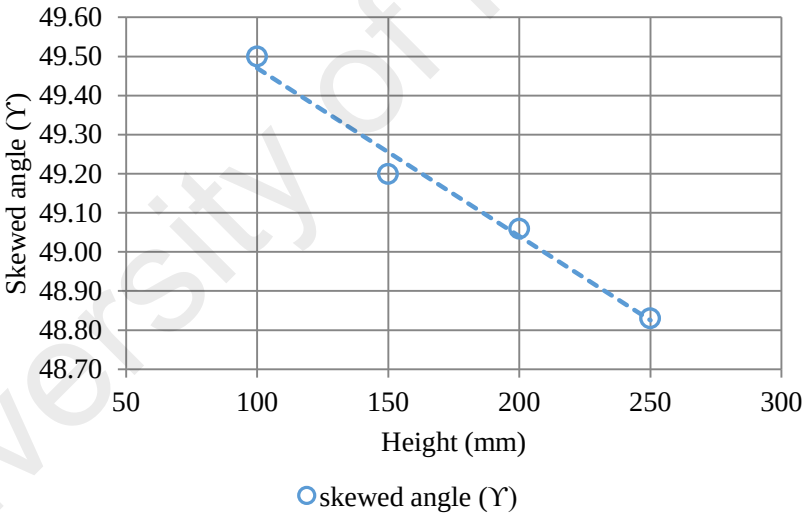

Figure 5.11: Skewed angle of CAWT on the gable rooftop for Y = 100 mm, 150 mm, 200 mm, and 250 mm

The higher skewed angle experience by the CAWT at 100 mm height also contributed to the improved performance of the CAWT at that position, Figure 5.11. At higher skewed angle the swept area of the turbine is increased due to the contribution of the downwind zone which counterparts the decrease of the projected frontal area with an overall increase of the available surface area to intercept the wind as reported by

Bianchini et al. (2012). Furthermore, Skewed flow increases the performance of H-VAWT by modifying the region of interaction of the downwind blade passage with the upwind generated wake. Increasing the skewed angle will increase the area of the downwind blades passage which is operating outside the upwind generated wake thus experiencing an incoming flow with larger energy content (Ferreira, 2006). While skewed angle is believed to improve the performance of wind turbine in urban buildings as reported by (Mertens et al., 2003; Ferreira et al., 2009; Balduzzi et al., 2012; Bianchini et al., 2012). Zanforlin & Letizia (2015) reported that for the case of cowling system the wind turbine in a skewed flow can lead to power loss of 11.6%. The skewed wind conditions in the cowling system generates excessive blockage thereby becoming an obstacle to the oncoming flow.

5.5 Performance comparison between CAWT and VAWT on vaulted rooftop

For the case of the vaulted rooftop, 10^o pitch angle was selected for the performance investigation of CAWT. The 10^o pitch angle is the optimum pitch angle for the horizontal blades for the case of the CAWT integrated on the vaulted rooftop. A comparative study was performed for the performance of the CAWT and the VAWT integrated on the vaulted rooftop. The heights of the two turbines (CAWT and VAWT) above the rooftop were varied for four (4) different heights i.e. Y = 100 to 250 mm, at wind speed of 4.5 m/s. For each case, the performance of the two turbines was evaluated based on the maximum C_p values and the rotational speed produced by the CAWT and the VAWT.

5.5.1 Variation of height above the vaulted rooftop

The height of the CAWT and the conventional straight bladed VAWT were varied from Y = 100 to 250 mm above the vaulted rooftop of the building. Figure 5.12 (a, b, c, and d) compares the C_p values between the building integrated CAWT and the conventional straight bladed building integrated VAWT at turbine height Y = 100 to 250

mm. Figure 5.12 (a-d) compares the coefficient of power against the tip speed ratio between the CAWT and the straight bladed VAWT integrated on the building model with vaulted rooftop. Based on the results obtained in Figure 5.12 (a-d), the CAWT outperformed the conventional straight bladed VAWT in all the configurations (i.e. *Y* = 100 to 250 mm).

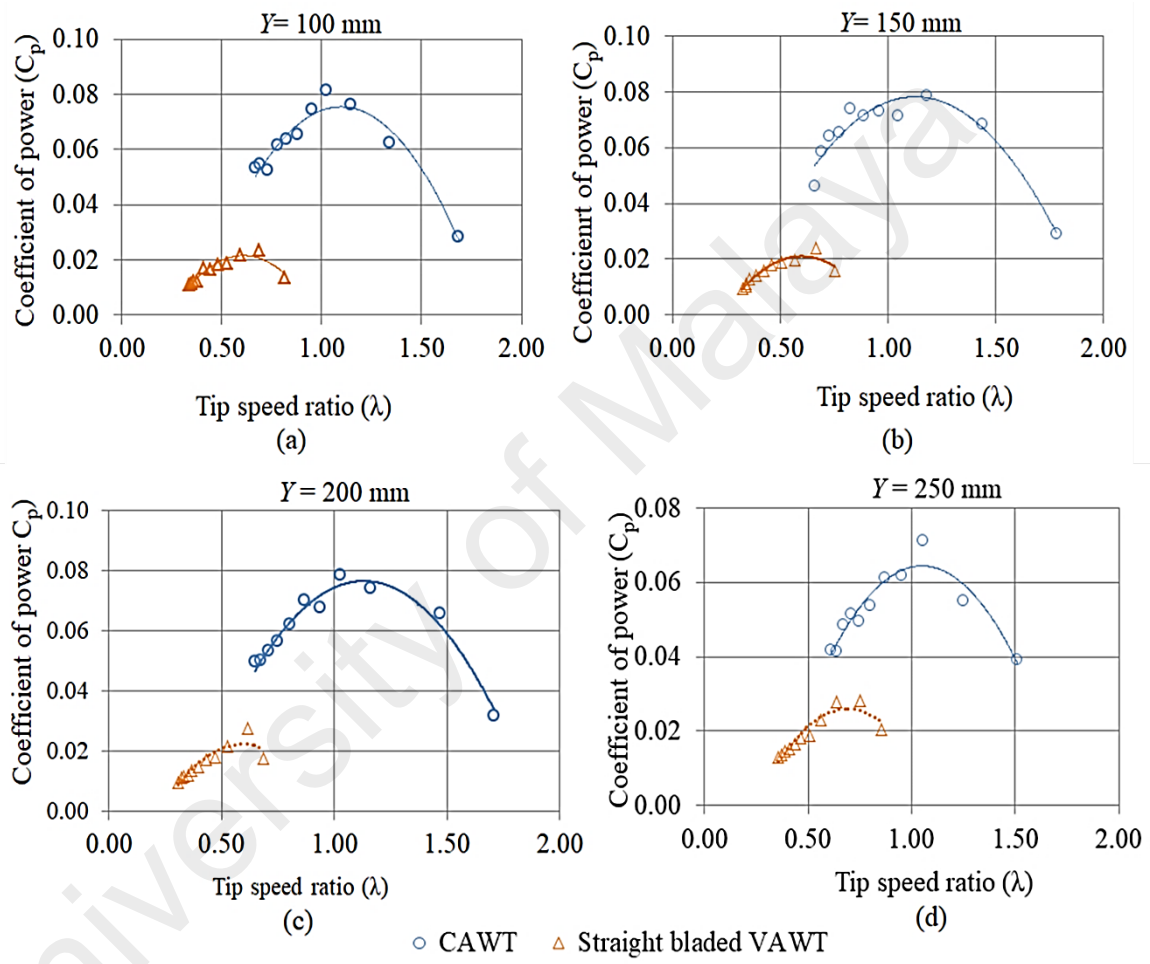

Figure 5.12: Coefficient of power against tip speed ratio for building integrated CAWT and VAWT at various heights above the vaulted rooftop for (a) *Y* = 100 mm; (b) *Y* = 150 mm; (c) *Y* = 200 mm; and (d) *Y* = 250 mm

The maximum C_p attained by the CAWT and the VAWT at *Y* = 100 mm height are 0.0814 at TSR of 1.03 and 0.0235 at TSR of 0.68 respectively. This shows that the CAWT outperformed the straight bladed VAWT by 246%. Similar improvement in the performance of CAWT is also observed for Y = 150 mm, 200 mm, and 250 mm where the CAWT outperformed the VAWT by 231%, 184%, and 154% respectively.

The improved performance of the CAWT is attributed to the cross axis orientation of the CAWT where the horizontal blades accept and utilized the increased wind speed that is deflected from the roof of the building to increase the torque output of the CAWT. This is possible through creating a larger area for the oncoming wind to interact with the turbine. The low C_p output of the conventional straight bladed VAWT is attributed to the radial arms (supporting struts) of the VAWT. The supporting struts of the VAWT inevitably affects the power output of the turbine by adding additional drag (parasitic drag) on the turbine therefore affecting the overall performance of the VAWT. The results are summarized in Table 5.3.

Table 5.3: Summary of the experimental results for the CAWT and the VAWT on the vaulted rooftop (data are presented for 10^o pitch angle)

Height (mm)	Parameter	CAWT	Straight bladed VAWT	Percentage of Improvement (%)
Y = 100	RPM	527	204	158
	$C_{p,\max}$	0.0814	0.0235	246
	TSR for $C_{p,\max}$	1.03	0.68	51
Y = 150	RPM	508	221	129
	$C_{p,\max}$	0.0788	0.0238	231
	TSR for $C_{p,\max}$	1.18	0.66	79
Y = 200	RPM	469	228	105
	$C_{p,\max}$	0.0781	0.0275	184
	TSR for $C_{p,\max}$	1.03	0.61	69
Y = 250	RPM	448	249	80
	$C_{p,\max}$	0.0711	0.0280	154
	TSR for $C_{p,\max}$	1.05	0.75	40

Figure 5.13 (a-d) compares the rotational speed of the CAWT and the straight bladed VAWT integrated on a building with a vaulted rooftop. It can be seen from the figure that the building integrated CAWT outperformed the building integrated VAWT in all the configurations mentioned above Figure 5.13 (a-d). These two turbines are mounted at the same height above the vaulted rooftop and subjected to the same experimental

conditions. This increase in rotational speed and coefficient of power by the CAWT may be attributed to the horizontal blades which serve as a horizontal axis wind turbine by interacting with the vertical airflow that is deflected from the building, and the pitch angle of the horizontal blades which exposes the horizontal blades at an optimum angle of attack of the vertical wind.

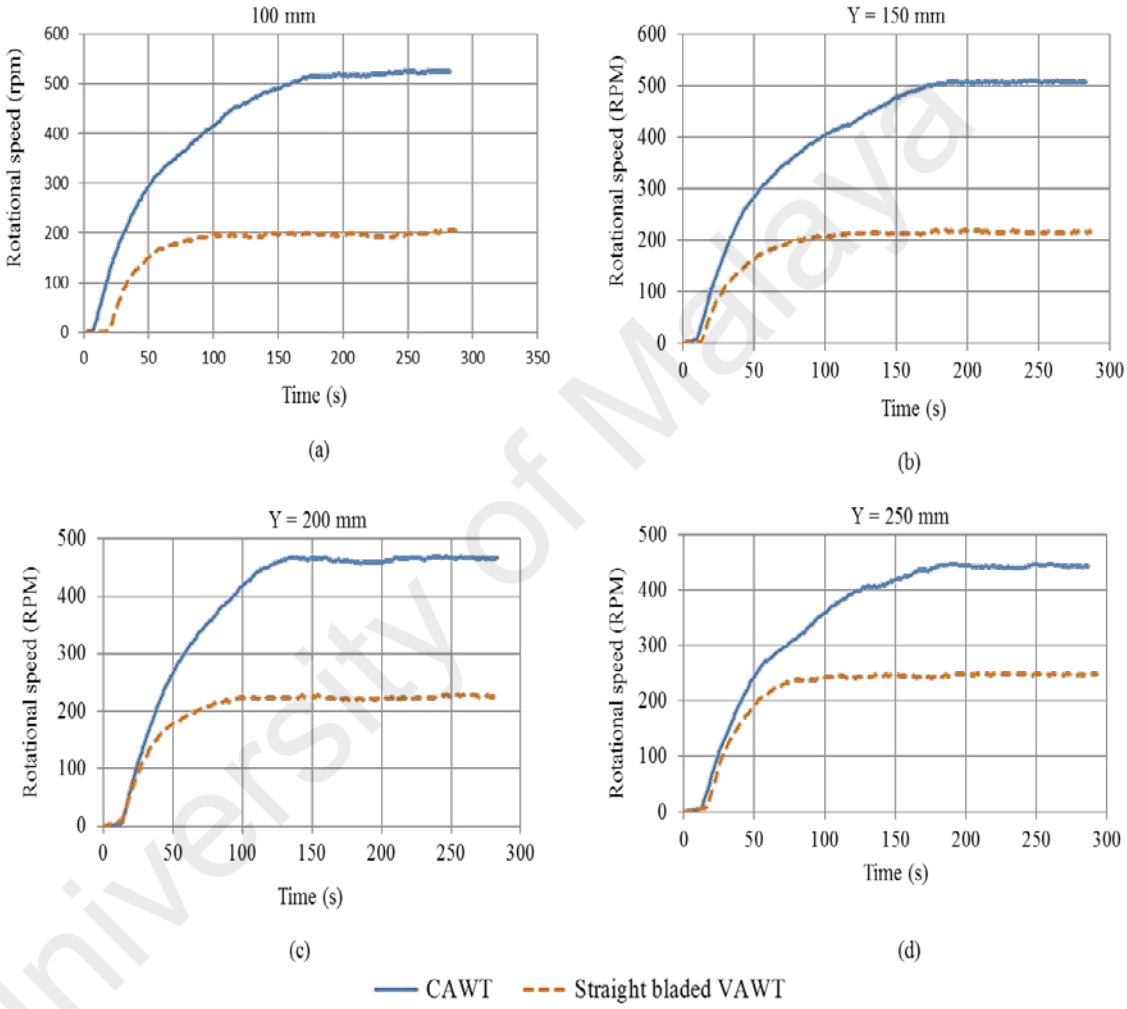

Figure 5.13: Rotational speed against time for building integrated CAWT, and VAWT at various heights above the vaulted rooftop for (a) *Y* = 100 mm; (b) *Y* = 150 mm; (c) *Y* = 200 mm; and (d) *Y* = 250 mm

5.5.2 Effect of increase in height on the performance of CAWT on vaulted rooftop

Further study was conducted on the effect of the increase in height of CAWT on the performance of the building integrated CAWT on the vaulted rooftop. The height of

the CAWT above the rooftop was varied Y = 100 to 250 mm in order to identify the suitable height for the mounting of the CAWT. The pitch angle used for this study is 5^{o} pitch angle at wind speed of 4.5 m/s. Comparisons were made between the performances of the building integrated CAWT at various heights above the vaulted rooftop. The result of the analysis is presented in Figure 5.14.

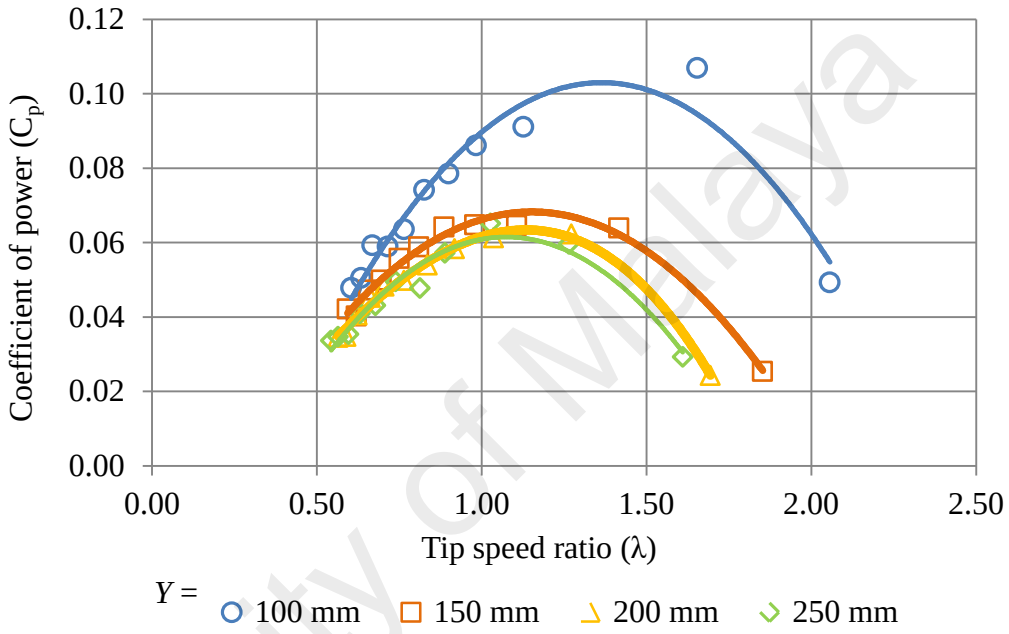

Figure 5.14: Coefficient of power against tip speed ratio for CAWT at different height above the vaulted rooftop

Figure 5.14 presents the C_p values against TSR of the building integrated CAWT at various heights above the vaulted rooftop. The Figure shows that the CAWT performs better when it is mounted closer to the rooftop. However, low performance of the CAWT is observed as it is mounted at higher positions above the rooftop of the building. This implies that the closer the CAWT is mounted above the rooftop, the better its performance. Moreover, the presence of the horizontal blades interacting with the deflected vertical winds enhances the self-starting capability, and improves the overall performance of the CAWT.

Figure 5.15 presents the RPM against time for the CAWT at various height Y =

100 to 250 mm above the vaulted rooftop. The shape of the rooftop is very vital in improving the performance of the CAWT. It can be seen from the figure that the rotational speed decreases with increase in height. At Y = 100 mm, the CAWT is able to attain a higher RPM of 609 rpm, As the height of the CAWT on the rooftop is increased from 100 mm to 150 mm, above the rooftop, the RPM decreases, 567 rpm (i.e. 7% decrease in RPM at higher height).

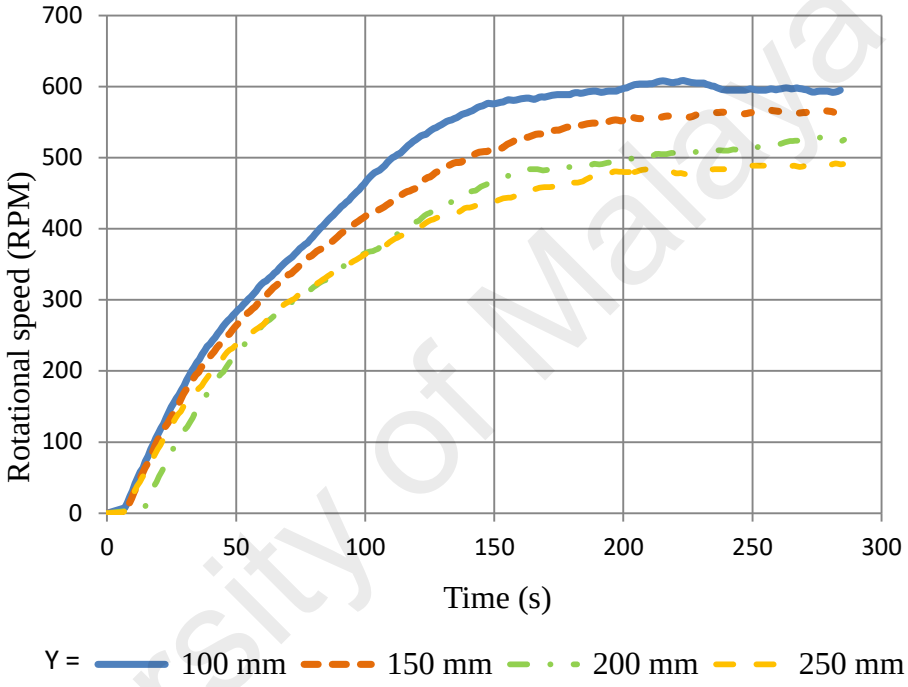

Figure 5.15: Rotational speed against time for CAWT at different height above the vaulted rooftop

This is because at higher height CAWT is position further away from the rooftop therefore reducing the deflected wind interacting with the horizontal blades of the CAWT. Similar observation is made for the case of Y = 200 mm, and 250 mm. Since there is non-uniform wind profile, the turbine at each position is expected to experience a different wind velocity and hence different amounts of available wind energy to be extracted. As explained earlier, Y = 100 mm is the minimum distance in which the CAWT can be mounted above the rooftop, at Y < 100 mm, the distance will be too close that the vertical blade almost touch the surface of the rooftop. When the height of the

CAWT above the rooftop of the building was increased from 100 to 150 mm and from 100 to 200 mm, the maximum C_p of the CAWT drops by 39% and 42%, respectively. The summary of the experimental results for the variation of height is presented in Table 5.4.

Table 5.4: Summary of the experimental results for the effect of increase in height of CAWT on the vaulted rooftop (data are presented for 5° pitch angle)

Parameter	Height (mm)			
	100	150	200	250
RPM	609	567	528	490
$C_{p,\max}$	0.106	0.065	0.062	0.065
TSR for $C_{p,\max}$	1.65	0.98	1.27	1.02

Using a simple CFD simulation the skewed angle of the wind at the rooftop was calculated for each height of the CAWT above the rooftop i.e. Y = 100 mm, 150 mm, 200mm, and 250 mm as shown in section 5.16.

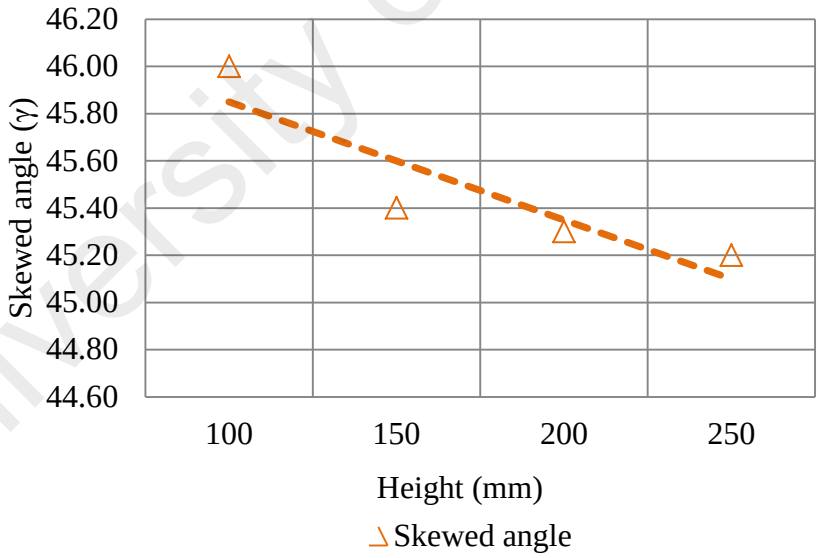

Figure 5.16: Skewed angle for CAWT on the vaulted rooftop for Y = 100 mm; 150 mm; 200 mm; and 250 mm

The results obtained from the simple CFD simulation carried out to verify the experimental result on the variation of height of CAWT above the rooftop (Figure 5.14 and Figure 5.15), indicates that the better performance experience by the CAWT at lower height is due to the higher skewed angle experienced by the CAWT at that

position. The result obtained for the calculated skewed angle agrees well with (Mertens et al., 2003), where the skewed angle is largest close to the windward side of the roof edge.

The improved performance of the CAWT at 100 mm height (Figure 5.14) is due to the high skewed angle experience by the CAWT at that position. At higher skewed angle the swept area of the turbine is increased due to the contribution of the downwind zone which counterparts the decrease of the projected frontal area with an overall increase of the available surface area to intercept the wind as reported by (Bianchini et al., 2012).

5.6 Bare-CAWT and bare-VAWT (stand-alone systems)

The results in this subsection are presented for the bare-CAWT and bare-VAWT where no roof is integrated with the turbine, and both wind turbines are placed at the same height i.e. 1464 mm from the ground level and are subjected to similar experimental conditions. The pitch angle for the horizontal blade for this study is 10^{o}, and the wind speed is set at 4.5 m/s. The graphs shown in Figure 5.17 shows the performance of bare-CAWT, and bare-VAWT, it can be seen from the figure that both the bare-CAWT and bare-VAWT have similar trend where each of the bare-CAWT and bare-VAWT attain peak coefficient of power C_p at different tip speed ratio (TSRs). The graphs illustrated that the bare-CAWT outperform the bare-VAWT. The maximum C_p produced by the bare-CAWT is $C_{p,max}$ is 0.0572 at TSR of 0.79, while the maximum C_p produced by the Bare-VAWT is 0.0345 at TSR of 0.59. In comparison, the $C_{p,max}$ value of bare-CAWT increases by 66%, (Table 5.5), compare to bare-VAWT.

Figure 5.17 show the free running RPM against time for the Bare-CAWT and bare-VAWT. The figure demonstrated that the bare-CAWT recorded a very high rotational speed of 279 RPM. In contrast, the maximum rotational speed recorded by the straight

bladed VAWT is 227 RPM, indicating an increment in RPM of 23%, by the bare-CAWT, Table 5.5 compared to the bare-VAWT. The improvement in the performance of the bare-CAWT is as a result of the lift created by the pitch angle of the horizontal blades which exposes the horizontal blade to a better angle of attack of the vertical wind. Another reason for the improved performance of the CAWT is supporting struts (i.e. the horizontal blades), the presents of the horizontal blades as the supporting struts reduces the drag force on the supporting struts and increases the angle of attack to its optimum which subsequently increases the lift force thereby improving the overall performance of the bare-CAWT. The case is not the same for the bare-VAWT, the supporting struts is a metal plate; this metal plates generate parasitic drag that reduces the net power out of the bare-VAWT (Islam et al. 2008, Ramkisoon & Manohar 2013). The results are summarized in Table 5.5.

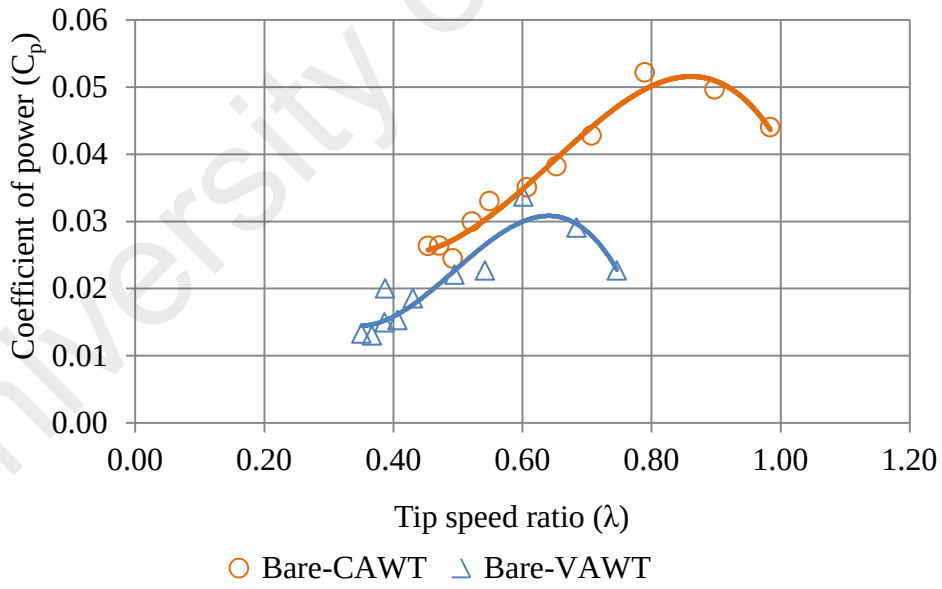

Figure 5.17: Coefficient of power for Bare-CAWT and Bare-VAWT

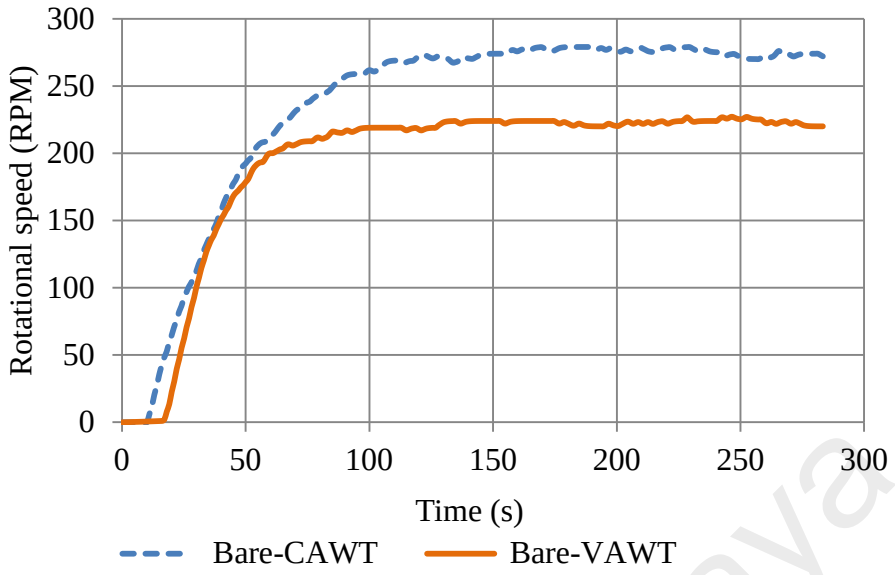

Figure 5.18: Rotational speed of Bare-CAWT and Bare-VAWT

Table 5.5: Summary of the experimental result for the bare-CAWT and bare-VAWT

Parameter	Bare-CAWT	Bare-VAWT	%increment
RPM	279	227	23
$C_{p,max}$	0.0572	0.0345	66
TSR	0.79	0.59	34

5.7 Effect of pitch angle on the performance of bare-CAWT

The effect of pitch angle on the performance of bare-CAWT was investigated through an experimental study. The result of the study is discussed in the following subsection.

5.7.1 Free-run test condition for bare-CAWT

The free-run tests, was conducted for the bare-CAWT at different pitch angle of the horizontal blades, the pitch angle was varied from, $\beta = 15^o$, 10^o, 5^o and 0^o, the results of this investigation is depicted in Figure 5.19. The RPM of the bare-CAWT was measured until a steady state conditions is achieved, the free-run test was carried out at a wind speed of 4.5 m/s. It can be observed from Figure 5.19 that the RPM of the CAWT decrease with increase in pitch. At $\beta = 0^o$, the bare-CAWT recorded the highest RPM compared to other pitch angles, although there is no significant difference in the

RPM at β = 5° and 10° pitch angle. However, a significant difference is observed for the 15° pitch angle, this is due to the higher pitch angle which leads to higher angle of attack that causes stall of the turbine.

Figure 5.20 depicts the C_p values against the TSR for the bare-CAWT at various pitch angle of the horizontal blades (β = 15°, 10°, 5° and 0°) of the CAWT. From the figure, it can be seen that the 10° pitch angle has the highest C_p values compared to other pitch angles. This shows that although the 0° has the highest RPM compared to the 10° pitch angle, however the 10° pitch angle has higher C_p values. This is attributed to the angle of attack which is optimum at 10° pitch angle. The 10° pitch angle creates more surface area for the horizontal blades to interact and extract more energy from the vertical wind stream. Therefore for the case of the bare-CAWT configuration, the 10° is considered as the optimum pitch angle for the horizontal blade. From the figure, the 15° pitch angle seems to have performed poorly, where it recorded the lowest value of C_p as compared to the 0° and the 5° pitch angle. At β = 15°, the angle of attack is very large, this expand the region where dynamics stall takes place and the blade deteriorate further, which lead to poor performance of the CAWT for the 15° pitch angle. The results are summarized in Table 5.6.

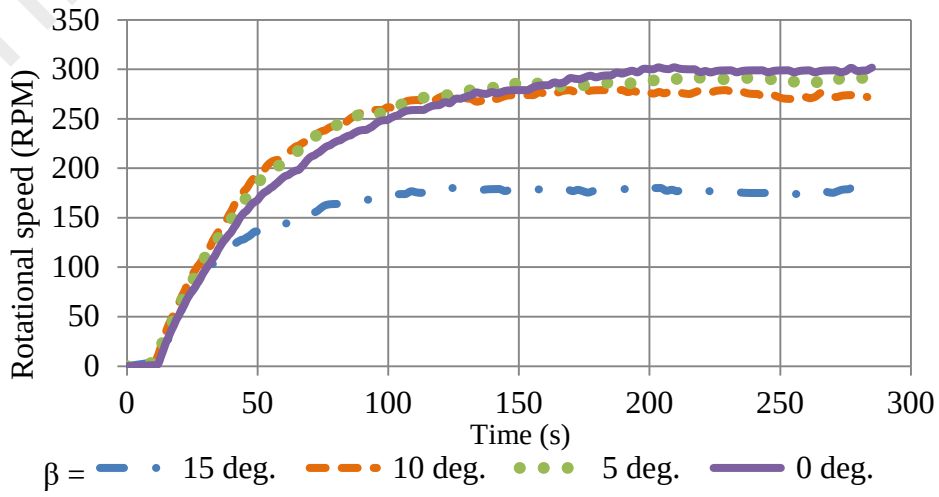

Figure 5.19: Free-run condition test for bare-CAWT at various pitch angles

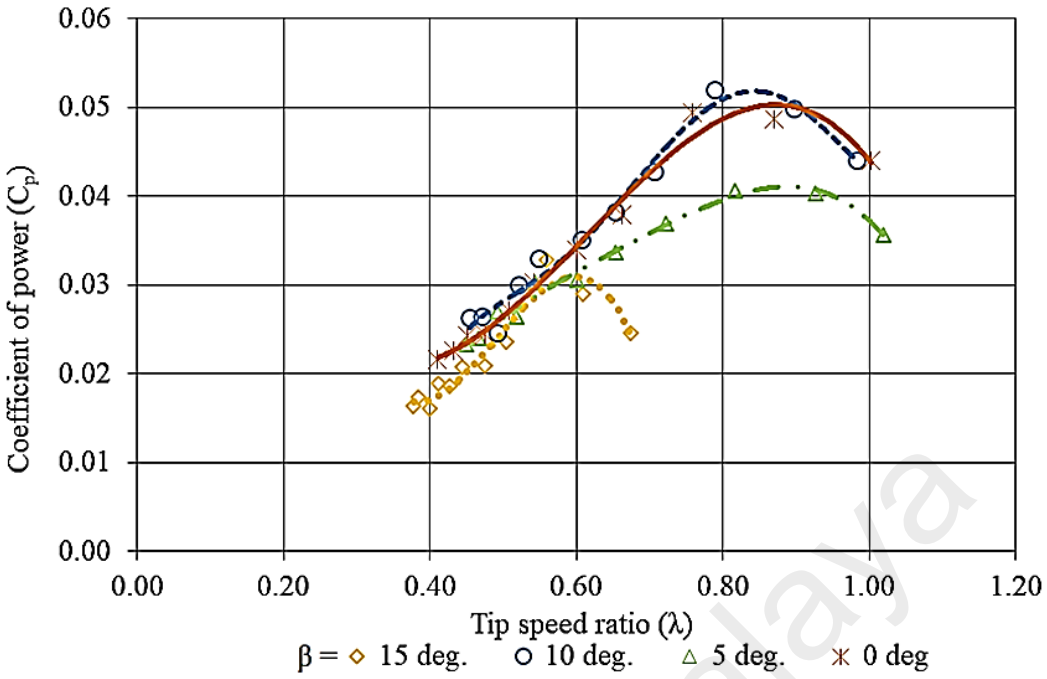

Figure 5.20: Coefficient of power against Tip speed ratio for Bare-CAWT

Table 5.6: Summary of experimental results for bare-CAWT at various pitch angles

Pitch angle	RPM	Cp	TSR
15^o	182	0.0328	0.56
10^o	279	0.0572	0.79
5^o	292	0.0405	0.81
0^o	302	0.049	0.75

5.8 Scale-up CAWT

A follow up study that was aimed to ascertain the effect of rotor diameter and chord length on the performance of the building integrated CAWT was conducted. A scale- up design of CAWT with a diameter of 500 mm, chord length of c = 70 mm, and solidity of σ = 0.42 was tested and compared with the small scale CAWT with the diameter of 350 mm, chord length, c = 50 mm, and solidity of σ = 0.43. The study was conducted with both the scale up and small scale CAWT mounted above the gable rooftop. The height of the CAWT for both the scale-up and small scale was varied from *Y*= 150-250 mm above the rooftop, the pitch angle for the horizontal blade of both the large scale

and small scale CAWT is 10^o, and the wind speed is set at 4.5 m/s, The horizontal blades of both the scale-up CAWT and the small scale CAWT were set at 10^o, and both the two turbines are subjected to similar experimental conditions. Y = 150 mm is the minimum distance to mount the large scale CAWT, at Y < 150 mm, the vertical blades of the large scale CAWT almost touch the surface of the rooftop. The gable rooftop is use as a case study for the integration of the large scale and small scale CAWT.

5.8.1 Performance comparison between large and small scale CAWT

Figure 5.21 compares the C_p values against the TSR for the building integrated CAWT for D = 350 mm, c = 50 mm, having a solidity, σ = 0.43, and D = 500 mm, c = 70 mm with a solidity σ = 0.42 for Y = 150 mm, 200 mm, and 250 mm. Figure 5.20 (a-c) shows the results for the coefficient of power against the tip speed ratio for all the height configurations, it can be seen from all the figures that the C_p values varies considerably with the TSR. The result in Figure 5.21 (a) is presented for Y = 150 mm one can see from the figure that the maximum C_p for the small scale is 0.1035 at TSR of 1.16. When the diameter, D, and the chord length c were increased from 350 mm to 500 mm, and c = 50 mm to 70 mm (σ = 0.42), the maximum C_p increases from 0.1035 at TSR of 1.16 to 0.1393 at TSR of 1.84. This represents an increment of 35% in C_p value for the large scale CAWT. The TSR also increases from 1.16 to 1.84 indicating an increment of 57% in the TSR for the large scale CAWT. Similarly, Figure 5.21 (b) and (c) presents the results for Y = 200 mm, and 250 mm height of CAWT with D = 350 mm, C = 50 mm (σ = 0.43) and D = 500 mm, C = 70 mm (σ = 0.42) respectively. The results showed for each case of the Y = 200 mm, and 250 mm height, the maximum C_p of the large scale building integrated CAWT is higher compared to the maximum C_p of the small scale building integrated CAWT. The increment in C_p, max for large scale CAWT is 43% and 42.8% for Y = 200 mm and 250 mm respectively. This results

obtained for these study indicates that the increment in diameter and the chord length can lead to an improvement in performance of the building integrated CAWT.

Figure 5.22 (a, b, and c) compares the rotational speed against time for the large scale CAWT, (D = 500 mm, c = 70 mm) and small scale CAWT (D = 350 mm, c = 50 mm) placed at turbine height (a) *Y* = 150 mm, 200 mm, and 250 mm above the gable rooftop. Figure 5.22 (a) presents the RPM against time for *Y* = 150 mm, It can be seen from figure that the small scale CAWT (D = 350 mm, c = 50 mm) produces higher RPM compared to the large scale CAWT (D = 500 mm, c = 70 mm). At *Y* = 150 mm, the small scale CAWT produce a peak RPM of 513 rpm while the peak RPM of the large scale CAWT is 450 rpm. The same observation can be made for *Y* = 200 mm, and *Y* = 250 mm. This result is expected because of the additional weight attached to the large scale CAWT. This weight can add additional drag which will affect the RPM of the large scale CAWT. Although the small scale CAWT (D = 350 mm, c = 50 mm) has higher RPM compared to the large scale CAWT in all the heights tested, the large scale, the scale-up CAWT produces higher C_p values compared to the small scale CAWT. This indicates that the large scale CAWT has produces higher torque values compared to the small scale CAWT.

In general, the low performance of the CAWT at the smaller diameter is due to the effect of the shaft and the downwind blades on the flow past the blades which decrease the velocity of the wind past the upwind blades. Moreover, when the radius of the CAWT is increased, the chord length also increases and this has significant effect in improving the performance of the CAWT, this can be explained due to the higher projected area which increases the aerodynamic forces on the blade and in turn increases Re number which results in higher coefficient of lift and reduce drag coefficient and increase the power coefficient of the turbine. Brusca et al. (2014)

reported that when the rotor diameter is increased, the Reynold number of the blade rises which in turn strongly influence the power coefficient of the turbine.

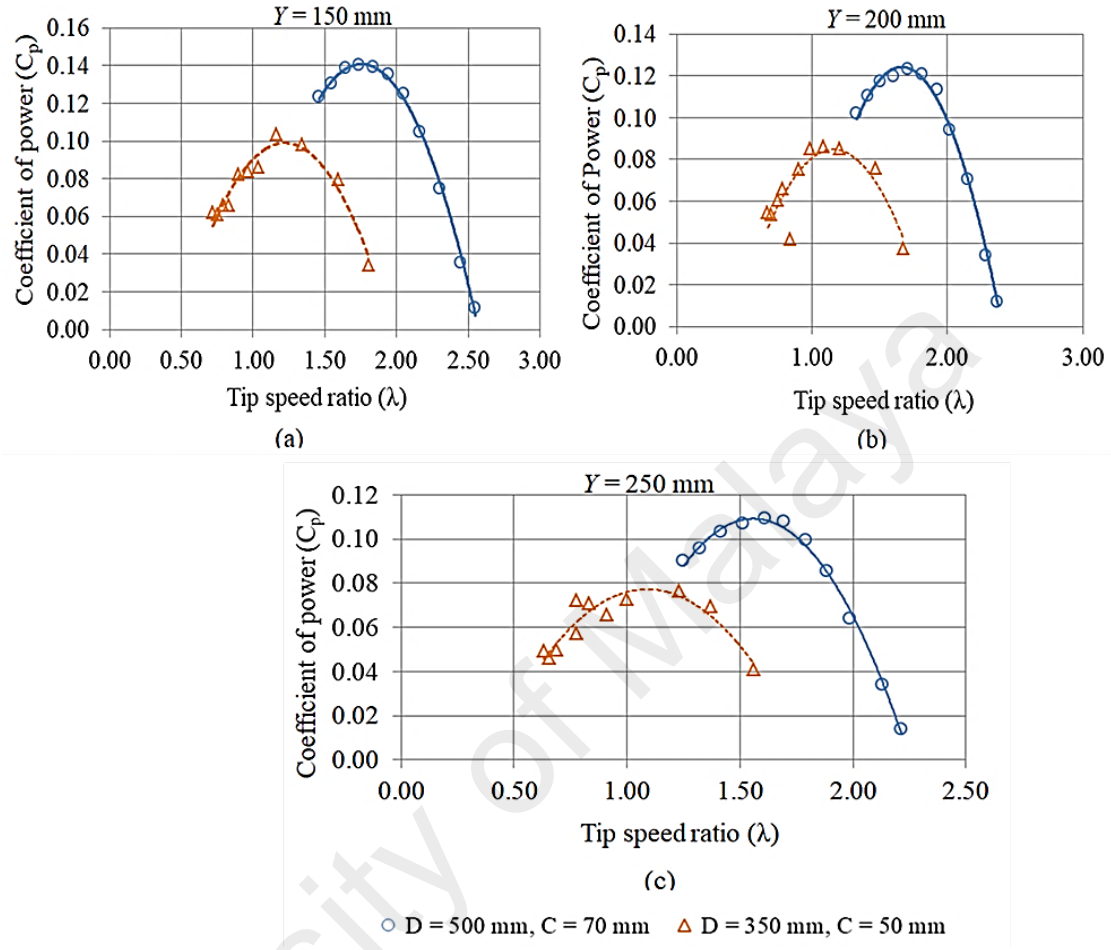

Figure 5.21: Coefficient of power against tip speed ratio for D = 500 mm, c = 70 mm, and D = 350 mm, c = 50 mm at (a) *Y* = 150 mm; (b) *Y* = 200 mm; (c) *Y* = 250 mm

El-Samanoudy et al. (2010) also presented a similar result where the coefficient of power of a VAWT increases with increase in both the radius and chord length of the turbine. Moreover, large scale CAWT has lower solidity ($\sigma = 0.42$) compared to the low scale CAWT ($\sigma = 0.43$). Low solidity minimizes blade wake interaction and consequent complexities, and avoids the occurrence of dynamic stall at moderate TSR. The results of these findings are summarized in Table 5.7.

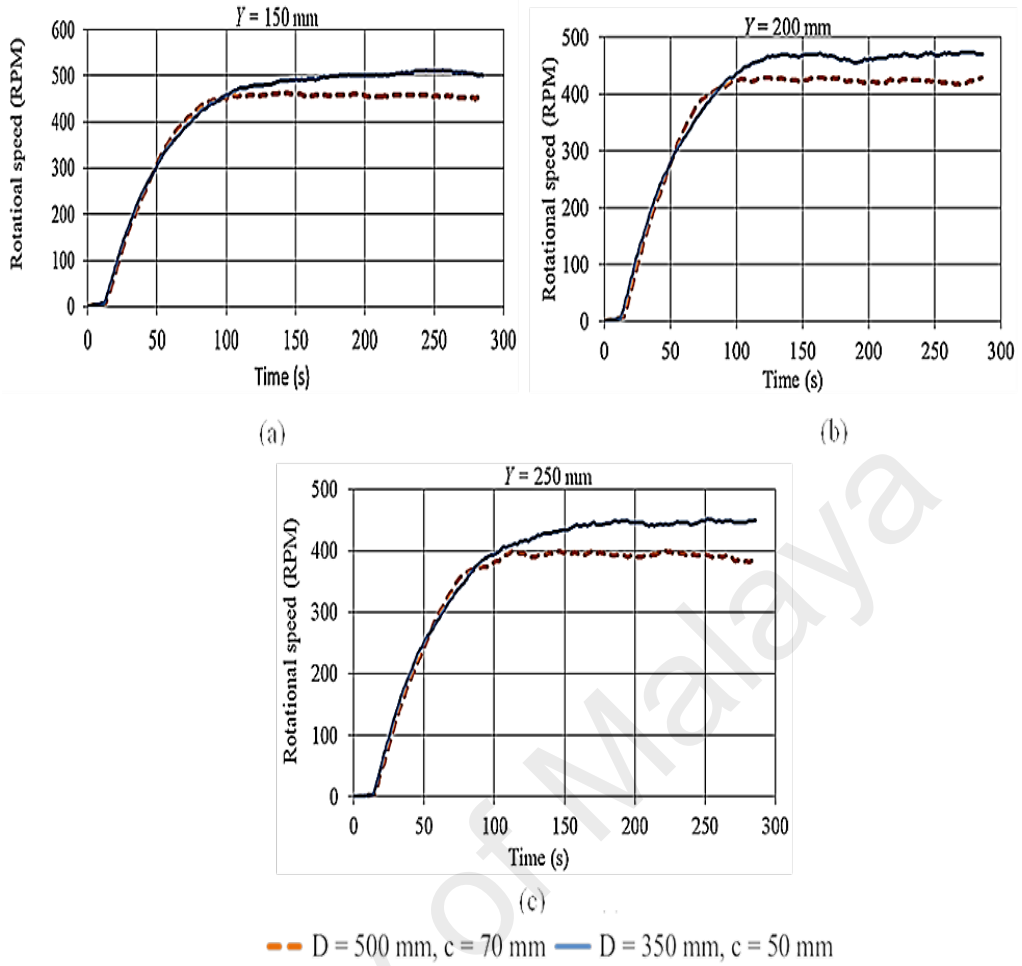

Figure 5.22: Rotational speed against time for D = 500 mm, c = 70 mm and D = 350 mm, c = 50 mm; at (a) *Y* = 150 mm; (b) *Y* = 200 mm; (c) *Y* = 250 mm

Table 5.7: Summary of the result for D = 500 mm, c = 70 mm and D = 350 mm, and c = 50 mm

	D = 500 mm, c = 70 mm			D = 350 mm, c = 50 mm		
	Height (mm)			Height (mm)		
	150	200	250	150	200	250
RPM	464	429	401	512	474	452
C_p,max	0.1393	0.1230	0.1093	0.1035	0.0859	0.0765
TSR	1.84	1.71	1.61	1.16	1.08	1.23

5.9 Effect of roof shapes on the performance of the CAWT

Wind turbines integrated on the buildings have a wide exposure to the prevailing winds from all directions, and the wind speed is higher than in the surroundings landscape (Ragheb 2016). In this section, the effect of roof shape on the performance of the CAWT was investigated. Three configurations were used for comparison, theses includes; the performance of the CAWT on the two rooftops i.e. gable rooftop, and

vaulted rooftop, and compared with the performance of the bare-CAWT (without the rooftop). 10^{o} pitch angle was used for the horizontal blade of the CAWT at an average wind speed of 4.5 m/s. The CAWT is mounted at a height, Y = 100 mm above the two rooftops, which is equivalent to 1464 mm from the ground level for the case of the bare-CAWT. In order to ascertain the rooftop that is more suitable for the integration of CAWT further comparisons were made between the performances of CAWT on the two rooftops (i.e. gable and vaulted rooftop). The comparisons were done by varying the height of the CAWT placed at Y =100-250 mm above the two rooftops The results are presented in Figure 5.23, and Figure 5.24, respectively.

5.9.1 Performance comparison of CAWT on gable, vaulted rooftop, and bare-CAWT

Figure 5.23 compares the C_p values against the TSR of the CAWT integrated on the two rooftops (i.e. gable and vaulted rooftop), and the bare-CAWT configuration (i.e. without rooftop). This Figure shows that the maximum power coefficient, $C_{p,max}$ of the building integrated CAWT is 0.1263 at TSR of 1.06 and 0.0786 at TSR of 1.03 for the gable and vaulted rooftop respectively. In comparison with the bare-CAWT which has $C_{p,max}$ of 0.0572 at TSR of 0.89, This indicates that the $C_{p,max}$ value of the building integrated CAWT increases by 121% and 37% respectively, compared to the bare-CAWT. This implies that mounting the CAWT on a building with gable and vaulted rooftops will yield 121% and 37% more energy respectively compared to the bare-CAWT indicating that the building roof shapes has significant effect in improving the performance of the CAWT integrated on the building as more power is produced when the CAWT is integrated on the rooftop of both the gable and vaulted rooftop compared to the bare-CAWT, Table 5.8.

Figure 5.24, depicts the rotational speed, RPM against time for the CAWT integrated on the gable and vaulted rooftop, and bare-CAWT. The results indicate that RPM of the CAWT integrated onto a building with gable and vaulted rooftops increases by 99% and 89 % respectively compared to the bare-CAWT. The increment in coefficient of power and RPM experienced by the building integrated CAWT is due to the accelerating effect at the rooftops, the presence of the horizontal blades as the supporting struts of the CAWT which interacts with the deflected vertical airflow from the building rooftop, and the pitch angle of the horizontal blades.

The building rooftops served as an augmentation device that further increase the wind speed due to the accelerating effect at the rooftop, the pitched angle which is set at 10^{o} exposes the horizontal blades to a better angle of attack of the vertical wind thereby enhancing the self-starting behavior and improving the overall performance of the building integrated CAWT. The horizontal blade which is also the supporting struts of the CAWT interacts with deflected airflow from the building to improve the self-starting capability of the CAWT at the rooftop compared to the bare-CAWT. With the unique axis of orientation of the CAWT, both the horizontal blades and the vertical blades contribute to the improved performance of the CAWT. Abohela eta al. (2013) presented a study on the effect of roof shapes on the performance of wind turbine, using a computational fluid dynamics simulation, where he tested for the performance of the wind turbine at various roof shapes, they concluded that integrating a wind turbine on the roof shape will yield 56% more energy compared to a free standing wind turbine.

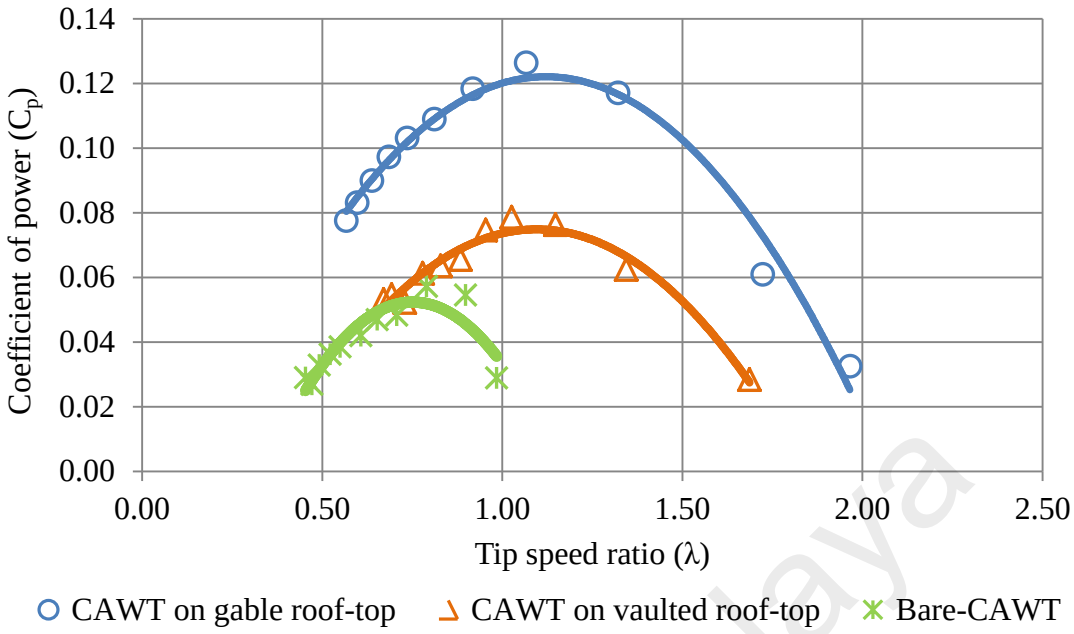

Figure 5.23: Coefficient of power against tip speed ratio for CAWT on gable rooftop, vaulted rooftop and bare-CAWT

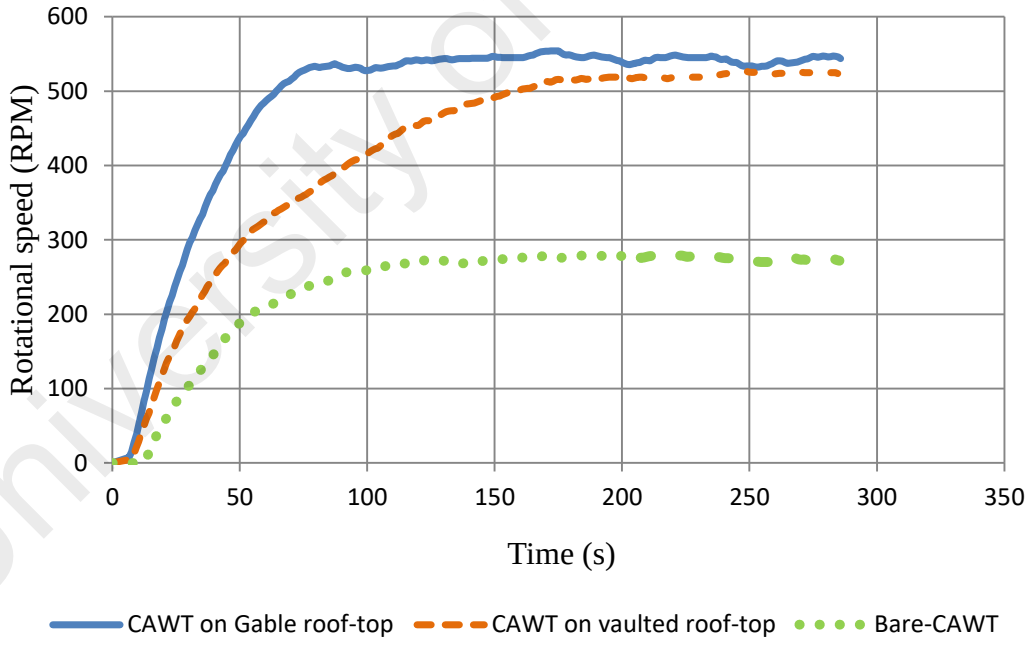

Figure 5.24: Rotational speed against time for CAWT on gable rooftop, vaulted rooftop, and bare-CAWT

The case is not the same for the bare-CAWT, there is little or no vertical wind to interact with the horizontal blades due to the lack of deflected wind streams either from the rooftop (for the case of the building integrated CAWT or guided by a guide van to further direct the deflected wind to the horizontal blades. This necessitates the bare-

CAWT to operate only with the wind streams coming from the horizontal directions, in that case most of the contribution to the performance of the CAWT comes from the vertical blades. The summary of the experimental results for the three configurations is presented in Table 5.8.

Table 5.8: Summary of experimental results on the effect of roofshape on the performance of CAWT on gable rooftop, vaulted rooftop, and bare-CAWT

Parameter	(CAWT on Gable Roof)	(CAWT on Vaulted roof)	Bare-CAWT	Increment on Gable roof (%)	Increment on Vaulted roof (%)
RPM	554	527	279	99	89
$C_{p,max}$	0.1263	0 .0786	0.0572	121	37
TSR, (λ)	1.06	1.03	0.79	34	30

5.9.2 Performance comparison of the CAWT on gable and vaulted rooftop

Figure 5.25 (a, b, c, and d) demonstrate the comparison of the C_P values against the TSR for the CAWT integrated on the gable and vaulted rooftop respectively. The pitch angle for the horizontal blades of the CAWT used in this experiment is 15^o at a wind speed of 4.5 m/s. The experiment was performed for Y = 100 to 250 mm, height of CAWT above the building rooftops. It can be seen from the Figure that the performance of the CAWT on the gable rooftop outperformed its performance on the vaulted rooftop for all the heights. Figure 5.25 (a) depicts the C_p values against the TSR for Y = 100 mm, the results showed that CAWT integrated on a gable rooftop recorded a $C_{p,max}$ of 0.1151 at TSR (λ) of 1.13. The $C_{p,max}$ recorded by the CAWT on the vaulted rooftop at the same height i.e. Y = 100 mm is 0.06913 at a TSR of 0.88, Figure 5.25 (a). The results reveals that integrating the CAWT on a building with a gable rooftop will yield 66% more energy compared to a vaulted rooftop under the similar experimental conditions.

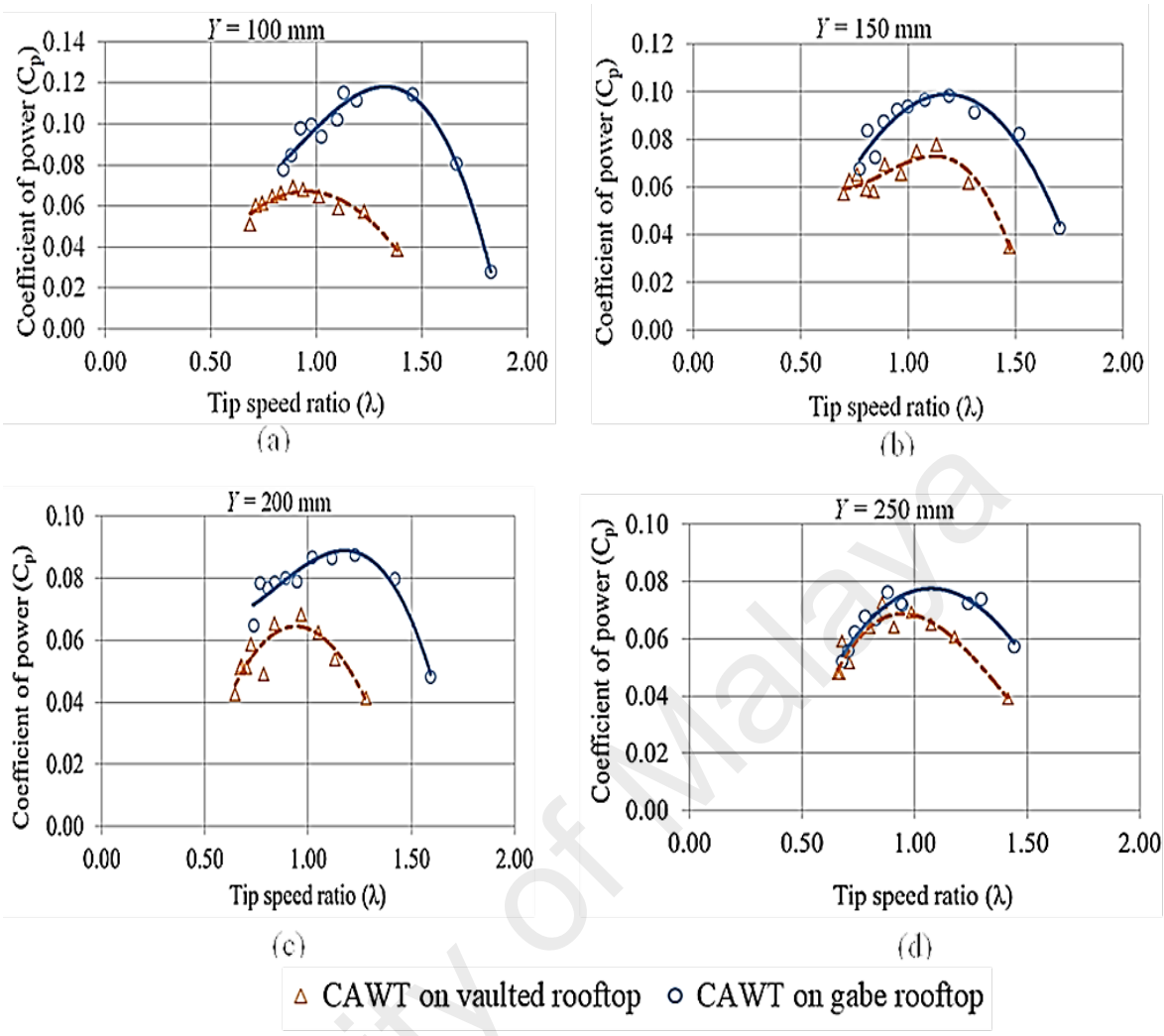

Figure 5.25: Coefficient of power against tip speed ratio for CAWT on gable and vaulted rooftop

Figure 5.25 (b, c, and d) presents the coefficient of power against the TSR for Y = 150 to 250 mm, a similar trend can be seen from the graph where the CAWT integrated on the gable rooftop have higher C_p values compared to the vaulted rooftop, the C_p values of the building integrated CAWT on the gable rooftop increases by 24%, 28% and 10 %, for Y = 150 mm. 200 mm, and 250 mm respectively. The results obtained from Figure 5.25 indicates that a building with gable rooftop is more suitable for mounting a CAWT as the integrated CAWT will yield more energy than a building with the vaulted rooftop.

Figure 5.26 (a, b, c, and d) shows the free-run rotational speed of the CAWT integrated on the gable and vaulted rooftop. All the figures show the same trend, however, it can

be observed from the figures that CAWT integrated on the gable rooftop starts to rotate earlier, and attain a higher rotational speed than the CAWT integrated on the vaulted rooftop. At Y = 100 mm, 31% increment in the RPM can be observed by CAWT integrated on the gable rooftop compared to the CAWT integrated on the vaulted rooftop. The trend is the same in all the height configurations i.e. Figure 5.26 (b-d) Y = 150 to 250 mm where the CAWT integrated on the gable rooftop outperformed its performance on the vaulted rooftop. The improve performance of CAWT on the gable rooftop is attributed to the shapes of the rooftops, The gable rooftop is shaped in such a way that it deflect and direct the deflected airflow to a certain angle known as the skewed angle, the higher the skewed angle, the better the performance of the CAWT. The skewed angle is higher on the gable rooftop compared to the vaulted rooftop as shown in Figure 5.27.

At higher skewed angle the swept area of the turbine is increased due to the contribution of the downwind zone which counterparts the decrease of the projected frontal area with an overall increase of the available surface area to intercept the wind (Bianchini et al., 2012). Furthermore, Skewed flow increases the performance of CAWT on the gable rooftop by modifying the region of interaction of the downwind blade passage with the upwind generated wake. Increasing the skewed angle will increase the area of the downwind blades passage which is operating outside the upwind generated wake thus experiencing an incoming flow with larger energy content (Ferreira, 2006). The summary of the results is shown in Table 5.9.

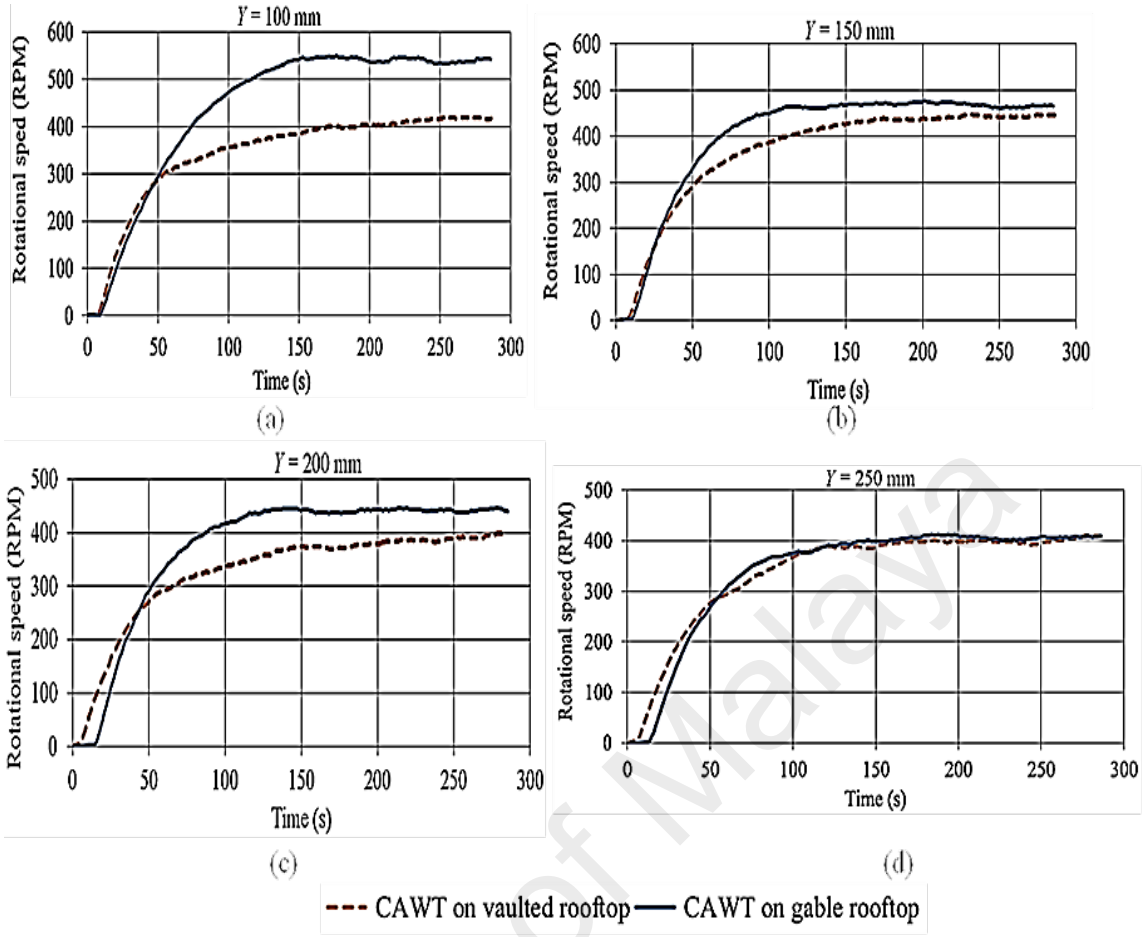

Figure 5.26: Rotational speed against time for CAWT on gable and vaulted rooftop

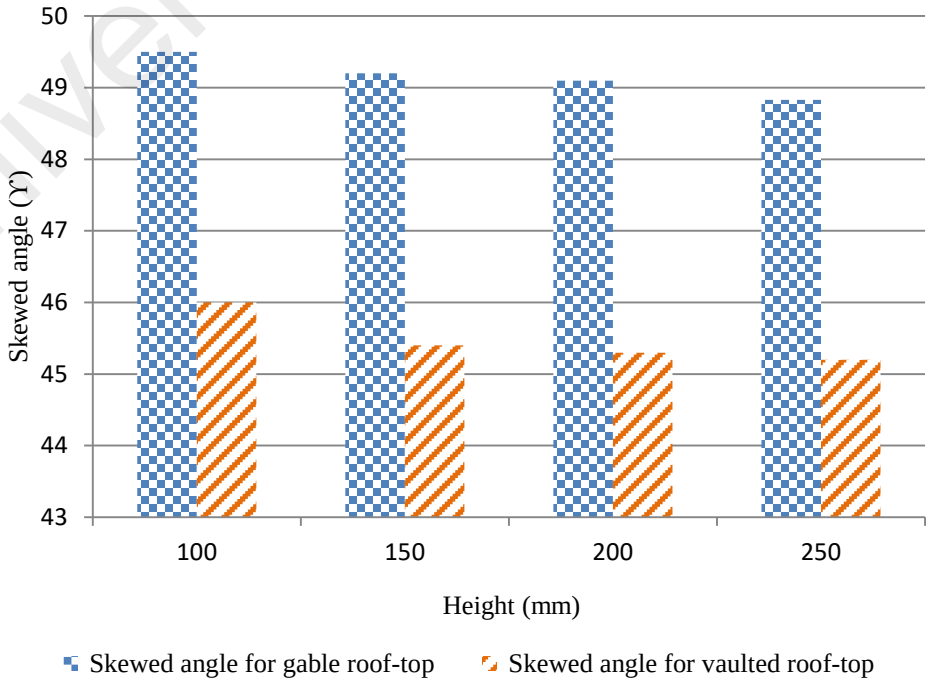

Figure 5.27: Skewed angle on the gable and vaulted rooftop

Table 5.9: Summary of experimental result for the performance comparison of CAWT on the gable and vaulted rooftop (data are presented for 15^{o} pitch angle

Height (mm)	Parameter	CAWT on gable rooftop	CAWT on vaulted rooftop	Increment by gable roof (%)
Y = 100	RPM	549	419	31
	$C_{p,\ max}$	0 .1151	0.06925	66
	TSR (λ)	1.13	0.88	28
Y = 150	RPM	475	447	6.3
	$C_{p,\ max}$	0.098	0.079	24
	TSR (λ)	1.18	1.13	4.4
Y = 200	RPM	447	399	12
	$C_{p,\ max}$	0.087	0.068	28
	TSR (λ)	1.23	0.97	21
Y = 250	RPM	412	411	0.2
	$C_{p,\ max}$	0.076	0.069	10
	TSR (λ)	0.88	0.98	-10

5.10 Simulation results

5.10.1 Flow simulation analysis on the gable and vaulted roof shape

A 2D CFD simulations was conducted for the two roof-shapes without the wind turbine on the rooftop to investigate the flow field around the two roofs. The parameters investigated in the CFD simulation are the streamline velocity, presure distribution, and turbulence kinetic energy around the two roof shapes. Figure 5.28 and Figure 5.29 depicts the velocity streamlines for the gable and vaulted roof shapes. From the figure, the boundary layer separates at the windward roof edge of the buildings and the flow forms a separation bubble on the roof (below the streamline above the roof). As a consequence, the velocity vector of the flow above the separation bubble makes an angle with the horizontal edge of the roof, Figure 5.28 and Figure 5.29. This angle is referred to as the skewed angle. The skewed angle is largest at the windward roof edge and decreases downwind (Mertens et al., 2003).

From the simulation, Figure 5.28, the wind velocity along the centre line of the roof at *Y* = 100 to 250 mm was found to be 5.36 m/s, 5.8 m/s, 5.95 m/s, and 5.97 m/s respectively, it shows that the wind speed achieved high velocity at this points due to

the accelerating effect on the building, and comparing with the inlet wind speed, 4.5 m/s, the wind velocity at the above mention heights of the CAWT increases by 19%, 29%, 32%, and 33% respectively. Hence the wind speed augmented factor, f =1.19, 1.28, 1.32, and 1.33 respectively. While for the case of the vaulted roof shape, Figure 5.29, the wind velocity along the centre line of the roof at Y = 100 to 250 mm, was found to be 6.98 m/s, 7.05 m/s, 6.99 m/s, and 6.82 m/s respectively, indicating an increase of 55%, 56%, 55.3%, and 52% respectively when compared with the inlet wind speed of 4.5 m/s. Hence the wind speed augmented factor, f =1.55, 1.56, 1.54, and 1.52 respectively.

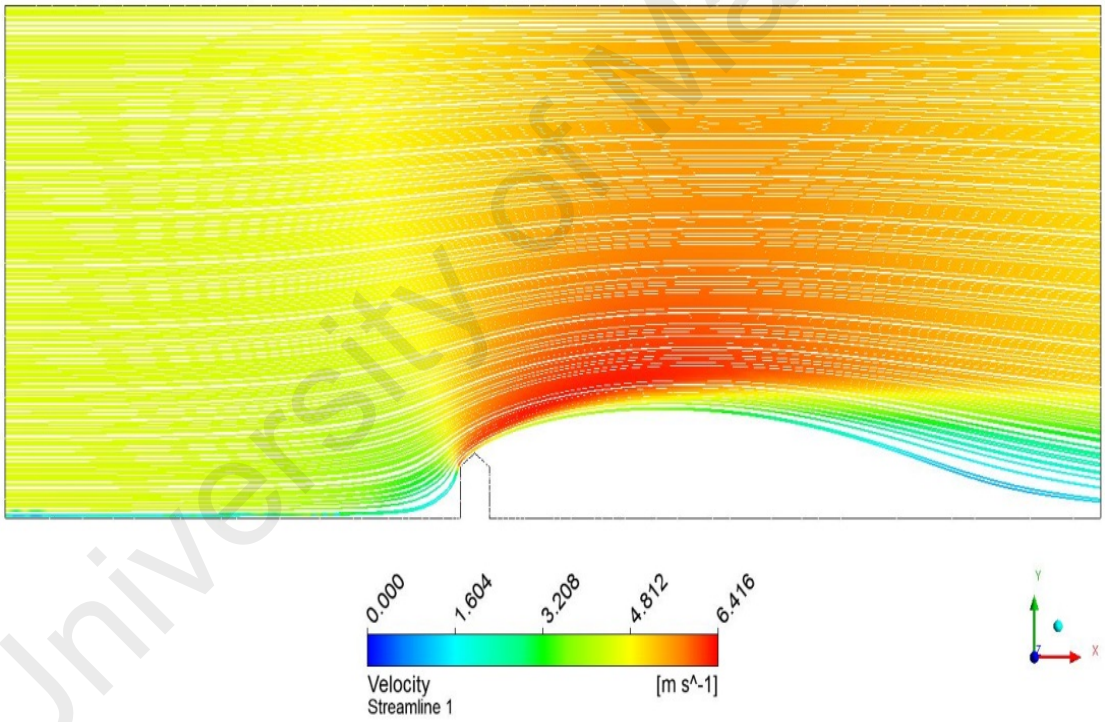

Figure 5.28: Velocity streamline for the gable rooftop

The instantaneous streamlines shows that the flow is periodical for the two roofs. A periodic increase in air velocity is observed by both rooftops. This shows that both the rooftops (gable and vaulted) can cause an increase in streamwise velocities above the roof. However, a higher increase in streamwise velocity is noticed on the vaulted

rooftop compared to the gable rooftop. The velocity profile for the gable and vaulted roof shape is presented in Figure 5.30.

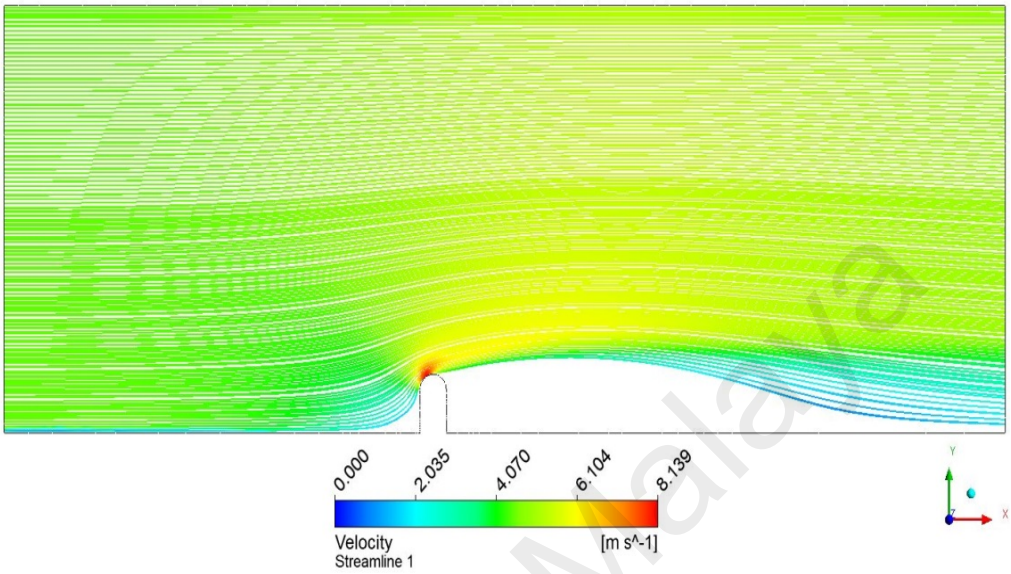

Figure 5.29: Velocity streamline for the vaulted rooftop

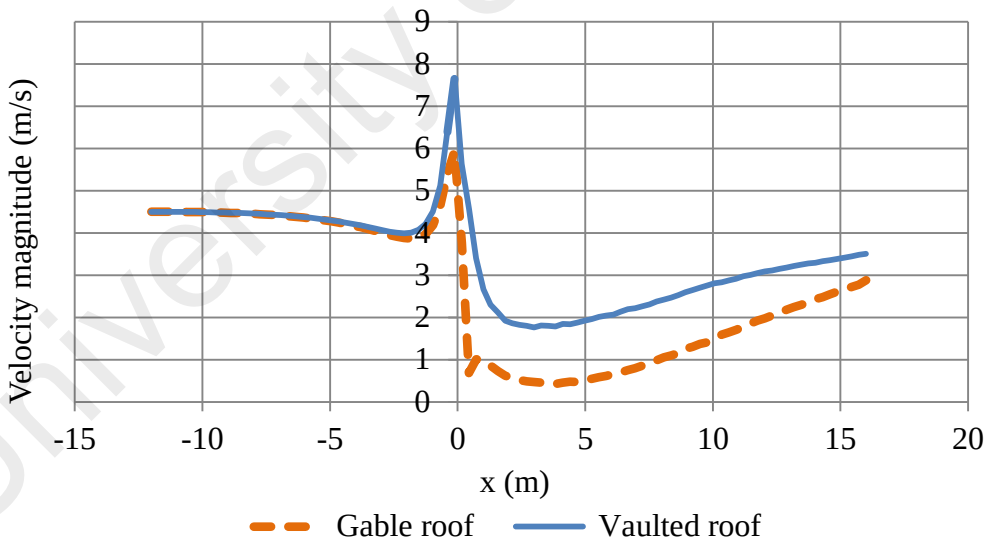

Figure 5.30: Velocity profile for the gable and vaulted rooftop

Additionally, the pressure contours on the two rooftops are presented in Figure 5.31 and Figure 5.32 respectively. Figure 5.31 shows the contour for the static pressure on the gable rooftop while Figure 5.32 shows the contour for the static pressure on the vaulted rooftop as the air comes in contact with the building. From these Figures it can be seen

that as the air stream came in direct contact with the building façade, a positive airside pressure is observed on the vertical wall of both buildings, this is due to the force that is directly perpendicular to the area of interaction. These cause a negative pressure to be generated on the opposite end at the immediate downstream of the building where the air velocity increased due to the streamlined body of the structure. Flow separation is seen around the rooftop, this flow separation can induce extreme low pressure that caused a pressure differential which was utilized by the turbine to generate higher lift force. The maximum positive pressure as observed from the figures was estimated at 7.2 pa and 5.46 pa for the gable and vaulted rooftop respectively. Also the maximum negative pressure was observed to be -9.45 pa and -21.907 pa for the gable and vaulted roof respectively. The analysis shows that the total pressure differential for both the gable and vaulted rooftop is 16.65 pa and 27.367 pa respectively was created for entire each geometry.

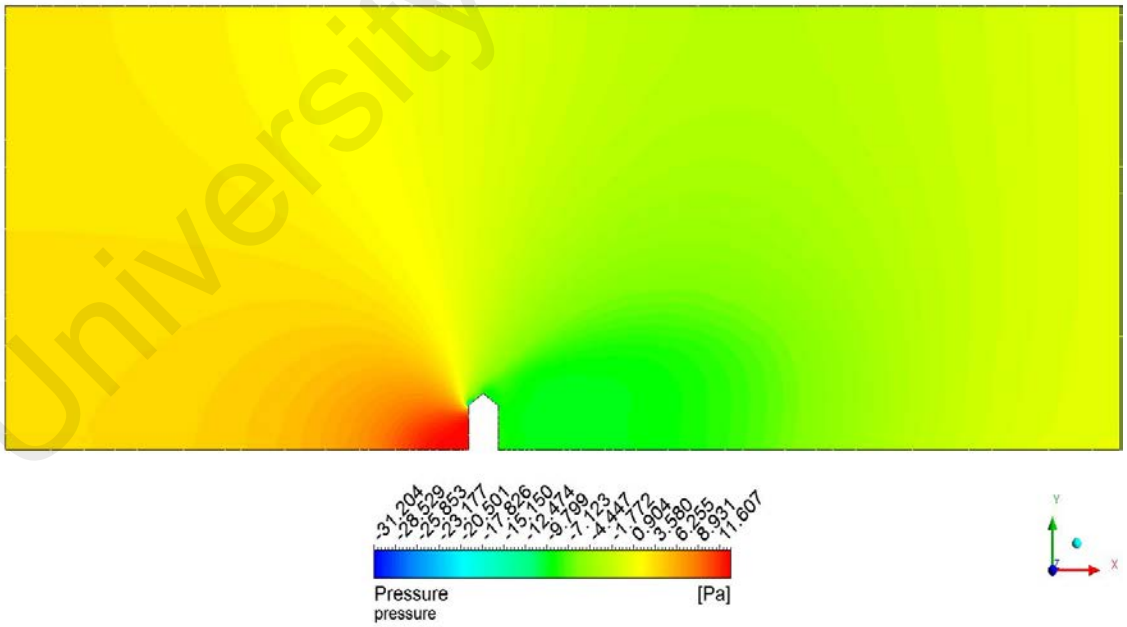

Figure 5.31: Pressure contour for the gable rooftop

The pressure profile showing a very sharp drop of pressure for the case of the vaulted rooftop is presented in Figure 5.33. Similarly, it can be observed that the gable rooftop

has higher positive pressure compared to the vaulted rooftop, the pressure differential between the windward side and the leeward side of the gable rooftop pushes the wind upward to the horizontal blade therefore creating more lift force for the CAWT thus enhancing its self-start behavior and improving its overall performance.

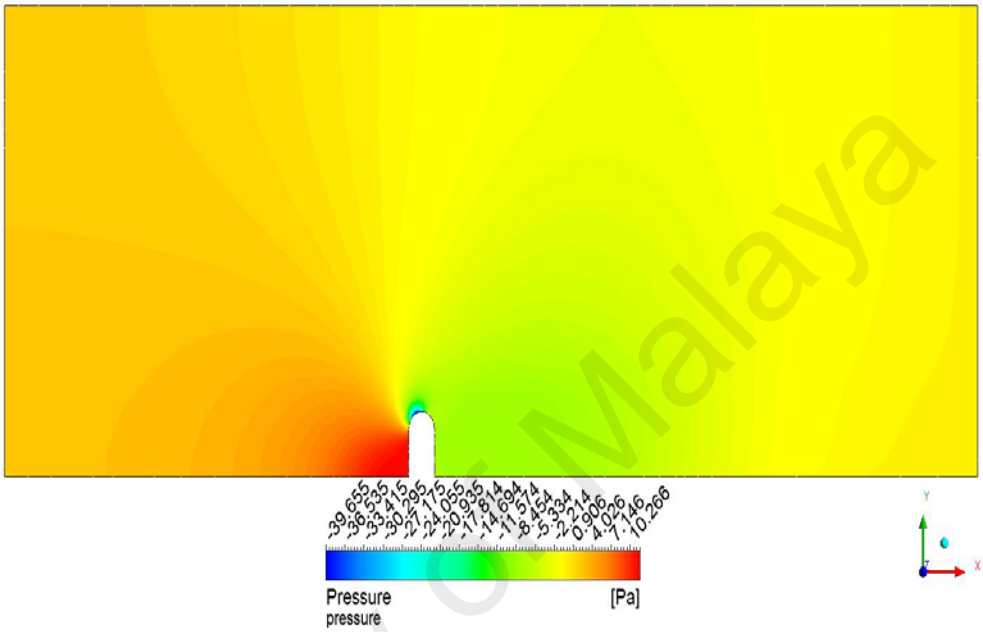

Figure 5.32: Pressure contour for the vaulted rooftop

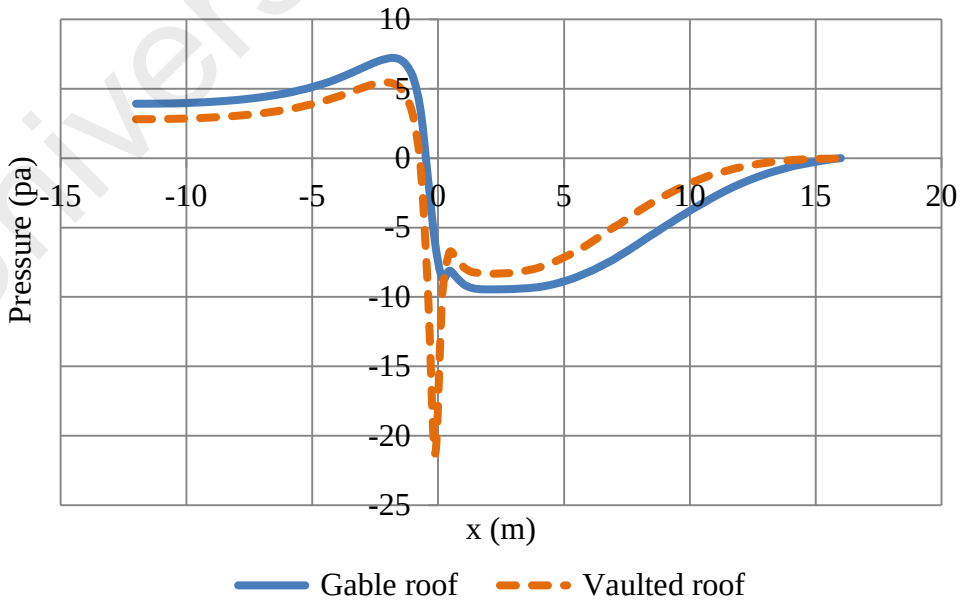

Figure 5.33: Pressure distribution for the gable and vaulted rooftop

The turbulence intensity for the two roof models are presented in Figure 5.34 and Figure 5.35. Figure 5.34 presents the turbulence intensity for the gable rooftop while Figure 5.35 presents the turbulent intensity for the vaulted rooftop. From these figures, it was observed that the gable rooftop experiences high turbulence intensity than the vaulted rooftop. This turbulence intensity has a significant influence on the performance of a wind turbine. Due to the cubic variation of power with wind speed more turbulent winds have greater power than less turbulent winds with the same mean wind speed (Cochran, 2002). Since the turbulence in the wake is an efficient mixer, it mixes the low velocity fluid in the wake with the high velocity fluid outside it. In this way momentum is transferred into the wake, the wake expands but the velocity deficit is reduced (Sanderse, 2009). Relating this with our current scenario, the gable roof shape has better performance because of the high turbulence experience by the CAWT on the gable rooftop. This high turbulence intensity increases the ability of the atmosphere to mix in high momentum air therefore enabling the induced wake to recover fast. Figure 5.35 shows the profile of the turbulence intensity on both the gable and the vaulted rooftop.

In general, despite the higher increment in wind velocity experienced by the vaulted rooftop, the result presented above shows that the mounting of CAWT on the gable rooftop performs better than on the vaulted rooftop this is attributed to the flow field on the rooftop. It was observed that the flow path is based on the shaped of the roof, It can be seen from Figure 5.28 that the flow on the gable rooftop is directed upward at a certain angle to the rooftop, this angle is called skewed angle, and higher skewed angle means higher performance.

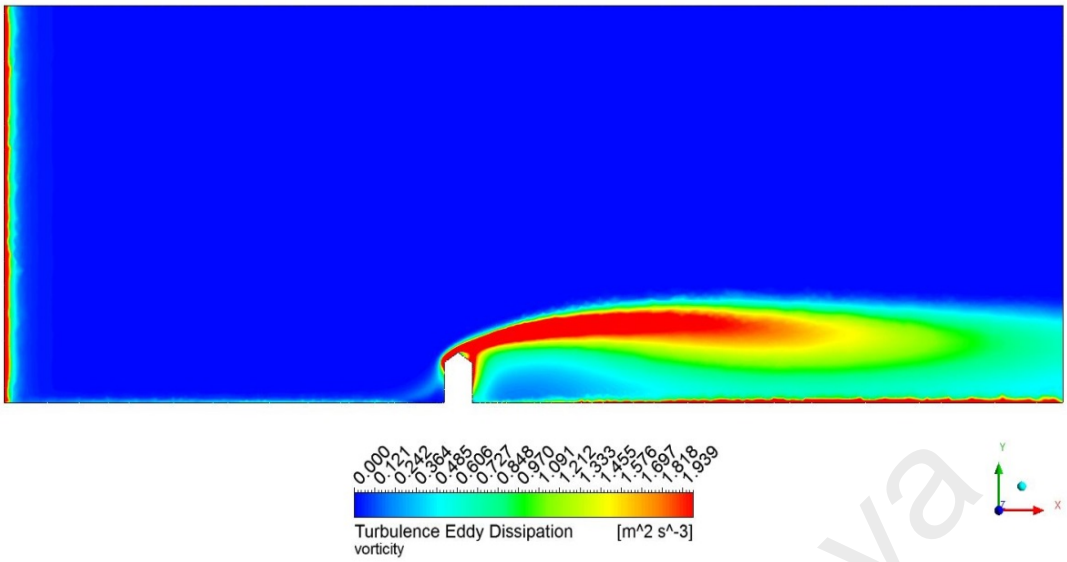

Figure 5.34: Turbulence eddy dissipation for gable rooftop

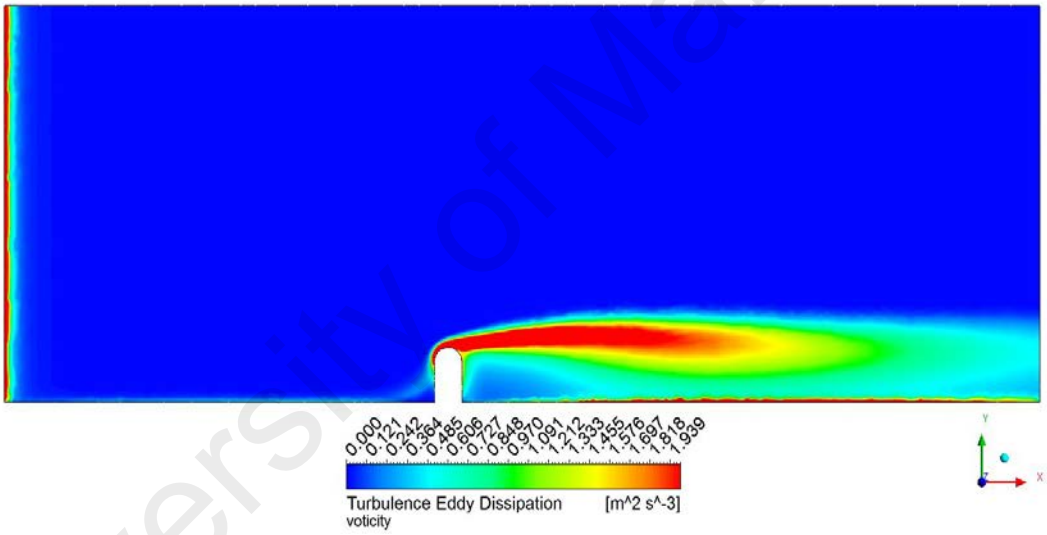

Figure 5.35: Turbulence eddy dissipation for vaulted rooftop

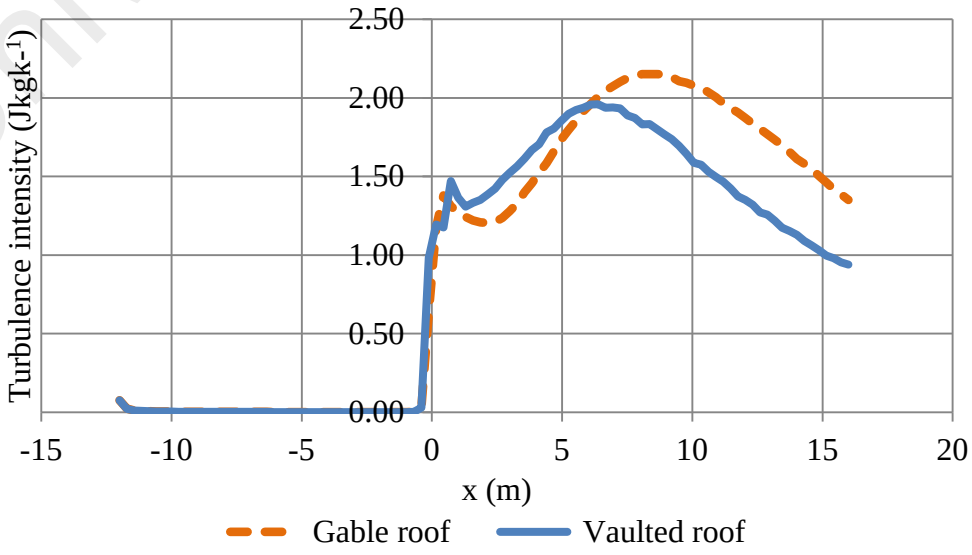

Figure 5.36: Turbulence eddy dissipation profile for gable and vaulted rooftop

On the gable rooftop, at the ridges, the wind speed compressed on the side of the building facing the wind, and once it reaches the top of the buildng and spills to the other side it can expand again in the low pressure area on the leeward side of the building. In Bernoulli's equation, the reduction in the static pressur is associated with an increase in kinetic pressure, and henc an increase in wind speed results (Ragheb 2016). The gable roof takes the advantage of the "roof effect" whereby the wind impacts the surface of the sloped face of the gabled roof and deflects the airflow upwards towards the ridge, thus directing the wind stream at an optimum angle of attack of the vertical wind before it intaracts with the horizontal blades. Unlike the vaulted rooftop, the wind stream on the vaulted roof shape takes the shape of the roof due to the curved nature of the vaulted rooftop the horizontal blades is deprived of the much needed deflected vertical wind to enhance its performance.

As earlier stated, the Figure 5.36 showed that the gable rooftop experience more turbulence compared to the vaulted rooftop. High turbulence experienced by the gable rooftop increases the performance of the CAWT. Based on previous researches, turbulence intensity actually improves the performance of wind turbines (Sanderse, 2009; Kurt S. Hansen et al., 2012; Lubitz, 2014). The power extraction is proportional to the cube of the relative velocity at the blade which increases with increase in turbulence (Mikkelsen, 2013). Higher turbulence appeared to increase the power production of CAWT mounted on the building with gable rooftop. At higher turbulence intensity, the turbine induces a wake (velocity deficit) recovers faster (Sanderse, 2009). The turbulence intensity has played a significant role in improving the overall performance of CAWT on the gable rooftop compared to the vaulted rooftop. According to Lubitz (2014), turbulence in the approaching wind can have a significant influence on the wind turbine power output; this is mainly significant for the smaller

wind turbines, which in practice are often situated near buildings, trees and other Impediments

5.10.2 Validation

This subsection provides a comparison between the experimental measurements and the computational data which was carried out to fully understand the flow structure around the building models. To verify the reliability of the simulation result, Figure 5.37 (a) shows the schematic diagram of the measuring locations while Figure 5.37 (b) indicates the comparison of the experimental data and the CFD data for the wind speed measurement. Eleven measuring points were used, the measuring distance starts from x (m) is the upwind side from 0.1 m to 0.5 m at 0.1 m interval, and, – x (m) in the downwind side from -0.1 m to -0.5 m, where x is the measuring distance. The averaged values of the velocity component were deduced for Y = 100 mm height above the building model. The results were compared with those obtained from the experimental measurement. The results showed that both the CFD results and the experimental data agree well with small discrepancies. The percentage error ranges from 8.6% on the upwind side of the building to 33% on the downwind side. The high discrepancies on the downwind side is due to the significant turbulence and vortex on the downwind side

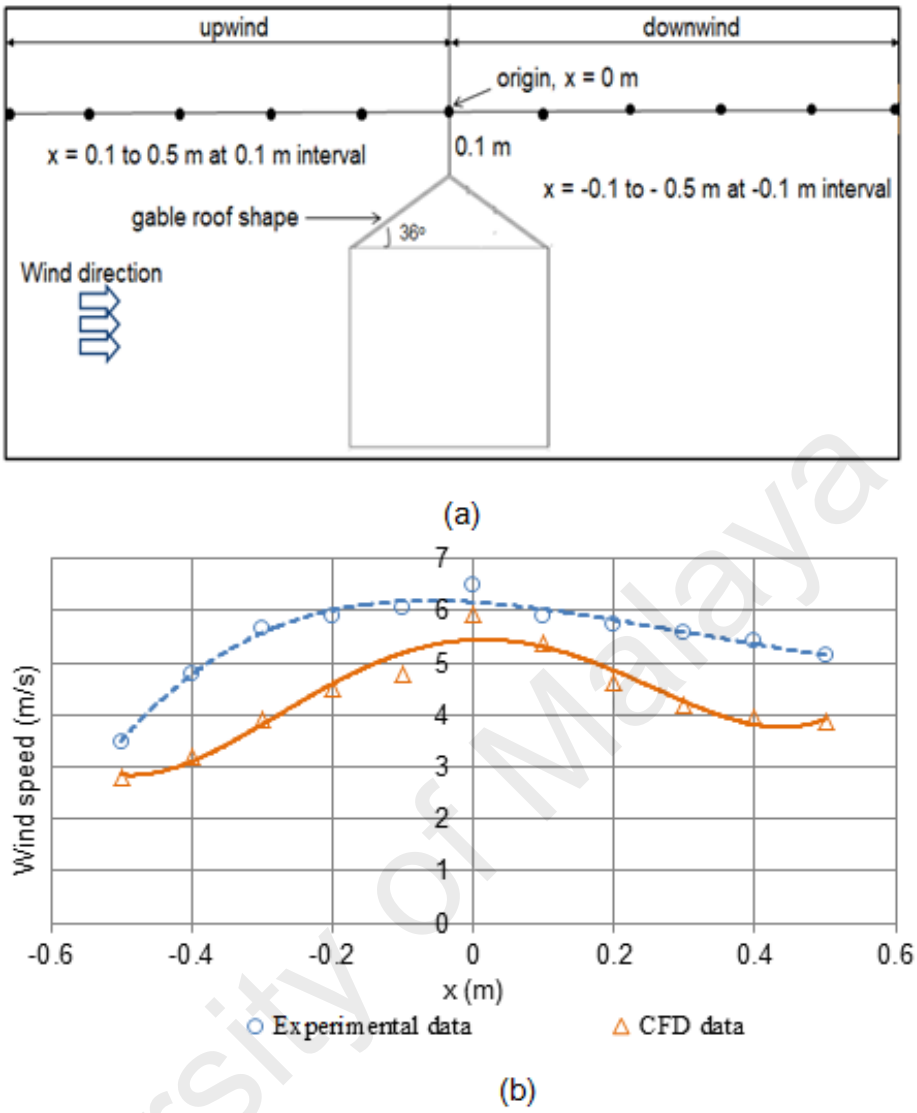

Figure 5.37; (a) Schematic diagram illustrating the measuring locations, (b) CFD simulation and experimental results

5.11 Analytical results

Analytical model based on the double multiple streamtube and blade element momentum method is proposed for calculating the rotor performance and aerodynamic blades forces for the CAWT. The detail discussion of these models is presented in chapter two subsection 2.11, and 2.13.1.

5.11.1 Local wind velocity profile on gable and vaulted rooftop

The local mean velocity profile for the two building models with different roof shapes at azimuth angles from 5° to 355° are plotted in Figure 5.38, and Figure 5.39.

Figure 5.38 presents the local mean velocity profile for the gable rooftop, while Figure 5.39 presents the local mean velocity profile for the vaulted rooftop at Y = 100 mm, 150 mm, 200 mm, and 250 mm. Different roof shapes produce different local wind velocity profiles throughout the azimuthal positions. The local wind velocity decreases gradually from azimuth angle of 5^{o} to 75^{o} for the case of the two rooftops. At the windward side of the building model, the wind velocity is high at azimuth angle of 5°, nearest to the local point. However, as the distance between the local point and the surface of the building increases, the deflected wind velocity reduces at these local positions.

Similar observations can be made for local points at azimuth angles of 95° to 175°. At the downstream position, i.e. the leeward side of the building models, the wind velocity decreases from 215° to 275° azimuth angle as a result of the leeward direction and the effect of the shaft, after these positions, the local wind velocity further increased from azimuth angle of 285° to 355°. Calculating the uncertainties for the measured local wind velocities showed that the maximum standard error of the mean velocities was below 10%, suggesting good repeatability.

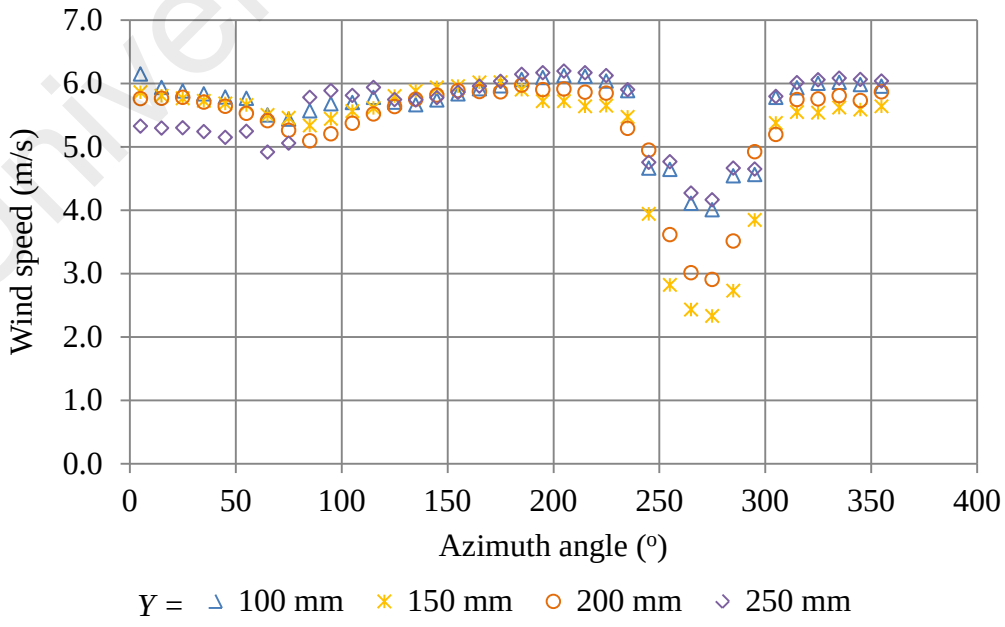

Figure 5.38: Local velocity profile for gable rooftop

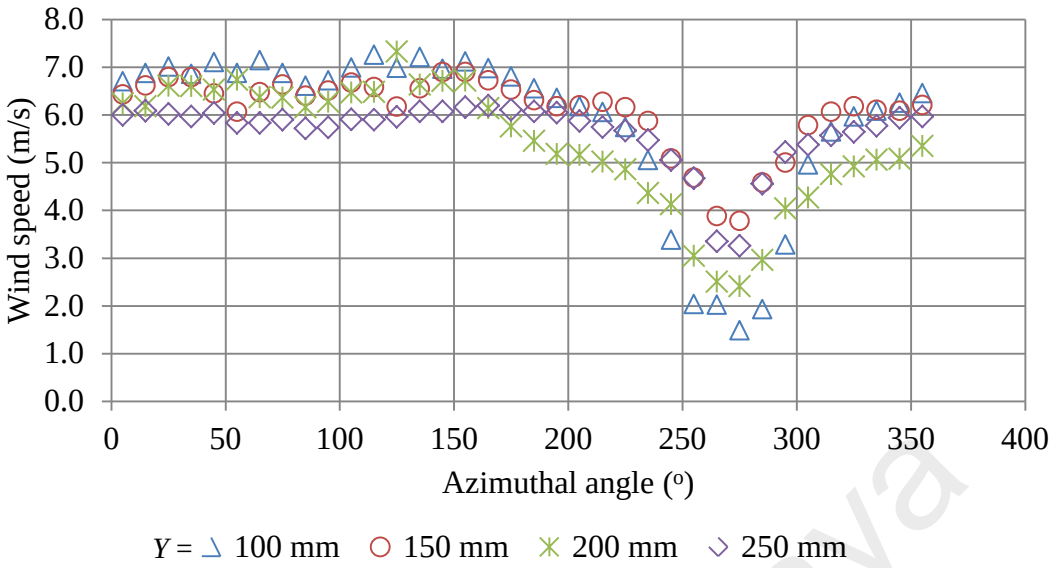

Figure 5.39: Local velocity profile for vaulted rooftop

5.11.2 Comparing the performance of CAWT (analytical and experimental method)

The performance of CAWT was predicted using the analytical approach outlined in section 2.11 and sub-section 2.13.1. To validate the proposed model, comparisons were made between the results of the experimental and the analytical studies. The performance of CAWT on both the gable, and the vaulted rooftop was used for the analytical studies. Using the approach outlined in Subsection 2.11, and sub section 2.13.1. For this analysis, the data for the 10^{o} and 15^{o} pitch angle of the horizontal blades of the CAWT were used as a case study since CAWT performs better at this pitch angles compared to the 5^{o} and 0^{o} pitch angles, Figure 5.5 and Figure 5.6. The calculation was done for different turbine height, Y = 100 mm, 150 mm, 200 mm, and 250 mm. The results are presented for the peak power from the experiments, DMST model, BEM model, and the power obtained from the combined method of the BEM and DMST models.

5.11.3 Comparison between experimental result and calculated results (CAWT on gable rooftop)

Figures 5.40 and Figure 5.41 present the comparisons between the power produced by the CAWT from experiment, DMST model, BEM model, and the combined power of the DMST and BEM model at different heights of the CAWT above the gable rooftop. The results are presented for 10^o and 15^o pitch angles for the horizontal blade. Figure 5.40 depicts the power produce by the CAWT for the 10^o pitch angle for Y = 100 to 250 mm. From the figure it can be seen that both the experimental power and theoretical power have similar trend where the power output decreases with increase in height of the CAWT above the rooftop. Though, there is an over prediction from the calculated power. The percentage error is less than 20% for both the 10^o, and 15^o pitch angles (appendix A). The calculated theoretical power is slightly higher compared to the experimental power; this is due to some factors such as the presence of the shaft, connecting struts and aerodynamic losses at the end of the blades. Furthermore, there are vibration factors and internal friction that lead to the power loss which were not taken into account in the analytical approach (Huleihil & Mazor, 2012). The theoretical power obtained is the combination of the power produced from the DMST and BEM model, it was observed from the figure that the total peak theoretical power produced by the CAWT for Y = 100 mm was calculated to be 0.871758 W, out of which the vertical blade (DMST) contributed 0.17584 W (i.e. 20.2%) and the horizontal blade contributed 0.695919 W (i.e. 79.8%).

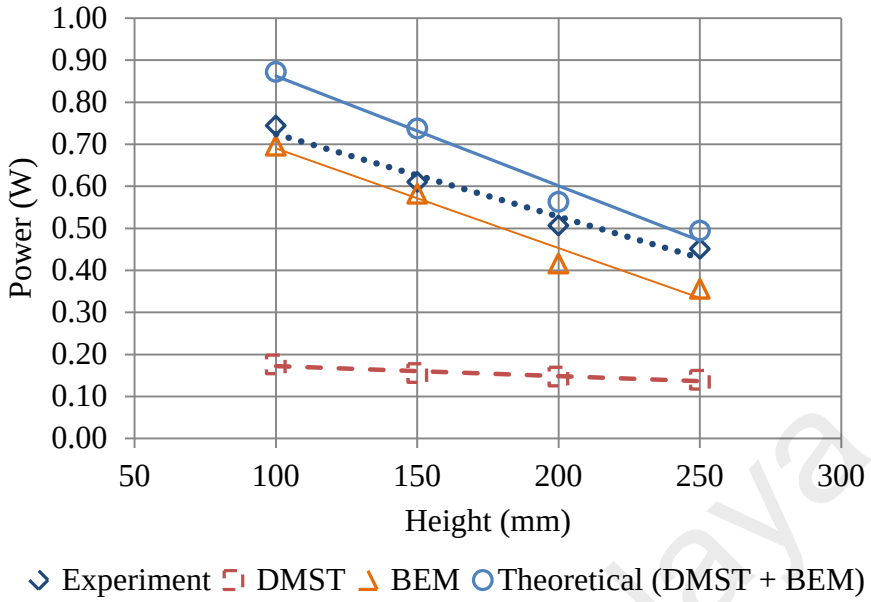

Figure 5.40: Comparison between the power obtained from experiment and analytical approach for 10^{o} pitch angle for CAWT on gable rooftop

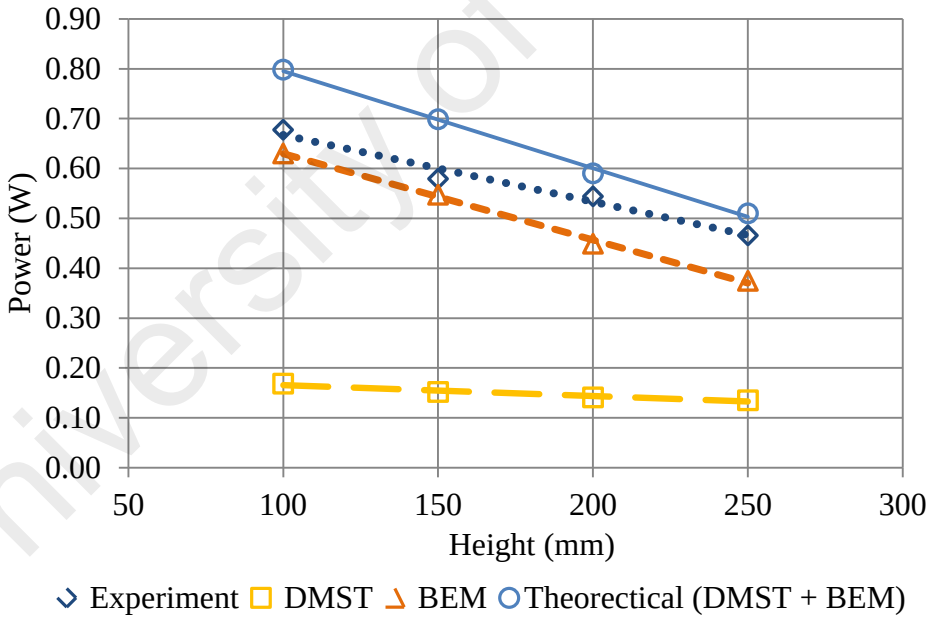

Figure 5.41: Comparison between the power obtained from experiment and analytical approach for 15^{o} pitch angle for CAWT on gable rooftop

Similarly, Figure 5.41 depicts the power produced by the CAWT for the 15^{o} pitch angle for Y = 100 - 250 mm, similar trend of increased power at lower height of CAWT is also observed. As the height of the CAWT increases, the power generated by the CAWT is low; the trend is the same both in the experimental, DMST, and the BEM

results. The general trend presented in Figure 5.40 and Figure 5.41 indicates that the calculated power decrease with increase in height of the CAWT above the rooftop. This results obtained is in agreement with the results obtained from the experimental study for both the 10^o and 15^o pitch angle, Figure 5.9 where the CAWT performance decreases with increase in height, similarly, the total peak theoretical power was obtained for CAWT at Y = 100 mm height. The peak power at this height was calculated to be 0.7977936 W, out of which the vertical blade (DMST) contributed 0.1682207 W (i.e. 21.1%) and the horizontal blade contributed 0.629716 W (i.e. 78.9%).

5.11.4 Comparison between experimental results and calculated results (CAWT on vaulted rooftop)

The comparison between the power produced by the CAWT integrated on the vaulted rooftop and the calculated power from the DMST and BEM models are presented in Figure 5.42 and Figure 5.43 for 10^o & 15^o pitch angle of the horizontal blades of the CAWT respectively. Similar trend of increased power at lower CAWT height was also observed. The percentage error due to prediction from the calculated power is less than 20% for both the 10^o, and 15^o pitch angles. As the height of the CAWT increases, the power generated by the CAWT decreases; the trend is the same both in the experimental, DMST, and the BEM results. This results obtained is in agreement with the results obtained from the experimental study for both the 10^o and 15^o pitch angle, Figure 5.14 where the CAWT performance decreases with increase in height. The total peak theoretical power produced by the CAWT was obtained at 100 mm height for both the 10^o and 15^o pitch angle. For the case of the 10^o pitch angle, this peak power was calculated to be 0.5667 W, out of which the vertical blade (DMST) contributed 0.18272 W (i.e. 32.2%) and the horizontal blade contributed 0.38399 W (i.e. 67.8%).

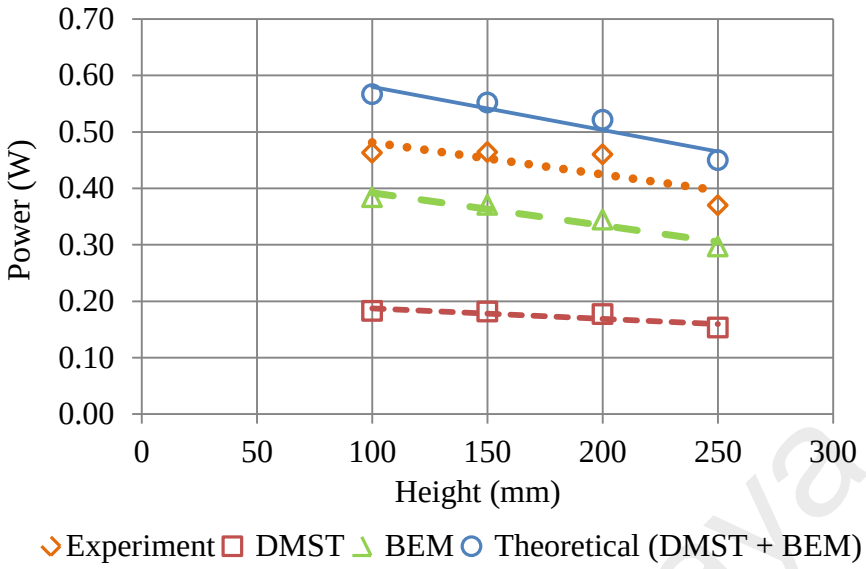

Figure 5.42: Comparison between the power obtained from experiments and analytical approach for 10^{o} pitch angle for CAWT on vaulted rooftop

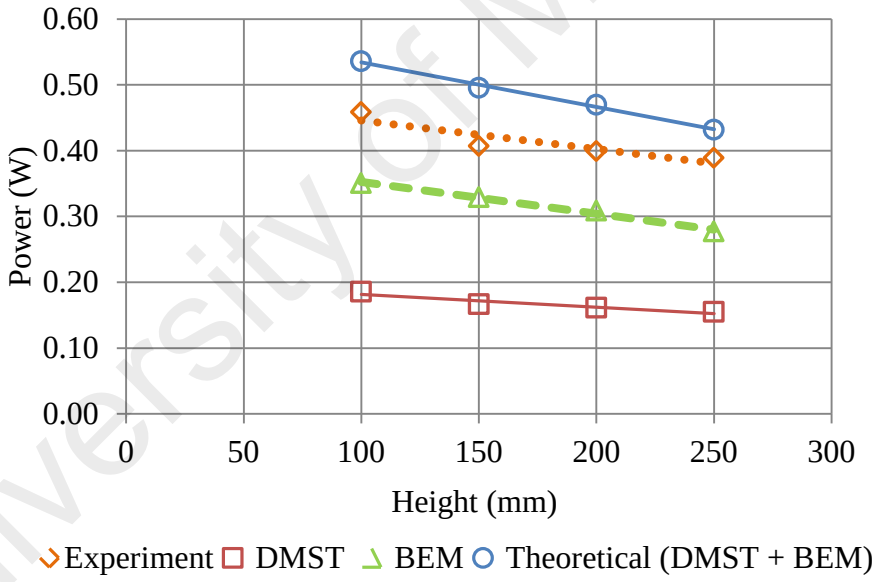

Figure 5.43: Comparison between the power obtained from experiments and analytical approach for 15^{o} pitch angle for CAWT on vaulted rooftop

And for the case of the 15^{o} pitch angle Figure 5.44, the peak power was calculated to be 0.5359 out of which the vertical blade (DMST) contributed 0.1854 W (35%) and the horizontal blade (BEM) 0.3504 W (i.e. 65%) of the total power produced by the CAWT.

5.11.5 Instantaneous torque and angle of attack (BEM Model)

Figure 5.44 (a, b, c, and d) shows the instantaneous torque and the angle of attack against the azimuth angle for *Y* = 100 mm, 150 mm, 200 mm, and 250 mm which is calculated using the BEM model along the whole blade span r/R = 91%, 69%, and 46% respectively. The data are obtained from the performance of the CAWT on the gable rooftop, and for 10^{o} pitch angle of the horizontal blades. From the Figures, it can be observed that similar trend of graph is observed in all the figures where the horizontal blades of the CAWT produces a negative torque at azimuth angle 5^{o}-45^{o} at the upstream, and azimuth angle 245^{o}-355^{o} at the downstream. At these azimuth positions the angle of attack, AOA of the turbine blade is less than 20^{o} for the entire blade spans, r/R = 91%, 69%, and 46% respectively for azimuth position 5^{o}-45^{o} which is not preferable to produce positive torque. At azimuth position of 265^{o}-355^{o} the negative torque produce by the horizontal blades is due to the low angle of attack experience by the blades at this azimuth positions. This is because lift is created by a pressure differential which occurs whenever the angle of attack is not equal to zero at these azimuth positions, since the AOA is negative, only a drag force exists.

However, lift begins to be created as the blades rotate out of these two positions as the angle of attack increases, positive torque are produced for all the blade span r/R; 91%, 69%, and 46% respectively when the blades rotates and passes these azimuth positions, hence positive power is expected at these azimuth positions. For the case of Figure 5.44 (a), *Y* = 100 mm, the torque produce by the horizontal blades gradually increase from a negative to a positive torque between azimuth angle 55^{o}-255^{o}, at this azimuth positions, the angle of attack is optimum for all the blade span r/R: 91%, 69%, and 46% respectively. A peak torque of 0.00336 Nm is observed at azimuth angle 95^{o} where at this azimuth position the angle of attack are 24.3^{o}, 30.7^{o}, and 40.8^{o}, for the 91%, 69%, and 46% blade span respectively.

For the case of Figure 5.44 (b), Y = 150 mm, the horizontal blade produces positive torque between azimuth angle 35°-245° at this azimuth position. A negative torque is seen around azimuth angle 5°-25° at the upstream and 255°-355° at the downstream, this negative torque arises as result of low angle of attack less than 5° at the upstream and negative angle of attack at the downstream. A total peak torque of 0.00257 Nm is observed at azimuth angle 135° where at this azimuth angle the angle of attack are 30.3°, 50.9°, and 80.7°, for the 91%, 69%, and 46% blade span respectively.

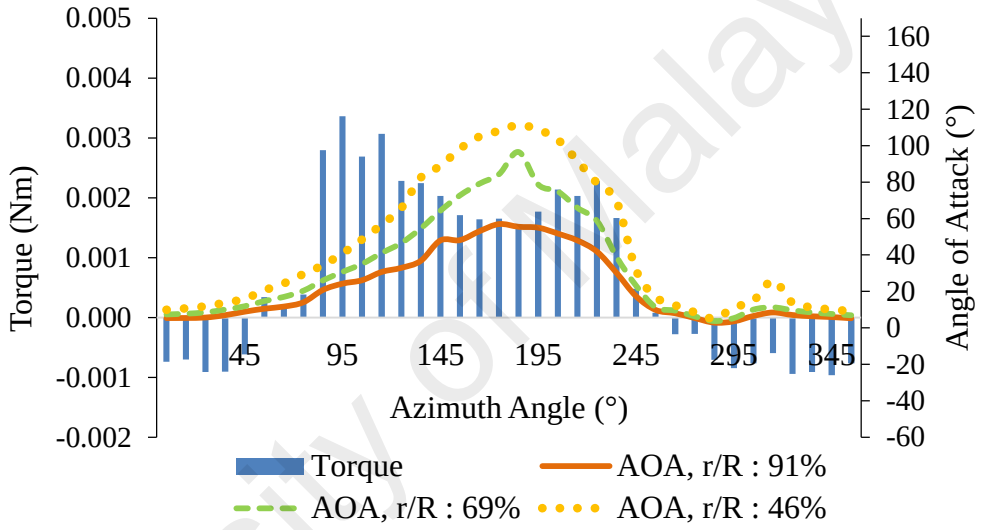

(a) *Y* = 100 mm

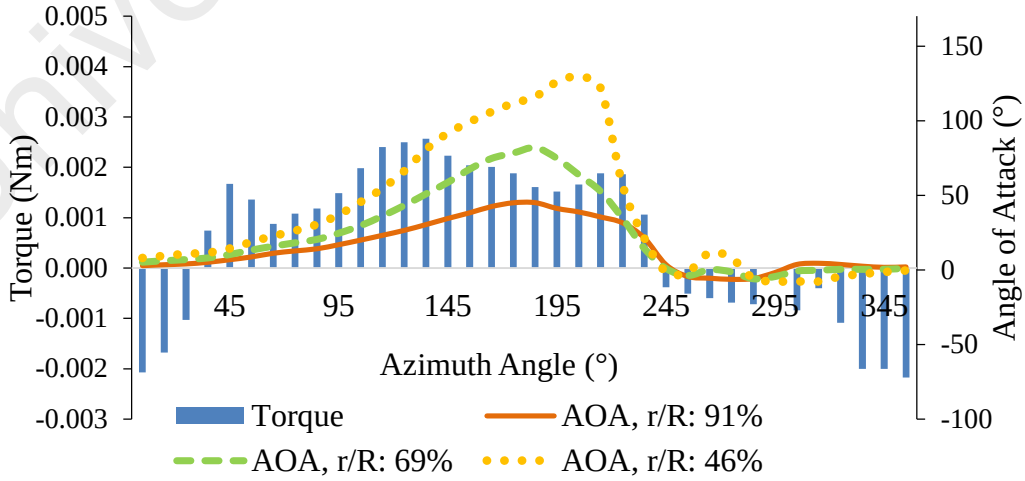

(b) *Y* = 150 mm

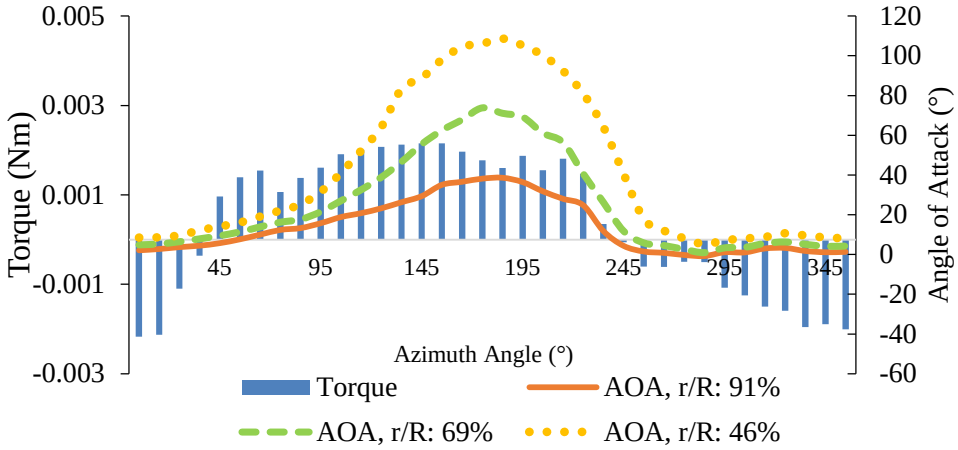

(c) *Y* = 200 mm

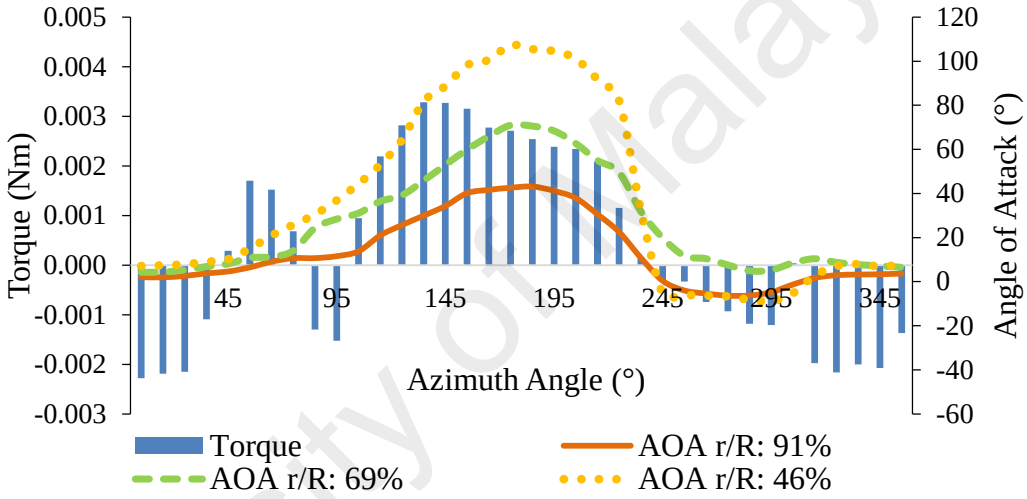

(d) *Y* = 250 mm

Figure 5.44: Instantaneous torque and angle of attack against azimuth angle for (a) *Y* = 100 mm; (b) *Y* = 150 mm; (c) *Y* = 200 mm; and (d) *Y* = 250 mm

Figure 5.44 (c, and d) presents the instantaneous torque and angle of attack against the azimuth angle for *Y* = 200 mm, and 250 mm height respectively. In Figure 5.44 (c), similar trend of negative torque is also observed where the horizontal blade of the CAWT produces negative torque between azimuth angle 5^{o}-35^{o} and 245^{o}-355^{o}. However, positive torque is produced at azimuth angle 45^{o}-235^{o}, at these azimuth positions, the angle of attack is ranges between 24^{o}-38^{o}, 26^{o}-73^{o}, and 19^{o}-106^{o} for blade span of 91%, 69%, and 46% respectively. The total peak torque produced by the CAWT is 0.00215 Nm at angle of attack of 29^{o}, 55^{o}, and 88^{o} for blade span of the 91%, 69%,

and 46% respectively. In Figure 5.44 (d), Y = 250 mm, a negative torque is seen between azimuth angle 5^o- 35^o, and a sharp drop in torque is seen between azimuth 85^o, and 95^o, and a negative torque between azimuth angle 245^o-345^o. This is due to the low angle of attack < 5^o found at these azimuth positions, the total peak torque produced by the CAWT is 0.00328 Nm at angle of attack of 29^o, 45^o, and 81^o for blade span of the 91%, 69%, and 46% respectively. The general trends of lift and drag coefficients of an airfoil behave much like a flat plate beyond the stall angle. The shape of the airfoil has little or no effect on its aerodynamics in the stall region due to the separation of flow which develops on the thick boundary layer of the airfoil (Montgomerie, 2004).

The instantaneous torque contribution along the blade span r/R: 91%, 69%, and 46% is presented in Figure 5.45 (a, b, and c) for Y = 100 mm for the purpose of discussing the instantaneous torque contribution along the blade span. Since the trend in the graph are similar, the instantaneous torque contribution along the blade span for Y = 150 mm, 200 mm, and 250 mm are presented in appendix E2, it can be seen from the figure that most of the section along the blade span have optimum angle of attack which give rise to positive torque except at the blade root section r/R: 46%, which means that most of the blade sections experience attack flow except for the root section. The Figure display that the 91% blade span contribute the highest amount of torque followed by the 69% blades span. The blade span with the least contribution of torque despites the positive angle of attack experience by the blade section is the 46% blade span. At 46% blade span the torque contribution is very small, many factors can lead to the low torque production at the 46% blade span, this includes; the blade location, the shaft effect and blockage effect.

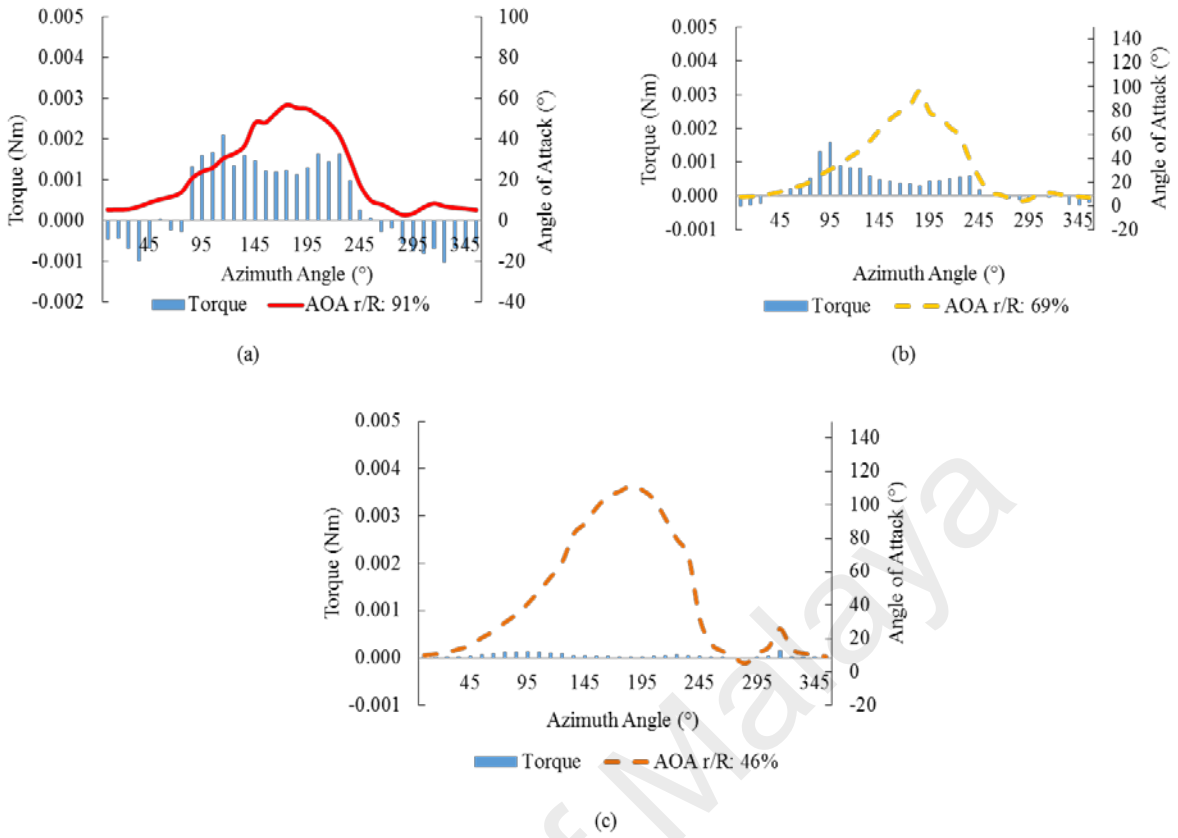

Figure 5.45: Instantaneous torque contribution and angle of attack against azimuth angle for (a) r/R: 91%; (b) r/R: 69%; and r/R: 46% blade span for *Y* = 100 mm

5.11.6 Instantaneous torque and angle of Attack (DMST Model)

Figure 5.46 (a-d) presents the DMST analysis of the distribution of the instantaneous torque and angle of attack against azimuth angle for the vertical blades of the CAWT for all the height i.e. *Y* = 100 mm, 150 mm, 200 mm, and 250 mm.

As can be seen from all the figures, the graph shows similar trend for all the CAWT configurations i.e. *Y* = 100 to 250 mm, where the angle of attack behave like a sinusoidal function when the tip speed ratio is high, thus it is assumed that the blades are under sinusoidal oscillatory motion as the VAWT is under operation. However, when the TSR is decreased, the effective angle of attack becomes larger, this expand the regions where dynamic stall takes place and the blade deteriorate further due to the situation around it which lead to poor performance of the VAWT. From all the figures, it can be observed that at the upstream side of the blade due to the low angle of attack

experience by the blade, negative torque is generated at azimuth angle 5^{o}-45^{o} as shown in Figure 5.46 (a & b). However, as the angle of attack increases gradually at this region, the torque output generated began to increase steadily, this occurs at azimuth angle 55^{o}-165^{o}. The angle of attack reaches its maximum at azimuth angle 125^{0}. The angle attack decreases after that and become negative at the downstream side. The torque value generated began to decrease as the angle of attack changes to a negative value i.e. at azimuth angle of 175^{o}-355^{o} at the downstream side of the blade. The positive torque is generated between azimuth angle 55^{o}-165^{o} as shown in Figure 5.46 (a & b).

Similar observation can be deduce for the case of Figure 5.46 (c & d), but in this case, the negative torque at the upstream side occurred at azimuth angle 5^{o}-55^{o}, when the angle of attack is low. As the angle of attack increases along with the azimuth angle, the torque values began to increase steadily until a peak torque value is achieved. The positive toque value is achieved at azimuth angle 65^{o}-155^{o}. After this position the angle of attack began to decrease steadily to a negative value, this cause the torque value to decrease gradually at the downstream side i.e. at azimuth angle 165^{o}-355^{o} as shown in in Figure 5.46 (a & b).

At Y = 100 mm Figure 5.46 (a) the peak torque produce by vertical blades of the CAWT is 0.0348 Nm at azimuth angle of 95°, and angle of attack of $\alpha = 33.4°$, and the total torque produce by the vertical blades of the CAWT at Y = 100 mm is 0.06415 Nm. At Y =150 mm Figure 5.46 (b) the peak torque produce by the vertical blades of the CAWT is 0.032377 Nm at azimuth angle and angle of attack of 105^{o} and 33^{o} respectively, the total torque produce by the CAWT at this position is 0.00519 Nm.

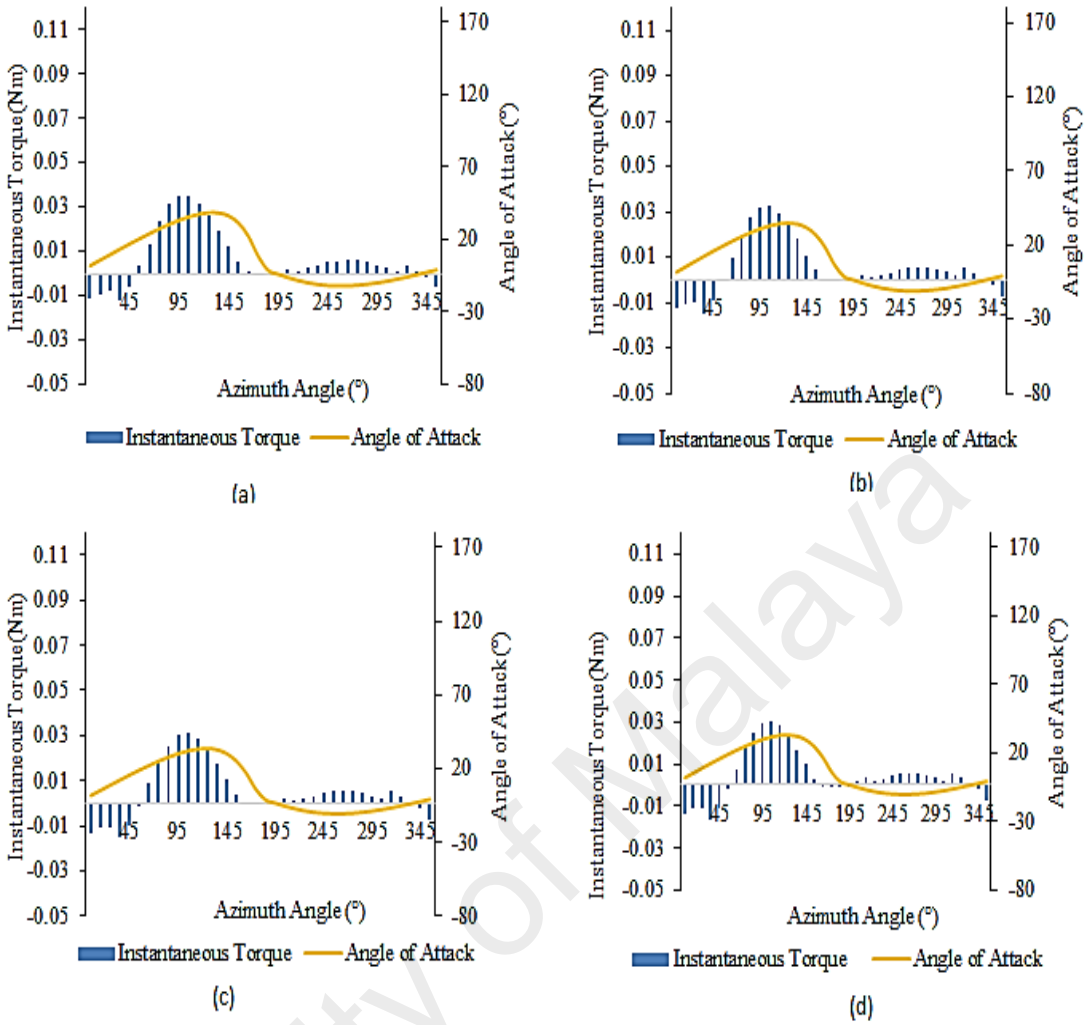

Figure 5.46: Instantaneous torque and angle of attack against azimuth angle for (a) *Y* = 100 mm; (b) *Y* = 150 mm; (c) *Y* = 200 mm; and (d) *Y* = 250 mm.

For the case of Figure 5.46 (c, and d) i.e. *Y* = 200 mm, and 250 mm, the peak torque of 0.031048 Nm and 0.029675 Nm are obtained at azimuth angle of 105^{o} and angle of attack of 32^{o}, and 31.3^{o} respectively. The total torque produce by vertical blades of the CAWT at *Y* = 200 mm, and 250 mm is calculated to be 0.004754 Nm and 0.004386 Nm respectively.

Based on the DMST theory, negative angle of attack experienced by the vertical blades of the CAWT is due to the switching of the blade to the downstream position. This happens on the third and fourth quadrants. According to Sheldahl and klismas (1981) the angle of attack of an airfoil of VAWT changes continuously from positive to negative and back to positive as it revolves round its vertical axis. This is the reason

why the instantaneous torque is low in these regions, due to the significant reduction in lift coefficients. From the figures, negative torque is observed at the first quadrant as the angle of attack increases steadily from the first to second quarter region. At the second quarter region, the instantaneous torque increases to a high value of 0.0348 Nm for the 10^{o} pitch angle or Y = 100 mm. The angle of attack further decreases to a negative value as the vertical blade rotates to the downstream position in the third and fourth quadrants.

5.12 Soft computing approach

A soft computing approach was used to predict the performance of power augmented vertical axis wind turbine. The results obtained from this approach are presented in the following sub-sections

5.12.1 Experimental results

Additional studies were conducted to predict the performance of power augmented vertical axis wind turbine using soft computing methodology. Firstly, experiments were conducted with and without the presence of the power augmentation guide vane (PAGV) integrated on the VAWT for different wind speeds. The experimental results without the PAGV show that the wind turbine cannot self-start by itself, hence requiring an external force to be applied on the rotor to enable the turbine to start. This is the reason why the rotational speed for the case of a wind turbine without the PAGV starts at about 20 RPM to 30 RPM. However, when the wind turbine was integrated with the PAGV, it was able to self-start without the influence of any external force. Furthermore, with the presence of PAGV, the average increments of the Sistan rotor wind turbine rotational speed is 29% for wind speeds of 4.24 ms^{-1} and approximately 25%. For wind speed 4.63 ms^{-1}. Figure 5.47 illustrates the results from the experiments. The results obtained from these experiments are use as input data for the soft computing methodology, using ANFIS (adaptive neuro-fuzzy inference system).

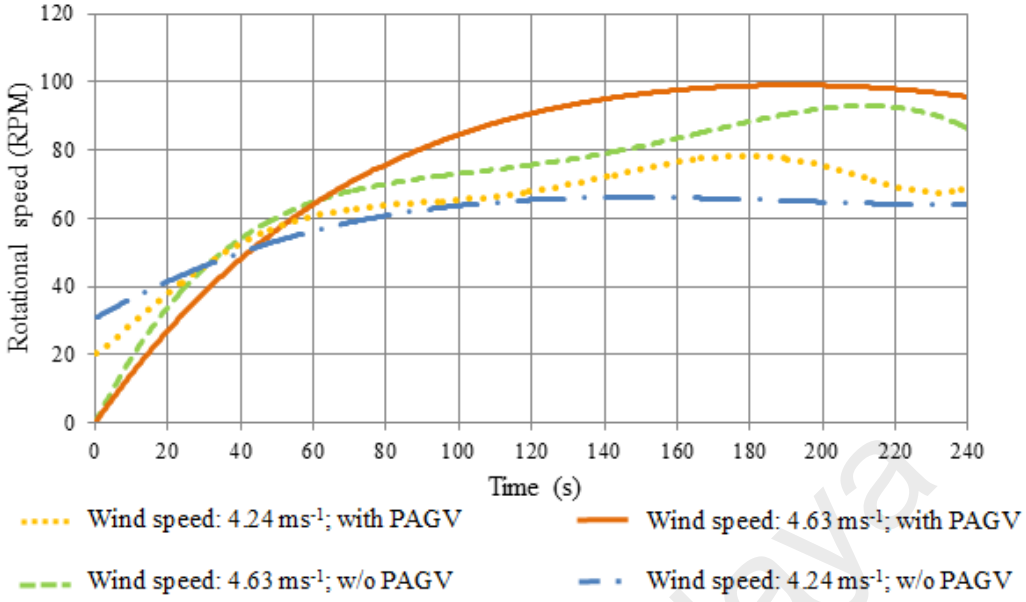

Figure 5.47: Wind turbine rotational speed and time (with PAGV and without PAGV) for different wind speeds

5.12.2 Input variables for the ANFS model

The data shown in Figure 5.47 was used for generating the ANFIS model. To get a more reliable evaluation and comparison, the ANFIS model is tested by evaluating a data set that was not used during the training process. The statistical parameters (wind speed, and rotor rotational speed with and without the presence of PAGV) for data sets are calculated and given in Table 5.10.

Table 5.10: Statistical parameters for data sets ([a] Stabilized rotor rotational speed)

Average wind speed (ms^{-1})	Rotational speed (RPM)[a] of the rotor	
	Without PAGV	With PAGV
4.24	70	90
4.63	80	100

5.12.3 ANFIS model analysis

5.12.3.1 Training of data set

Training is a learning process of the developed model. The model is trained until the results are obtained with minimum error. To design an ANFIS system for real world problems, it is essential to select the parameters for the training process and testing of data set (Vaidhehi, 2014). In this study, approximately 70% of the data generated for the ANFIS model was used for training purposes, and the remaining 30% was used for testing purposes of the ANFIS model. Three bell-shaped membership functions were used to fuzzify the inputs of the ANFIS. After the training process, the ANFIS networks were tested to determine the wind turbine rotational speed without the presence of the PAGV and with the presence of the PAGV. The predicted data is used to correlate with the rotor rotational speed test data extracted from the experiment, Figure. 5.47.

The average computation time for the ANFIS modeling was around 300 seconds for 1000 training epochs using a PC with the Intel Core Duo CPU E7600 @3.06GHz and 2-GB RAM. For the ANFIS modeling, MATLAB software was used. The predicted rotor rotational speed values using ANFIS model for a wind turbine without the PAGV are presented in Figure 5.48 (a) and 5.48 (b). Whereas, Figure. 5.49 (a), and 5.49 (b) illustrate the predicted values using ANFIS model for a wind turbine with the PAGV.

As seen in the figures, the R^2 correlation coefficients are very high. Therefore, the ANFIS model used for the study has a very good correlation with the wind turbine model with and without the PAGV. Note that the R^2 correlation is higher for the wind turbine with the PAGV, which translates to a better correlation. The output from the ANFIS shows that the model can be used to predict the wind turbine performance for any future sites. By feeding the site's wind speed data into the ANFIS model, the output

of rotor rotational speed for wind turbine models with and without the PAGV can be predicted.

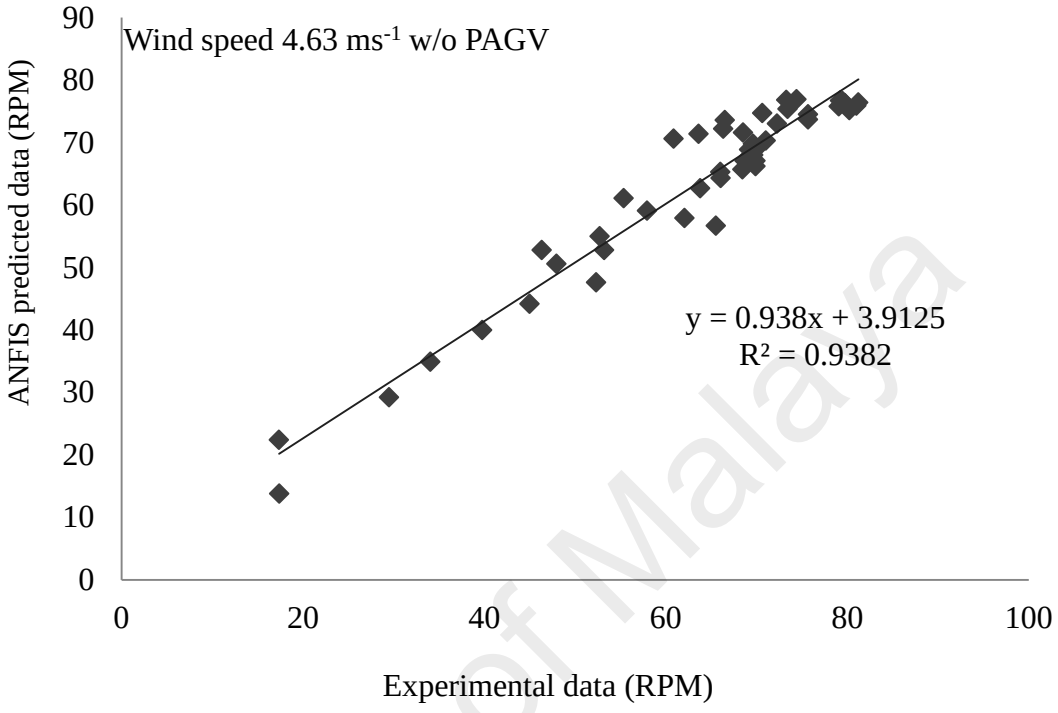

(a)

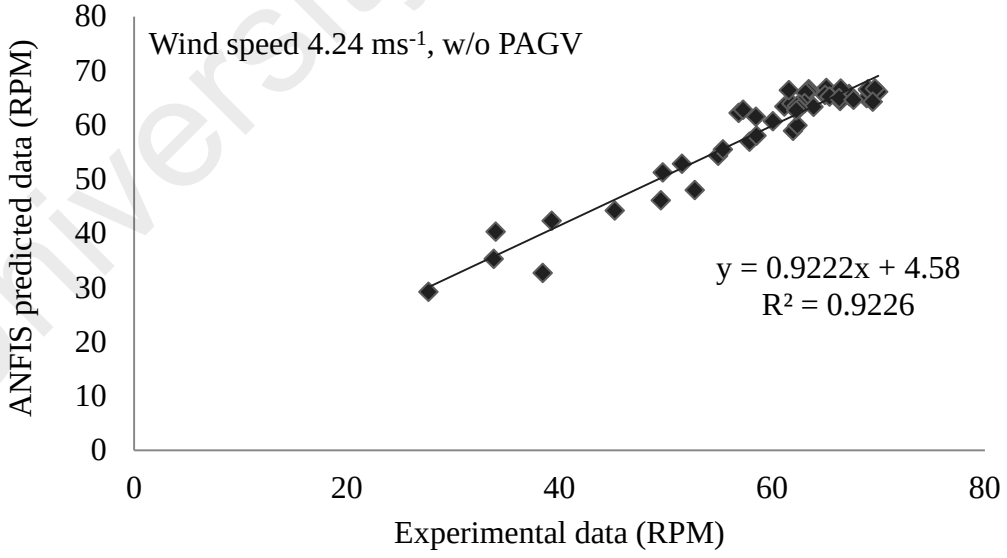

(b)

Figure 5.48: Scatter plots of predicted and experimental data of rotational speeds (RPM) without PAGV using ANFIS model for wind speed (a) 4.63 ms^{-1} and (b) 4.24 ms^{-1}

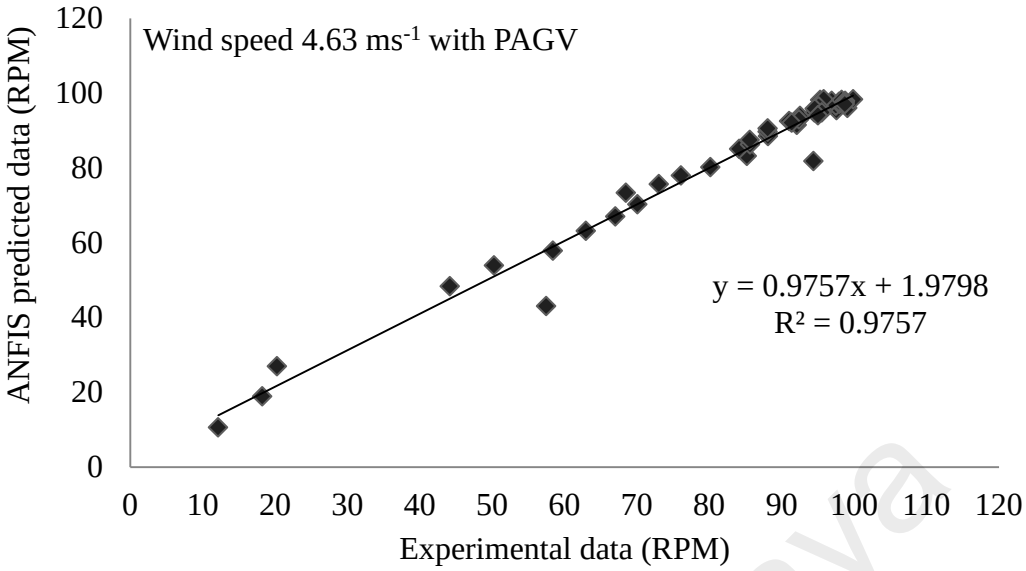

(a)

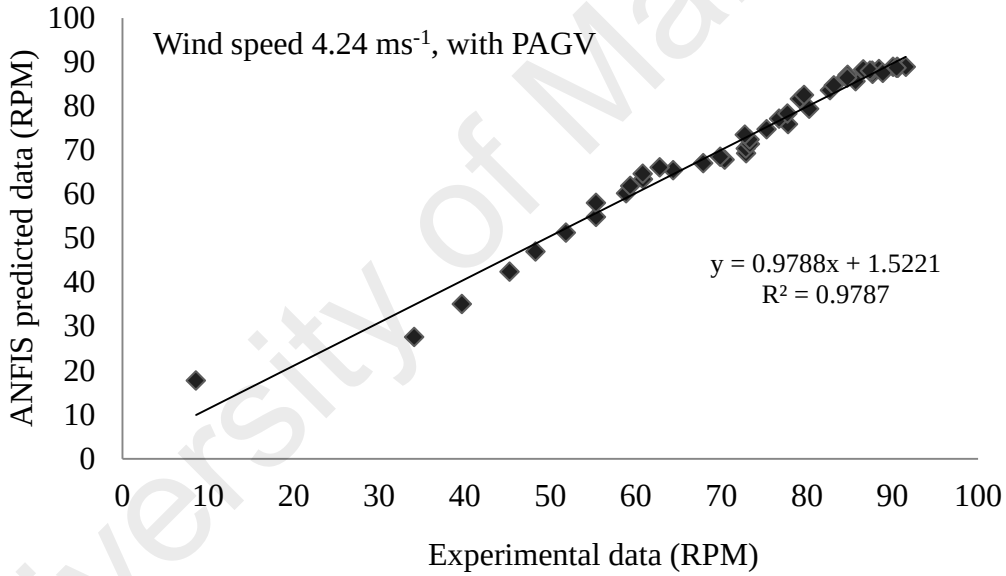

(b)

Figure 5.49: Scatter plots of predicted and experimental data of rotational speeds with PAGV using ANFIS model for wind speed for (a) 4.63 ms^{-1}, and (b) 4.24 ms^{-1}

To illustrate, Figure 5.50 (a) and 5.50 (b) show the predicted rotor rotational speed data extracted from the ANFIS model for a period of 240s. The predicted data output from the ANFIS model can be used as an efficient indicator to evaluate a site's wind performance, therefore reducing time and cost. For the current study, the ANFIS model

is trained with a wind speed of 4.24 m/s and 4.63 m/s only. However, for future study, the ANFIS model can be trained and tested with larger range of wind speed.

The evaluation of the ANFIS model performance for the estimation of the rotor rotational speed was also conducted in a tangible manner based on RMSE and R^2. The output from the ANFIS testing phase confirms the RMSE statistics as shown in Table 5.11. The presented results in Table 5.11 show average results after much iteration in order to find optimal results. It therefore shows that the proposed ANFIS model can be used for forecasting wind turbine rotational speed with high reliability.

ANFIS already has shown high prediction accuracy for power augmented wind turbines. For example in article (Petkovic et al., 2014) ANFIS methodology for estimation of building augmented wind turbine performances was presented where ANFIS was used to determine factors of wind and power increasing due to building augmentation of the wind turbine performances. However in article (Petkovic et al., 2014) different inputs are used in comparison with this study.

In another similar research (Vlastimir et al., 2015). ANFIS was used to estimate diffuser effect on wind turbine performances. ANFIS was used to determine power and torque coefficient changing of the wind turbine with a diffuser. It also estimated the wind turbine rotational performances according to wind speed and blade solidity (the number of wind turbine blades in percentage).

Table 5.11: Performance statistics of the ANFIS model in wind turbine rotational speed estimation

	RMSE	R^2	R
Wind speed 4.63 ms^{-1}; w/o PAGV	1.386773	0.9382	0.9686
Wind speed 4.24 ms^{-1}; w/o PAGV	1.023119	0.9226	1.01149
Wind speed 4.63 ms^{-1}; with PAGV	1.230114	0.9757	0.9877
Wind speed 4.24 ms^{-1}; with PAGV	0.906654	0.9787	0.9892

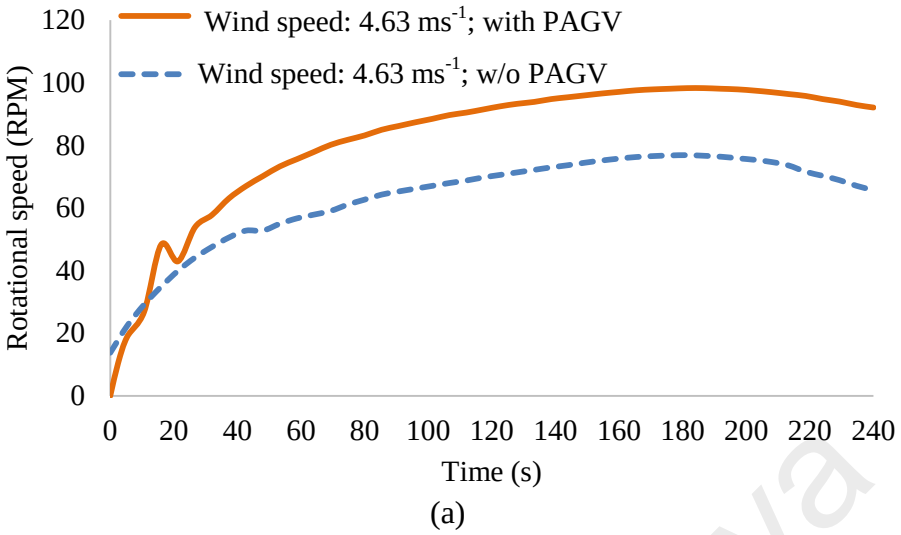

(a)

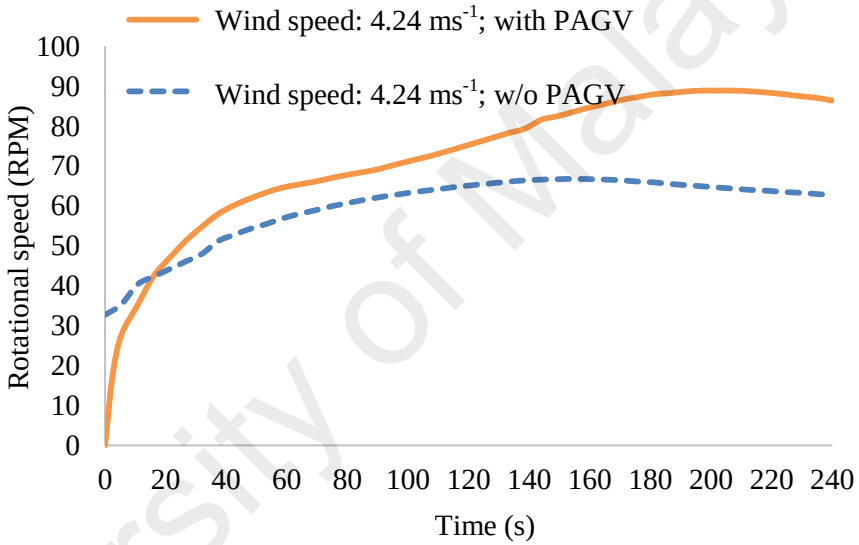

(b)

Figure 5.50: ANFIS forecasting of wind turbine rotational speed for wind speeds for (a) 4.63 ms^{-1}, and (b) 4.24 ms^{-1}.

The investigation (Vlastimir et al., 2015) also concluded that ANFIS prediction has better results with slower wind speeds which confirm results in this investigation also where one can see in Table 5.11 that ANFIS has better performances for wind speed of 4.24 ms^{-1} than for wind speed of 4.63 ms^{-1}.

5.13 Uncertainty Analysis

The accuracy of measurements of physical quantities in the laboratory is error prone therefore there can be discrepancies of measured data. These discrepancies can be classified as precision error and the bias errors. The major sources of the precision error are due to parallax, while the bias errors are mostly caused by a calibration error in measuring apparatus. With the complexity of experimental measurements in this study, the error in the acquired data is both precision and systematic. A sample data for the performance of the CAWT on the gable rooftop at 100 mm height was used for the uncertainty analysis. The rotational speed, torque, and mechanical power are the parameters that are used for this analysis. The mean values of the data is i.e. rotational speed, mechanical power and torque calculated using the equation below

$$\text{Mean } (x_{AV}) = \frac{1}{n}\sum_{n=1}^{n} x_1 = \frac{1}{n}(X_1 + X_2 + X_3 + \ldots\ldots\ldots + n) \quad (5.1)$$

Where n is the number of repeated measurement and the standard deviation σ is calculated using

$$\sigma = \sqrt{\frac{1}{n-1}[(x_1 - x_{AV})^2 + (x_2 - x_{AV})^2 + \ldots\ldots\ldots + (x_n - x_{AV})^2]} \quad (5.2)$$

where the standard deviation σ is the sum of squares of deviation from the average value divided by (n-1). The standard error (SE) is calculated using

$$SE = \frac{\sigma}{\sqrt{n}} \quad (5.3)$$

Figure 5.51 presents the percentage uncertainty analysis in the rotational speed of the CAWT placed at 100 mm height above the gable rooftop. The mean value, standard deviation and standard error is calculated to be 262 RPM, +/- 7.95, and a standard error of 0.499.

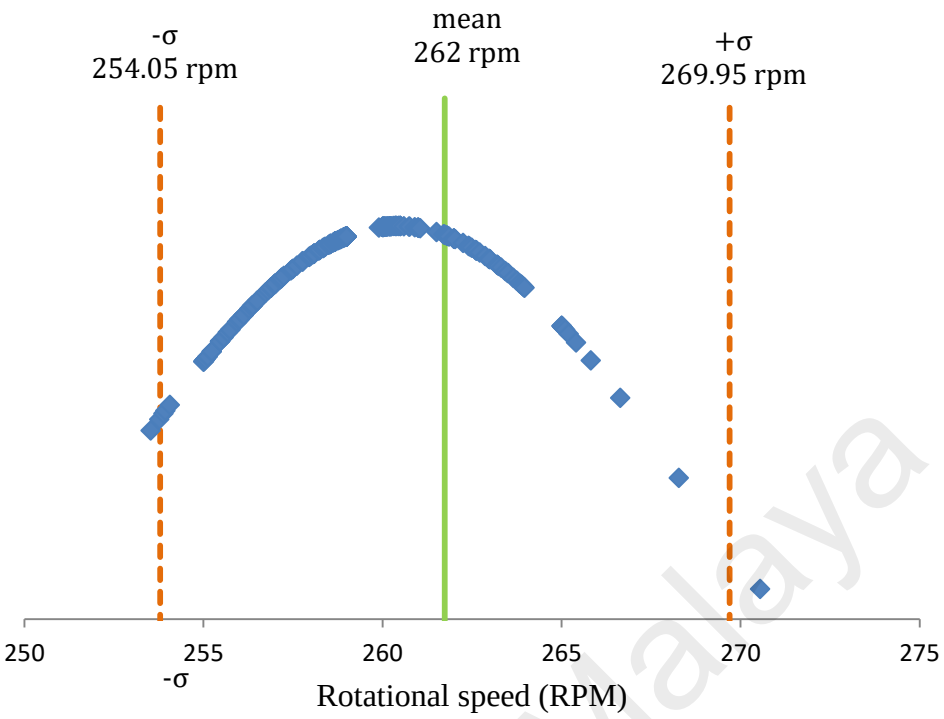

Figure 5.51: Normal distribution of rotational speed of CAWT

Figure 5.52 shows the normal distribution for the mechanical power of the CAWT it can be seen from the figure that the mean value, standard deviation and standard error for the mechanical power 0.744 W, +/- 0.044, and 0.00293 respectively.

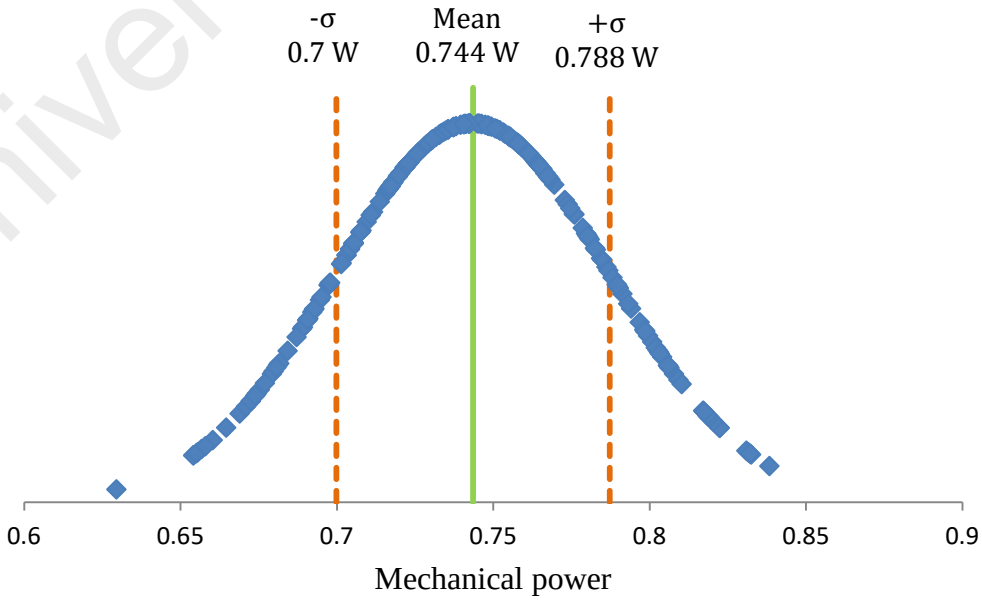

Figure 5.52: Normal distribution of mechanical power

The uncertainty analysis for the torque measurement is presented in Figure 5.53. From the figure, it can be observed that the mean value, the standard deviation and the standard error is calculated to be 0.0271 Nm, +/- 0.001657, and 0.00011. Considering the size of the CAWTs used in this study, the error estimates is reasonable.

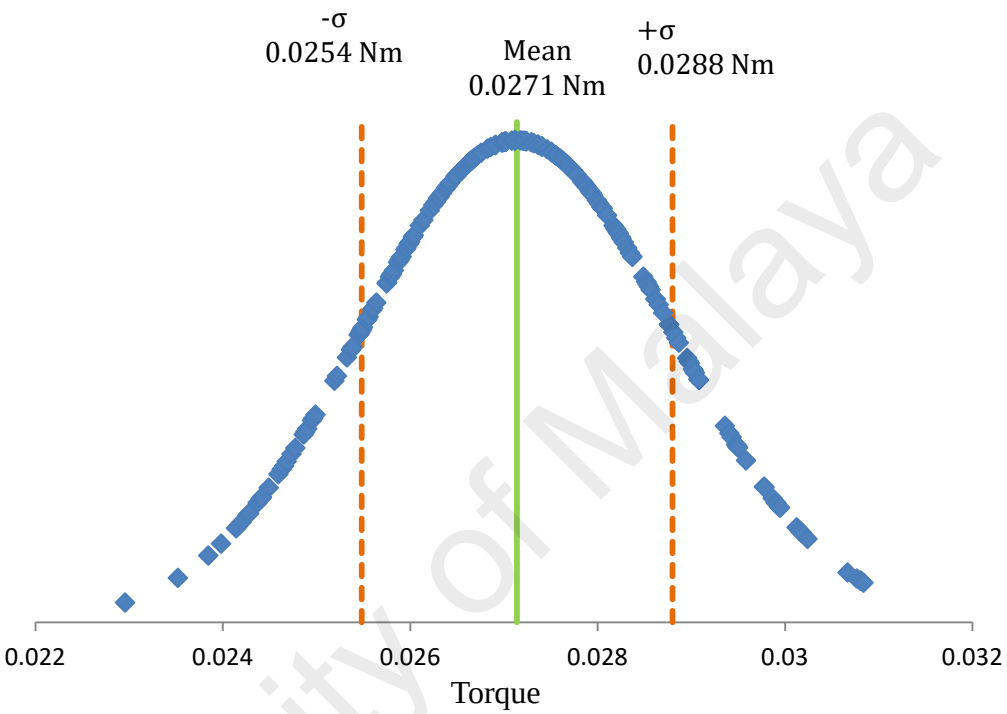

Figure 5.53: Normal distribution of Torque

CHAPTER 6: CONCLUSION AND RECOMMENDATION

6.1 Conclusion

A highly efficient wind turbine with cross axis orientation for application in urban buildings has been designed and tested. The effect of the roof shapes on the performance of the CAWT and the suitability of rooftops in integrating CAWT was investigated in the experiment. Comparisons between the performances of a building integrated CAWT with a building integrated straight bladed VAWT was analyzed on both the gable and the vaulted rooftop of a scaled down building model. The results obtained from the study showed that the coefficient of power (C_p) of the building integrated CAWT improved significantly compared to the building integrated straight-bladed VAWT. At Y = 100 mm height on both the gable and vaulted rooftop, the $C_{p,max}$ value of the CAWT increased by 266% at a TSR (λ) of 1.1 and 246% at λ of 1.03 at a wind speed of 4.5 m/s compared to the straight-bladed VAWT under the same experimental conditions. Similar improvement in performance of CAWT is also observed for all conditions of height on both rooftops i.e. Y = 150 mm, 200 mm, and 250 mm where the CAWT outperformed the VAWT. The results obtained from the variation of height of CAWT above the rooftop showed that the closer the height of CAWT to the building rooftop, the better the performance of the CAWT. The result was verify from the CFD simulation which indicates that the 100 mm height has the highest skewed angle which helps to improves the performance of the building integrated CAWT. The 10^o pitch angle for the horizontal blade is the optimum pitch angle for the CAWT. Furthermore, integrating CAWT on building with gable and vaulted rooftops respectively will produce an increased power output compared to bare-CAWT (without roof). The results obtained demonstrates that 121% and 37 more power can be obtained when CAWT is integrated on the gable and vaulted rooftops respectively compared to the bare-CAWT. Further results showed that the gable rooftop is more suitable for

integrating the CAWT as mounting a CAWT on a building with gable rooftop will yield 66% more energy compared to the vaulted rooftop. Moreover, in both rooftops the centre position is more suitable for the installation of the CAWT compared to the side's positions. The analytical approach employed indicates a good agreement with the experimental results. In addition, the results obtained from the CFD simulation shows that the calculated skewed angle and the increased turbulence intensity on the gable rooftop influence the improved performance of the CAWT on the gable rooftop compared to the vaulted roof shape. Moreover, the employed soft computing methodology, adaptive neuro-fuzzy inference system (ANFIS) used to predict the performance of power augmented vertical axis wind turbine has demonstrated that the developed ANFIS model is very effective and reliable in predicting the performance of power augmented VAWT.

Building integrated CAWT represents the future outlook of wind turbines in urban environments. The innovative design of the CAWT was intended to be very versatile and to excel in many different environments. It is an ideal solution for on-site building integrated wind turbines especially in urban areas with relatively low to moderate wind speeds and a high level of turbulence. The uniqueness of this design gives rise to its technical advantages over the conventional wind turbines and can minimize or completely eliminate the disadvantages of the conventional wind turbines. The idea of using horizontal blades as connecting struts for the CAWT is shown to have played a significant role in the improved rotational speed, power output and self-starting behavior of the CAWT.

6.2 Recommendation

The findings of the studies performed in this research mainly serve as recommendations to the improvement of the performance of the building integrated CAWT. As a new type of wind turbine, CAWT still encounter many challenges towards commercialization in a utility scale, the information presented in this thesis provides valuable insights to help understanding the performance of this new type of wind turbine. While analysis performed capture the general operating characteristics and performance of CAWT under different roof shaped of the buildings and as a stand-alone system. There is need for further research in several areas before the potential of small CAWTs as prime movers in urban buildings can be fully assessed. In view of these, the following recommendations were made to further enhance the current analysis.

- Beyond the initial design stage, more precise and reliable numerical methods such as vorticity transport modeling can be utilized to detail the three-dimensional flow field around CAWT and the VAWT. Measurement of flow field parameters in the wake of the CAWT and the region between them can shed more lights on the underlying physics of their interaction.
- Since the experiments were performed on a semi-open wind tunnel where the flow is not controlled, the turbulence in the experimental area cannot be controlled due to the limitations of instruments and costs. The turbulence could affect the wind turbine performance; therefore, it is necessary to study the CAWT in a proper wind tunnel with variable wind speed at higher Reynolds number flow regime and higher accuracy instruments.
- Future research to compliment the current study can be “investigating the effect of turbulence and blade effects on the aerodynamic performance of building integrated CAWT”.

REFERENCES

Abohela, I., Hamza, N., & Dudek, D. (2011). *Effect of Roof Shape on Energy Yield and Positioning of Roof Mounted Wind Turbines*. Paper presented at the 12th Conference of International Building Performance Simulation Association, Sydney.

Abohela, I., Hamza, N., & Dudek, S. (2013). Effect of roof shape, wind direction, building height and urban configuration on the energy yield and positioning of roof mounted wind turbines. *Renewable Energy, 50*, 1106-1118.

Ackermann, T., & Soder, L. (2000). Wind energy technology and current status: a review". *Renewable and Sustainable Energy Reviews, 4*, 315–374.

AID Airfoil Investigation Database. Retrieved from http://www.airfoildb.com/foils/377

Akcayol, M. A. (2004). Application of adaptive neuro-fuzzy controller for SRM. *Advances in Engineering Software, 35*(3-4), 129-137.

Alam, J. M., & Iqbal, M. T. (2009). Design and development of hybrid vertical axis turbine *IEEE,* 1178-1183.

Alidadi, M., & Calisal, S. (2014). A numerical method for calculation of power output from ducted vertical axis hydro-current turbines. *Computers & Fluids, 105*, 76-81.

Altan, B. D., Atılgan, M., & Özdamar, A. (2008). An experimental study on improvement of a Savonius rotor performance with curtaining. *Experimental and Thermal Fluids science, 32*, 1673–1678.

Allaei, D., & Andreopoulos, Y. (2014). INVRLOX: Description of a new concept in wind power and its performance evaluation. Energy, 69, 336-334.

Allaei, D., Tarnowski, D., Andreopoulos, Y. (2015). INVRLOX with multiple wind turbine generator systems. Energy, 93, 1030-1040.

Amirante, R., De Palma, P., Distaso, E., La Scala, M., Tamburrano, P. , Design of a novel open space test rig for small scale wind turbine. 72th Conference of the Italian thermal mechines engineering association, ATI2017, 6-8 September 2017, Lecce, Italy.

ANSYS Fluent 14.0 User's Guide. ANSYS Inc.

ANSYS Fluent User's Guide Released 14.0 ANSYS Inc. Retrieved from http://www.ansys.com

Armstrong, S., Fiedler, A., & Tullis, S. (2012). Flow separation on a high Reynolds number, high solidity vertical axis wind turbine with staright and canted blades and canted blades with fences. *Renewable Energy, 41*, 13-22.

Arifin S., Soeparman, S., Wahyudi, S., Yuliati, L. (2017) Performance Analysis of a combined blade Savonius wind turbine. International Journal of Fluid machinery and Systems 10(1), 1882-9554.

Aslam Bhutta, M. M., Nasir Hayat, A. U., Zain Ali, F., Rehan, J. S., & Zahid, H. (2012). Vertical axis wind turbine – A review of various configurations and design techniques. *Renewable & Sustainable Energy Reviews, 16*, 1926-1939.

Bahaj, A. S., Myers, L., & James, P. A. B. (2007). Urban energy generation: Influence of micro-wind turbine output on electricity consumption in buildings. *Energy and Buildings, 39*, 154-165.

Balduzzi, F., Alessandro, B., Ennio Antonio, C., Lorenzo F., & Magnani, S. (2012). Feasibility analysis of a Darrieus vertical-axis wind turbine installation in the rooftop of a building *Applied Energy, 97*, 921-929.

Barker, J. (1983). Features to aid or enable self-starting of fixed pitch low solidity vertical axis wind turbines. . *Wind Engineering and Industrial Aerodynamics., 15*, 369–380.

Batista, N. C., Melício, R., Mendes, V. M. F., Calderón, M., & Ramiro, A. (2015). On a self-start Darrieus wind turbine: Blade design and field tests. *Journal of Renewable and Sustainable Energy Reviews, 52*, 508-522.

Batista, N. C., R. Melício, Matias, J. C. O., & Catalão, J. P. S. (2012). *Vertical Axis Wind Turbine Performance Prediction: An Approach to the Double Multiple Streamtube Model*. Paper presented at the International Conference on Renewable Energies and Power Quality (ICREPQ'12), Santiago de Compostela (Spain).

Bailey L. J., & John, T. B. (26, August 2010). Shrouded vertical axis dual-turbine generator. US patent. PCT No.: PCT/US2008/004269,1-4.

Beri, H., & Yao, Y. (2011). Double Multiple StreamTube Model and Numerical Analysis of Vertical Axis Wind Turbine. *Energy and Power Engineering, 3*, 262-270.

Beri, H., & Yao, Y. (2011). Effect of camber on self starting of vertical axis wind turbine. *Environmental Science and Technolology, 4*(3), 302-312.

Biadgo, A. M., Simonovic, A., Komarov, D., & Stupar, S. (2013). Numerical and Analytical Investigation of Vertical Axis Wind Turbine. *FME Transactions, 41*, 49-58.

Bianchini, A., Ferrara, G., Ferrari, L., & Magnani, S. (2012). An Improved Model for the Performance Estimation of an H-Darrieus Wind Turbine in Skewed Flow. *Wind Engineering, 36*(6), 667-686.

Bianchini, A., Ferrari, L., & Magnani, S. (2011, 6-11 June 2011). *Start-up Behavior of a Three-Bladed H-Darrieus VAWT : Experimental and Numerical Analysis.* Paper presented at the Proceedings of ASME Turbo Expo 2011 GT2011 June 6-10, 2011, Vancouver, British Columbia, Canada, Canada.

Blackmore, P. (2010). *Building-mounted micro-windvturbines on high-rise and commercial buildings.* Watford: BRE.

Boatner, B. (2010 [accessed 10.05.2016]). *A summary overview of the blackhawk wind turbine,http://coen.boisestate.edu/windenergy/files/2011/10/BlackhawkOverview-BruceBoatner1.pdf.*

Bravo, R., Tullis, S., & Ziada, S. (2007). *Performance testing of a small scale vertical-axis wind turbine.* Paper presented at the 21st Canadian Congress of Applied Mechanics, June 3-7, Toronto.

Brusca, S., Lanzafame, R., & Messina, M. (2014). Design of a vertical-axis wind turbine: how the aspect ratio affects the turbine's performance. *International Journal of Energy Environment Engineering, 5*, 333–340.

Cantwell, L., & Amargosa, V. N. (2014). Low wind, vertical axis dual stage wind turbine power generator. US Patent No. US 8,790,068B2.

Casini, M. (2016). Small Vertical Axis Wind Turbines for Energy Efficiency of Buildings *Journal of Clean Energy Technologies, 4*(1) 56-65.

Castelli, M. R., De Betta, S., & Benini, E. (2012). Effect of Blade Number on a straight-bladed Vertical axis Darrieus wind turbine. *International journal of Mechanical, Aerospace, Industrial, Mechatronic and Manufacturing Engineering, 6*(1), 68-74.

Chong, W. T., Fazlizan, A., Poh, S. C., Pan, K. C., & Ping, H. W. (2012). Early development of an innovative building integrated wind, solar, and rain water harvester for urban high rise application. *Energy and Buildings, 47*, 201–207.

Chong, W. T., Pan, K. C., Poh, S. C., Fazlizan, A., Oon, C. S., Badarudin, A., & Nik-Ghazali, N. (2013). Performance investigation of a power augmented vertical axis wind turbine for urban high-rise application. *Renew Energy, 51*, 388-397.

Chong, W. T., Poh, S. C., Fazlizan, A., Pan, K. C. (2012); Vertical axis wind turbine with omni-directional guide vane for urban high rise buildings. J. Cent. South Univ. (2012) 19: 727−732.

Chong W. T., & Kong, Y. Y. (2016) Cross Axis Wind turbine; patent No: PCT/MY2016/050031.

Cochran, B. (2002). *The influence of atmospheric turbulence on the kinetic energy available during small wind turbine power performance testing.* Retrieved from Soria, Spain.

Cochran, B. C., & Damiani, R. R. (2008). Harvesting wind power form tall buildings. *WindPower*.

Cochran, B. C., & Damiani, R. R. (2008). Integrating Wind Energy into the Design of Tall Buildings -A Case Study of the Houston Discovery Tower. *Wind Power*, 1-11.

Dannecker, R. K. W., & Andrew, D. G. (2002). Investigations of a Building-Integrated Ducted Wind Turbine Module. *Wind Enrgy, 5*, 53–71.

Dayan, E. (2006). Wind energy in building: Power generation in the urban environment-where it is need most. *Refocus*, pp. 33-38.

Dennis, G. S. (2009). historical Development of the Wind Mill. In A. S. David (Ed.), *Wind Turbine Technology; Fundamental Concepts of Wind Turbine Engineering* (2nd ed., pp. 1). New York: ASME press.

De Jesus Henriques, T. A., Hedges, T. S., Owen, I., Poole, J. R. (2016); the influence of blade pitch angle on the performance of a model horizontal axis tidal stream turbine operating under wave-current interaction. Energy 102, 166-175.

DNV/Riso (2002). *Guidelines for Design of Wind Turbines* (2nd ed.). Denmark: Jydsk Centraltrykkeri,ISBN 87-550-2870-5.

Dominy, R., Lunt, P., Bickerdyke, A., & Dominy, J. (2006). Self-starting capability of a Darrieus turbine. *Journal of Power and Energy, Vol. 221 Part A.*

Dominy, R., Lunt, P., Bickerdyke, A., & Dominy, J. (2007). Self-starting capability of a Darrieus turbine. *Journal of Power and Energy, Proc. IMechE 221 Part A* 111-120.

Donald, C. F. (1999). Dual turbine wind.electricity converter. US Patent No. 5,969,430.

Dutton, A. G., Halliday, J. A., & Halliday, M. J. (2005). The Feasibility of Building Mounted/Integrated Wind Turbines (BUWTs): Achieving their Potential for Carbon Emission Reductions. *Final Report of Carbon Trust Contract 2002-07-028-1-6, Energy research Unit, Rutherford Appleton Laboratory, Science and Technology Facilities Counci, Oxfordshire, UnitedKingdom*, 1-109.

Drew, D., Barlow, J., & Cockerill, T. (2013). Estimating the potential yield of small wind turbines in urban areas; A case study of Greater London UK. *Journal of Wind Energy and Industrial Aerodynamic, 115*, 104-111.

Energy Information and Administration, eia; Internaltional energy outlook May, 2016, DOE/EIA-0484. www.eia.gov/forecasts/ieo pp1

Ekici, B. B., & Aksoy, U. T. (2011). Prediction of building energy needs in early stage of design by using ANFIS. *Expert Systems with Applications, 38*(5), 5352-5358.

Eriksson, S., Benhoff, H., & Leijon, M. (2008). Evaluation of different turbine concept for wind power. *Renewable Energy, 12*, 1219-1234.

El-Samanoudy, M., Ghorab, A.A.E., Youssef, Sh.Z. (2010); Effect of some design parameters on the performance of a Giromill vertical axis wind turbine. Ain Shams Engineering Journal 1, 85–95.

ESMAP/WB. (2011.). Greening the Wind: Environmental and Social Considerations for Wind Power Developmentin Latin Americaand Beyond. *Energy Sector*

Management Assistance Program (ESMAP) and World Bank (WB), Washington DC, 170.

Ferreira, C. (2006). *Wind tunnel hotwire measurements, flow visualization and thrust measurement of a VAWT in skew.* Paper presented at the 44th AIAA Aerospace Sciences Meeting and Exhibit, 9-12 January, Reno, Nevada.

Ferreira, C., Dixon, K., Hofemann, C., Kuik, G. V., & Gerard, V. B. (2009). *The VAWT in Skew: Stereo-PIV and Vortex Modeling.* Paper presented at the 47th AIAA Aerospace Sciences Meeting Including the New Horizons Forum and Aerospace Exposition, 5–8 January. Orlando, USA.

Fluent 5 User's Guide 2. Fluent Inc. Lebanon, USA, 9-8.

Gasch, R., & Twele, J. (2012). *Wind Power Plants: Fundamentals, Design, Construction, and Operation*. Berlin Heidelberg: Springer-Verlag.

Geurts, B., Simao Ferreira, C., & Van Bussel, G. (2010). *Aerodynamic Analysis of a Vertical Axis Wind Turbine in a Diffuser.* Paper presented at the 3rd EWEA Conference-Torque 2010: The Science of making Torque from Wind, Heraklion, Crete, Greece, 28-30 June 2010.

Gipe, P. (2004). *Wind Power: Renewable Energy for Home, Farm, and Business*. Tehnology & Engineering. Chelsea Green Publishing, 512 pages.

Global Wind Report. (2014). *Annual market update*. Retrieved from http://www.gwec.net/publications/global-wind-report-2/global-wind-report-2014-annual-market-update.

Gorelov, A., (1998). Development of the helical reaction hydraulic turbine, final technical report July 1, 1996- June 30, 1998. US Department of Energy. Office of energy efficiency and renewable energy, 56 pages.

Grigorie, T. L., & Botez, R. M. (2009). Adaptive neuro-fuzzy inference system-based controllers for smart material actuator modelling. *Journal of Aerospace Engineering, 223*(6), 655-668.

Gupta, R., Deb, B., Misra, R, D. (2013). Performance anslsys of Helical Savonius rotor with shaft at 45^{o} twist angle using CFD. Mechanical Engineering Research, 3(1), 118-129.

GWEC. (2014). Wind power works ; Saving C02 everyday.

Haase, M., & Lofstrom, E. (2015). *Building Augmented Wind Turbines -BAWT, Integrated solutions and technologies of small wind turbines* SINTEF Research 34, Blindern, Norway.

Hameed, M. S., & Afaq, S. K. (2013). Design and analysis of a straight-bladed vertical axis wind turbine blade using analytical and numerical techniques. *Ocean Engineering, 57*, 248–255.

Hanjun, S., Yun, L., & Nicolas, B. (2012). Vertical axis wind turbine. US2012/0099997A1.

Hara, Y., A. Shiozaki, H. Nishiono, S. Saito, K. Shioya, S. Kogo, *et al.*, (2014). "Experiments of a Butterfly wind turbine with aluminium circular blades and performance predictions," *Wind Energy*, vol. 38, pp. 16-21.

Hara, Y., Kawamura, T., Hiromichi, A., Kenji, T., Takuju, N., & Kentaro, M. (2014). Predicting Double-Blade Vertical Axis Wind Turbine Performance by a Quadruple-Multiple Streamtube Model. *International Journal of Fluid Machinery and Systems, 7*(1), 16-24.

Haslenda, H., & Ho, W. (2011). Renewable energy policies and initiatives for a sustainable energy future in Malaysia. *Renewable and Sustainable Energy Reviews, 15*, 4780-4787.

Hau, E. (2006). *Wind Turbines; Fundamentals, Technologies, Application, Economics* (2nd ed.). Berlin, Germany: Springer.

Heymann, M. (1998). Signs of hubris: the shaping of wind technology styles in Germany, Denmark, and the United States, 1940–1990. *Technology and Culture, 39*(4), 641-670.

Hill, N., Dominy, R., Ingram, G., & Dominy, J. (2009). Darrieus turbines: the physics of self-starting. *Journal of Power and Energy, ImechE 223 Part A*, 21-29.

Huleihil, M., & Mazor, G. (2012). *Wind turbine power: the Betz limit and beyond*. Advances in Wind Power. InTech: Rijeka, Croatia.

Hwang I. Seong, Hwang Chang Sup, Min Seung Yong, Jeong In Oh, Lee Yun Han, Kim Seung Jo. Efficiency improvement of cycloidal wind turbine by active control of blade motion. 16th International conference on adaptive structures and technologies, October 9–12, Paris, France, 2005**.**

Hyun, B., Choi, D., Han, J., Jin, J., & Roo, C. (2012). Performance analysis and design of vertical axis tidal stream turbine. *Journal of Shipping and Ocean Engineering, 2*, 191-200.

Ibrahim, M. T., A. Allet, & Paraschivoiu, I. (1995). Aerodynamic Analysis Models for Vertical-Axis Wind Turbines. *International Journal of Rotating Machinery, 2*(1), 15-21.

Igra, O. (1975). *Shrouds for aerogenerator, AIAA Journals. 14(10), 1481-1483*. Retrieved from Ben Gurion University.

İnal, M. (2008). Determination of dielectric properties of insulator materials by means of ANFIS: A comparative study. *Journal of Materials Processing Technology, 195*(1-3), 34-43.

International Renewable Energy Agency. (2012). *Renewable Energy Technologies: Cost Analysis Series, Wind Power*. IRENA.

Irabu, K., & Roy, J. N. (2007). Characteristics of wind power on Savonius rotor using a guide-box tunnel. *Experimental and Thermal Science, 32*, 580-586.

Islam, M., David, S. K., & Ting, A. F. (2008). Aerodynamic models for Darrieus-type straight-bladed vertical axis wind turbines. *Renewable & Sustainable Energy Reviews, 12*, 1080-1109.

Islam, M., Fartaj, A., & Carriveau, R. (2008a). Analysis of the Design Parameters related to a Fixed-pitch Straight-Bladed Vertical Axis Wind Turbine. *Wind Engineering, 32*, 491-507.

Islam, M., David, S. K., & Ting, A. F. (2007). Design of special-purpose airfoil for smaller-capacity straight-bladed VAWT. Wind Engineering, 31(6), 401-424.

Islam, M. R., Saidur, R., Rahim, N. A., & Solangi, K. H. (2009). Renewable Energy Research in Malaysia. *Engineering e-Transaction,, 4*(2), 69-72.

Jang J-SR. (1993). ANFIS: adaptive-network-based fuzzzy inference systems. *IEEE Transyst, Man, and Cybernet, 23(3)*, 665-685.

Jha, A. R. (2011). *Wind Turbine Technology*. London New York: CRC Press Taylor and Francis Group.

Joe, C. (2008). Vertical axis dual vortex downwind inward flow impulse wind turbine, US Patent No. US0317582 A1.

Johnson, G. L. & Manhattan, K. S.(2001). Wind Energy Systems, Electronic Edition.

Joo-soo, K., & Busan, K. (2013). High-performance wind turbine generator that can be driven in horizontal/vertical axis directions with the use of 3D active intelligent turbine blades. US 2013/0241200 A1.

Joselin Herbert, G. M., Iniyan, S., Sreevalsan, E., & Rajapandian, S. (2007). A review of wind energy technologies. *Renewable & Sustainable Energy Reviews, 11*, 1117-1145.

Kamoji, M. A., Kedare, S. B., & Prabhu, S. V. (2009). Performance tests on helical Savonius rotors. *Renewable Energy, 34* 521–529.

Kumar, N. M., Subathra, M.S.P, Cota, O. D. (2015). Design and wind tunnel testing of funnel based wind energy harvesting system. Procedia Technology, 21, 33-40.

Kentfield, J. A. C. (1996). The fundamentals of wind-driven water pumpers. *Taylor and Francis, London, U.K.*

Khajeh, A., Modarress, H., & Rezaee, B. (2009). Application of adaptive neuro-fuzzy inference system for solubility prediction of carbon dioxide in polymers. *Expert Systems with Applications, 36*(3), 5728-5732.

Kirke, B. K. (1998). *Evaluation of self-starting vertical axis wind turbines for stand-alone applications.* (PhD Thesis), Griffith Univerisity Gold Coast Campus.

Kulunk, E. (2011). Aerodynamics of Wind Turbines. In R. Carriveau (Ed.), *Fundamental and Advanced Topics in Wind Power*, pp. 3-6. InTech. Croatia.

Kurt S. Hansen, Rebecca J. Barthelmie, Leo E. Jensen, & Sommer, A. (2012). The impact of turbulence intensity and atmospheric stability on power deficits due to wind turbine wakes at Horns Rev. wind farm. *Wind Energy, 15*, 183–196.

Lapin, E. E. (1975). Theoretical performance of vertical axis wind turbines. *American Society of Mechanical Engineers*, winter annual meeting, Houston, Tex., Nov. 30-Dec. 4, pp 11.

Lawan, S. M., Abidin, W. A. W. Z., Chai, W. Y., Baharun, A., & Masri, T. (2014). An overview of energy sector and wind power potential in Malaysia. *British Journal of Applied Science and Technology, 4*(7), 1042-1059. Retrieved from www.sciencedomain.org

Ledo, L., Kosasih, P. B., & Cooper, P. (2011). Roof mounting site analysis for micro-wind turbines. *Renewable Energy, 36*(5), 1379-1391.

Letcher, T. (2010). *Small Scale Wind Turbines Optimized for Low Wind Speeds* The Ohio State University, Columbus, OH. Unpublished

Li, D., Wang, S., & Yuan, P. (2010). A Review of Micro Wind Turbines in the Built Environment, Power and energy engineering conference (APPEEC), 28-31 Mar. Chengdu, China.

Li, Y., & Calisal, S. M. (2010). Three-dimensional effects and arm effects on modeling a vertical axis tidal current turbine. *Renewable Energy, 35*, 2325-2334.

Li, Q. Maeda, T., Kamada, Y. Murata, J., Kawabata, T., Kogaki, T. (2014) Study on flow around straight-bladed vertical axis wind turbine under low tip speed ratio, J. Fluid Sci. Technol. 9 (3). JFST0051-JFST0051.

Li, Q. Maeda, T., Kamada, Y. Murata, J., Kawabata, T., Ogasawara, T. Kogaki, T, (2016) Study on power performance for straight-bladed vertical axis wind turbine by field and wind tunnel test, Renew. Energy 90, 291-300.

Lubitz, W. D. (2014). Impact of ambient turbulence on performance of a small wind turbine. *Renewable Energy, 61*, 69-73.

Lu, L., & Sun, K. (2014). Wind power evaluation and utilization over a reference high-risebuilding in urban area. *Energy and Buildings, 68*, 339-350.

Maalawi, K. (2011). Special Issues on Design Optimization of Wind Turbine Structures. In I. Al-Bahadly (Ed.), *Wind Turbines* (Vol. 1). Croatia: Intech Janeza Trdine 9, 51000 Rijeka.

Magdi, R., & Adam, M. R. (2011). wind Turbines Theory - The Betz Equation and Optimal Rotor Tip Speed Ratio *Fundamental and Advanced 20 Topics in Wind Power*, pp. 20.

Manabu, T., Hiroyuki, T., Yohei, S., Takao, M., Yasunari, K., & Kazuhiko, T. (2009, May 31 - June 5, 2009). *Experimental study of a straight-bladed vertical axis wind turbine with a directed guide vane row.* Paper presented at the Proceedings of the ASME 2009 28th International Conference on Ocean, Offshore and Arctic Engineering OMAE2009, Honolulu, Hawaii, USA.

Manwell, J. F., McGowan, J. G., & Rogers, A. L. (2002). *Wind Energy Explained* (1st ed.). Amherst, USA: Wiley.

Manwell, J. F., Mcgowan, J. G., & Rogers, A. L. (2009). *Wind Energy Explained: Theory, Design and Application* (Second Edition ed.). United Kingdom: A John Wiley and Sons, Ltd, publication.

Mathew, S. (2006). *Wind Energy fundamentals, Resource Analysis and Economics*. Natherland: Springer.

Menet, J.-L. (2004). Adouble-step Savonius rotor for local production of electricity: a design study. *Renewable Energy, 29*, 1843–1862.

Menter, F. R., Kuntz, M., & Langtry, R. (2003). *Ten years of industrial experience with the SST turbulence model.* Paper presented at the Fourth International Conference on Turbulence, Heat and Mass Transfer, Redding, Begell House Inc.

Mertens, S. (2002). *Wind energy in urban areas: Concentrator effects for wind turbines close to buildings*. *Refocus*, pp. 22-24. Retrieved from www.re-focus.net

Mertens, S. (2003). The energy yield of roof mounted wind turbines. *Wind Engineering, 27*(6), 507-517.

Mertens, S. (2003). *The wind conditions at flat roofs for small wind turbines*. Paper presented at the EWEC, June 16-19, Madrid.

Mertens, S., Kuik, G. V., & van Bussel, G. (2003). Performance of an H-Darrieus in the skewed flow on a roof[1]. *Journal of solar Energy Engineering, 125*, 433-440.

Messam Abbas Naqvi, Akhtar Abbas, Maria Hamid, Hasan Tarar, & Ahmed., L. (2015). Aerodynamic Design Optimization of Residential Scale Wind Turbine Blades for Lower Wind Speeds. *Journal of Renewable Energy Research, 5*, (2), 373-385.

Mikkelsen, K. (2013). *Effect of free stream turbulence on wind turbine performance.* (Masters thesis), Norwegian University of Science and Technology.

Mithraratne, N. (2009). Rooftop wind turbines for microgeneration in urban houses in New Zealand. *Energy and Buildings, 41*, 1013-1018.

Mohamed, A., & Lee, K. (2006). Energy for sustainable development in Malaysia: energy policy and alternative energy *Energy Policy, 34*(15), 2388–2397.

Mohammed, M. H. (2013). Impacts of solidity and hybrid system in small wind turbines performance. *Energy, 57*, 495-504.

Montgomerie, B. (2004). Methods for Root Effects, Tip Effects and Extending the Angle of Attack Range to ±180, with Application to Aerodynamics for Blades on Wind Turbines and Propellers. *Tech. Rep FOI*.

Mostafaeipour, A. (2011). Productivity and Development Issues of Global wind Turbine Inssues of Global wind Turbine Industry. In I. Al-Bahadly (Ed.), *Wind Turbines*. Croatia: Intech Janeza Trdine 9, 51000 Rijeka.

Mukund, R. P. (1999). *Wind and Solar Power Systems*. New York Washington, D.C.: CRC Press.

Muller, G., Jentsch, M., & Stoddart, E. (2009). Vertical axis resistance type wind turbines for use in buildings. *Renewable Energy, 34*, 1407-1412.

Nilesh, N. S., & Shiekh, S. M. (2014). Design and Development of Micro Vertical Axis Wind Turbine for Rural Application. *International Journal Of Engineering And Computer Science, 03*(07), 7035-7704.

Nils, E. G., Lyngholt, & Akuneyri, I. (2000). Horizontal axis wind turbine United State Patent No.: 290/55;290/44.

Nobile, R., Vahdati, M., Barlow, J. F., & Mewburn-Crook, A. (2013). *Unsteady flow simulation of a vertical axis wind turbine: a two-dimensional study*. Paper presented at the 2nd Engineeing conference.

Oh, T. H., Shen, Y. P., & Shing , C. C. (2010). Energy policy and alternative energy in Malaysia: Issues and challenges for sustainable growth. *Renewable and Sustainable Energy Reviews, 14*, 1241-1252.

Ozmen, Y., Baydar, E., & Beeck, v. (2016). Wind flow over the low-rise building models with gable roofs having different pitch angles. *Building and Environment, 95*, 63-74.

Padmanabhan, K. K. (2013). Study on increasing wind power in buildings using TRIZ Tool in urban areas. *Energy and Buildings, 61*, 344-348.

Paraschivoiu., I. (2002). Wind Turbine Design With Emphasis on Darrieus Concept. *Presses internationales Polytechnique*

Paraschivoiu I, Trifu O, Saeed F. (2009) H-Darrieus wind turbine with blade pitch control. International Journal of Rotating machinery, article ID 505343. 7 pages.

Park, J., Jung, HJ, Lee, SW., Jiyoung, P. (2015), A New Building-Integrated Wind Turbine System Utilizing the Building. *Energies* 2015, *8*, 11846-11870.

Petković, D., Issa, M., Pavlović, N. D., Pavlović, N. T., & Zentner, L. (2012). Adaptive neuro-fuzzy estimation of conductive silicone rubber mechanical properties. *Expert Systems with Applications, 39* (10), 9477-9482.

Petković, D., Issa, M., Pavlović, N. D., Zentner, L., & Ćojbašić, Ž. (2012). Adaptive neuro-fuzzy controller for adaptive compliant robotic gripper. *Expert Systems with Applications, 39*(18), 13295-13304.

Petkovic, D., Shamshirband, S., ojbašic´, Z. a. C., Vlastimir N., Nor Badrul, A., Aznul Qalid Md, S., & Shatirah, A. (2014). Adaptive neuro-fuzzy estimation of building augmentation of wind turbine power. *Computer & Fluids, 97*, 188-194.

Poh, K. M., & Kong, H. W. (2002). Renewable energy in Malaysia: a policy analysis; Energy for Sustainable Development, *6*(3) 31-39.

Pope, K., Dincer, I., & Naterer, G. F. (2010). Energy and exergy efficiency comparison of horizontal and vertical axis wind turbines. *Renewable Energy, 35*, 2102-2113.

Qu, J. , M. Xu, and Y. Mei, "Aerodynamic model of vertical axis wind turbine with wind speed self-adapting in drag-mode," *Advanced Materials Research*, vol. 347-353, pp. 340-343, 2012.

Rafailidis, S. (1997). Influence of building areal density and roof shape on the wind characteristics above a town *Bound Lay, Meteorology, 85*(2), 255-271.

Ragheb, M. (2013). Aerodynamics of Rotor Blades, pp 1-23.

Ragheb, M. (2014). Optimal Rotor tip speed ratio, pp 1-10.

Ragheb, M. (2014). Wind Turbine in Urban Environment, pp 1-18.

Ragheb, M. (2015). Vertical axis wind turbines, pp 1-40.

Rainbird, J. M., Bianchini, A., Balduzzi, F., Peiró, J., Graham, J. M. R., Ferrara, G., & Ferrari, L. (2015). On the influence of virtual camber effect on airfoil polars for use in simulations of Darrieus wind turbines. *Energy Conversion and Managment, 106*, 373-384.

Ramkissoon, R., & Manohar, K. (2013). Increasing the Power Output of the Darrieus Vertical Axis Wind Turbine. *British Journal of Applied Science & Technolog, 3*(1), 77-90.

Raymond, E. P., & Winchester, V. (2010). Roof Ridge wind turbine. US Patent No. US 2010/0126086 A1.

Rezaeiha, A., Kalkman, I., Blocken, B., (2017). Effect of pitch angle on power Performance and aerodynamics of a vertical axis wind turbine. Applied Energy 97, 132-150.

Ren 21. (2012). *Renewables 2012 Global Status Report*. Retrieved from Paris: (Ren 21 Secretariat): http://www.ren21.net/REN21Activities/GlobalStatusReport.

Ren 21. (2014). *Renewable energy policy network for the 21st century*. http://www.ren21.net/REN21Activities/GlobalStatusReport.

Ren 21. (2014 a). Renewable energy policy network for the 21st century. Retrieved from Robert, H., Ning, Q., Jonathan, E., Naveed, D. i. Wind tunnel and numerical study of a small vertical axis wind turbine. *Renewable Energy* (5), 412-422.

Ren 21. (2017). Renewable energy policy network for the 21st century. Renewables 2017; Global Status Report. http:/www.ren21.net/REN21Activities /GlobalStatusReport.

Robert, H., Ning, Q., Jonathan, E., & Naveed, D. i. (2010). Wind tunnel and numerical study of a small vertical axis wind turbine. *Renewable Energy, 35* 412–422.

Saha, U. K., & Rajkumar, M. J. (2006). On the performance analysis of Savonius rotor with twisted blades. *Renewable Energy, 31* 1776–1788.

Sahin, A. (2005). Progress and recent trends in wind energy. Progress in Energy and Combustion Science. *An International Review Journal, 30* 501–543.

Saidur, R., Rahim, N. A., Islam, M. R., & Solangi, K. H. (2011). Environmental impact of wind energy. *renewable and Sustainable Energy Reviews, 15*, 2423-2430.

Sanderse, B. (2009). *Aerodynamics of wind turbine wakes: Literature review. Energy research center of Netherland. ECN-e--09-016.* Retrieved from wwwpublications/E/2009/ECN-E--09-016.ecn.nl

Sayed Mohamed, A., Kandil Hamdy, A., & Ahmed., S. (2012). Aerodynamic analysis of different wind-turbine-blade profiles using finite-volume method. *Energy Conversion and Managment, 2*(64), 541-550.

Shahizare, B., Nik-Ghazali, N., Chong, W. T., Tabatabaeikia, S., Izadyar, N., & Esmaeilzadeh, A. (2016). Novel investigation of the different Omni-direction-guide-vane angles effects on the urban vertical axis wind turbine output power via three-dimensional numerical simulation. *Energy Conversion and Managment, 117*, 206–217.

Shamshirband, S., Iqal, J., Petkovic, D., & Mirhashemi, A. M. (2014). Survey of four models of probability density functions of wind speed and directions by adaptive neuro-fuzzy methodology. *Advances in Engineering Software, 76*, 148-153.

Sharpe, T., & Proven, G. (2010). Crossflex: Concept and early development of a true building integrated wind turbine. *Energy and Buildings, 42*(12), 2365-2375.

Sheldahl, R. E., &, Klimas, P. C., *Aerodynamic characteristics of seven symmetrical airfoil sections through 180-degree angle of attack for use in aerodynamic analysis of vertical axis wind turbines* Sandia National Laboratories. Report SAND80-2114. 1981 (1980) Retrieved from Albuquerque, United States: http://www.osti.gov/scitech//servlets/purl/6548367.

Shepherd, D. G. (2009). Historical Development of the Windmill. In D. A. Spera (Ed.), *Wind Turbine Technology Fundamental Concepts of Wind Turbine Engineering* (Second Edition ed.). New York, USA ASME Press.

Siddiqui, M. S., Naveed, D., & Imran, A. (2015). Quantification of the effects of geometric approximations on the performance of a vertical axis wind turbine. *Renewable Energy, 75*, 661-670.

Simao Ferreira, C. J., van Bussel, G., & van Kuik, G. (Febuary 27-March 2, 2006). *An analytical methods to predict the variation in performance of a H-Darrieus in skewed flow and its experimental validation.* Paper presented at the European Wind Energy Conference, Athens (Greece).

Simiu, Emil and Scanlan, & Robert. (2011). *Wind Power Plant ;Fundamentals, Design, Construction and Operation*: Springer.

Simiu, S., & Scanlan, R. H. (1996). *Wind Effects on Structures*. New York: Wiley and Sons, inc.

Sitti, M. R. S., Norizah, M., & Syafrudin, M. (2011). The Evaluation of Wind Energy Potential in Peninsular Malaysia. *International Journal of Chemical and Environmental Engineering, 2*(4), 284.

Soraghan, C., Leithead, W., Feuchwang, J., & Hong. Y. (2013). *Double multiple stream model for variable pitch vertical axis wind turbines*. Paper presented at the 31st AIAA Applied Aerodynamics Conference.

Song, S.H. S. Kang, N. Hahm, Implementation and control of grid connected AC-DC-AC power converter for variable speed wind energy conversion system, in: Applied Power Electronics Conference and Exposition, 2003. APEC'03. Eighteenth Annual IEEE. IEEE, 1, 2003, 154-158.

Stankovic, S., Campbell, N., & Harries, A. (2009). *Urban wind energy*. London Earthscan, UK. Pp 1-20.

Streamlining and Aerodynamics. (27 September, 2016). Retrieved from http://www.aerospaceweb.org/question/aerodynamics/q0094b.shtml

Strickland, J. H. (1975). *The Darrieus Turbine: Performance prediction model using multiple streamtube*. Retrieved from Albuquerque, New Mexico 87115.

Strom, B., Brunton, S., Polagye, B., (2015); Consequences of Preset Pitch Angle on Cross-Flow Turbine Hydrodynamics, Proceedings of the 11th European Wave and Tidal Energy Conference (11th EWTEC, 2015), 6-11th Sept 2015, Nantes, France.

Sudhamshu, A. R., Manik, C. P., Nivedh, S., Satish, N. S., Vivek, M., & Ratna, K. V. (2016). Numerical study of effect of pitch angle on performance characteristics of a HAWT. *Engineering Science and Technology, an International Journal, 19*(1), 632-641.

Takao, M., Kuma, H., Maeda, T., Kamada, Y., Oki, M., & Minoda, A. (209). A straight-bladed vertical axis wind turbine with a directed guide vane row; Effect of guide vane geometry on the performance *Journal of Thermal Science, 18*(1), 54-57.

Takao, M. , H. Takita, and Y. Saito, "Experimental study of a straight-bladed vertical axis wind turbine with a directed guide vane row," in *Proceedings of the 28th*

International Conference on Ocean, Offshore, and Arctic Engineering, Honolulu, HI 2009.

Tan, C. S., Maragatham, K., & Leong, Y. P. (2013). *Electricity Energy Outlook in Malaysia*. Paper presented at the 4th International Conference on Energy and Environment (ICEE 2013).

Tourlidakis, A., Vafiadis, K., Fintikakis, H., & Zaproudis, I. (2014). *Computational analysis of a shrouded small scale vertical axis wind turbine*. Paper presented at the EWEA 2014, Barcelona, Spain: Europe's Premier Wind Energy Event.

Turan, S., Peacock, A. D., & Newborough, M. (2007). Micro and small wind turbine applications in the built environment. *ISESCO Scinece Tech. Vison, 3*, 106-110.

Vaidhehi, V. (2014). The role of Dataset in training ANFIS System for Course Advisor. *International Journal of Innovative Research in Advanced Engineering (IJIRAE), 1*(6), 2349-2163.

Valsamidis, M. (1995). Wind Turbine Cross wind machine. US Patent No.; US 5,380149.

van Bussel, G. J. W., Mertens. S., Polinder, H., & Sidler, H. F. A. (2004). *TURBY®concept and realisation of a small VAWT for the built environment* Paper presented at the EAWE/EWEA Special Topic conference "The Science of making Torque from Wind" 2004 Delft, The Netherlands.

van de Wiel, J., (2015) "Global and Aerodynamic Optimization of a high solidity mid-size VAWT," (Masters Thesis) Delft University of Technology.

Vlastimir, N., Petkovic, D., Shamshirband, S., & Zarko, C. (2015). Adaptive neuro-fuzzy estimation of diffuser effects on wind turbine performance. *Energy, 89*, 324-333.

Wahidabanu, R. S. D., Shakilabanu, A., & Manoj, D. (2011). Identification and Control of Nonlinear Systems using Soft Computing Techniques. *International Journal of Modeling and Optimization, 1*(1), 24-28.

Walker, S. L. (2011). Building mounted wind turbines and their suitability for the urban scale- a review of methods of estimating urban wind resource. *Energy and Buildings, 43*, 1852-1862.

Wang, Y., Sun, X., Dong, X., Zhu, B., Huang, D., & Zheng, Z. (2016). Numerical investigation on aerodynamic performance of a novel vertical axis wind turbine with adaptive blades. *Energy Conversion and Management, 108*, 275-286.

Wei, T. (2010). Fundamental of wind energy. In W. Tong (Ed.), *Wind Power Generation and Wind Turbine Design* (pp. 9). Southampton, Boston: WITpress.

Wei, T. (2010). *Wind Power Generation and Wind turbine Design*. Southamton, UK: WIT Press.

WINEUR. (2007). *Wind Energy Integration in the Urban Environment*. Retrieved from European Commission.

Worasinchai, S., Ingram, G. L., & Dominy, R. G. (2015). The physics of H-Darrieus turbine starting behavior. *Journal of Engineering for Gas Turbines and Power, 138*(6), 1-27.

Zanforlin, S., & Letizia, S. (2015). *Improving the performance of wind turbines in urban environment by integrating the action of a diffuser with the aerodynamics of the rooftops.* Paper presented at the ATI 2015 - 70th Conference of the ATI Engineering Association.

Zhao, Z. Y., Wen-Jun, L., George, Z., & Jian, Z. (2012). Comparative assessment of performance of foreign and local wind turbine manufacturers in Chna. *Renewable Energy, 39*, 424-432.

Zhang, Lx, Liang, Yb., Liu, Xh., Guo, J.(2014). Effect of blade pitch angle on aerodynamic performance of straight-bladed vertical axis wind turbine. Journal of Central South university, V0l. 21(4), 1417-1427.

List of publications and papers presented

Wen Tong Chong, **Mohammed Gwani,** Chin Joo Tan, Wan Khairul Muzammil, Sin Chew Poh, and Kok Hoe Wong, (2017). Design and Testing of a Novel Building Integrated Cross Axis Wind Turbine. Appl. Sci. 7,251; doi:10.3390/app7030251. (ISI).

W. T. Chong, **M. Gwani,** S. Shamshirband, W.K. Muzammil, C.J. Tan, A. Fazlizan, S.C. Poh, Dalibor Petković, K.H. Wong, (2016) Application of adaptive neuro-fuzzy methodology for performance investigation of a power-augmented vertical axis wind turbine. Energy, 102, 630-636, (ISI).

Conferences

Mohammed Gwani; Design and Testing of a Novel Building Integrated Cross Axis Wind Turbine. Paper presented at Doctoral Research Seminar on Renewable Energy & Green Energy, 10 March 2016, Faculty of Engineering, University of Malaya.

Gwani, M., Feasibility study and optimization analysis of a stand-alone wind-PV hybrid energy system with omni-direction guide vane in Malaysia; An application of HOMER; 7^{th} international conference on researches in Engineering, Technology and Sciences (ICRETS), July 16-27, 2015, Kuala Lumpur, Malaysia.